# Out-of-Equilibrium Replication and the Amplification of Chirality

**Sarah M. Morrow**

A thesis submitted for the degree of

**Doctor of Philosophy**

of the

**University of Oxford**




University College

Michaelmas Term 2018

# Declaration

This thesis describes work conducted under the supervision of Professor Stephen Fletcher in the Chemistry Research Laboratory, Oxford, between February 2015 and August 2018. The thesis is entirely my own work except where otherwise indicated and acknowledged. It has not been submitted for any other degree at this university or at any other institution.

Sarah M. Morrow

# Acknowledgements

Thanks go first to University College, the Oxford Radcliffe Scholarship, the EPSRC, and all the industrial sponsors of the SBM for their support and for funding my four years of study. It's been a pleasure to meet the individuals behind these sponsorships.

Thank you to Steve for welcoming me into the Fletcher group and for proposing the challenging and intellectually rewarding projects in this thesis. I am grateful for all the opportunities you have offered me over the four years, not least of all teaching and all those conferences in far-flung places.

Thank you to the whole of the Fletcher group, past and present (especially Andrew, Mireia, Masha and Wieland) for being fantastic advice-givers (scientific or otherwise), travel companions, and karaoke-enforcers. I am indebted to all of my very thorough proof-readers. Special thanks go to Ignacio for the valuable ideas which have contributed hugely to this thesis.

Thank you to 4 Parker Street, the house and its occupants. And to blissful Sunday mornings post-run eating breakfast in the garden. That reminds me of summertime, and a bank-holiday-hike from Moreton-in-Marsh with Nod and Jason, who are both very special to me.

My greatest thanks go to Lilja and to my parents, Diane and Rod. Their unwavering support has been wonderful. I hope that I've made that clear to you

all over my time in Oxford. Here's to more camping adventures, dancing, and wine and cheese nights together, Lilja. And here's to more mid-week sherry, weekend negroni's, Friday night pizzas, and fell-walking, M and D.

# Abstract

This thesis explores physical autocatalysis, or the replication of supramolecular aggregates of surfactants such as micelles. There is a focus on the out-of-equilibrium and non-linear behaviours that can be extracted from a process of physical autocatalysis and which characterise lifelike dynamics and properties.

Chapter 2 describes a study of reversibly-formed surfactants which form micelles within a dynamic combinatorial library. Though the system does not demonstrate a process of replication, the study of surfactants containing reversibly-formed bonds is of use towards the design of an out-of-equilibrium replicator. Thus, Chapter 3 describes the development of a physical replicator constructed by thiol-disulfide exchange which can persist, out-of-equilibrium, by the consumption of a chemical fuel, mimicking dissipative biological structures.

The second half of this thesis introduces an ambitious design for a process of physical autocatalysis with amplification of chirality. Chapters 5 and 6 detail two experimental attempts. Chapter 5 describes the study of a chiral surfactant constructed by a native chemical ligation reaction, which shows interesting differences in reactivity between homogeneous and biphasic reaction conditions. However, a process of replication is not observed, nor the amplification of chirality. A more successful system is the study in Chapter 6 on the formation of a chiral surfactant based on the autocatalytic reaction studied in Chapter 3. An interesting sense of asymmetry is established; the chiral surfactant appears to be autocatalytic and partitions into a precipitate of enhanced ee and a solution phase of diminished ee.

# Abbreviations

| | |
|---|---|
| 4° | quaternary |
| Å | angstrom(s) |
| a.u. or arb. unit | arbitrary unit |
| Ac | acetyl |
| aq. | aqueous |
| Ar | aromatic |
| Bn | benzyl |
| Boc | *tert*-butyloxycarbonyl |
| °C | degrees Celsius |
| cac | critical aggregation concentration |
| cat. | catalytic |
| $cm^{-1}$ | wavenumber |
| cmc | critical micelle concentration |
| DLS | dynamic light scattering |
| DOSY | diffusion-ordered spectroscopy |
| ee | enantiomeric excess |
| eq. | equivalents |
| g | gram(s) |
| h | hour(s) |
| HetAr | heteroaromatic |
| HPLC | high performance liquid chromatography |
| HRMS | high resolution mass spectrometry |
| Hz | hertz |
| iPr | *iso*-propyl |
| IR | infrared |
| iSCAT | interferometric scattering microscopy |
| *J* | coupling constant |
| kg | kilogram(s) |
| kHz | kilohertz |
| L | litre(s) |
| LRMS | low resolution mass spectrometry |
| m/z | mass to charge ratio |
| m | metre(s) |
| M | molar |
| Me | methyl |
| MHz | megahertz |
| mM | millimolar |
| min | minute(s) |
| mL | millilitre(s) |
| mM | millimolar |
| mm | millimetre(s) |
| mmol | millimole(s) |
| mol | mole(s) |
| mol% | mole percent |
| mQ | milliQ $H_2O$ |
| MS | mass spectrometry |
| nm | nanometre(s) |
| NMR | nuclear magnetic resonance |
| Np | napthyl |
| pH* | measured “pH” by pH probe of a $D_2O$ solution |
| ppm | parts per million |
| PTFE | polytetrafluoroethylene |
| R | general organic group |
| rac | racemic |
| $R_h$ | hydrodynamic radius |
| rpm | revolutions per minute |
| rt | room temperature |
| mPa | millipascal(s) |
| s | second(s) |
| sat. | saturated |
| s.d. | standard deviation |
| SFC | supercritical fluid chromatography |
| TFA | trifluoroacetic acid |
| µL | microlitre(s) |
| µm | micrometre(s) |
| µM | micromolar |
| µmol | micromole(s) |
| UPLC | ultra high performance liquid chromatography |
| UV | ultraviolet |
| $\tilde{\nu}_{max}$ | infrared absorption maximum |

# General Experimental Details

$^{1}H$ NMR and $^{13}C$ NMR spectra were recorded on a 400 MHz or 500 MHz spectrometer in $(CD_3)_2SO$, $(CD_3)_2CO$, $D_2O$ and $CDCl_3$ and referenced to residual solvent peaks. Chemical shifts are quoted in ppm (parts per million) to the nearest 0.01 ppm with signal splitting recorded as singlet (s), doublet (d), triplet (t), quartet (q), multiplet (m), broad singlet (br. s) and broad doublet (br. d). Coupling constants, *J*, are measured in Hz to the nearest 0.5 Hz. $^{1}H$ and $^{13}C$ NMR spectra were recorded at room temperature. Infrared spectra were recorded as thin films of neat samples on a Bruker Tensor 27 FT-IR spectrometer equipped with Attenuated Total Reflectance sampling accessories. Peaks labelled (w) are weak. High resolution mass spectra are given to four decimal places and were recorded on a Bruker MicroTof (resolution = 10000 FWHM) under conditions of electrospray ionisation (ESI), atmospheric pressure chemical ionisation (APCI), or electron ionisation (EI). Low resolution MS were recorded using a Walters LCT premier XE. Optical rotations were recorded using a Perkin-Elmer 241 polarimeter at 25 °C in a 10 cm cell in the stated solvent. $[\alpha]_D$ values are given in $10^{-1}deg \cdot cm^2g^{-1}$, with concentration c given as g/100 mL. Column chromatography was performed using silica gel (60 Å, 0.033-0.070 mm, BDH). Chemicals and reagents were obtained from Sigma Aldrich, Alfa-Aesar, Apollo Scientific, Strem chemicals, Acros Organics, TCI UK and Fluorochem, and were used directly as supplied (unless indicated otherwise as detailed in procedures). All anhydrous reactions were carried out in flame-dried glassware and under an inert atmosphere of argon provided by a balloon or Schlenk line. Reaction solvents dichloromethane ($CH_2Cl_2$), diethyl ether ($Et_2O$), tetrahydrofuran (THF), methanol (MeOH), acetonitrile (MeCN), dimethylformamide (DMF), and ethyl acetate (EtOAc) were dried by purification through two activated alumina purification columns. All reactions were stirred with magnetic followers. Cooling of reaction mixtures to 0 °C was performed using an ice/water bath. Heating was performed using Drysyn® heating blocks.

# Contents

**Chapter 1 Replication Out-of-Equilibrium ..... 1**

1.1 Molecular replication and lifelike dynamics ..... 2

1.2 How does a molecule replicate? ..... 3

1.3 Replication under dynamic regimes ..... 17

1.4 Beyond thermodynamic control: replication out-of-equilibrium ..... 30

1.5 Project aim: towards an out-of-equilibrium replicator ..... 46

1.6 References ..... 48

**Chapter 2 Physical Autocatalysis in a Dynamic Combinatorial Library .... 53**

2.1 Introduction ..... 54

2.2 “Dynamic Combinatorial Evolution within Self-Replicating Supramolecular Assemblies” ..... 55

2.3 Our study ..... 60

2.4 Conclusions ..... 66

2.5 Experimental ..... 68

2.6 References ..... 95

**Chapter 3 A Chemically Fuelled Out-of-Equilibrium Replicator ..... 97**

3.1 Introduction ..... 98

3.2 The discovery of a metastable physical replicator ..... 99

3.3 Out-of-equilibrium replication ..... 110

3.4 Conclusions ..... 118

3.5 Experimental ..... 119

3.6 References ..... 150

**Chapter 4 Molecular Replication and the Amplification of Chirality ..... 153**

4.1 A hallmark of life ..... 154

4.2 Autocatalysis and the amplification of chirality ..... 155

4.3 Replication of micelles and the amplification of chirality ..... 160

4.4 Project Aim ..... 168

4.5 References ..... 169

**Chapter 5 Chiral Surfactant Formation by Native Chemical Ligation ..... 171**

5.1 Introduction ..... 172

5.2 System design ..... 172
5.3 Surfactant characterisation ..... 174
5.4 Optimisation of the biphasic reaction ..... 175
5.5 Test for autocatalysis ..... 180
5.6 Test for the amplification of chirality ..... 183
5.7 Conclusions ..... 184
5.8 Experimental ..... 186
5.9 References ..... 201
**Chapter 6 Chiral Surfactant Formation by Thiol-Disulfide Exchange ..... 203**
6.1 Introduction ..... 204
6.2 Enantioselective physical autocatalysis: system design ..... 204
6.3 Scenario 1: a chiral hydrophilic disulfide ..... 206
6.4 Scenario 2: a chiral hydrophobic thiol ..... 211
6.5 Conclusions ..... 223
6.6 Experimental ..... 225
6.7 References ..... 243
**Chapter 7 Conclusions and Future Work ..... 245**
7.1 Out-of-equilibrium replication ..... 246
7.2 Replication and the amplification of chirality ..... 251
7.3 Concluding remarks ..... 255
7.4 References ..... 256

# 1

## Replication Out-of-Equilibrium

## 1.1 Molecular replication and lifelike dynamics

A process of replication is vital to life, allowing for persistence, propagation, mutation and evolution in the environment.[1–3] However, the modern biological mechanisms for replication are highly complex and heavily evolved themselves. The design of minimal replication, without biological machinery, is a synthetic and intellectual challenge and may help us understand a transition from non-living to living.[4–6]

Since the late 1980's, many molecular systems capable of simple replication without enzymatic apparatus have been designed and studied.[4–6] It is systems like these which teach us about the minimal requirements for life without confinement to the molecules which make life as we know it at present. Still, however, the majority of minimal replicators studied are the thermodynamic or kinetically trapped products of the system,[4–6] arising from simple conversion to stable products. Life itself is characterised by more dynamic regimes: it persists out-of-equilibrium, maintaining high energy, dissipative and functional states by the continuous consumption of energy.[7] This behaviour is evident across scales, from chemically-fuelled metabolic cycles, to the maintenance of strong but adaptable microtubules responsible for cell integrity and division.

It is therefore important to design and study systems and structures undergoing minimal replication, without biological machinery,[4–6] under dissipative out-of-equilibrium and fuelled regimes,[6,8–11] coupling two processes which are intimately associated with lifelike processes and dynamics. High energy, metastable

replicators can be maintained out-of-equilibrium by the continuous consumption of energy. Ultimately, being out-of-equilibrium may be a requirement for a process of replication subject to open-ended evolution, and the synthesis of life itself. Put most simply, the continuous consumption of energy by a system of replicators may allow for a continuous increase in order and function away from the thermodynamic minimum.[2,3,12–16]

The design of any dissipative out-of-equilibrium system is non-trivial, let alone the design of a dissipative out-of-equilibrium replicator. We must begin simply: first, we explore the early development of molecular replicators in closed systems, with the formation of stable thermodynamic or kinetically trapped products. We then follow their development towards more dynamic systems, examining replication within dynamic combinatorial libraries whose members are subject to processes of competition and destruction. Finally, we consider the realisation of replicators which persist, despite their metastability, with the consumption of fuel energy, out-of-equilibrium.

## 1.2 How does a molecule replicate?

Most simply, a process of replication is where a product acts as a catalyst for its own formation.[4–6] This process is known as autocatalysis (Figure 1.2.1). In the reaction between A and B to form replicator C, C is a catalyst for its own formation. Autocatalytic reactions are ideally characterised by an exponential reaction profile, where the rate of reaction is proportional to the concentration of product. There is therefore a lag period in the production of product at the start

of the reaction, but the continuous production of catalyst results in exponential growth before starting materials are depleted (Figure 1.2.1). Where the reaction is less efficient (where not all product is available for catalysis, for example) sub-exponential growth results in sigmoidal, or 'S'-shaped, rather than exponential profiles. This is a primitive model for the 'selection of the fittest' replicators,[17] where exponential replicators outcompete less efficient catalysts. There is also a positive relationship between initial product concentration and initial rate; an increased quantity of product seeded into the reaction at the beginning increases the initial rate, shortening or removing the lag period (Figure 1.2.1b).

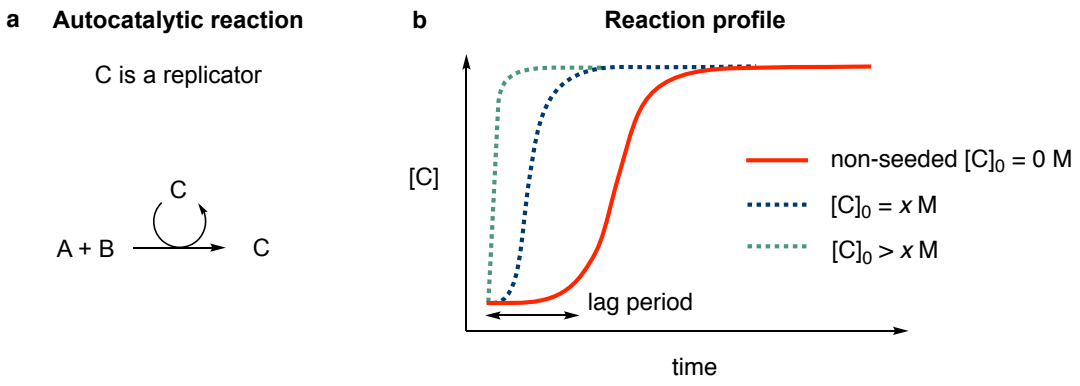



**Figure 1.2.1 a** In an autocatalytic reaction, the product C is a catalyst for its own formation and is therefore a replicator. **b** Autocatalytic reaction profiles: ideally the production of product C is exponential, with the continuous increase in concentration of the catalyst matched by a continuous increase in rate. Seeding the reaction with product C removes or shortens the lag phase, and the initial reaction rate increases with an increasing quantity of seeded product.

The types of molecules which undergo a process of minimal replication may be divided into two camps: template replicators and physical replicators.[4] Their

mechanisms are explored in detail in the following sections. Broadly, template replicators are inspired by the well-defined recognition afforded by hydrogen bonding between nucleobases in strands of DNA. Physical replication concerns the replication of supramolecular structures, often mediated by less well-defined interactions.

The earliest developed synthetic replicators of both types were formed by irreversible reactions, and usually from a limited pool of starting materials (Figure 1.2.2). They display the simplest autocatalytic dynamics, forming stable products, whether thermodynamic or kinetically trapped. Nevertheless, these studies introduce us to the fundamental mechanisms of minimal, molecular replication which can be developed to more dynamic systems. They are explored in the following sections.

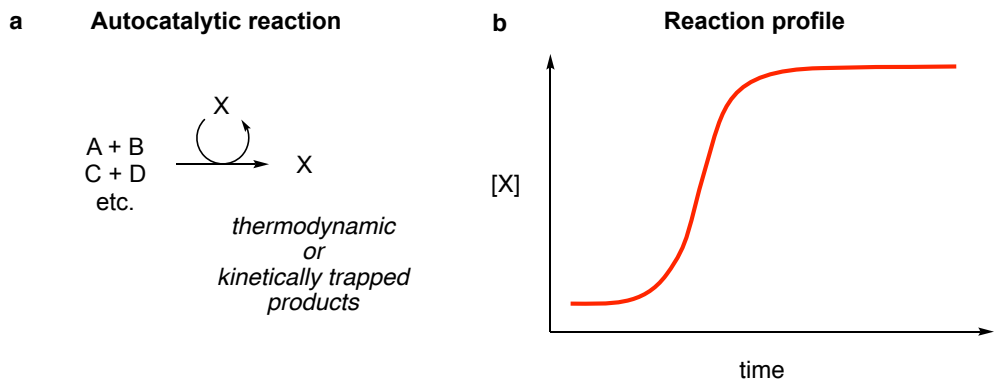



**Figure 1.2.2 a** An autocatalyst X is formed *via* an irreversible reaction from a pool of starting materials. **b** Irreversibly formed autocatalyst X is the thermodynamic or kinetically trapped product of the reaction and is stable.

## 1.2.1 Template replication

A minimal model for a template replication is presented in Figure 1.2.3. A template replicator T contains functional groups which act as recognition elements for the binding of precursor molecules A and B. Their pre-organisation by template T allows for their increased rate of reaction to form a second template molecule T. Successful dissociation of the template dimer therefore releases both the 'old' template and a new template, both of which can continue to catalyse their own formation. Template T is therefore an autocatalyst, or replicator.

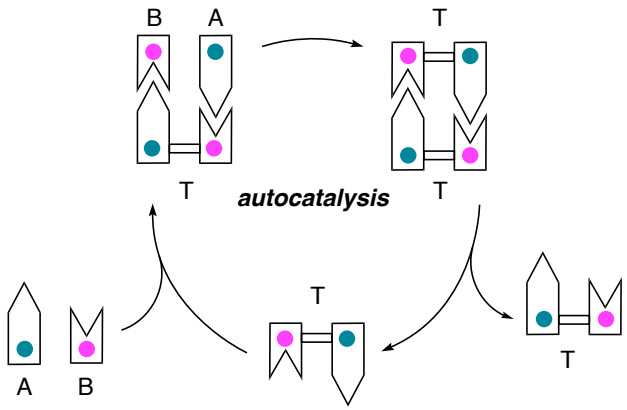



**Figure 1.2.3** Template replicator T contains recognition elements for the binding of precursor molecules A and B, catalysing the formation of a second template T by pre-organisation.

The very first report of a synthetic replicator was that of a template replicator,[18] and this mechanism has since been harnessed most notably in the replication of small oligonucleotides, peptides, and small molecules.[4–6] They are all governed by specific interactions between functional groups and are sensitive to structural and chemical changes.

As an illustrative example, Ghadiri and co-workers presented the first example of a replicating peptide, based on a simple protein folding motif.[19–21] Electrostatic interactions between charged residues and inter-helical recognition between hydrophobic residues allowed successful binding and pre-organisation of electrophilic and nucleophilic fragments of the peptide for template-catalysed native chemical ligation (Figure 1.2.4). The formation of a single product by irreversible bond formation placed this system firmly in the simplest scenario of replicator dynamics and the formation of a thermodynamic or kinetically trapped product (Figure 1.2.2), even where larger networks of peptide replicators were created.[22–25]

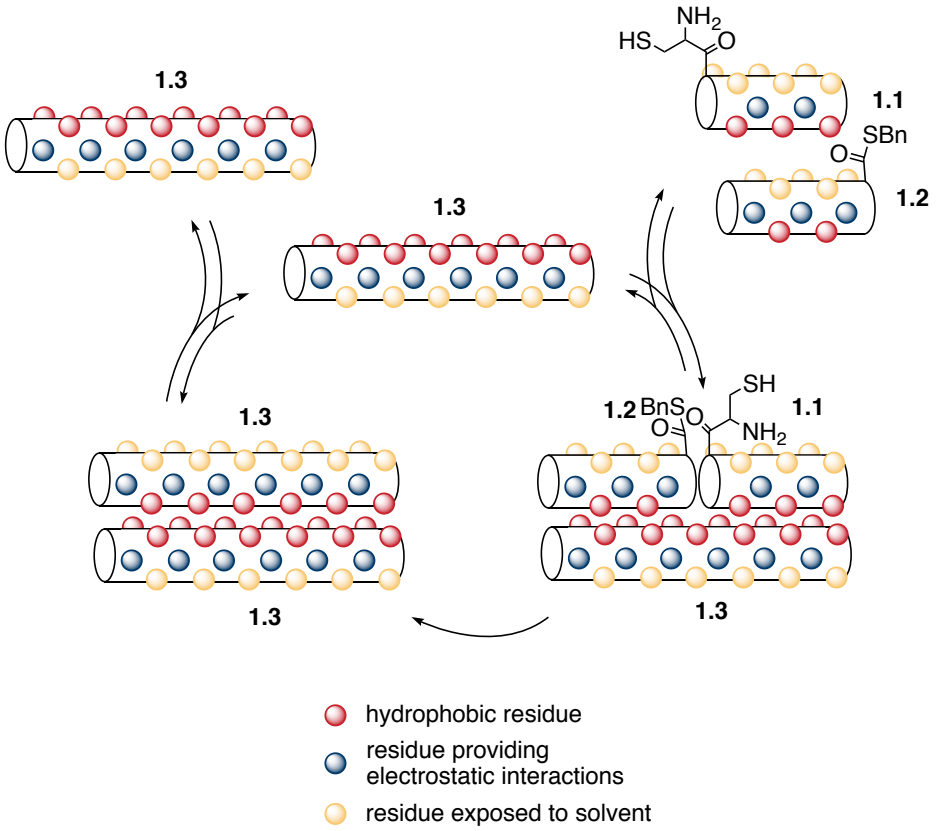



**Figure 1.2.4** An alpha helical coiled coil peptide, **1.3**, is capable of replication by the binding of precursors **1.1** and **1.2**. Binding is driven by recognition between hydrophobic resides and electrostatic interactions between charged residues. Adapted with permission from references[6,19].

Template replicators display interesting, emergent behaviour, and have obvious analogy to the replication of biological informational polymers. They are structurally sensitive systems which makes their function, whether oligonucleotide, peptide, or small molecule, idiosyncratic and non-general.[23,26,27] A more general, more accessible mode of minimal replication belongs to the replication of supramolecular aggregates. Interest in their design and realisation is not confined to this property; they have their own biological relevance. Rather than mimicking the replication of informational polymers, physical replication

mimics the creation and replication of biological boundaries such as primitive cell membranes.

### 1.2.2 Physical replication: the replication of micelles and other supramolecular aggregates

Most relevant to the work in this thesis, and the interest of the group, is the study of the replication of micelles.[4,28,29]

The historical interest in the replication of aggregates like micelles and vesicles can be explained by the fact that life, and its origins, has always been associated with the creation of a boundary. Indeed, attempts to define life gave rise to a theory of autopoiesis, developed by Maturna and Varela.[30,31] An autopoietic unit is a system capable of sustaining itself by maintaining an inner network of reactions which regenerates all the system's components, including the boundary itself. In more modern takes on the origins of life, networks of replicating molecules operating within replicating membrane vesicles allow for competition and evolution.[32] Indeed, work towards coupling boundary replication with the replication of informational, genetic material within it has been experimentally realised by some groups.[33–37]

A general scheme for physical replication,[4,28,29] the reproduction of aggregates like micelles and vesicles, is in Figure 1.2.5. Reaction between phase-separated components A and B is slow but produces a surfactant product C (Figure 1.2.5). Above the critical aggregation concentration (cac), newly produced C

spontaneously aggregates (in Figure 1.2.5 aggregation into micelles above the cmc is shown).

These aggregates act to increase mixing between the phases by solubilising the hydrophobic component in the aqueous layer, thereby increasing the rate of reaction to form the surfactant product and components of the aggregate; it is a replicator. They are inherently not ‘faithful’ in the synthesis of new surfactant precursors and, in theory, an aggregate could catalyse any biphasic reaction. This is in contrast to the high degree of complementarity between a template replicator and its fragments. Furthermore, unlike template replication, there is no well-defined catalyst-substrate interaction.[4,29,38–40]

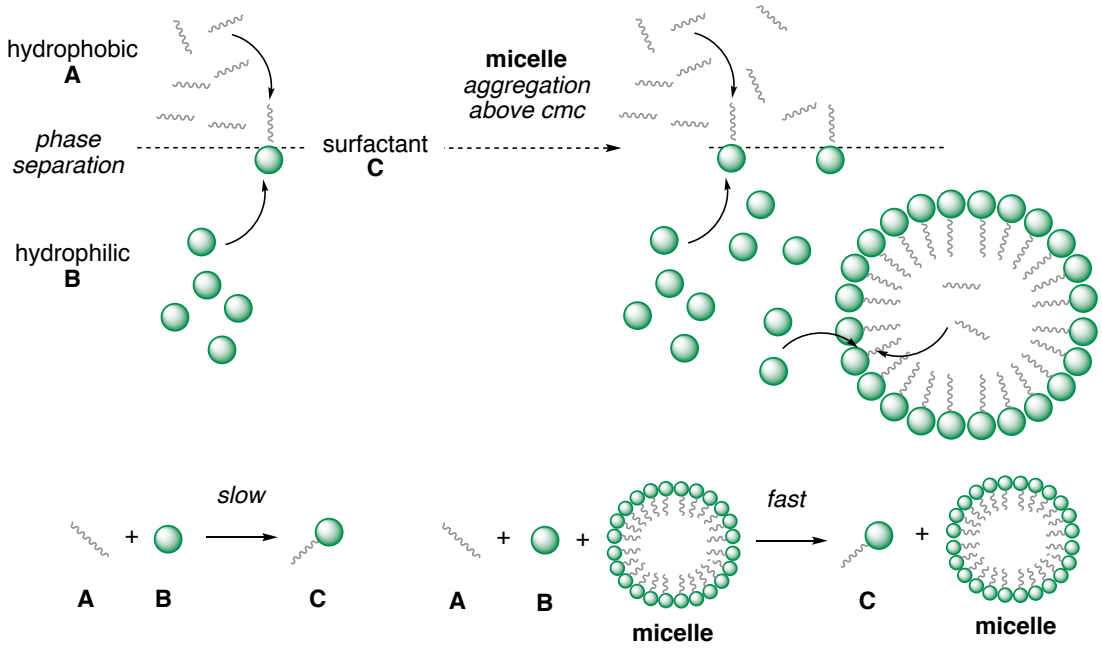



**Figure 1.2.5** Reaction between phase-separated components A and B is initially slow but produces surfactant molecule C. Above the critical aggregation concentration (cac), or here the cmc for the formation of micelles, the surfactant spontaneously aggregates. Aggregates act to increase mixing between the phases and therefore increase the rate of the reaction.

The creation of a minimal autopoietic system was in the mind of Luisi *et al.* in the first demonstration of the physical replication of reverse and aqueous micelles.[41–43] Most prominent was the production of octanoate micelles (Figure 1.2.6).[44] The hydrolysis of hydrophobic ethyl octanoate **1.4** produced octanoate **1.5**, and, on account of the phase separation, the reaction was slow for the first ~ 26 hours. However, after this lag period, the rate of hydrolysis became exponential. The increase in rate was ascribed to the fact that octanoate micelles, formed above the critical micelle concentration (cmc) of octanoate (~ 0.1 M determined under these reaction conditions), effectively solvated the hydrophobic ethyl octanoate

molecules in the aqueous phase, thus increasing the surface area for reaction (Figure 1.2.6). An increasing concentration of produced octanoate resulted in an increasing concentration of micelles, and thus an increased number of catalysts. The lag period could be reduced by an increased stirring rate, or by seeding the reaction with pre-formed octanoate (Figure 1.2.6). The formation of the stable thermodynamic product again placed this system in the simplest scenario of replicator dynamics (Figure 1.2.2).

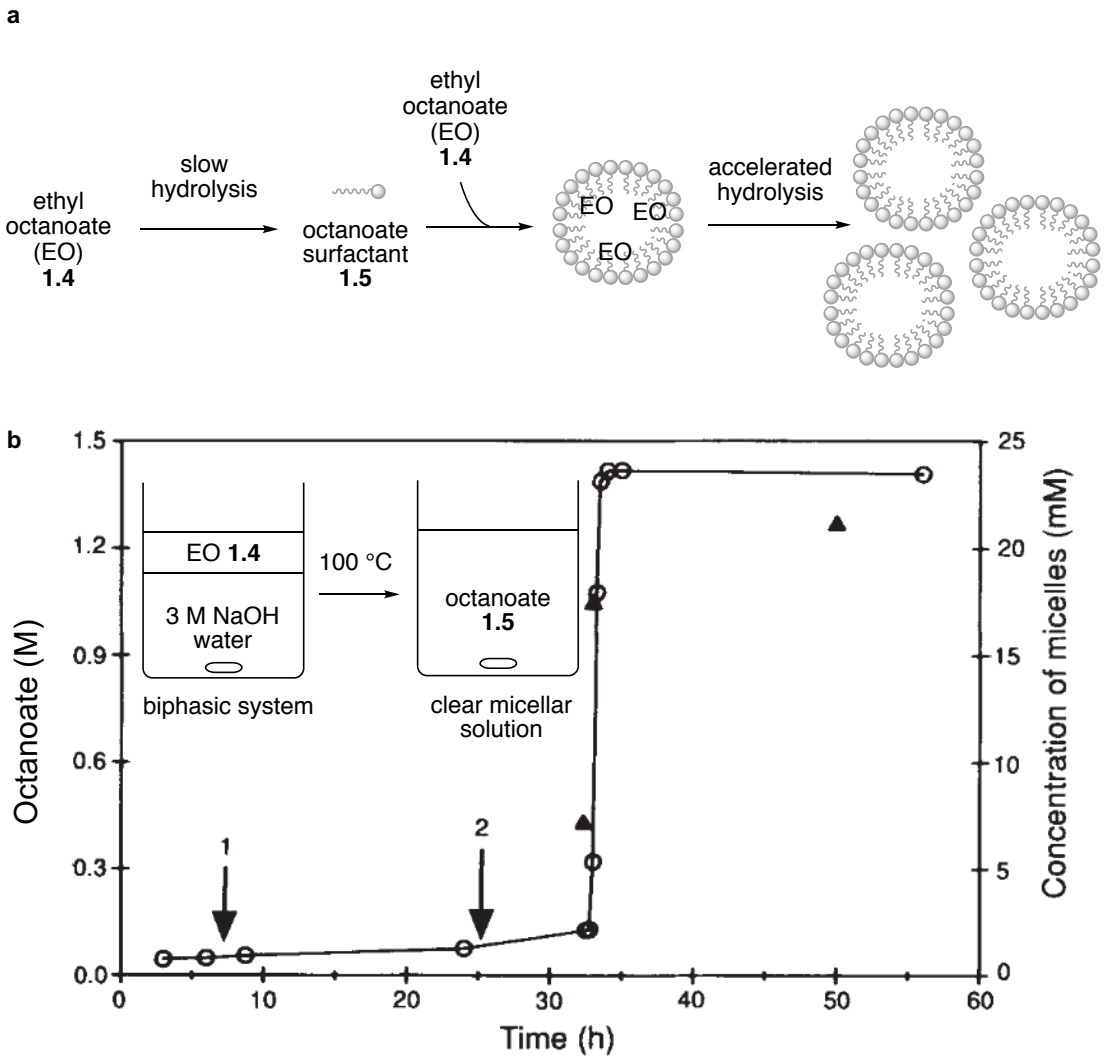



**Figure 1.2.6 a** The physical replication of aqueous micelles as described by Luisi *et al.*.[31,44] Ethyl octanoate (EO) **1.4** undergoes initially slow hydrolysis in 3 M NaOH. At a critical point, the product octanoate **1.5** aggregates into micelles, after which point hydrolysis is greatly accelerated. **b** Concentration of octanoate (open circles) measured by Fourier-transform infrared spectroscopy, and of micelles (triangles) by time-resolved fluorescence quenching during the course of the reaction. The inset drawing illustrates the reaction set-up. The onset time for exponential growth could be reduced by an increase in stirring rate (arrow 1) and by seeding the reaction with preformed octanoate **1.5** (arrow 2). Drawings adapted and graph reproduced with permission from references[31,44].

Initial investigations into systems undergoing physical autocatalysis conducted in the Fletcher group by Dr Andrew Bissette were based on irreversible bond formation, beginning with the 1,4-conjugate addition of a thiol to an α,β-unsaturated carbonyl (Figure 1.2.7).[45,46] Two systems were developed; one reaction was conducted at high pH/pD, and one under milder conditions, more relevant for the design of model protocells, at pD 7.85 (Figure 1.2.7).

Only the data for the reaction at pD 7.85 are shown in Figure 1.2.7 but are characteristic of both systems. A lag period was observed on reaction between **1.9** (100 mM, 1.0 eq.) and **1.10** (10 eq.), before a rapid increase in rate of the depletion of **1.9** (Figure 1.2.7, diamonds). The lag period was eliminated on seeding the reaction with pre-formed product **1.11** at concentrations above the measured cmc (measured as 4.8 mM for the isolated compound **1.11**; triangles = seeding with 20 mM **1.11**, circles = seeding with 70 mM **1.11**).

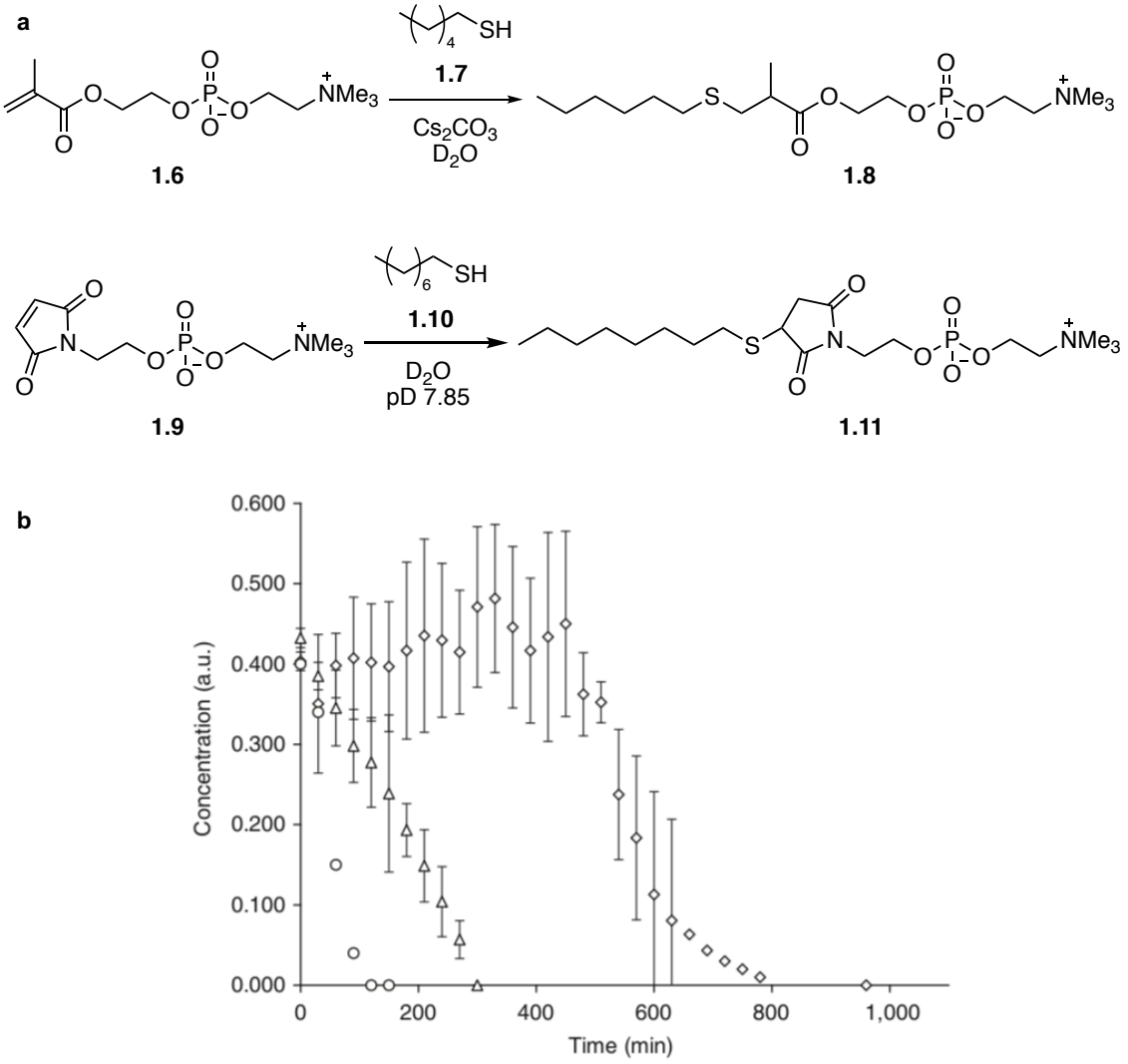



**Figure 1.2.7 a** First and second generation systems: a base-catalysed 1,4-conjugate addition of a thiol to an α,β-unsaturated carbonyl compound to produce a surfactant. **b** Examination of the 2nd generation system: concentration of **1.9** measured by $^{1}$H NMR spectroscopy over the course of the reaction. The control reaction (diamonds), containing starting materials only, displayed a lag period followed by an increase in reaction rate. On seeding the reaction with 20 mM **1.11** (triangles), the lag period was removed. Seeding at 70 mM (circles) further increased the rate of reaction. Control and 20 mM seeding reactions are plotted as the average of three entire experimental repeats (error bars = s.d.). Graph reproduced with permission from reference[45].

A derivative of the system at high pD (Figure 1.2.8) was also studied at the single aggregate level in collaboration with the Kukura group, University of Oxford, using interferometric scattering microscopy.[47] With this technique the group could directly observe the reactive interface between thiol **1.12** and aqueous **1.6**, giving insight into the nature and dynamics of aggregate formation in the non-homogenous system (Figure 1.2.8).

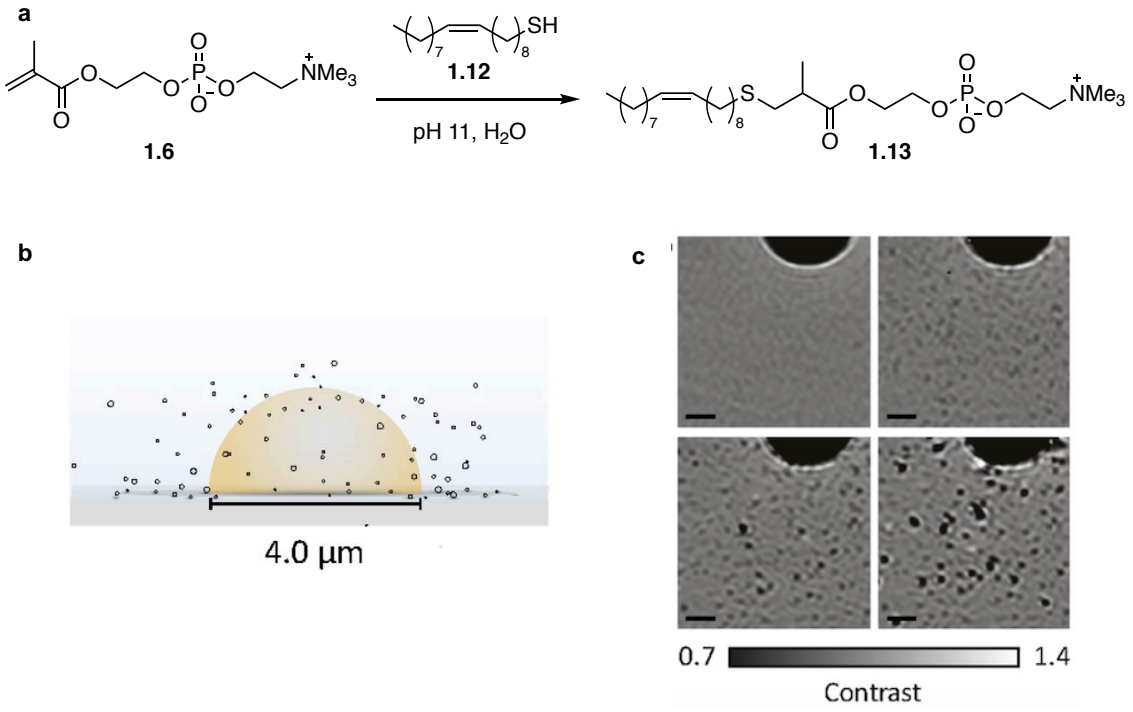



**Figure 1.2.8** **a** The autocatalytic reaction under study by interferometric scattering microscopy. **b** Reaction geometry: the hemisphere is a droplet of neat thiol **1.12**, flooded by an aqueous solution of electrophile **1.6** on a microscope coverslip. The black rings illustrate newly produced aggregates of **1.13**. **c** Flat field images of the reaction at the thiol-water interface. The reaction progress is from left to right and top to bottom. The production of new aggregates of **1.13** is measured by the appearance of black spots on the background. Their size is directly proportional to their contrast. Scale bar = 1 µm. Reproduced with permission from reference[47].

## 1.3 Replication under dynamic regimes

The preceding short review of both template replication and physical replication has encompassed only irreversibly-formed, stable replicators. Indeed, these were the first developed examples of any synthetic molecule undergoing a process of replication. Both have some biological relevance, whether that is the mimicry of the replication of informational polymers, or the replication of membranes. However, a movement towards more lifelike dynamics and out-of-equilibrium replication requires the study of high energy, metastable replicators.[6,8–10]

The study of replicators in systems containing an increased number of components and subject to pressures of replicator competition and destruction is, in some way, considered as a preliminary step towards this goal. A simple increase in the number of components brings with it unpredictable, emergent behaviour of the entire network which has analogy to lifelike processes.[6] This phenomenon has best been explored by the construction of replicators within a dynamic combinatorial library, examined in the following section.

### 1.3.1 Replication in dynamic combinatorial libraries

A dynamic combinatorial library (DCL) is constructed by the mixing of building blocks which can undergo reversible covalent or non-covalent association between each other; the so-formed library members continuously interconvert between each other and their distribution, (usually) under thermodynamic control,

is responsive to stimuli such as templates or changes in the environment, minimising the energy of the system as a whole.[48]

It is therefore interesting to study the formation of replicators – themselves a form of template – in dynamic combinatorial libraries.[6,48–50] A simplified scheme of their dynamics is shown in Figure 1.3.1, with the production of transient, high energy kinetic products, leading to thermodynamic products, or the formation of kinetically trapped products. Exploring replication within DCLs is an interesting study of the coupling of thermodynamic and kinetic control, and the emergent behaviour of multiple competing species.

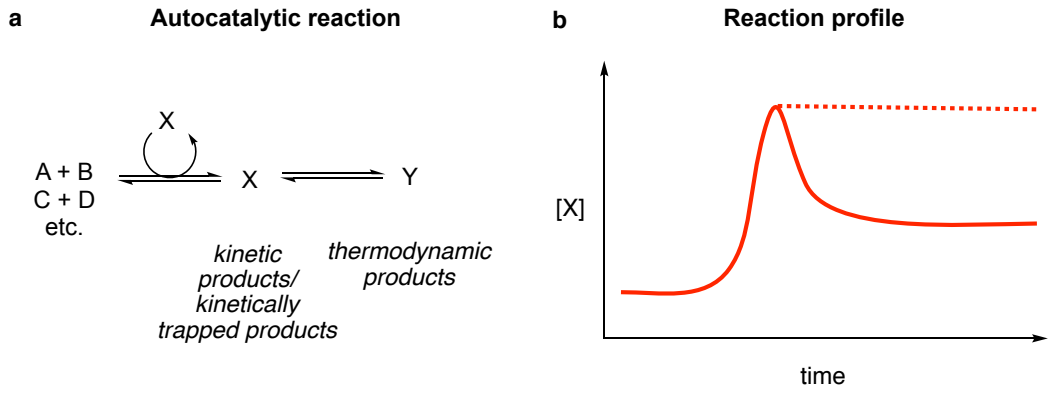



**Figure 1.3.1 a** A simplified scheme of replication in a dynamic combinatorial library and (**b**) its associated reaction profile: replicator X may be reversibly formed from a pool of starting materials but, unless kinetically trapped (dashed line), is unstable towards thermodynamic products Y. The system has the potential to explore different states and the reaction profile is a function of the various kinetic and thermodynamic stabilities of the library members.

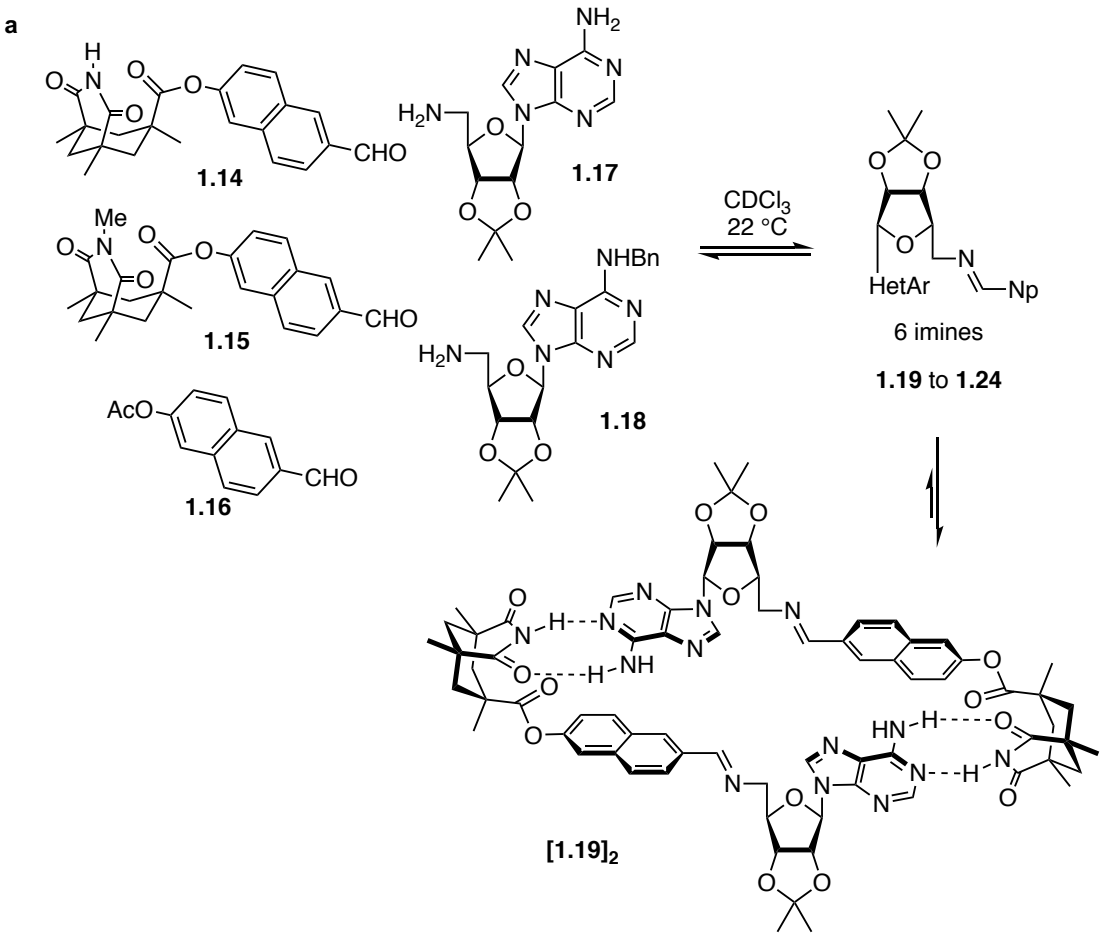
The study of systems which eventually evolve to the thermodynamic minimum of the entire system, or which become kinetically trapped, at first appears counterproductive for the design and realisation of *out-of*-equilibrium states, in which high energy, metastable species are maintained and prevented from destruction to the thermodynamic minimum by the consumption of energy. However, exploring the nature of replicators that are constructed in DCLs, and the reactions that are used for their construction and destruction, could help us to design these metastable states in the first place. The non-trivial translation to an out-of-equilibrium replicator would then involve the maintenance of the otherwise transient kinetic states with the consumption of energy.

Further, even fully under thermodynamic control DCLs have their own analogy to "lifelike" processes. The dynamic, responsive system, whose components are reversibly formed and can be subject to destruction, can undergo processes of 'error checking' and 'error correction',[6] which have been likened to evolutionary processes. The increase in "complexity" that arrives with the consideration of an increased number of components better matches the finely-tuned and emergent interactions between multiple components in biological systems. The study of replication within DCLs is therefore of interest in its own right.

Xu and Giuseppone exploited an imine condensation in the design of their reversibly-formed template replicator, inspired by Rebek (Figure 1.3.2 and 1.3.3).[51–53] The component capable of self-recognition, and therefore replication, was amplified in the equilibrating pool. Amplification was initially kinetically controlled, based on a pre-association between **1.14** and **1.17**, and **1.19** reached

a peak in concentration before movement towards equilibrium and a reduction in the quantity of this replicator to make way for other species. The thermodynamic stability of **1.19** ensured that the molecule capable of self-recognition still remained amplified, far from a statistical distribution, in the final equilibrium distribution. Direct competitors, which possessed one half of the replicator structure (**1.20**, **1.21**, **1.23**), were therefore suppressed.

**a**




**b**

| | | amine | |
|---|---|---|---|
| | | **1.17** | **1.18** |
| aldehyde | **1.14** | **1.19** | **1.20** |
| | **1.15** | **1.21** | **1.22** |
| | **1.16** | **1.23** | **1.24** |

**Figure 1.3.2 a** 11 library members, individual aldehyde and amine components **1.14** to **1.18** and their six condensation products, **1.19** to **1.24**, can equilibrate between each other. Imine **1.19** undergoes a process of self-recognition, forming [**1.19**]$_2$. **b** Table showing the origin of each condensation product **1.19** to **1.24**. Adapted with permission from reference[53].

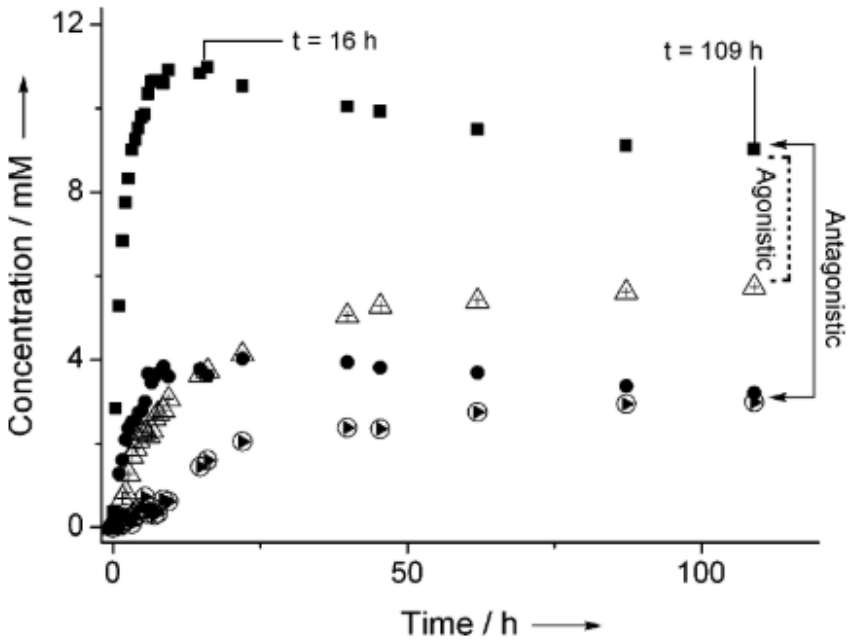


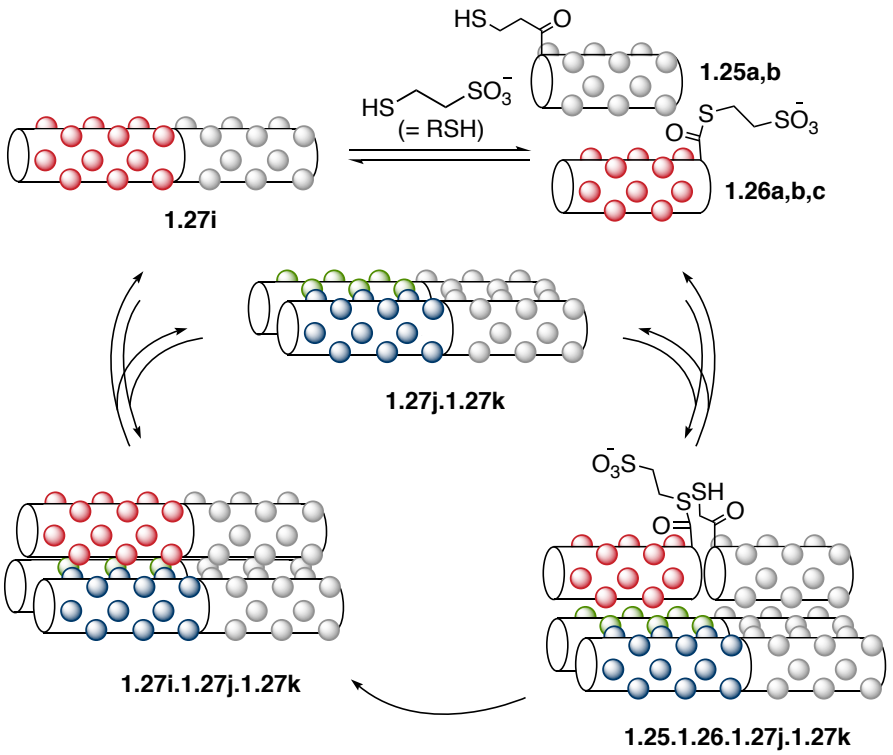

**Figure 1.3.3** Formation of condensation products from components **1.14** to **1.18** (15 mmol each) in the library as a function of time measured by $^{1}$H NMR spectroscopy. **1.19** (■), **1.20** (●), **1.21** (○), **1.22** (+), **1.23** (▸), **1.24** (△) (some are coincident). **1.19** is amplified both as a kinetic product (at 16 h) and in the final equilibrium distribution (109 h) relative to a library in which no recognition can take place and in which a statistical distribution is formed. Reproduced with permission from reference[53].

Ashkenasy has also explored similar dynamics based on the reversible formation of replicating coiled-coils of peptides (Figure 1.3.4).[54,55] A large network is constructed from two nucleophilic fragments **1.25a**,**b** and three electrophilic fragments **1.26a,b,c**, differing in amino acid sequence, for the possible formation of six reversibly formed peptide molecules **1.27a-f**. These peptides arrange into coiled-coils (individual cylinder in Figure 1.3.4), and can associate with each other, acting as templates for new peptide formation *via* both autocatalysis and cross-catalysis, where one replicator acts as the template for the formation of a

different replicator (Figure 1.3.4). As a small aside, a process of cross-catalysis is therefore an 'unfaithful' mode of replication for a template replicator, with important implications for processes of mutation and evolution.[23,56] The differing auto- and cross-catalytic efficiencies of the sequences, competing for a limited resource, as well as their inherent thermodynamic stability and kinetic stability to uncoiling under different environmental conditions, influences the distribution of products over the course of reaction (Figure 1.3.5). Thus, the system is reported be operating under "partial thermodynamic control", and unstable replicators are consumed to make way for more thermodynamically stable species over the course of reaction.

For example, under initially template-free conditions (Figure 1.3.5a) there is a consumption of quickly-formed but unstable replicators (for example, **1.27b**) to make way for more stable ones (for example, **1.27a** and **1.27c**). Further, the system is responsive; when instructed with non-reversibly formed template **1.28**, which can act as a template for **1.27b** formation, the network distribution is altered again and replicator **1.27b** is amplified (Figure 1.3.5b).

a




b

| | | thioester | | |
|---|---|---|---|---|
| | | **1.26a** | **1.26b** | **1.26c** |
| thiol | **1.25a** | **1.27a** | **1.27b** | **1.27c** |
| | **1.25b** | **1.27d** | **1.27e** | **1.27f** |

**Figure 1.3.4** General peptide replicators **1.27i,j,k** (representing peptide replicators **1.27a-f**) are constructed from thiols **1.25a,b** and thioesters **1.26a,b,c**, as detailed in the table in panel **b**. A dimer **1.27i.1.27j** consisting of two coiled-coils of peptide acts as a template for the formation of a new replicator **1.27i**, constructed from one nucleophilic fragment **1.25**, and one electrophilic fragment **1.26**. They may all have the same sequence and form a homotrimer (i=j=k), or all different, or mixed sequences (i≠j≠k or i=j≠k or i≠j=k) and form a heterotrimer. **b** Table detailing the origin of replicators **1.27a-f** from individual thiol and thioester components. Adapted with permission from references[6,55].

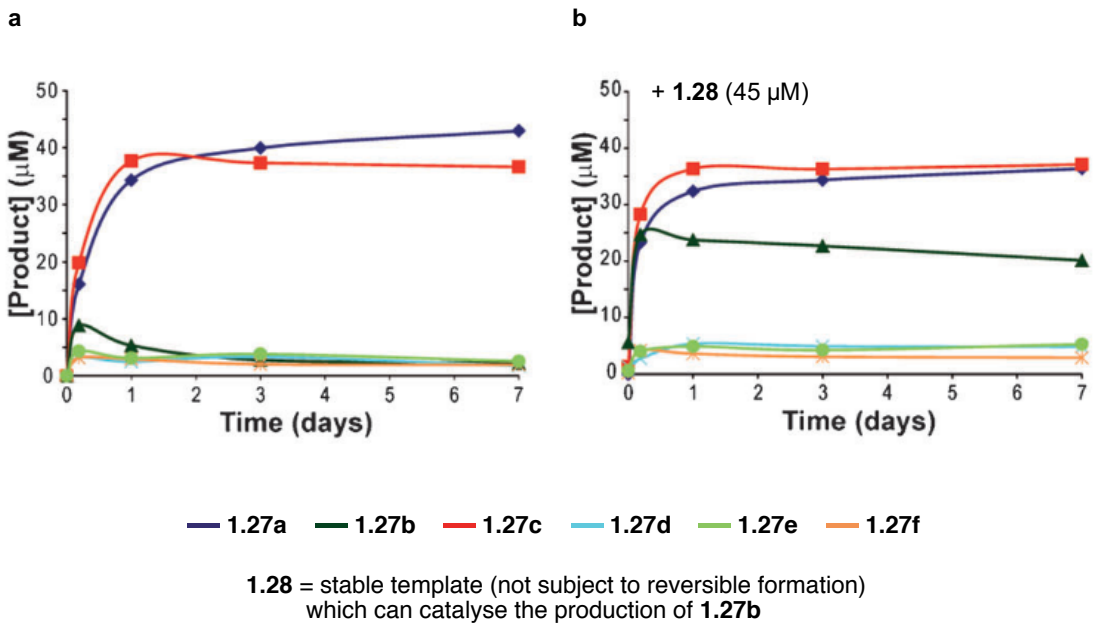



**Figure 1.3.5 a** Formation of replicators **1.27a-f** measured by HPLC from an initial composition of [**1.25a**]=[**1.25b**]=[**1.26a**]=[**1.26b**]=[**1.26c**]=150(±10) μM **b** Formation of replicators **1.27a-f** measured by HPLC from the same initial composition as **a** plus template **1.28** (45 μM). For the construction of all species **1.27a-f**, see Figure 1.3.4. Reproduced with permission from reference[55].

Beyond small molecules and peptides,[57,58] the templated replication of supramolecular assemblies within dynamic combinatorial libraries has been well established by the Otto group.[59,60] Dithiol building blocks are capable of forming macrocyclic disulfides under gentle oxidation and equilibrate between various ring sizes by thiol-disulfide exchange with remaining free thiol (Figure 1.3.6).

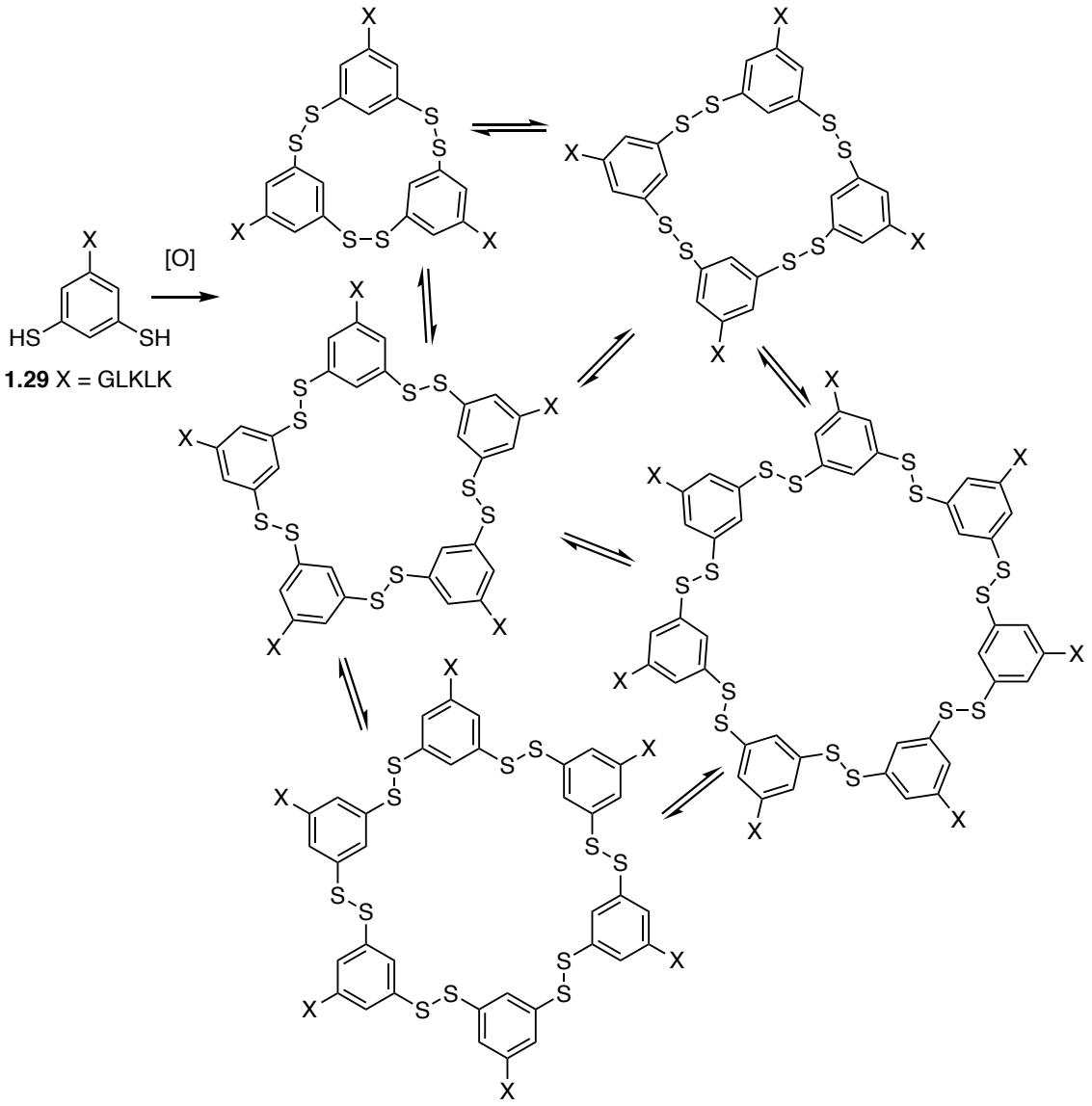



**Figure 1.3.6** Under gentle oxidation dithiol building blocks **1.29** appended with a short peptide sequence (GLKLK = Gly-Leu-Lys-Leu-Lys-OH) form macrocyclic species which can equilibrate between each other by thiol-disulfide exchange. Adapted with permission from reference[59].

Building blocks appended with a short peptide sequence at first equilibrated between trimeric and tetrameric species (Figure 1.3.7a). However, they were capable of forming fibrous stacks of heptameric and hexameric macrocycles by interaction between the oligopeptide chains of neighbouring macrocycles in a β-sheet structure. Under a regime of stirring a process of fibre elongation and breakage, revealing an increased number of new fibre 'ends' for macrocycle association, resulted in autocatalytic kinetics (Figure 1.3.7a) and the formation of the most efficient autocatalyst, the heptameric macrocycle.

However, the distribution of the replicator network was dependent on whether the solutions were shaken or stirred, inducing different shear strains in the vials.[59] Whilst the regime of stirring resulted in the autocatalytic formation of heptamer (Figure 1.3.7a), the same solution under a regime of shaking resulted in the autocatalytic formation of hexamer (Figure 1.3.7b), playing on differences in the susceptibility of heptamer and hexamer to fibre breakage under each regime and their different inherent autocatalytic efficiencies. The formation of fibres was a powerful kinetic trap for these systems, with a different distribution of library members depending on the sample's history.[60]

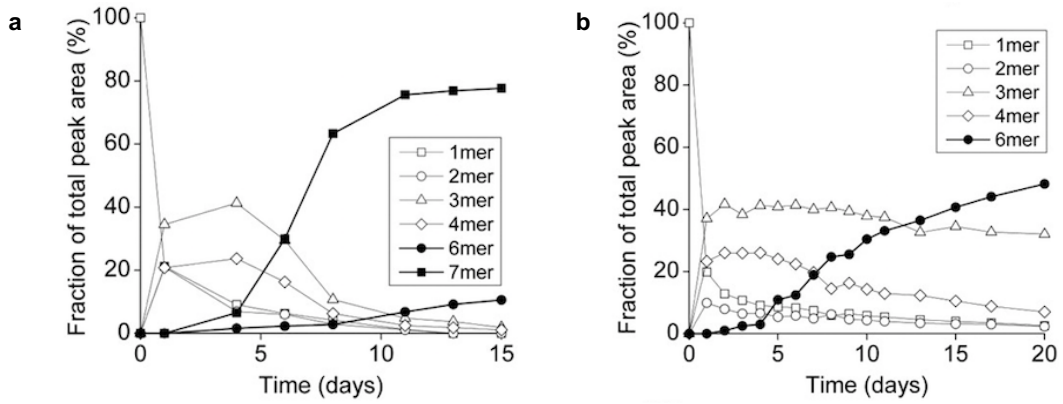



**Figure 1.3.7 a** A 3.8 mM solution of **1.29** under a regime of stirring (1200 rpm) results in the autocatalytic formation of heptamer on account of the formation of fibrous stacks of this macrocycle. **B** The same solution under a regime of shaking (500 rpm) results in the autocatalytic formation of hexamer. Reproduced with permission from reference[59].

Finally, of particular interest to our group was an example of the replication of surfactant molecules which are formed within a DCL, reported by Nguyen *et al.*, with the construction of "dynablock" surfactants by reversible imine bond formation (Figure 1.3.8).[61] A thermodynamically stable imine surfactant **2.3** formed from **2.1** and **2.2c** aggregates into micelles, and performs physical autocatalysis by the increase in concentration of hydrophobic aldehyde **2.1** in the aqueous phase. A later mechanistic study also revealed the influence of empty and "activated" sites on the micelle surface, acting as templates for imine bond formation.[62] This dynablock can outcompete non-replicating, thermodynamically unstable surfactant formed from amine **2.2a** which requires the same hydrophobic aldehyde for its construction.

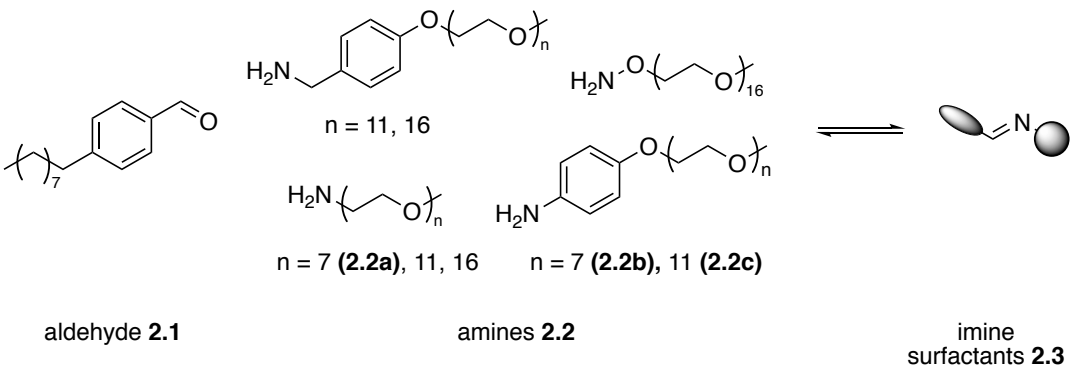



**Figure 1.3.8** Aldehyde and amine components **2.1** and **2.2** reversibly form imine bonds, resulting in the formation of an equilibrating set of imine surfactants or dynablocks **2.3**. These dynablock surfactants are capable of aggregating into micelles in water and can catalyse their own formation by physical autocatalysis, increasing the concentration of aldehyde **2.1** in the aqueous phase. "Activated" sites on the micelle surface may also catalyse the condensation reaction.[62] Adapted with permission from reference[61].

Thus, replication within a dynamic combinatorial library under conditions of reversible replicator formation gives rise to new and interesting behaviour; the composition of the system can change dramatically during the course of reaction, and high energy replicators can be subject both to the pressure of competition with other replicators and destruction to other, lower energy, species. These systems are highly responsive and dynamic and make an important contribution to the study of lifelike dynamics.

## 1.4 Beyond thermodynamic control: replication out-of-equilibrium

The examination of replication in dynamic combinatorial libraries, with the formation of metastable replicators, is undoubtedly a leap to more dynamic regimes from systems in which replicators are formed irreversibly.

However, in total, replication within a dynamic combinatorial library is still controlled by equilibration to the most thermodynamically stable distribution or to a kinetically trapped state (Figure 1.3.1). Whilst it is perhaps a 'first step toward the far-from-equilibrium character of life',[63] life itself is characterised by the formation of energy-consuming and out-of-equilibrium states, or the maintenance of high energy, metastable states by the consumption of energy. The functions of even the simplest biological structures, such as microtubules, rely on the consumption of chemical energy, out-of-equilibrium, to maintain dissipative, high energy and functional states. They do not evolve to the thermodynamic nor the kinetically trapped product.

Establishing a regime of molecular replication under the same energy-consuming, out-of-equilibrium regime could give rise to dynamic behaviour far beyond that which can be achieved in the closed systems we have examined so far. The replicator would be highly dynamic and adaptable, and its presence determined by the controlled consumption of fuel. Ultimately, processes of replication out-of-equilibrium might allow for the continuous increase in order and

function, away from the thermodynamic minimum, that is demanded for a process of open-ended evolution.[2,3,12–16]

The translation of the replication processes we have already examined into out-of-equilibrium states has been little explored.[64–67] The design of any out-of-equilibrium system is non-trivial. Their design rules and their emergent behaviours can be illustrated by examination of a biological system: the construction of a microtubule.[68]

## 1.4.1 Systems operating out-of-equilibrium

A classical and relatively simple example of the dynamics which characterise life is the formation of microtubules, which provide structural integrity to cells and form part of the cell division machinery (Figure 1.4.1). Alpha-beta tubulin bound to guanosine triphosphate (GTP) undergoes non-covalent self-assembly, driven by hydrophobic and electrostatic interactions, into a polymeric microtubule. However, the structure is subject to an orthogonal destructive step. The individual tubulin dimers act as enzymes, binding to GTP and inducing its hydrolysis, which in turn causes structural changes within the polymer and a build-up of strain. Once the hydrolysis reaches the tip of the microtubule, ‘catastrophe’ results and the entire structure dissociates. It is only under the continuous consumption of GTP fuel, therefore, that the thermodynamically unstable microtubule structure may persist; it is highly ordered, highly functional, and out-of-equilibrium (Figure 1.4.1).[69]

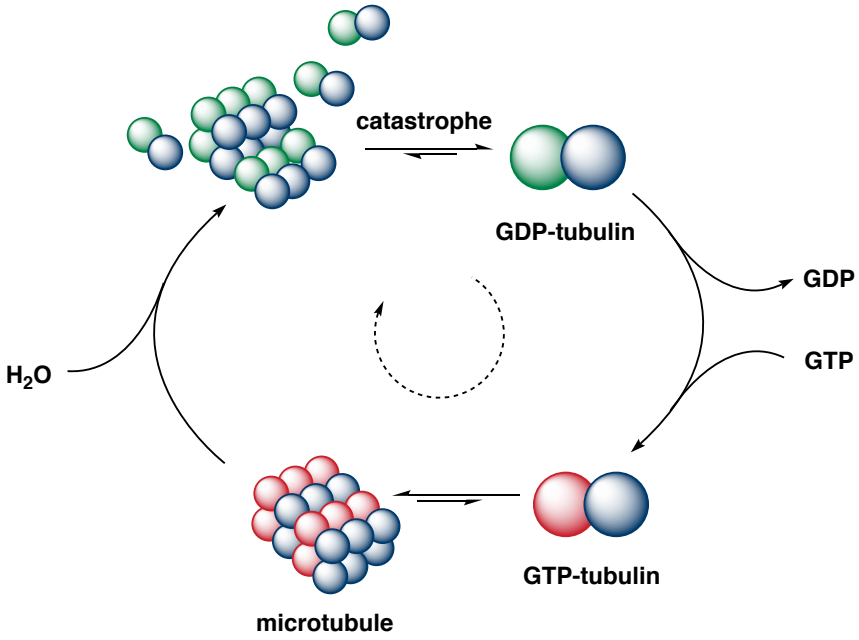



**Figure 1.4.1** The simplified assembly and dynamics of microtubules.[68,70] GTP = guanosine triphosphate, GDP = guanosine diphosphate.

Biology has harnessed out-of-equilibrium systems and structures like these because the equilibrium state is of no energetic value to an organism. It is the change in free energy as the system continuously moves clockwise around the cycle, trying to gain the equilibrium state, that is the driving force behind all biological processes.[68,71] In microtubule dynamics, for example, it is the thermodynamically favourable 'catastrophe' event and release of energy that powers cell division.[69] The persistence of high energy, low entropy functional supramolecular structures like microtubules is no longer determined by their thermodynamic stability and is instead controlled by the supply of fuel. This releases us from the normal rules of self-assembly, and these systems are highly adaptable and dynamic. Their function can be controlled in time and space.

The emergent behaviour of biological systems has inspired the design of a multitude of synthetic supramolecular materials and networks, whose functions can also be controlled in time and space. They have been described in a number of excellent recent reviews which highlight the current excitement in the field.[8–11,68,70,72–75] Some aim to mimic microtubule dynamics, with the manipulation of the physical properties of supramolecular materials such as hydrogels by the consumption of chemical fuel.[76–81] The directional motion of both light- and chemically-driven molecular motors was pioneered by Feringa, Stoddart and Sauvage, and recognised by their receipt of the 2016 Nobel Prize in Chemistry.[11,72,82–86] In addition, all biological oscillators are out-of-equilibrium networks of chemical reactions, controlling rhythms across different scales of time and space; both mechanical oscillations[87] and oscillations in the concentrations of biologically-relevant small molecules have been realised under out-of-equilibrium regimes with the continuous consumption of energy.[65,66]

The most prominent example, and a conceptually simple one, is work by van Esch *et al.* (Figure 1.4.2), in a process which closely resembles microtubule dynamics.[78] At the basis of the design was a molecule that could be switched between a non-associating and an associating state by the removal of a repulsive ionic charge. A rapid 'activation' reaction, the methylation of **1.30** to produce ester **1.31**, transformed the non-associating molecule to the associating state, consuming a simple chemical fuel, dimethyl sulfate (DMS), in the process. The esterified molecule could undergo assembly into fibres, forming a hydrogel. However, it was also subject to a 'deactivation' process, a simple ester hydrolysis,

which returned the molecule to the non-associating state. In the gelated state, therefore, the system was considered to be out-of-equilibrium.

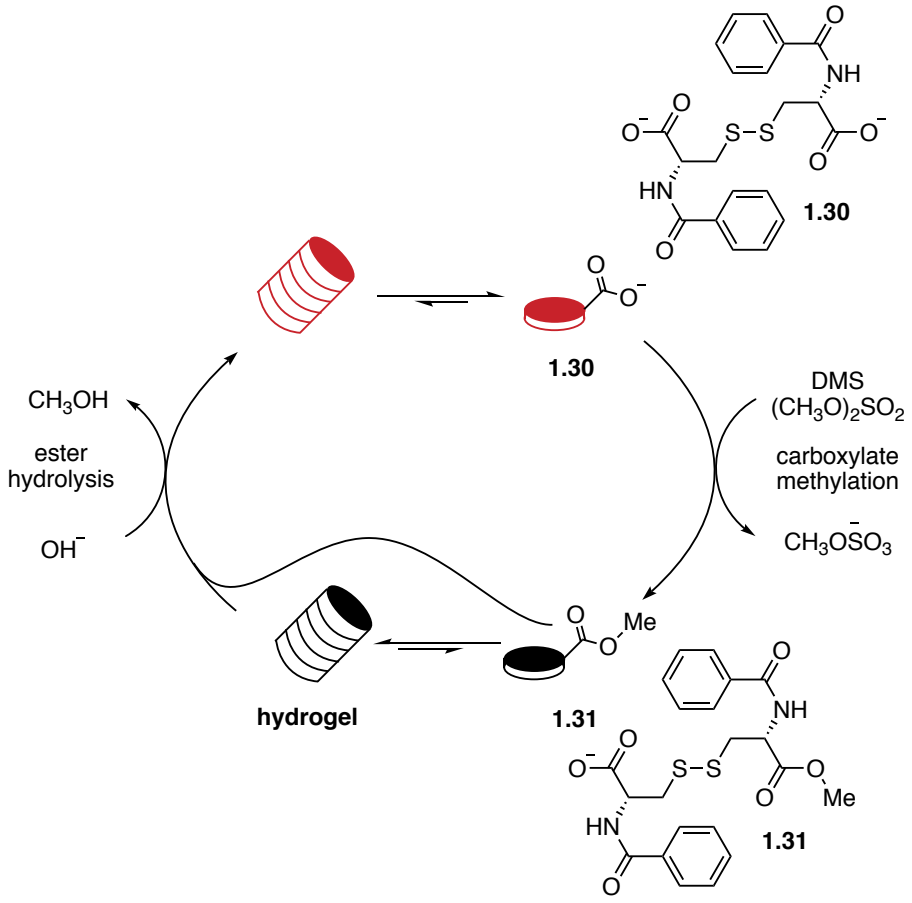



**Figure 1.4.2** In a reaction cycle, carboxylate groups on the inactive monomer **1.30**, incapable of assembly, react with dimethyl sulfate (DMS) to produce methyl esters **1.31**. These methyl esters are 'activated' and can undergo self-assembly into fibres, forming a hydrogel. Methyl esters **1.31** in both the aggregated and monomeric state are susceptible to hydrolysis under the basic conditions of the system back to the inactive, monomeric carboxylate **1.30**.[68,78]

Reaction rates and fuel levels, rather than the equilibrium distribution, were the controlling factors in the system. Both the lifetime and stiffness of the gel could be tuned by the quantity of available fuel (DMS) and the pH of the reaction solution. Closer analysis of the system by microscopy revealed that fibres tended to collapse stochastically, and that fibres shrunk only at their tips. There was also a period in which both growing and shrinking fibres were observed simultaneously in close proximity. Observations showed remarkable similarity to the dynamics observed in microtubule depolymerisation.

However, this sophisticated system and many other synthetic systems still have limitations, making it difficult to define their out-of-equilibrium character.[68] For example, the fuel in this system, as well as many other synthetic systems, is supplied in batch. More interesting behaviour is expected when the chemical fuel is added continuously, rather than in a batch or semi-batch process, allowing for the continuous maintenance of the out-of-equilibrium material.[11,72,75] Furthermore, a clear sense of directionality must be supplied to the system. In Figure 1.4.1 and microtubule formation, it is GTP-tubulin in its aggregated form, rather than in the non-aggregated state, which preferentially undergoes enzymatic hydrolysis. Further, non-aggregated GDP-tubulin preferentially interacts with the GTP fuel, rather than GDP-tubulin in the aggregated state. Both processes drive the cycle in a clockwise manner, and this directionality is important for the observation of an out-of-equilibrium state. It was not made clear whether the same asymmetry was installed in the synthetic system presented by Boekhoven *et al.*,[68,78] though based on the close examination of hydrogel dynamics this asymmetry seems likely.[68]

The synthetic system in Figure 1.4.2, and its biological counterpart in Figure 1.4.1, give us some essential design rules for the establishment and maintenance of out-of-equilibrium states. Despite the importance of a process of replication out-of-equilibrium, purely synthetic replicators which harness these design rules have been little explored.[64–67,81]

## 1.4.2 Out-of-equilibrium replication: system design

The cycles in Figure 1.4.1 and Figure 1.4.2 highlight the essential design features of out-of-equilibrium systems that can be applied to the realisation of a synthetic replicator in an out-of-equilibrium state.

First, a high energy replicator must be formed by the consumption of a chemical fuel, which is ideally supplied continuously to the system. Second, this high energy replicator must be subject to a destruction step, and these 'formation' and 'destruction' steps must occur along different pathways with different transition states. In microtubule construction, the formation of GTP-tubulin from GDP-tubulin, by supply of GTP fuel, is not the microscopic reverse of the hydrolysis step from GTP-tubulin back to monomeric GDP-tubulin. If the two reactions ran along the same path, then the addition of reagents would simply shift the position of equilibrium between the two and we would reach a new equilibrium state, $\Delta G = 0$, incapable of maintaining a high energy self-assembled state away from the equilibrium position or performing work.

Designing the formal forward and reverse reactions which do not run along the same pathway is difficult, and few examples of this type of reactivity are known which can operate in the same flask and under similar enough reaction environments.[11]

A subtly different, albeit less elegant, design links most processes of replication under out-of-equilibrium conditions that have been attempted to date (Figure 1.4.3). Whilst the 'destruction' step in microtubule formation involves the hydrolysis of GTP-tubulin to GDP-tubulin, and therefore the regeneration of precursors for the reconstruction of the high energy state (Figure 1.4.1), it is possible to imagine a system in which the 'destruction' step is to a different state altogether, without the direct regeneration of starting materials for the system (Figure 1.4.3). This completely avoids the problem of microscopic reversibility: here, the formation and destruction steps are completely separated. Indeed, this design links the majority of examples of replication under out-of-equilibrium regimes.

In a closed system, a quickly-formed replicator which is the kinetic product of the reaction may build up in concentration. However, if it is subject to a slower destruction step for the formation of thermodynamic products Y, then once equilibrium is reached the kinetic product is destroyed (Figure 1.4.3a,b). A sense of direction in the system is clearly established.

In an open system, however, the continuous supply of starting materials (the fuel supply) would allow us to maintain the metastable replicator out-of-equilibrium

(Figure 1.4.3c,d). Both its concentration and persistence in time are no longer determined by its thermodynamic stability, and instead are controllable by fuel supply. Importantly, once the supply of fuel is halted the system degrades back to the equilibrium position (Figure 1.4.3d). This degradation back to the equilibrium position once fuel supply is halted allows us to recognise and define the out-of-equilibrium state under continuous fuel supply.

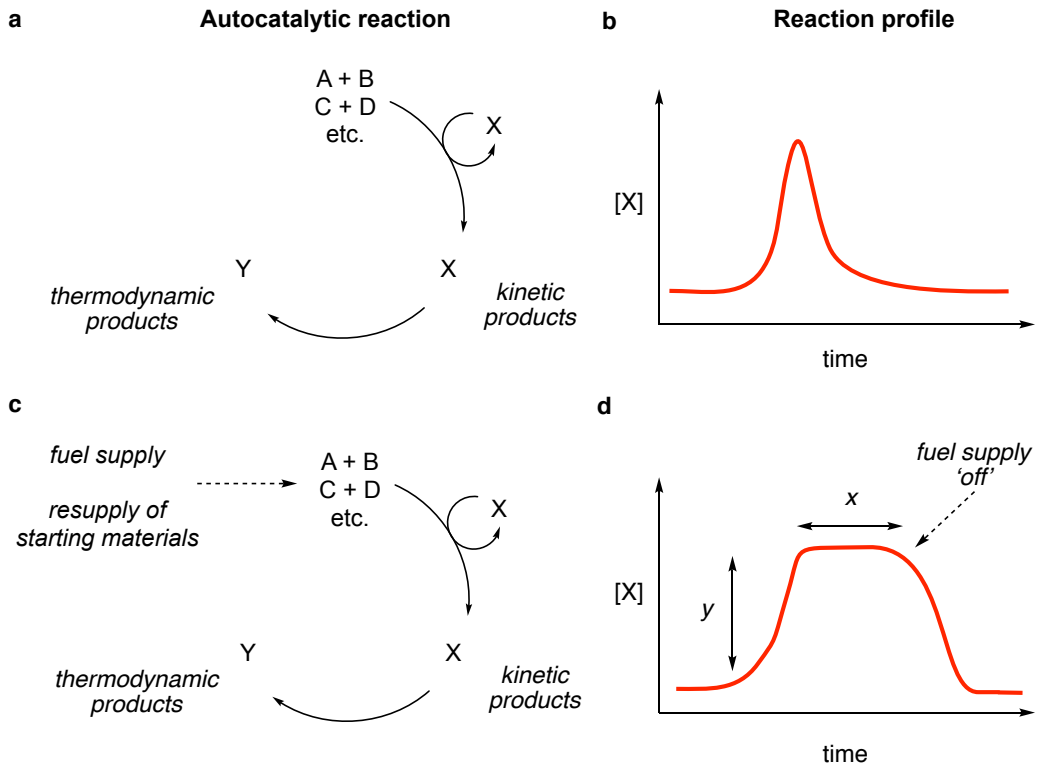



**Figure 1.4.3 a,b** Replicator X is the kinetic product and, in a closed system, is completely degraded towards the thermodynamic product Y. **c,d** In an open system, with the continuous resupply of starting materials, the kinetic product X can be maintained, out-of-equilibrium. The concentration (*y*) and persistence in time (*x*) of the replicator X are no longer determined by its thermodynamic stability, and instead by fuel supply.

## 1.4.3 Experimental realisation

Even with use of the simplified design in Figure 1.4.3, the actual experimental realisation of a process of replication operating under out-of-equilibrium conditions has been significantly limited.[64–67] The coming together of all necessary parts of the system – simultaneous formation and destruction steps, the input of chemical fuel – is difficult both to design and to achieve experimentally. Further, the scheme in Figure 1.4.3 is limited also by the continuous build-up of multiple waste products of the system, which can disturb the operation of an out-of-equilibrium state.[11,75]

The most prominent attempts have focused on the physical replication of micelles and vesicles. This is perhaps not surprising; the construction of supramolecular materials under out-of-equilibrium regimes, whether replicating or not, is of interest since the manipulation of their physical properties is of interest in the design of new materials. The coupling of these out-of-equilibrium structures with other processes is easy to imagine in contrast to template replicators whose functions are confined to specific and spatially-organised interactions between well-defined functional groups.[88] Furthermore, the inhomogeneous nature of the reaction has been harnessed in the realisation of other out-of-equilibrium structures,[89] often used to better separate the formation and destruction steps.

The simplest way to induce a ‘destruction’ process and to fuel the system is by set up of a continuous stirred tank reactor (CSTR). Precursors for replicator formation are fed into the tank, replicators are synthesised autocatalytically within

the tank, and then are 'destroyed' by the simple process of a continuous outflow of material (Figure 1.4.4). This scheme is the basis of experimental work by Buhse *et al.*,[90] which adapted Luisi's original system[44] into a CSTR and, as a result, established an out-of-equilibrium system of micelle reproduction which displayed bistability.[67]

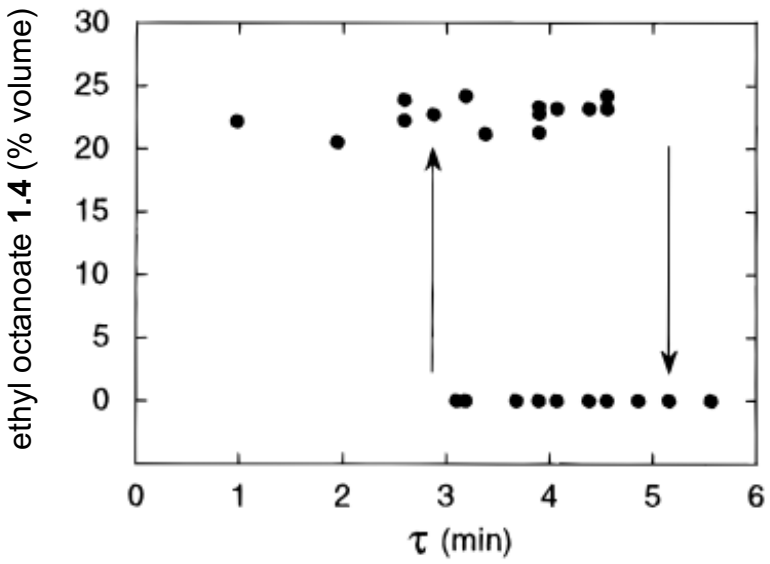



**Figure 1.4.4** The stationary state quantity of ethyl octanoate **1.4** present under biphasic alkaline hydrolysis conditions (see Figure 1.2.6) as a function of residence time ($\tau$) in a CSTR. The system displays bistability and hysteresis, with the stationary state quantity of ethyl octanoate **1.4** between residence times of ~ 3 minutes and ~ 5 minutes being determined by the history of the system. Reproduced with permission from reference[90].

A chemical destruction step was considered by Luisi *et al.*, and a process of homeostasis was established in an open system (Figure 1.4.5).[91] Here, the autocatalytic production of vesicles of oleate **1.32** in borate buffer was powered by the continuous feeding of the system with oleic anhydride **1.33**. This reaction

was counteracted by the simultaneous destruction of the oleate vesicles by oxidation with osmium tetroxide, achieved by continuous feeding of the system with potassium ferricyanide to regenerate $OsO_4$.

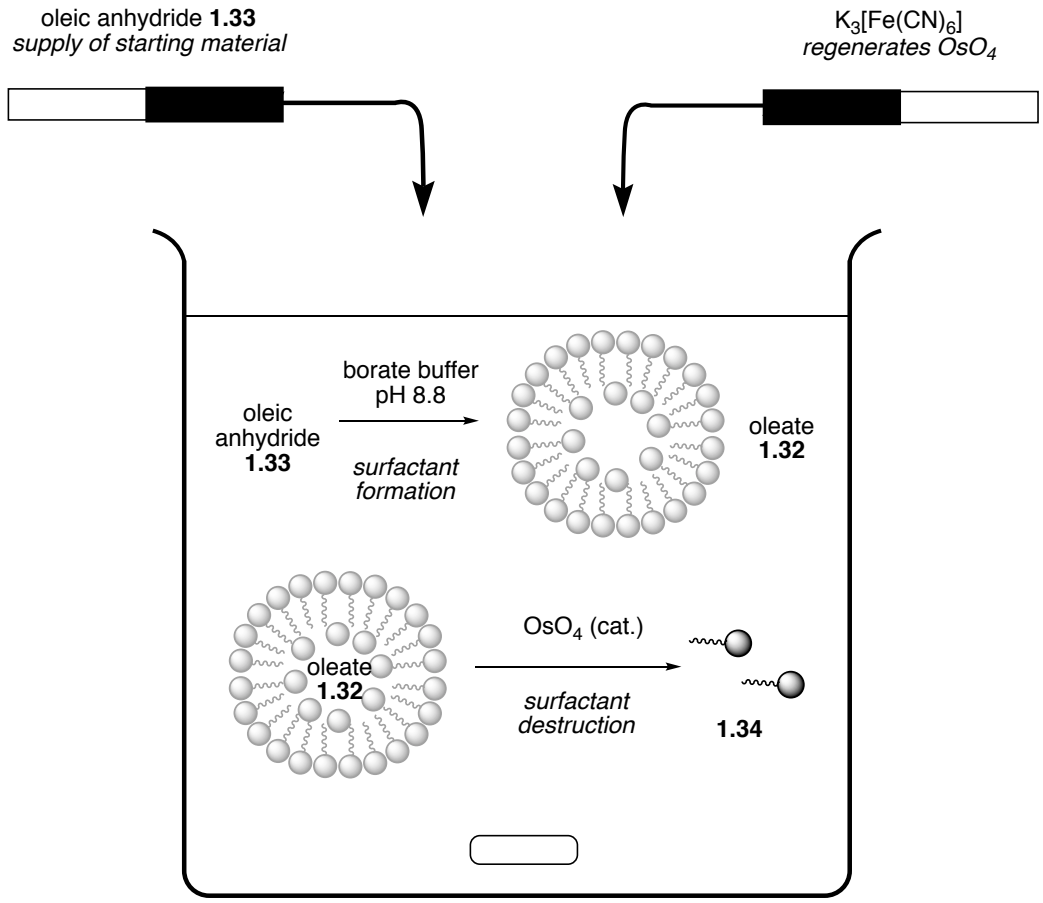



**Figure 1.4.5** The formation of oleate surfactants **1.32** by physical autocatalysis is fuelled by the supply of oleic anhydride **1.33**. At the same time, the surfactant is subject to an oxidation reaction with $OsO_4$, producing **1.34**, which is unable to aggregate. Catalytic $OsO_4$ is regenerated by a supply of $K_3[Fe(CN)_6]$. Adapted with permission from reference[91].

If the rates of the formation and destruction processes were successfully balanced then a steady state in oleate was successfully established (Figure 1.4.6).

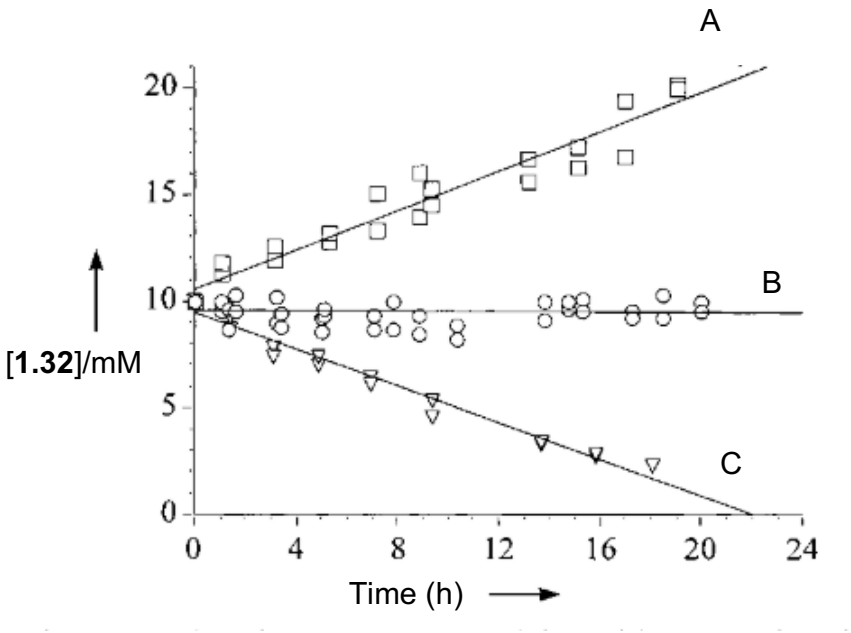



**Figure 1.4.6** Concentration of oleate surfactant **1.32** in time. Variation in the rates of supply of oleic anhydride **1.33** and $K_3[Fe(CN)_6]$ to the system (Figure 1.4.5) results in regimes of continuous oleate **1.32** formation (A) (rate formation > rate destruction), homeostasis (B) (rate formation = rate destruction), or continuous oleate **1.32** destruction (C) (rate formation < rate destruction). Reproduced with permission from reference[91].

However, though a destructive step was established in this open system, and a steady state was established, we do not define the system to be persisting out-of-equilibrium. Since fuel is required both for the formation and destruction steps, removal of the fuel supply would, in theory, 'trap' the system; it would not move

towards a different, equilibrium, state and the complete destruction of the replicator.

Working in the Fletcher group, Ignacio Colomer made a step to an out-of-equilibrium replicator by establishing a physical replicator which could be transiently amplified but which was thermodynamically unstable and, in a closed system, was fully consumed (Figure 1.4.7 and 1.4.8).[92]

First, a surfactant replicator **1.37** was constructed by an alkene metathesis reaction between two phase-separated components, **1.35** and **1.36**. There was a lag period (Figure 1.4.8) before the surfactant **1.37** self-assembled into micelles, increasing mixing between the phases and inducing an increased rate of reaction to form more surfactant **1.37**; the micelles were therefore able to replicate (Figures 1.4.7 and 1.4.8).

However, once starting materials were almost fully consumed, a second reaction between the surfactant and the activated ruthenocarbene **1.38** came to dominate and resulted in the degradation of the replicator to thermodynamically stable product **1.39** (Figures 1.4.7 and 1.4.8). Mechanistic studies revealed that phase separation was vital both for the observation of autocatalysis and for the destruction step to take place.

Once the replicator had been depleted, the system could be ‘restarted’, and the replicator built up again, by the manual supply of batches of fuel, effectively repeating the reaction within the same flask. However, this work did not establish

conditions under which the high energy, functional replicator could be *maintained* out-of-equilibrium, avoiding decomposition to the equilibrium state. The fall towards the thermodynamic minimum was inevitable in the closed system or between batchwise additions of the fuel.

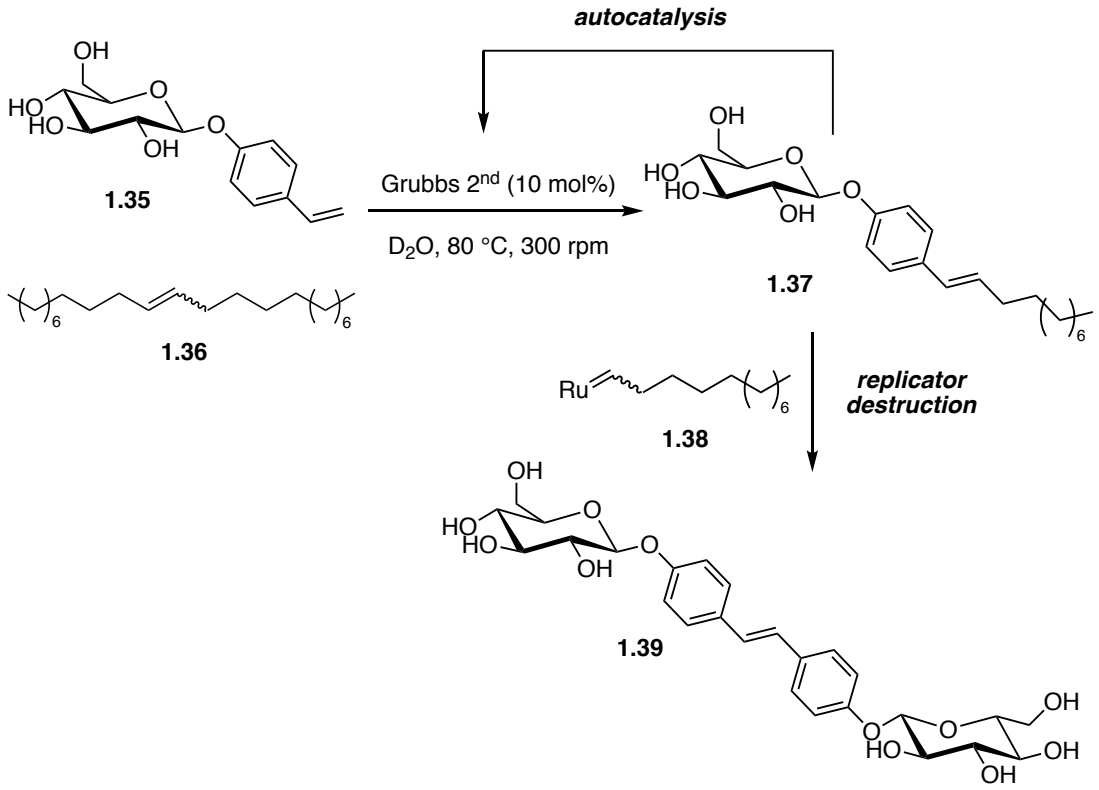



**Figure 1.4.7** Phase-separated reactants **1.35** and **1.36** undergo an alkene metathesis reaction to form surfactant **1.37**. Micelles composed of surfactant **1.37** increase mixing between the phases and therefore increase the rate of reaction to form their own components. However, in the aggregated state, surfactant **1.37** is subject to a destruction reaction to form thermodynamic product **1.39**. Adapted with permission from reference[92].

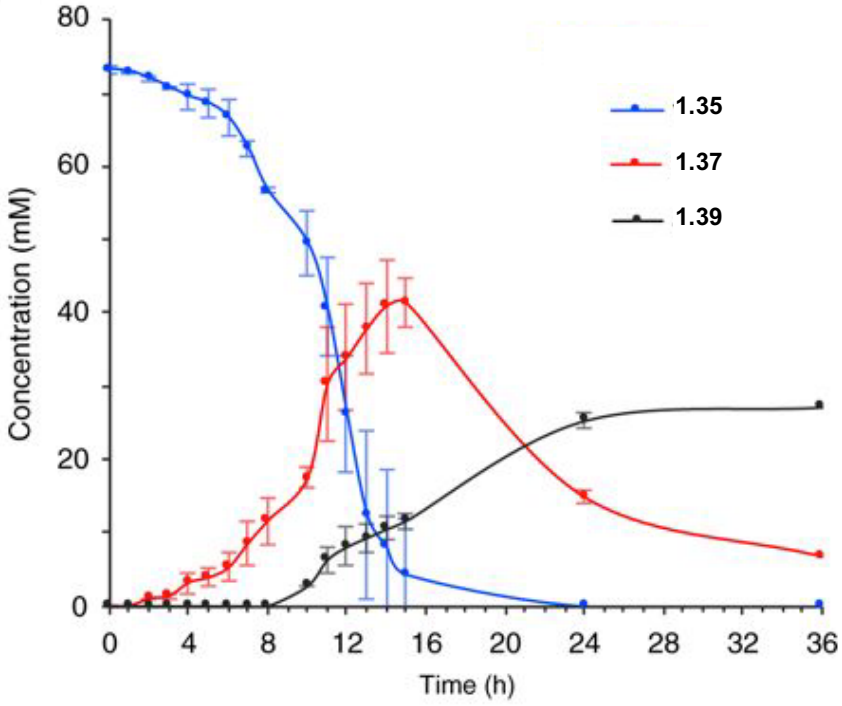



**Figure 1.4.8** The concentration of reaction components over time monitored by UPLC, plotted as an average of three experiments with error bars representing the standard deviation. Surfactant **1.37** is transiently amplified by autocatalysis after a lag period but, in a closed system, succumbs to destruction at equilibrium. Reproduced with permission from reference[92].

The importance of establishing a replicator which persists out-of-equilibrium, as well as the general interest in supramolecular structures out-of-equilibrium, makes a focus on the construction of an out-of-equilibrium physical replicator of great interest. Experimental attempts had, thus far, been limited.

## 1.5 Project aim: towards an out-of-equilibrium replicator

### 1.5.1 Replication in a dynamic combinatorial library

To begin the work in this thesis, we were interested in the work published by the Giuseppone group as an example of a physical replicator constructed in a dynamic combinatorial library.[61] Examination of a replicator formed in a DCL would allow us to explore a system under both kinetic and thermodynamic control with a set of competing replicators. The system was in contrast to the Fletcher group's previously reported systems of irreversibly formed, thermodynamically stable replicators, which had been examined both in the bulk and at the single aggregate level using interferometric scattering microscopy (in collaboration with the Kukura group). We wanted to examine the autocatalytic formation of this reversibly formed replicator at the single aggregate level and hoped that close examination of the system would increase our insight into replication operating under biphasic conditions in DCLs.

This work is discussed in Chapter 2.

The simultaneous processes of replicator formation and destruction contained within DCL chemistry, and the production of transient kinetic products, had made some contribution towards the construction of out-of-equilibrium systems.[6,67] The exploration of replicators constructed *via* dynamic combinatorial chemistry with processes such as imine bond formation and thiol-disulfide exchange explored in

Section 1.3.1, would be a stepping stone towards the realisation of an out-of-equilibrium replicator.

### 1.5.2 A chemically-fuelled replicator

Inspired by previous attempts of molecular replication, out-of-equilibrium, we wanted to design a metastable physical replicator whose population could be maintained, out-of-equilibrium, by the action of a chemical fuel. This fuelling step would allow for the continuous regeneration of the replicator and its supramolecular structure. Thus, whilst individual molecules would continuously be subject to a process of destruction, the population as a whole could be maintained and prevented from falling into the thermodynamic sink. Once fuel supply was removed the entire system would move towards the equilibrium state and the destruction of all replicators.

The system would incorporate two important lifelike processes: the maintenance of metastable supramolecular structure, out-of-equilibrium, and a process of replication.

The design and realisation of a chemically-fuelled replicator is the subject of Chapter 3.

## 1.6 References


1. Ruiz-Mirazo, K., Briones, C. & de la Escosura, A. Prebiotic systems chemistry: new perspectives for the origins of life. *Chem. Rev.* **114,** 285–366 (2014).
2. Duim, H. & Otto, S. Towards open-ended evolution in self-replicating molecular systems. *Beilstein J. Org. Chem.* **13,** 1189–1203 (2017).
3. Schwille, P. How Simple Could Life Be ? *Angew. Chem. Int. Ed.* **56,** 10998–11002 (2017).
4. Bissette, A. J. & Fletcher, S. P. Mechanisms of Autocatalysis. *Angew. Chem. Int. Ed.* **52,** 12800–12826 (2013).
5. Clixby, G. & Twyman, L. Self-replicating systems. *Org. Biomol. Chem.* **14,** 4170–4184 (2016).
6. Kosikova, T. & Philp, D. Exploring the emergence of complexity using synthetic replicators. *Chem. Soc. Rev.* **46,** 7274–7305 (2017).
7. Schrodinger, E. What is life? The physical aspects of the living cell. (Cambridge University Press, 1994).
8. Grzybowski, B. A., Fitzner, K., Paczesny, J. & Granick, S. From dynamic self-assembly to networked chemical systems. *Chem. Soc. Rev.* **46,** 5647–5678 (2017).
9. Grzybowski, B. A. & Huck, W. T. S. The nanotechnology of life-inspired systems. *Nat. Nanotechnol.* **11,** 585–592 (2016).
10. Mattia, E. & Otto, S. Supramolecular systems chemistry. *Nat. Nanotechnol.* **10,** 111–119 (2015).
11. Ashkenasy, G., Hermans, T. M., Otto, S. & Taylor, A. F. Systems chemistry. *Chem. Soc. Rev.* **46,** 2543–2554 (2017).
12. Higgs, P. G. Chemical Evolution and the Evolutionary Definition of Life. *J. Mol. Evol.* **84,** 225–235 (2017).
13. Pross, A. *What is Life? How chemistry becomes biology*. (Oxford University Press, 2016).
14. England, J. L. Dissipative adaptation in driven self-assembly. *Nat. Nanotechnol.* **10,** 919–923 (2015).
15. England, J. L. Statistical physics of self-replication. *J. Chem. Phys.* **139,** 121923 (2013).
16. Pascal, R., Pross, A. & Sutherland, J. D. Towards an evolutionary theory of the origin of life based on kinetics and thermodynamics. *Open Biol.* **3,** 130156 (2013).
17. Szathmáry, E. & Gladkih, I. Sub-exponential growth and coexistence of non-enzymatically replicating templates. *J. Theor. Biol.* **138,** 55–58 (1989).
18. von Kiedrowski, G. A Self-Replicating Hexadeoxynucleotide. *Angew. Chem. Int. Ed. Engl.* **25,** 932–935 (1986).
19. Lee, D. H., Granja, J. R., Martinez, J. A., Severin, K. & Ghadiri, M. R. A self-replicating peptide. *Nature* **382,** 525–528 (1996).
20. Severin, K., Lee, D. H., Kennan, A. J. & Ghadiri, M. R. A synthetic peptide ligase. *Nature* **389,** 706–709 (1997).

21. Severin, K., Lee, D. H., Martinez, J. A. & Ghadiri, M. R. Peptide self-replication via template-directed ligation. *Chem. Eur. J.* **3,** 1017–1024 (1997).
22. Lee, D. H., Severin, K., Yokobayashi, Y. & Ghadiri, M. R. Emergence of symbiosis in peptide self-replication through a hypercyclic network. *Nature* **390,** 591–594 (1997).
23. Severin, K., Lee, D. H., Martinez, J. A., Vieth, M. & Ghadiri, M. R. Dynamic Error Correction in Autocatalytic Peptide Networks. *Angew. Chem. Int. Ed.* **37,** 126–128 (1998).
24. Saghatellan, A., Yokobayashi, Y., Soltani, K. & Ghadiri, M. R. A chiroselective peptide replicator. *Nature* **409,** 797–801 (2001).
25. Yao, S., Ghosh, I., Zutshi, R. & Chmielewski, J. Selective amplification by auto- and cross-catalysis in a replicating peptide system. *Nature* **396,** 447–450 (1998).
26. Luther, A., Brandsch, R. & Von Kiedrowski, G. Surface-promoted replication and exponential amplification of DNA analogues. *Nature* **396,** 245–248 (1998).
27. Kosikova, T. & Philp, D. A Critical Cross-Catalytic Relationship Determines the Outcome of Competition in a Replicator Network. *J. Am. Chem. Soc.* **139,** 12579–12590 (2017).
28. Bissette, A. J. & Fletcher, S. P. Novel applications of physical autocatalysis. *Orig. Life Evol. Biosph.* **45,** 21–30 (2015).
29. Dyson, F. *Origins of Life*. (Cambridge University Press, 1985).
30. Varela, F. G., Maturana, H. R. & Uribe, R. Autopoiesis: The organization of living systems, its characterization and a model. *BioSystems* **5,** 187–196 (1974).
31. Luisi, P. L. Autopoiesis: a review and a reappraisal. *Naturwissenschaften* **90,** 49–59 (2003).
32. Szostak, J. W., Bartel, D. P. & Luisi, P. L. Synthesizing life. *Nature* **409,** 387–390 (2001).
33. Murtas, G., Kuruma, Y., Bianchini, P., Diaspro, A. & Luisi, P. L. Protein synthesis in liposomes with a minimal set of enzymes. *Biochem. Biophys. Res. Commun.* **363,** 12–17 (2007).
34. Kurihara, K. *et al.* Self-reproduction of supramolecular giant vesicles combined with the amplification of encapsulated DNA. *Nat Chem* **3,** 775–781 (2011).
35. Adamala, K. & Szostak, J. W. Competition between model protocells driven by an encapsulated catalyst. *Nat. Chem.* **5,** 495–501 (2013).
36. Matsumura, S. *et al.* Transient compartmentalization of RNA replicators prevents extinction due to parasites. *Science* **354,** 1293–1296 (2016).
37. Engelhart, A. E., Adamala, K. P. & Szostak, J. W. A simple physical mechanism enables homeostasis in primitive cells. *Nat. Chem.* **8,** 448–453 (2016).
38. Wintner, E. A., Conn, M. M. & Rebek, J. Studies in Molecular Replication. *Acc. Chem. Res.* **27,** 198–203 (1994).
39. Stano, P. & Luisi, P. L. Achievements and open questions in the self-reproduction of vesicles and synthetic minimal cells. *Chem. Commun.* **46,** 3639–3653 (2010).
40. Luisi, P. L. The Emergence of Life. From Chemical Origins to Synthetic Biology. (Cambridge University Press, 2006).

41. Angelica Bachmann, P., Walde, P., Luigi Luisi, P. & Lang, J. Self-Replicating Reverse Micelles and Chemical Autopoiesis. *J. Am. Chem. Soc.* **112,** 8200–8201 (1990).
42. Bachmann, P. A., Luisi, P. L. & Lang, J. Self-replicating Reverse Micelles. *Chimia* **45,** 266–268 (1991).
43. Bachmann, P. A., Walde, P., Luisi, P. L. & Lang, J. Self-Replicating Micelles: Aqueous Micelles and Enzymatically Driven Reactions in Reverse Micelles. *J. Am. Chem. Soc.* **113,** 8204–8209 (1991).
44. Bachmann, P. A., Luisi, P. L. & Lang, J. Autocatalytic self-replicating micelles as models for prebiotic structures. *Nature* **357,** 57–59 (1992).
45. Bissette, A. J., Odell, B. & Fletcher, S. P. Physical autocatalysis driven by a bond-forming thiol–ene reaction. *Nat. Commun.* **5,** 4607 (2014).
46. Post, E., Bissette, A. & Fletcher, S. P. Self-reproducing micelles coupled to a secondary catalyst. *Chem. Commun.* **54,** 8777–8780 (2018).
47. Ortega-arroyo, J., Bissette, A. J., Kukura, P. & Fletcher, S. P. Visualization of the spontaneous emergence of a complex, dynamic, and autocatalytic system. *Proc. Natl. Acad. Sci.* **113,** 11122–11126 (2016).
48. Li, J., Nowak, P. & Otto, S. Dynamic Combinatorial Libraries: From Exploring Molecular Recognition to Systems Chemistry. *J. Am. Chem. Soc.* **135,** 9222–9239 (2013).
49. Hunt, R. A. R. & Otto, S. Dynamic combinatorial libraries: New opportunities in systems chemistry. *Chem. Commun.* **47,** 847–858 (2011).
50. del Amo, V. & Philp, D. Integrating replication-based selection strategies in dynamic covalent systems. *Chem. Eur. J.* **16,** 13304–13318 (2010).
51. Tjivikua, T., Ballester, P. & Rebek, J. A Self-replicating system. *J. Am. Chem. Soc.* **112,** 1249–1250 (1990).
52. Nowick, J. S., Feng, Q., Tjivikua, T., Ballester, P. & Rebek, J. Kinetic Studies and Modeling of a Self-Replicating System. *J. Am. Chem. Soc.* **113,** 8831–8839 (1991).
53. Xu, S. & Giuseppone, N. Self-duplicating amplification in a dynamic combinatorial library. *J. Am. Chem. Soc.* **130,** 1826–1827 (2008).
54. Dadon, Z., Samiappan, M., Wagner, N. & Ashkenasy, G. Chemical and light triggering of peptide networks under partial thermodynamic control. *Chem. Commun.* **48,** 1419–1421 (2012).
55. Dadon, Z. *et al.* Competition and cooperation in dynamic replication networks. *Chem. Eur. J.* **21,** 648–654 (2015).
56. Vaidya, N. *et al.* Spontaneous network formation among cooperative RNA replicators. *Nature* **491,** 72–77 (2012).
57. Del Amo, V., Slawin, A. M. Z. & Philp, D. Manipulating replication processes within a dynamic covalent framework. *Org. Lett.* **10,** 4589–4592 (2008).
58. Sadownik, J. W. & Philp, D. A simple synthetic replicator amplifies itself from a dynamic reagent pool. *Angew. Chem. Int. Ed.* **47,** 9965–9970 (2008).
59. Carnall, J. M. A. *et al.* Mechanosensitive self-replication driven by self-organization. *Science* **327,** 1502–1506 (2010).
60. Sadownik, J. W., Mattia, E., Nowak, P. & Otto, S. Diversification of self-replicating molecules. *Nat. Chem.* **8,** 264–269 (2016).
61. Nguyen, R., Allouche, L., Buhler, E. & Giuseppone, N. Dynamic

Combinatorial Evolution within Self-Replicating Supramolecular Assemblies. *Angew. Chem. Int. Ed.* **48,** 1093–1096 (2009).
62. Nguyen, R. *et al.* Autopoietic Behavior of Dynamic Covalent Amphiphiles. *Chem. Eur. J.* **24,** 17125–17137 (2018).
63. Otto, S. Dynamic Molecular Networks: From Synthetic Receptors to Self-Replicators. *Acc. Chem. Res.* **45,** 2200–2210 (2012).
64. Bottero, I., Huck, J., Kosikova, T. & Philp, D. A Synthetic Replicator Drives a Propagating Reaction-Diffusion Front. *J. Am. Chem. Soc.* **138,** 6723–6726 (2016).
65. Semenov, S. N. *et al.* Rational design of functional and tunable oscillating enzymatic networks. *Nat. Chem.* **7,** 160–165 (2015).
66. Semenov, S. N. *et al.* Autocatalytic, bistable, oscillatory networks of biologically relevant organic reactions. *Nature* **537,** 656–660 (2016).
67. Mukherjee, R., Cohen-Luria, R., Wagner, N. & Ashkenasy, G. A Bistable Switch in Dynamic Thiodepsipeptide Folding and Template-Directed Ligation. *Angew. Chem. Int. Ed.* **54,** 12452–12456 (2015).
68. Ragazzon, G. & Prins, L. J. Energy consumption in chemical fuel-driven self-assembly. *Nat. Nanotechnol.* **13,** 882–889 (2018).
69. Hess, H. & Ross, J. L. Non-equilibrium assembly of microtubules : from molecules to autonomous chemical robots. *Chem. Soc. Rev.* **46,** 5570–5587 (2017).
70. Merindol, R. & Walther, A. Materials learning from life: concepts for active, adaptive and autonomous molecular systems. *Chem. Soc. Rev.* **46,** 5588–5619 (2017).
71. Newsholme, E. A. *Regulation in Metabolism*. (John Wiley & Sons, 1973).
72. van Rossum, S. A. P., Tena-Solsona, M., van Esch, J. H., Eelkema, R. & Boekhoven, J. Dissipative out-of-equilibrium assembly of man-made supramolecular materials. *Chem. Soc. Rev.* **46,** 5519–5535 (2017).
73. Sorrenti, A., Leira-iglesias, J., Markvoort, A. J., de Greef, T. F. A. & Hermans, T. M. Non-equilibrium supramolecular polymerization. *Chem. Soc. Rev.* 5476–5490 (2017).
74. Heinen, L. & Walther, A. Celebrating Soft Matter's 10th Anniversary: Approaches to program the time domain of self-assemblies. *Soft Matter* **11,** 7857–7866 (2015).
75. Sorrenti, A., Leira-Iglesias, J., Sato, A. & Hermans, T. M. Non-equilibrium steady states in supramolecular polymerization. *Nat. Commun.* **8,** 15899 (2017).
76. Solís Muñana, P. *et al.* Substrate-Induced Self-Assembly of Cooperative Catalysts. *Angew. Chem. Int. Ed.* 10.1002/anie.201810891
77. Ravensteijn, B. G. P. Van, Hendriksen, W. E., Eelkema, R., Esch, J. H. Van & Kegel, W. K. Fuel-Mediated Transient Clustering of Colloidal Building Blocks. *J. Am. Chem. Soc.* **139,** 9763–9766 (2017).
78. Boekhoven, J., Hendriksen, W. E., Koper, G. J. M., Eelkema, R. & van Esch, J. H. Transient Self-Assembly of Active Materials Fueled by a Chemical Reaction. *Science* **349,** 1075–1079 (2015).
79. Boekhoven, J. *et al.* Dissipative Self-Assembly of a Molecular Gelator by Using a Chemical Fuel. *Angew. Chem. Int. Ed.* **49,** 4825–4828 (2010).
80. te Brinke, E. *et al.* Dissipative adaptation in driven self-assembly leading to self-dividing fibrils. *Nat. Nanotechnol.* **13,** 849–855 (2018).
81. Leira-Iglesias, J., Tassoni, A., Adachi, T., Stich, M. & Hermans, T. M.

Oscillations, travelling fronts and patterns in a supramolecular system. *Nat. Nanotechnol.* **13,** 1021–1027 (2018).
82. Erbas-Cakmak, S. *et al.* Rotary and linear molecular motors driven by pulses of a chemical fuel. *Science* **358,** 340–343 (2017).
83. Fletcher, S. P., Dumur, F., Pollard, M. M. & Feringa, B. L. A Reversible, Unidirectional Molecular Rotary Motor Driven by Chemical Energy. *Science* **310,** 80–82 (2005).
84. Collins, B. S. L., Kistemaker, J. C. M., Otten, E. & Feringa, B. L. A chemically powered unidirectional rotary molecular motor based on a palladium redox cycle. *Nat. Chem.* **8,** 860–866 (2016).
85. Koumura, N., Zijlstra, R. W. J., Delden, R. A. Van, Harada, N. & Feringa, B. L. Light-driven monodirectional molecular rotor. *Nature* **401,** 152–156 (1999).
86. Astumian, R. D. Optical vs. chemical driving for molecular machines. *Faraday Discuss.* **195,** 583–597 (2016).
87. He, X. *et al.* Synthetic homeostatic materials with chemo-mechano-chemical self-regulation. *Nature* **487,** 214–218 (2012).
88. Maiti, S., Fortunati, I., Ferrante, C., Scrimin, P. & Prins, L. J. Dissipative self-assembly of vesicular nanoreactors. *Nat. Chem.* **8,** 725–731 (2016).
89. Tena-Solsona, M., Wanzke, C., Riess, B., Bausch, A. R. & Boekhoven, J. Self-selection of dissipative assemblies driven by primitive chemical reaction networks. *Nat. Commun.* **9,** 2044 (2018).
90. Buhse, T., Pimienta, V., Lavabre, D. & Micheau, J. C. Experimental Evidence of Kinetic Bistability in a Biphasic Surfactant System. *J. Phys. Chem. A* **101,** 5215–5217 (1997).
91. Zepik, H. H., Blöchliger, E. & Luisi, P. L. A Chemical Model of Homeostasis. *Angew. Chem. Int. Ed.* **40,** 199–202 (2001).
92. Colomer, I., Morrow, S. M. & Fletcher, S. P. A transient self-assembling self-replicator. *Nat. Commun.* **9,** 2239 (2018).

# 2

## Physical Autocatalysis in a Dynamic Combinatorial Library

The results of this this chapter have been published in *Tetrahedron*.[1]

## 2.1 Introduction

Replicators within dynamic combinatorial libraries (DCLs), explored in Chapter 1, may be rapidly formed in a process of autocatalysis. However, they are subject to competition with other library members and processes of destruction to more thermodynamically stable states. The entire system is dynamic and responsive to alterations in the environment or instruction by templates. The construction of replicators in dynamic combinatorial libraries could be considered a preliminary step towards the realisation of out-of-equilibrium systems.[2,3]

The work published by Nguyen *et al.* on "Dynamic Combinatorial Evolution within Self-Replicating Supramolecular Assemblies",[4] briefly discussed in Chapter 1, was an example of a dynamic combinatorial library containing physical replicators. The replicating aggregates were subject to destructive steps and the formation of other species on changes in the environment. The reversible formation of the surfactant replicators was in direct contrast to the Fletcher group's previous studies of physical autocatalysis based on irreversible bond formation,[5–7] and examining this system would help us to design more dynamic and responsive replicators.

Furthermore, within the group, a physical autocatalytic reaction based on a 1,4-conjugate addition of a hydrophobic thiol to a polar electrophile had been studied extensively both in the bulk and at the single aggregate level using interferometric

scattering microscopy (iSCAT) in collaboration with the Kukura group, Oxford.[5,6,8] In contrast to fluorescence microscopy, the interferometric detection of scattering can directly image nanoscopic particles without labels, minimising disturbance of the system under analysis, and with excellent sensitivity and time resolution. Collaboration with the Kukura group therefore put us in the unique position to be able to observe and take measurements on the formation of single micelles in real time. We were interested in examining reversibly-formed replicators using this technique, gaining insight into the dynamics of the reaction at the single aggregate level.

In the next section we report the findings of the original study, before exploring the details of the study conducted for this thesis.

## 2.2 "Dynamic Combinatorial Evolution within Self-Replicating Supramolecular Assemblies"

In their report, Nguyen *et al.* design a system based on the replication of micelles.[4,9] The amphiphilic components, or "dynablocks",[10–13] are constructed by the reversible formation of an imine bond between a hydrophobic aldehyde **2.1** and a set of hydrophilic amines **2.2**, with the potential formation of a DCL of equilibrating imines **2.3** (Figure 2.2.1). On aggregation in $D_2O$, the imines are reported stable to hydrolysis and may undergo a process of replication *via* physical autocatalysis, concentrating the hydrophobic component in the aqueous

phase. A mechanistic study published much later also emphasised a templation effect.[13]

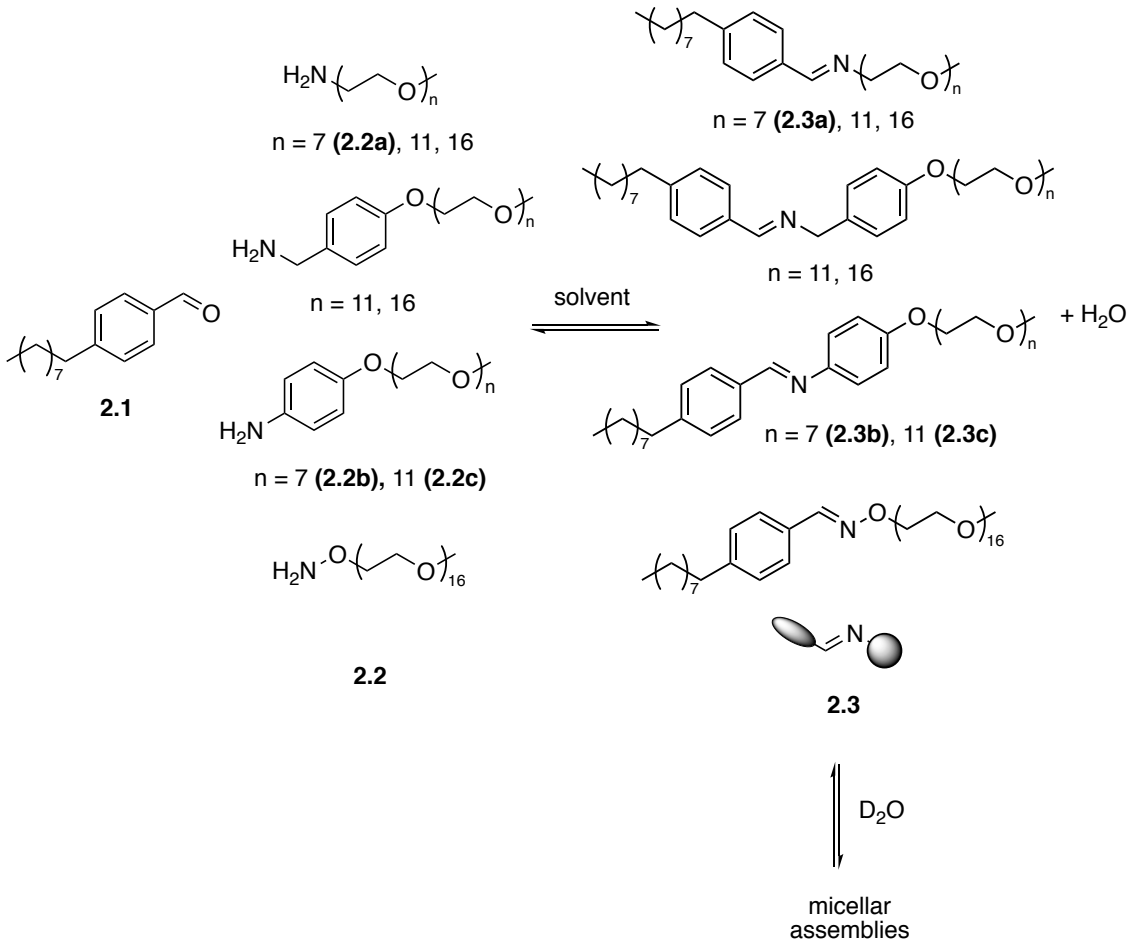



**Figure 2.2.1** Reaction between aldehyde **2.1** and amines **2.2** in a DCL results in the formation of imines **2.3** which aggregate into supramolecular structures in $D_2O$.

Reported reaction between aldehyde **2.1** and amine **2.2c** in isolation resulted in the sigmoidal growth of imine **2.3c** associated with autocatalysis (black squares, Figure 2.2.2). Seeding experiments confirmed that imine **2.3c** was a catalyst for its own formation, with initial reaction rate increasing with increasing quantity of seeded imine.

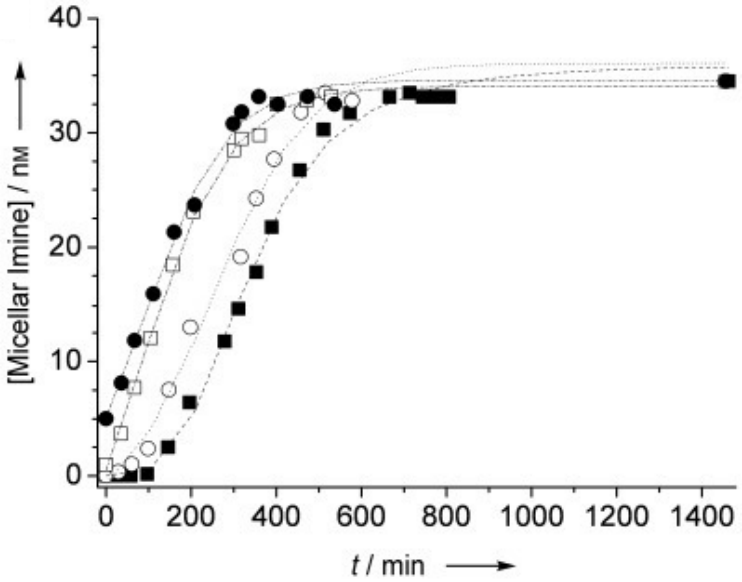



**Figure 2.2.2** Concentration of imine **2.3c** versus time starting from **2.1** and **2.2c** (50 mM each) in $D_2O$ with different amounts of initially added imine **2.3c** (concentration in mM): (■) = 0 mM, (○) = 0.1 mM, (□) = 1.0 mM, (●) = 5.0 mM. Reproduced with permission from reference[4].

The responsive nature of their system, enabled by reversible bond formation, was highlighted in a competition experiment between amines **2.2a** and **2.2c** for aldehyde **2.1**, illustrating replication within a (small) DCL (Figure 2.2.3). Here, imine **2.3a** is the dominant equilibrium species in deuterated acetonitrile ($CD_3CN$ or $d_3$-MeCN), but once the solvent is exchanged for $D_2O$ the increased thermodynamic stability of imine **2.3c** in $D_2O$ wins out and it is produced autocatalytically at the expense of imine **2.3a**.

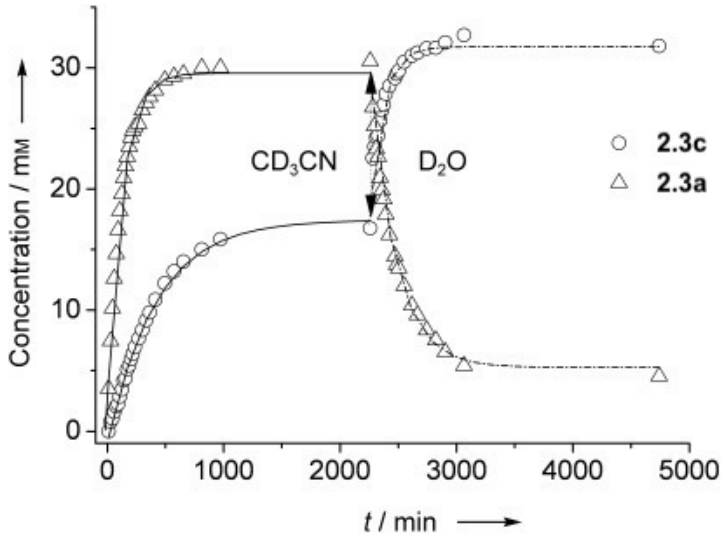



**Figure 2.2.3** Concentration of imines **2.3a** and **2.3c** formed from an equimolar mixture of **2.1**, **2.2a**, and **2.2c** (50 mM each) in $CD_3CN$ and, after reaching equilibrium, on changing the solvent to $D_2O$. Reproduced with permission from reference[4].

If amines **2.2a** and **2.2c** were mixed with aldehyde **2.1** in $D_2O$ from the beginning then imine **2.3c** would win out and be produced autocatalytically at the expense of imine **2.3a** (Figure 2.2.4).

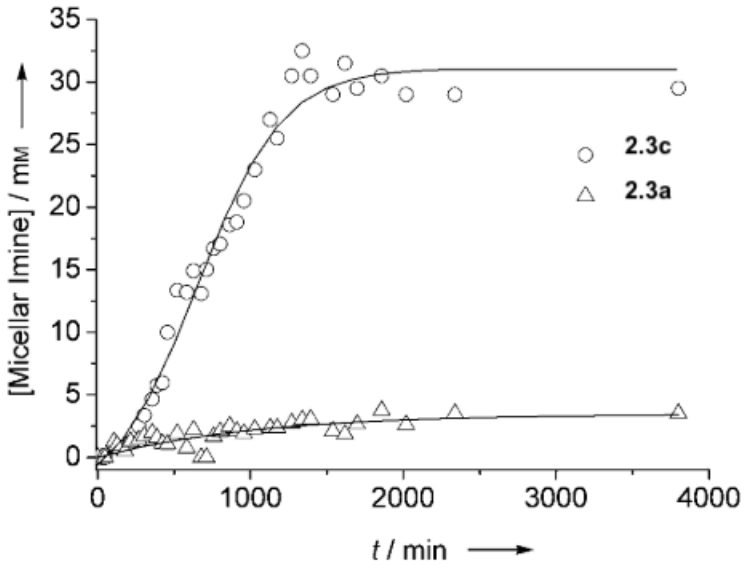



**Figure 2.2.4** Concentration of imines **2.3a** and **2.3c** formed from an equimolar mixture of **2.1**, **2.2a**, and **2.2c** (50 mM each) in $D_2O$. Reproduced with permission from reference[4].

The reported system was more dynamic than the Fletcher group's reported systems based on irreversible bond formation,[5–7] and the lability of the imine bond allowed for processes of competition and selection. Both kinetic and thermodynamic controls were in operation: the fast, autocatalytic step for replicator construction was coupled with the thermodynamic equilibration of the library. Examination of this system both in the bulk and at the single aggregate level would help us to develop our own physical replicators responsive to their environment, subject to competition and destruction.

## 2.3 Our study

### 2.3.1 Chosen substrates

We chose to examine amines **2.2a** and **2.2b** (Figure 2.2.1), allowing comparison between hydrophilic components of different nucleophilicity and $pK_a$ with the same polyethylene glycol chain length. We were confident that imine **2.3b**, by its similarity to imine **2.3c** and reports of its aggregation and thermodynamic stability, would show autocatalytic behaviour. Synthesis of amines **2.2a** and **2.2b** was achieved following the procedure of a later report,[12] and the synthesis of aldehyde **2.1** was achieved following the procedure of an independent publication (Section 2.5).[14]

### 2.3.2 Thermodynamic stability and autocatalysis of imine surfactants

In accordance with the original report, the thermodynamic stability of imines **2.3a** and **2.3b** under homogeneous conditions was first determined by rapidly stirring each amine **2.2a** and **2.2b** with an equivalent of aldehyde **2.1** in $d_3$-MeCN at room temperature for 24 hours before taking a $^1$H NMR spectrum (Figure 2.3.1). Increased condensation was observed for amine **2.2a**, as was reported by Nguyen *et al.*,[4] on account of the increased thermodynamic stability of imine **2.3a** relative to imine **2.3b**. Diffusion-ordered spectroscopy confirmed that no aggregate structures were formed under these homogeneous conditions and that

the free aldehyde and amine components diffused independently of imines **2.3a** and **2.3b** (Table 2.5.1).

To determine the thermodynamic stability of imines **2.3** under phase separated conditions, Nguyen *et al.* dilute the experiment performed in $d_3$-MeCN with $D_2O$ before removal of $d_3$-MeCN *in vacuo*.[4] It is unclear whether the mixture was given time to equilibrate after the solvent exchange and hence whether it was a true equilibrium measurement. Instead, analogously to the experiment performed in $d_3$-MeCN, we simply stirred the amine and aldehyde components in $D_2O$ at room temperature (Figure 2.3.1). Rapid stirring over 48 hours before analysis of the solution by $^1$H NMR spectroscopy resulted in no imine formation for either amine, which was surprising. Although Nguyen *et al.* reported relatively little condensation between amine **2.2a** and aldehyde **2.1**, the report for amine **2.2b** recorded nearly complete (>95%) condensation for the formation of imine **2.3b** at equilibrium.[4] Its aqueous stability had been attributed to its self-assembly intro supramolecular aggregates, providing protection against hydrolysis.

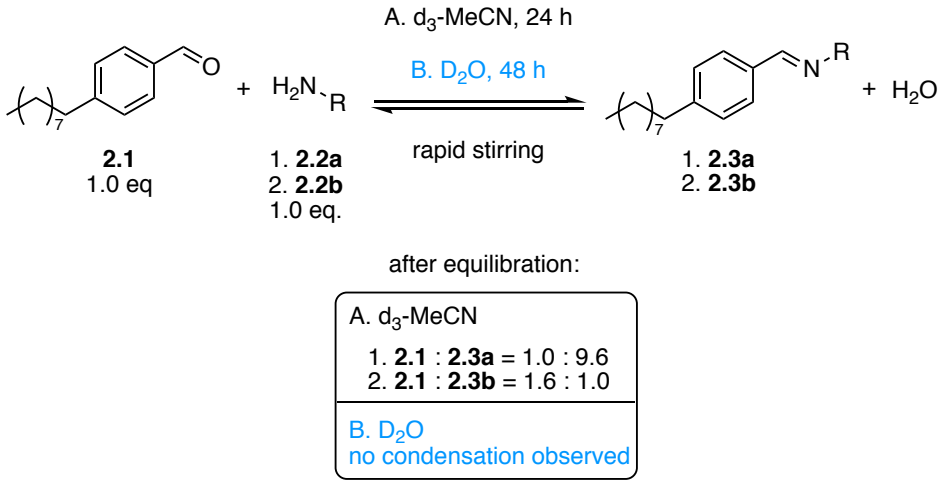



**Figure 2.3.1** Equilibrium formation of imine **2.3a** (set 1) and imine **2.3b** (set 2) in $d_3$-MeCN (conditions A) and $D_2O$ (conditions B).

As a second test of the equilibrium distribution, we synthesised imines **2.3a** and **2.3b** under anhydrous conditions before dissolving them in $D_2O$ (50 mM). Both imines were subject to extensive hydrolysis over approximately 15 hours, monitored by $^1H$ NMR spectroscopy, with complete hydrolysis to starting materials over several days (Figure 2.5.13 and Figure 2.5.14). In our hands, under neutral aqueous conditions, imines **2.3a** and **2.3b** were thermodynamically unstable in $D_2O$.

Though the study by Nguyen *et al.* had reported only the use of neutral aqueous solutions,[4] later reports from the same group also explored stability over a range of pH/pD values.[10–13] We were therefore encouraged to assess the stability of imines **2.3a** and **2.3b** at increased pD. Solutions of imines **2.3a** and **2.3b** were prepared at pH* 12 (pD 12.45)[15] and their thermodynamic stability monitored by $^1H$ NMR spectroscopy. No increase in stability was observed for imine **2.3a**, which hydrolysed to aldehyde and amine components. However, imine **2.3b** displayed much enhanced stability, with no evidence of hydrolysis over 13 hours. Encouraged by this result, we attempted to observe the autocatalytic formation of imine **2.3b** from aldehyde and amine components at pD 12.45. The reaction was conducted as shown in Figure 2.3.1, but using a solution of $D_2O$ at pD 12.45 and monitoring over 20 hours. Unfortunately only trace quantities of imine **2.3b** were observed and no autocatalytic process appeared to take place.

The findings were frustrating. We had indeed not chosen to reproduce the most extensively studied component in the previous report, amine **2.2c**, and the only component that was explicitly stated to participate in physical autocatalysis.

However, the reported stability and aggregate formation of imines **2.3a** and **2.3b** had encouraged us that they might show similar behaviour.

## 2.3.3 Physical characterisation

Despite failing to observe autocatalysis, we were able to confirm that imines **2.3a** and **2.3b** formed aggregates in aqueous solution (before their hydrolysis and disassembly) by DOSY and by DLS.

DOSY of imine **2.3a** was more facile than of imine **2.3b** since it was well solvated with sharp, well-resolved peaks in its $^1$H NMR spectrum in $D_2O$. Imine **2.3a** was found to diffuse with a hydrodynamic radius of 6.0 nm, comparable to the reported value of 5 nm and consistent with the formation of supramolecular aggregates (Table 2.3.1).[4] A small quantity of aldehyde **2.1** was present in the sample since imine **2.3a** was not purified following synthesis. DOSY revealed this hydrophobic molecule to be associated with the aggregates, diffusing at a similar rate to imine **2.3a** and much more slowly than the control (*cf.* entries 1 and 4, Table 2.3.2).

DOSY of imine **2.3b** was less facile on account of the relatively broad peaks observed in the $^1$H NMR spectrum in $D_2O$, but a hydrodynamic radius of 8.1 nm was extracted (Table 2.3.1). DLS experiments on this species recorded micelles with a hydrodynamic radius of 6.1 nm. Nguyen *et al.* report aggregates too large to observe by DOSY spectroscopy for this species, which may explain the broad peaks we observed; neutron scattering experiments in their study revealed cylindrical micelles of 6 × 34 nm in size.

| | | Hydrodynamic radii $R_h$/nm | | | | |
|---|---|---|---|---|---|---|
| | | This study | | Literature values | | |
| Entry | Species | DOSY | DLS | DOSY | DLS | SANS[a] |
| 1 | **2.3a** | 6.0 | - | 5 | - | - |
| 2 | **2.3b** | 8.1 | 6.1 | - | - | 6 x 34[b] |

**Table 2.3.1** Hydrodynamic radii recorded in $D_2O$, 50 mM. [a] Small angle neutron scattering. [b] diameter × length: small angle neutron scattering found cylindrical micelles.

| | | Diffusion coefficient D/$10^{-10}$ $m^2s^{-1}$ | | | | |
|---|---|---|---|---|---|---|
| Entry | Species present | **2.1** | **2.2a** | **2.2b** | **2.3a** | **2.3b** |
| 1 | **2.1** | 1.41 | - | - | - | - |
| 2 | **2.2a** | - | 4.23 | - | - | - |
| 3 | **2.2b** | - | - | 3.70 | - | - |
| 4 | **2.3a** | 0.26 | n.d.[a] | - | 0.41 | - |
| 5 | **2.3b** | n.d.[b] | - | n.d.[a] | - | 0.30 |

**Table 2.3.2** Diffusion coefficients measured by DOSY NMR spectroscopy. All components were measured at a concentration of 50 mM in $D_2O$ (assuming 100% purity). The presence of a small quantity of aldehyde **2.1** and amines **2.2a** and **2.2b** in measurements of **2.3a** and **2.3b** (entries 4 and 5) are a result of their synthesis without purification. [a] Could not determine D due to overlap of peaks. [b] Aldehyde peak too small for accurate integration.

Both an inability to probe the exact dimensions of non-spherical aggregates and the apparent differences in sample stability with the reported system makes it difficult to directly compare all values between our study and that of Nguyen *et al.*. However, we could be confident that both imines **2.3a** and **2.3b** aggregated in aqueous solution. The full comparison of our data and those reported by Nguyen *et al.* is shown in Table 2.3.1.[4]

## 2.3.4 Examination at the single aggregate level using iSCAT

Despite the failure to observe imine formation in the bulk, we were still interested to observe the system at the single aggregate level, using iSCAT, in accordance with the original aims of the project. Biphasic reactions on the microlitre scale and on a glass coverslip are subject to significantly different parameters than are found in the bulk in a well-stirred solution. We were able to observe supramolecular aggregates of pre-formed imine **2.3b** in $H_2O$, consistent with the binding of micelles (Figure 2.3.2 and Section 2.5.5). Unfortunately, however, the mixing of aldehyde **2.1** and amine **2.2b** resulted in no apparent micelle formation on the glass coverslip under observation (Figure 2.5.19).

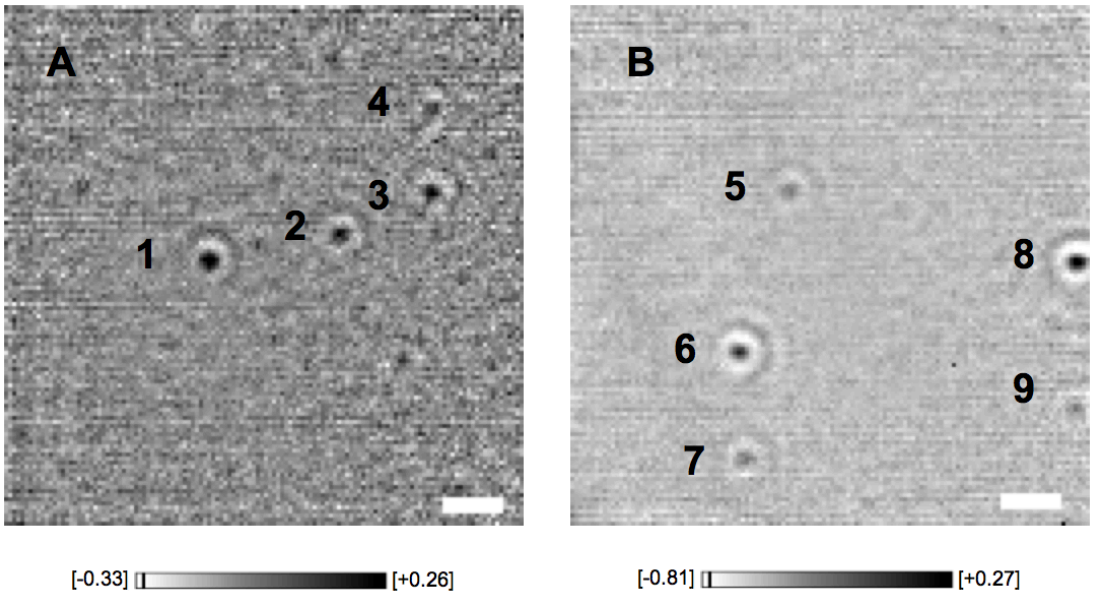



**Figure 2.3.2** Images A and B are independent images of the binding of imine **2.3b** (~1 mM in $D_2O$) to the microscope coverslip as aggregates (individual aggregates are numbered within each image). Each image is the average of 100 frames. Scale bar = 1 μm. The bar below the images represent the contrast range of each image; the individual contrast of each aggregate provides a measure of its size (Section 2.5.5).

## 2.4 Conclusions

Nguyen *et al.* reported the physical replication of imine **2.3c**, whose dominance in a DCL, in competition with imine **2.3a**, resulted from its autocatalytic production and high thermodynamic stability in $D_2O$. Its similarity to imine **2.3b** and the high reported stability of other DCL components encouraged us that we might be able to observe physical autocatalysis for other library members and examine their formation under the pressure of competitors, potentially observing the formation

of transiently formed kinetic products which were subject to destruction and competition.

However, though imines **2.3a** and **2.3b** formed micelles in aqueous solution (as determined by DLS, DOSY and iSCAT), we found these structures to be thermodynamically unstable to the reformation of starting materials, hydrolysing fully to aldehyde and amine components in neutral aqueous solution. The enhanced stability offered at increased pD did not induce imine formation from aldehyde and amine starting materials; the trace conversion observed by NMR spectroscopy was not great enough for the onset of autocatalysis. These observations precluded any investigation of their behaviour when in competition with each other.

The strong dependence of the system on pH/pD, variation in sample preparation, hydrophilic chain length, and on parameters explored in later publications such as reaction stoichiometry,[10–13] demonstrate the sensitivity of the system and the precise conditions which may be required for significant imine stability and the observation of autocatalysis. Further work on this system would of course begin with the exact replication of studies on imine **2.2c**, the only species explicitly shown to undergo a process of autocatalysis in $D_2O$.

Nevertheless, the examination of replication in DCLs was the starting point for the realisation of a system of physical replication out-of-equilibrium. This is explored in Chapter 3.

## 2.5 Experimental

## 2.5.1 Synthesis and characterisation of the compounds used in this study

### 2.5.1.1 Aldehyde **2.1**

The route for the synthesis of aldehyde **2.1** was taken from *J. Med. Chem.* **45,** 4629–4638 (2002) (Figure 2.5.1).[14]

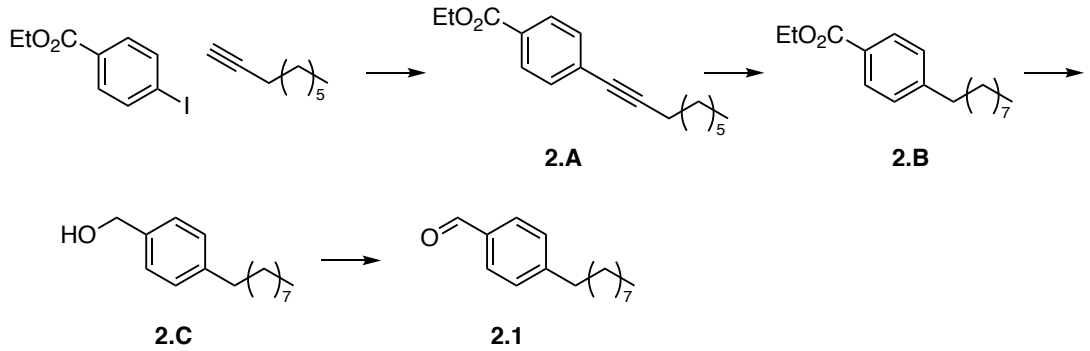



**Figure 2.5.1** Schematic route for the synthesis of aldehyde **2.1**.

Ester **2.A**

A flame-dried round-bottom flask was charged with a solution of 4-iodoethylbenzoate (1.50 g, 5.43 mmol, 1.00 eq.) in MeCN (15 mL) and covered with aluminium foil. Nonyne (1.3 mL, 8.2 mmol, 1.5 eq.), $^{i}Pr_2NH$ (1.2 mL, 8.2 mmol, 1.5 eq.), $PdCl_2(PPh_3)_2$ (38 mg, 54 µmol, 1.0 mol%), and CuI (21 mg, 110 µmol, 2.0 mol%) were added at 0 °C. The mixture was stirred under an argon atmosphere for 4.5 hours and then diluted with $Et_2O$ (15 mL). The reaction mixture was washed with an aq. solution of $KHSO_4$ (5 wt%, 15 mL), an aq. solution of $Na_2S_2O_3$ (5 wt%, 15 mL), and brine (15 mL). The organic layer was dried over $MgSO_4$ and concentrated *in vacuo*. Purification by column

chromatography ($SiO_2$, petrol ether:$Et_2O$ 99.5:0.5) afforded ester **2.A** as an orange oil (1.26 g, 85% yield). **$^1$H NMR** (400 MHz, $CDCl_3$): δ 7.96–7.94 (2H, m, 2× C(Ar)–H), 7.44–7.42 (2H, m, 2× C(Ar)–H), 4.36 (2H, q, *J* = 7.0 Hz, $CO_2CH_2CH_3$), 2.42 (2H, t, *J* = 7.0 Hz, C≡C–$CH_2$), 1.65–1.57 (2H, m, 1× $CH_2$), 1.48–1.25 (11H, m, 4× $CH_2$ and $CO_2CH_2CH_3$), 0.89 (3H, t, *J* = 7.0 Hz, $(CH_2)_6CH_3$); **$^{13}$C NMR** (101 MHz, $CDCl_3$): δ 166.5 (C=O), 131.7 (2× C(Ar)–H), 129.7 (2× C(Ar)–H), 129.5 (4° C(Ar)), 129.2 (4° C(Ar)), 94.2 (1× C≡C), 80.5 (1× C≡C), 61.3 ($CO_2CH_2CH_3$), 32.1, 29.2, 29.2, 28.9, 23.0 (5× $CH_2$), 19.8 (C≡C–$CH_2$), 14.6 ($CO_2CH_2CH_3$), 14.4 ($(CH_2)_6CH_3$); **HRMS** (ESI+, m/z): calc. for $C_{18}H_{25}O_2^+$ $[M+H]^+$ 273.1849, found 273.1850; **IR** $\tilde{\nu}_{max}$ (film)/ $cm^{-1}$: 2929, 2857, 2230 (w), 1718, 1607.

Ester **2.B**

A flame-dried round-bottom flask was charged with a solution of **2.A** (500 mg, 1.84 mmol, 1.00 eq.) in MeOH (2.5 mL) under an argon atmosphere. Activated carbon (270 mg) and a solution of $Pd(OAc)_2$ (30 mg, 0.13 mmol, 7.0 mol%) in THF (3.0 mL) were added. The reaction mixture was stirred for 5.5 hours and continuously bubbled with hydrogen gas (3 balloons). The mixture was then filtered through a Celite pad and concentrated *in vacuo*. Purification by column chromatography ($SiO_2$, petrol ether:EtOAc 99:1) afforded ester **2.B** as a colourless oil (404 mg, 79% yield). **$^1$H NMR** (400 MHz, $CDCl_3$): δ 7.97–7.94 (2H, m, 2× C(Ar)–H), 7.24–7.22 (2H, m, 2× C(Ar)–H), 4.36 (2H, q, *J* = 7.0 Hz, $CO_2CH_2CH_3$), 2.65 (2H, t, *J* = 8.0 Hz, C(Ar)–$CH_2$), 1.65–1.58 (2H, m, 1× $CH_2$), 1.38 (3H, t, *J* = 7.0 Hz, $CO_2CH_2CH_3$), 1.31–1.26 (12H, m, 6× $CH_2$), 0.88 (3H, t, *J* = 7.0 Hz, $(CH_2)_8CH_3$); **$^{13}$C NMR** (101 MHz, $CDCl_3$): δ 167.0 (C=O), 148.7 (4°

C(Ar)), 129.9 (2× C(Ar)–H), 128.7 (2× C(Ar)–H), 128.3 (4° C(Ar)), 61.1 ($CO_2CH_2CH_3$), 36.3 (C(Ar)–$CH_2$), 32.2, 31.5, 29.9, 29.8, 29.6, 29.6, 23.0 (7× $CH_2$), 14.7 ($CO_2CH_2CH_3$), 14.5 ($(CH_2)_8CH_3$); **HRMS** (ESI+, m/z): calc. for $C_{18}H_{29}O_2^+$ $[M+H]^+$ 277.2162, found 277.2164; **IR** $\tilde{\nu}_{max}$ (film)/$cm^{-1}$: 2929, 2857, 1718, 1607.

Alcohol **2.C**

A flame-dried round-bottom flask was charged with $Et_2O$ (2.0 mL) and a solution of $LiAlH_4$ in $Et_2O$ (4.0 M; 0.54 mL, 3.0 eq.) under an argon atmosphere. A solution of ester **2.B** (200 mg, 720 µmol, 1.00 eq.) in $Et_2O$ (2.5 mL) was added dropwise at 0 °C. The reaction was stirred for 2 hours, diluted with $Et_2O$ and quenched with an aq. sat. solution of $Na_2SO_4$. The aqueous layer was extracted with $Et_2O$ (3× 15 mL) and the combined organic layers were washed with brine (15 mL), dried over $MgSO_4$, and concentrated *in vacuo*. Purification by column chromatography ($SiO_2$, petrol ether:EtOAc 80:20) afforded the alcohol **2.C** as a colourless solid (158 mg, 94% yield). **$^1$H NMR** (400 MHz, $CDCl_3$): δ 7.28 (2H, d, *J* = 8.0 Hz, 2× C(Ar)–H), 7.18 (2H, d, *J* = 8.0 Hz, 2× C(Ar)–H), 4.65 (2H, s, C$H_2$OH), 2.61 (2H, t, *J* = 8.0 Hz, C(Ar)–C$H_2$), 1.77 (1H, s, OH), 1.65–1.57 (2H, m, 1× $CH_2$), 1.32–1.27 (12H, m, 6× $CH_2$), 0.89 (3H, t, *J* = 7.0 Hz, $(CH_2)_8CH_3$); **$^{13}$C NMR** (101 MHz, $CDCl_3$): δ 142.9 (4° C(Ar)), 138.4 (4° C(Ar)), 128.9 (2× C(Ar)–H), 127.4 (2× C(Ar)–H), 65.6 ($CH_2OH$), 36.0 (C(Ar)–$CH_2$), 32.2, 31.9, 29.9, 29.9, 29.8, 29.7, 23.0 (7× $CH_2$), 14.5 ($(CH_2)_8CH_3$); **HRMS** (ESI+, m/z): calc. for $C_{16}H_{26}ONa^+$ $[M+Na]^+$ 257.1876, found 257.1876; **IR** $\tilde{\nu}_{max}$ (film)/$cm^{-1}$: 3305, 2923, 1513.

Aldehyde **2.1**

A flame-dried round-bottom flask was charged with a solution of alcohol **2.C** (1.52 g, 6.47 mmol, 1.00 eq.) in $CH_2Cl_2$ (70 mL) and activated $MnO_2$ (5.63 g, 64.7 mmol, 10.0 eq.). The reaction mixture was stirred at room temperature for 23 hours and was then filtered through a Celite pad, rinsed with $CH_2Cl_2$, and concentrated *in vacuo*. Purification by column chromatography ($SiO_2$, petrol ether:$Et_2O$ 95:5) afforded the aldehyde **2.1** as a colourless oil (1.43 g, 95% yield). **$^1$H NMR** (400 MHz, $CDCl_3$): δ 9.96 (1H, s, CHO), 7.79 (2H, d, *J* = 8.0 Hz, 2× C(Ar)–H), 7.33 (2H, d, *J* = 8.0 Hz, 2× C(Ar)–H), 2.68 (2H, t, *J* = 8.0 Hz, C(Ar)–C*H*$_2$), 1.67–1.60 (2H, m, 1× $CH_2$), 1.31–1.26 (12H, m, 6× $CH_2$), 0.88 (3H, t, *J* = 7.0 Hz, ($(CH_2)_8$C*H*$_3$)); **$^{13}$C NMR** (101 MHz, $CDCl_3$): δ 192.3 (C=O), 150.8 (4° C(Ar)), 134.7 (4° C(Ar)), 130.2 (2× C(Ar)–H), 129.4 (2× C(Ar)–H), 36.5, 32.2, 31.4, 29.8, 29.8, 29.6, 29.6, 23.0 (8× $CH_2$), 14.4 ($(CH_2)_8$C*H*$_3$); **HRMS** (ESI+, m/z): calc. for $C_{16}H_{25}O^+$ $[M+H]^+$ 233.1900, found 233.1901; **IR** $\tilde{\nu}_{max}$ (film)/cm$^{-1}$: 2924, 2854, 1701, 1606, 1576. The data are consistent with those reported in *J. Med. Chem.* **45,** 4629–4638 (2002).[14]

## 2.5.1.2 Amines **2.2a**, **2.2b**

The route for the synthesis of amines **2.2a** and **2.2b** was taken from procedures described in *Soft Matter* **10,** 3926–3937 (2014) (Figure 2.5.2).[12]

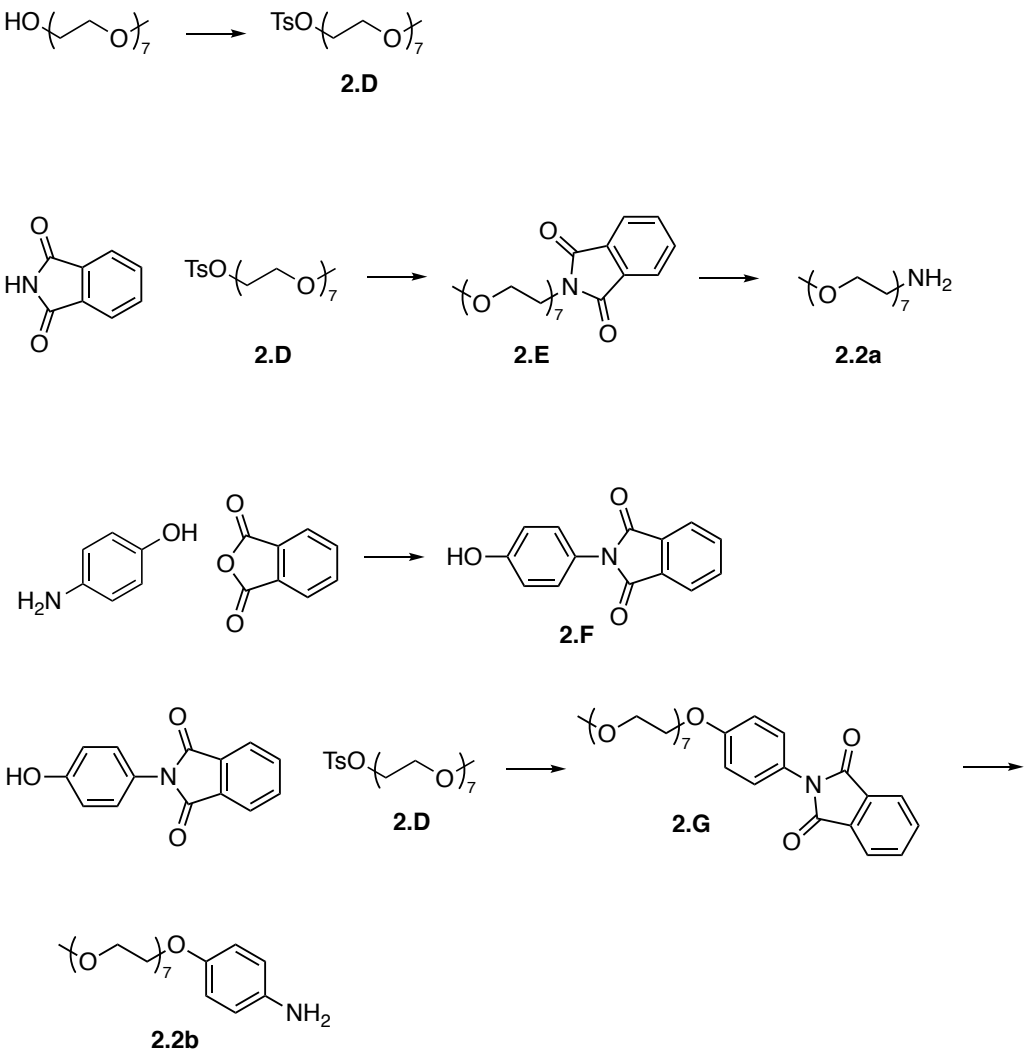



**Figure 2.5.2** Schematic routes for the synthesis of amines **2.2a** and **2.2b**.

Tosylate **2.D**

A round-bottom flask was charged with a solution of heptaethylene glycol monomethyl ether (2.50 g, 7.34 mmol, 1.00 eq.) in THF (4.3 mL). A solution of NaOH (881 mg, 22.0 mmol, 3.00 eq.) in $H_2O$ (4.3 mL) and a solution of TsCl (1.82 g, 9.55 mmol, 1.30 eq.) in THF (3.0 mL) were added to the solution and the mixture was stirred at room temperature for 28 hours. The reaction mixture was extracted with $Et_2O$ (3× 20 mL) and the combined organic layers washed with an aq. solution of NaOH (10 wt%; 50 mL), brine (50 mL), and $H_2O$ (50 mL). The organic layer was then dried over $MgSO_4$, filtered, and concentrated *in vacuo*. Purification by column chromatography ($SiO_2$, $CH_2Cl_2$:MeOH 97:3) afforded the tosylate **2.D** as a colourless oil (2.57 g, 71% yield). **$^1$H NMR** (400 MHz, $CDCl_3$): δ 7.76 (2H, d, *J* = 8.0 Hz, 2× C(Ar)–H), 7.31 (2H, d, *J* = 8.0 Hz, 2× C(Ar)–H), 4.12 (2H, t, *J* = 5.0 Hz, 1× $CH_2$), 3.66–3.50 (26H, m, 13× $CH_2$), 3.34 (3H, s, $OCH_3$), 2.42 (3H, s, C(Ar)-$CH_3$); **$^{13}$C NMR** (101 MHz, $CDCl_3$): δ 145.0 (4° C(Ar)), 133.2 (4° C(Ar)), 130.1 (2× C(Ar)–H), 128.2 (2× C(Ar)–H), 72.2, 71.0, 70.8 - 70.7, 69.5, 68.9 (14× $CH_2$), 59.3 ($OCH_3$), 21.9 (C(Ar)-*C*$H_3$); **HRMS** (ESI+, m/z): calc. for $C_{22}H_{38}O_{10}NaS$ $[M+Na]^+$ 517.2078, found 517.2074; **IR** $\tilde{\nu}_{max}$ (film)/$cm^{-1}$: 2871, 1598. The data are consistent with those reported in *Soft Matter* **10,** 3926–3937 (2014).[12]

Phthalimide **2.E**

A round-bottom flask equipped with a reflux condenser was charged with a solution of tosylate **2.D** (500 mg, 1.01 mmol, 1.00 eq.) in MeCN (20 mL). $K_2CO_3$ (168 mg, 1.21 mmol, 1.20 eq.), followed by phthalimide (178 mg, 1.21 mmol, 1.20 eq.) were added to the solution. The mixture was stirred for 7 hours under

reflux and then concentrated *in vacuo*. $H_2O$ (20 mL) was added, and the aqueous layer was extracted with $CH_2Cl_2$ (4× 20 mL). The combined organic layers were dried over $MgSO_4$, filtered, and concentrated *in vacuo*. Purification by column chromatography ($SiO_2$, EtOAc:MeOH 92:8) afforded the phthalimide **2.E** as a brown oil (181 mg, 38% yield). **$^1$H NMR** (400 MHz, $CDCl_3$): δ 7.83–7.81 (2H, m, 2× C(Ar)–H), 7.70–7.68 (2H, m, 2× C(Ar)–H), 3.87 (2H, t, *J* = 6.0 Hz, 1× $CH_2$), 3.71 (2H, t, *J* = 6.0 Hz, 1× $CH_2$), 3.63–3.51 (24H, m, 12× $CH_2$), 3.35 (3H, s, $OCH_3$); **$^{13}$C NMR** (101 MHz, $CDCl_3$): δ 168.5 (2× C=O), 134.2 (2× 4° C(Ar)), 132.4 (2× C(Ar)–H), 123.5 (2× C(Ar)–H), 72.2, 70.9 - 70.8, 70.4, 68.2 (13× $CH_2$), 59.3 ($OCH_3$), 37.5 (1× $CH_2$); **HRMS** (ESI+, m/z): calc. for $C_{23}H_{35}O_9N_{23}Na$ [M+Na]+ 492.2204, found 492.2204; **IR** $\tilde{\nu}_{max}$ (film)/$cm^{-1}$: 2869, 1773, 1710.

Amine **2.2a**

A round-bottom flask was charged with a solution of phthalmide **2.E** (220 mg, 0.47 mmol, 1.00 eq.) in THF (6.5 mL). An aqueous solution of hydrazine (40–50 wt%; 1.2 mL, ~ 40 eq.) was added. The reaction mixture was stirred for 2 hours at room temperature and then concentrated *in vacuo*. $H_2O$ (15 mL) was added and the aqueous layer was extracted with $CHCl_3$ (3× 15 mL). The combined organic layers were dried over $MgSO_4$, filtered, and concentrated *in vacuo* to obtain amine **2.2a** as a colourless oil (128 mg, 80% yield). **$^1$H NMR** (400 MHz, $CDCl_3$): δ 3.62–3.59 (24H, m, 12× $CH_2$), 3.52–3.46 (4H, m, 2× $CH_2$), 3.34 (3H, s, $OCH_3$), 2.83 (2H, br. s, $NH_2$); **$^{13}$C NMR** (101 MHz, $CDCl_3$): δ 73.6, 72.2, 70.8 - 70.8, 70.5 (13× $CH_2$), 59.3 ($OCH_3$), 42.0 (1× $CH_2$); **HRMS** (ESI+, m/z): calc. for $C_{15}H_{34}O_7N$ $[M+H]^+$ 340.2330, found 340.2328; **IR** $\tilde{\nu}_{max}$ (film)/$cm^{-1}$: 3446, 2872.

Phthalimide **2.F**

A flame-dried round-bottom flask equipped with a vigreux column was charged with 4-aminophenol (2.00 g, 18.3 mmol, 1.00 eq.) and phthalic anhydride (2.85 g, 19.2 mmol, 1.05 eq.). DMF (20 mL) was added and the reaction mixture was stirred for 2 hours at 100 °C. The mixture was then filtered through a sinter funnel. The residue was dissolved in glacial acetic acid (38 mL) in a round-bottom flask equipped with a vigreux column. The reaction mixture was stirred at 80 °C for 4 hours and then filtered through a sinter funnel to afford phthalimide **2.F** as a pale yellow solid (1.87 g, 43% yield). **$^{1}$H NMR** (400 MHz, $(CD_3)_2SO$): δ 9.80 (1H, s, OH), 7.96–7.92 (4H, m, 4× C(Ar)–H), 7.26–7.24 (2H, m, 2× C(Ar)–H), 6.93–6.91 (2H, m, 2× C(Ar)–H); **$^{13}$C NMR** (101 MHz, $(CD_3)_2SO$): δ 168.3 (2× C=O), 158.2 (4° C(Ar)), 135.5 (2× C(Ar)–H), 132.5 (2× 4° C(Ar)), 129.7 (2× C(Ar)–H), 124.2 (2× C(Ar)–H), 123.8 (4° C(Ar)), 116.3 (2× C(Ar)–H); **LRMS** (ESI-, m/z): 238.1 $[M-H]^-$. The data are consistent with those reported in *Soft Matter* **10,** 3926–3937 (2014).[12]

Phthalimide **2.G**

A round-bottom flask equipped with a reflux condenser was charged with a solution of tosylate **2.D** (500 mg, 1.01 mmol, 1.00 eq.) in MeCN (20 mL). $K_2CO_3$ (168 mg, 1.21 mmol, 1.20 eq.) and phthalimide **2.F** (290 mg, 1.21 mmol, 1.20 eq.) were added to the solution. The mixture stirred under reflux for 7 hours and then concentrated *in vacuo*. $H_2O$ (20 mL) was added, and the aqueous layer was extracted with $CH_2Cl_2$ (4× 20 mL). The combined organic layers were dried over $MgSO_4$, filtered, and concentrated *in vacuo*. Purification by column chromatography ($SiO_2$, EtOAc:MeOH 92:8) afforded the phthalimide **2.G** as a bright yellow solid (213 mg, 37% yield). **$^{1}$H NMR** (400 MHz, $CDCl_3$): δ 7.93–7.91

(2H, m, 2× C(Ar)–H), 7.77–7.75 (2H, m, 2× C(Ar)–H), 7.32–7.29 (2H, m, 2× C(Ar)–H), 7.03–7.00 (2H, m, 2× C(Ar)–H), 4.15 (2H, t, *J* = 5.0 Hz, 1× $CH_2$), 3.86 (2H, t, *J* = 5.0 Hz, 1× $CH_2$), 3.72–3.61 (22H, m, 11× $CH_2$), 3.54–3.52 (2H, m, 1× $CH_2$), 3.35 (3H, s, $OCH_3$); **$^{13}$C NMR** (101 MHz, $CDCl_3$): δ 167.8 (2× C=O), 158.7 (4° C(Ar)), 134.6 (2× C(Ar)–H), 132.1 (2× 4° C(Ar)), 128.2 (2× C(Ar)–H), 124.7 (4° C(Ar)), 123.9 (2× C(Ar)–H), 115.4 (2× C(Ar)–H), 72.2, 71.1, 70.9 - 70.8, 69.9, 68.0 (14× $CH_2$), 59.3 ($OCH_3$); **HRMS** (ESI+, m/z): calc. for $C_{29}H_{39}O_{10}NNa$ $[M+Na]^+$ 584.2466, found 584.2463; **IR** $\tilde{\nu}_{max}$ (film)/$cm^{-1}$: 2872, 1716, 1513. The data are consistent with those reported in *Soft Matter* **10,** 3926–3937 (2014).[12]

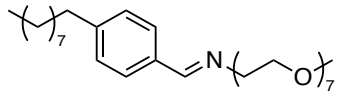
Amine **2.2b**

A round-bottom flask was charged with a solution of phthalmide **2.G** (1.36 g, 2.43 mmol, 1.00 eq.) in THF (40 mL). An aqueous solution of hydrazine (40-50 wt%; 6.1 mL, ~ 40 eq.) was added and the reaction mixture was stirred at room temperature for 2 hours. The mixture was concentrated *in vacuo* and $H_2O$ (50 mL) was added. The aqueous layer was extracted with $CHCl_3$ (3× 50 mL). The combined organic layers were dried over $MgSO_4$, filtered, and concentrated *in vacuo* to obtain amine **2.2b** as a colourless solid (885 mg, 84% yield). **$^1$H NMR** (400 MHz, $CDCl_3$): δ 6.73–6.69 (2H, m, 2× C(Ar)–H), 6.60–6.56 (2H, m, 2× C(Ar)–H), 4.01 (2H, t, *J* = 5.0 Hz, 1× $CH_2$), 3.77 (2H, t, *J* = 5.0 Hz, 1× $CH_2$), 3.69–3.59 (22H, m, 11× $CH_2$), 3.52–3.50 (2H, m, 1× $CH_2$), 3.46 (2H, br. s, $NH_2$), 3.34 (3H, s, $OCH_3$); **$^{13}$C NMR** (101 MHz, $CDCl_3$): δ 152.0 (4° C(Ar)), 140.5 (4° C(Ar)), 116.5 (2× C(Ar)–H), 116.0 (2× C(Ar)–H), 72.1, 71.0, 70.8 - 70.7, 70.1, 68.3 (14× $CH_2$), 59.2 ($OCH_3$); **HRMS** (ESI+, m/z): calc. for $C_{21}H_{38}O_8N$ $[M+H]^+$ 432.2592, found

432.2581; **IR** $\tilde{\nu}_{max}$ (film)/cm$^{-1}$: 3355, 2871, 1512. The data are consistent with those reported in *Soft Matter* **10,** 3926–3937 (2014).[12]

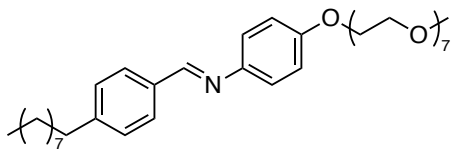
## 2.5.1.3 Imines **2.3a**, **2.3b**

Imine **2.3a**



A flame-dried round-bottom flask was charged with $MgSO_4$ (106 mg, 880 µmol, 1.50 eq.) and $CH_2Cl_2$ (2.0 mL) under an argon atmosphere. A solution of aldehyde **2.1** (137 mg, 590 µmol, 1.00 eq.) in $CH_2Cl_2$ (1.0 mL) and a solution of amine **2.2a** (200 mg, 590 µmmol, 1.00 eq.) in $CH_2Cl_2$ (1.0 mL) were added to the mixture. The reaction was stirred for 24 hours at room temperature and then filtered through a sinter funnel and rinsed with dry $CH_2Cl_2$. The filtrate was concentrated *in vacuo* to afford imine **2.3a** as a colourless oil (317 mg, 97% yield). **$^1$H NMR** (400 MHz, $CDCl_3$): δ 8.27 (1H, s, CHN), 7.63 (2H, d, *J* = 8.0 Hz, 2× C(Ar)–H), 7.20 (2H, d, *J* = 8.0 Hz, 2× C(Ar)–H), 3.78 (4H, m, 2× $CH_2$), 3.67–3.61 (22H, m, 11× $CH_2$), 3.55–3.53 (2H, m, 1× $CH_2$), 3.37 (3H, s, $OCH_3$), 2.62 (2H, t, *J* = 8.0 Hz, 1× $CH_2$), 1.62–1.59 (2H, m, 1× $CH_2$), 1.30–1.25 (12H, m, 6× $CH_2$), 0.87 (3H, t, *J* = 7.0 Hz, $(CH_2)_8CH_3$); **$^{13}$C NMR** (101 MHz, $CDCl_3$)**:** δ 163.0 (CHN), 146.3 (4° C(Ar)), 134.1 (4° C(Ar)), 129.0 (2× C(Ar)–H), 128.4 (2× C(Ar)–H), 72.3, 71.2, 70.9 - 70.7 , 61.5 (14× $CH_2$), 59.4 ($OCH_3$), 36.2, 32.2, 31.6, 29.9, 29.8, 29.6, 29.6, 23.0 (8× $CH_2$), 14.4 ($(CH_2)_8CH_3$); **HRMS** (ESI+, m/z): calc. for $C_{31}H_{56}O_7N$ $[M+H]^+$ 554.4051, found 554.4052; **IR** $\tilde{\nu}_{max}$ (film)/cm$^{-1}$: 2924, 1856, 1647.

Imine **2.3b**

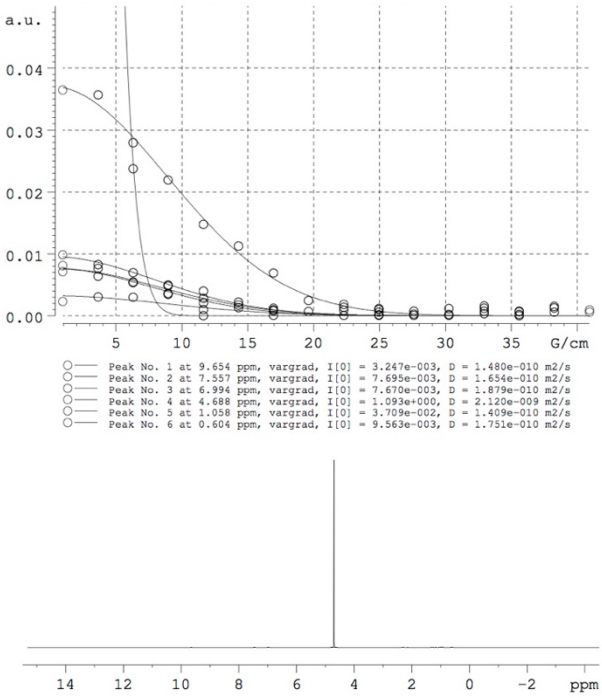


A flame-dried round-bottom flask was charged with $MgSO_4$ (84.0 mg, 700 µmol, 1.50 eq.) and $CH_2Cl_2$ (2.0 mL) under an argon atmosphere. A solution of aldehyde **2.1** (108 mg, 460 µmol, 1.00 eq.) in $CH_2Cl_2$ (1.0 mL) and a solution of amine **2.2b** (200 mg, 460 µmol, 1.00 eq.) in $CH_2Cl_2$ (1.0 mL) were added to the mixture. The reaction was stirred for 24 hours at room temperature and then filtered through a sinter funnel and rinsed with dry $CH_2Cl_2$. The filtrate was concentrated *in vacuo* to afford imine **2.3b** as a colourless oil (295 mg, 99% yield). **$^1$H NMR** (400 MHz, $CDCl_3$): δ 8.44 (1H, s, CHN), 7.79 (2H, d, *J* = 8.0 Hz, 2× C(Ar)–H), 7.26 (2H, d, *J* = 8.0 Hz, 2× C(Ar)–H), 7.19 (2H, d, *J* = 9.0 Hz, 2× C(Ar)–H), 6.93 (2H, d, *J* = 9.0 Hz, 2× C(Ar)–H), 4.15 (2H, t, *J* = 5.0 Hz, 1× $CH_2$), 3.87 (2H, t, *J* = 5.0 Hz, 1× $CH_2$), 3.75–3.72 (2H, m, 1× $CH_2$), 3.69–3.62 (20H, m, 10× $CH_2$), 3.55–3.53 (2H, m, 1× $CH_2$), 3.37 (3H, s, $OCH_3$), 2.65 (2H, t, *J* = 8.0 Hz, 1× $CH_2$), 1.67–1.60 (2H, m, 1× $CH_2$), 1.31–1.26 (12H, m, 6× $CH_2$), 0.88 (3H, t, *J* = 7.0 Hz, $(CH_2)_8CH_3$); **$^{13}$C NMR** (101 MHz, $CDCl_3$): δ 158.9 (CHN), 157.6 (4° C(Ar)), 146.9 (4° C(Ar)), 145.7 (4° C(Ar)), 134.4 (4° C(Ar)), 129.2 (2× C(Ar)–H), 128.9 (2× C(Ar)–H), 122.4 (2× C(Ar)–H), 115.5 (2× C(Ar)–H), 72.3, 71.2, 71.0 – 70.9, 70.9, 70.1, 68.1 (14× $CH_2$), 59.4 ($OCH_3$), 36.3, 32.2, 31.6, 29.9, 29.8, 29.6, 29.6, 23.0 (8× $CH_2$), 14.4 ($(CH_2)_8CH_3$); **HRMS** (ESI+, m/z): calc. for $C_{37}H_{60}O_8N$ $[M+H]^+$ 646.4313, found 646.4313; **IR** $\tilde{\nu}_{max}$ (film)/$cm^{-1}$: 2924, 2856, 1625, 1503.

## 2.5.2 DOSY NMR

DOSY NMR measurements were performed using a 500 MHz spectrometer equipped with a TFI probehead at 298 K using the 2D sequence for diffusion measurement using double stimulated echo for convection compensation and longitudinal eddy current delay, using bipolar gradient pulses for diffusion, and using three spoil gradients (Bruker terminology: dstebpgp35) pulse sequence. The samples were thoroughly mixed using a Vortex Genie 2 mixer (Scientific Industries) and were then clarified using a hand centrifuge (Hettich, model 1011) before measurement. For biphasic experiments sufficient $D_2O$ was used to ensure that the hydrophobic layer was not detectible by the NMR probe. Experiments were performed in two stages: initially 1D edited DOSY experiments were used to optimise the diffusion period $\Delta$ (d20) for each compound. The 2D dstebpgp35 sequence was then used, based on the optimised $\Delta$ from the previous procedure and with $\delta$ = 4 ms, with gradient amplitude ranging from 2% to 85% with 16 points in between. Data were analysed using the T1T2 module in TOPSPIN 3.2, and plots were generated using the eddosy module.

## 2.5.2.1 In $D_2O$ (Table 2.3.2)




```
Current Data Parameters
NAME                  SMM1-049
EXPNO                       20
PROCNO                       1

F2 - Acquisition Parameters
Date_               20150322
Time                    23.20
INSTRUM                 avb500
PROBHD    5 mm PATXI 1H/
PULPROG          dstebpgp3s
TD                       65536
SOLVENT                    D2O
NS                          16
DS                           4
SWH                 10000.000 Hz
FIDRES                0.152588 Hz
AQ                    3.2767999 sec
RG                          144
DW                     50.000 usec
DE                      6.50 usec
TE                     298.0 K
D1                  3.00000000 sec
D16                 0.00020000 sec
D20                 0.40000001 sec
D21                 0.00500000 sec

======== CHANNEL f1 ========
SFO1                499.9827499 MHz
NUC1                        1H
P1                       9.61 usec
P2                      19.22 usec
PLW1                13.06200027 W

====== GRADIENT CHANNEL =====
GPNAM[6]          SMSQ10.100
GPNAM[7]          SMSQ10.100
GPNAM[8]          SMSQ10.100
GPNAM[9]          SMSQ10.100
GPZ6                   100.00 %
GPZ7                   -13.17 %
GPZ8                   -17.13 %
GPZ9                   -15.37 %
P19                    600.00 usec
P30                   2000.00 usec

F1 - Acquisition parameters
TD                          16
SFO1                 499.9827 MHz
FIDRES               322.497406 Hz
SW                     10.320 ppm
FnMODE                      QF

F2 - Processing parameters
SI                       32768
SF                  499.9800000 MHz
WDW                         EM
SSB          0
LB                      0.50 Hz
GB           0
PC                     10.00

F1 - Processing parameters
SI                          16
MC2                         QF
SF                  499.9800000 MHz
WDW                         no
SSB          0
LB           0 Hz
```

**Figure 2.5.3** DOSY NMR of aldehyde **2.1** in $D_2O$ (50 mM) (entry 1, Table 2.3.2)

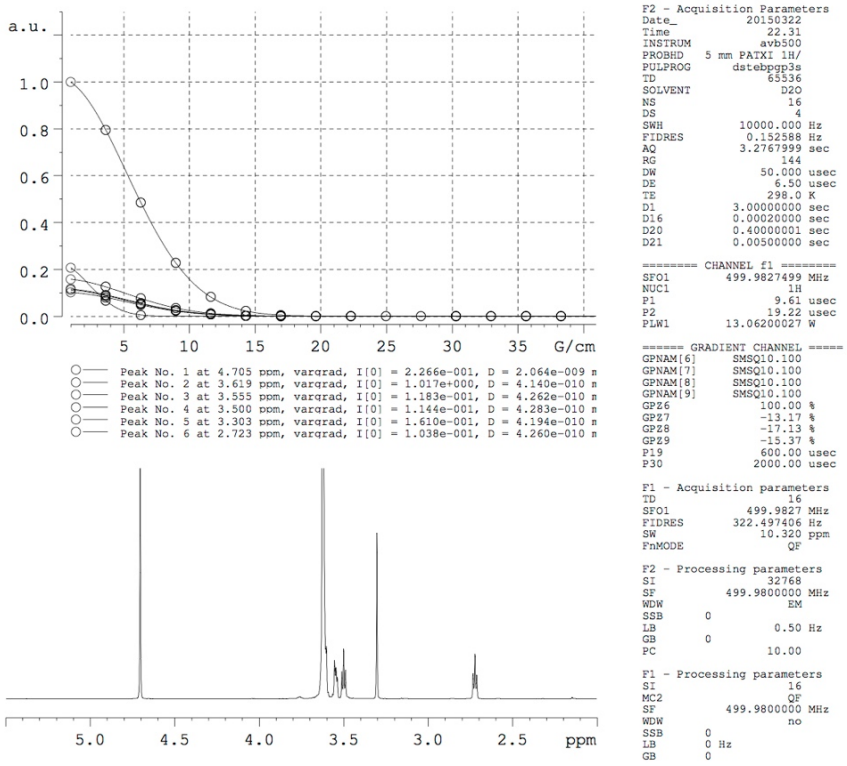



**Figure 2.5.4** DOSY NMR of amine **2.2a** in $D_2O$ (50 mM) (entry 2, Table 2.3.2)

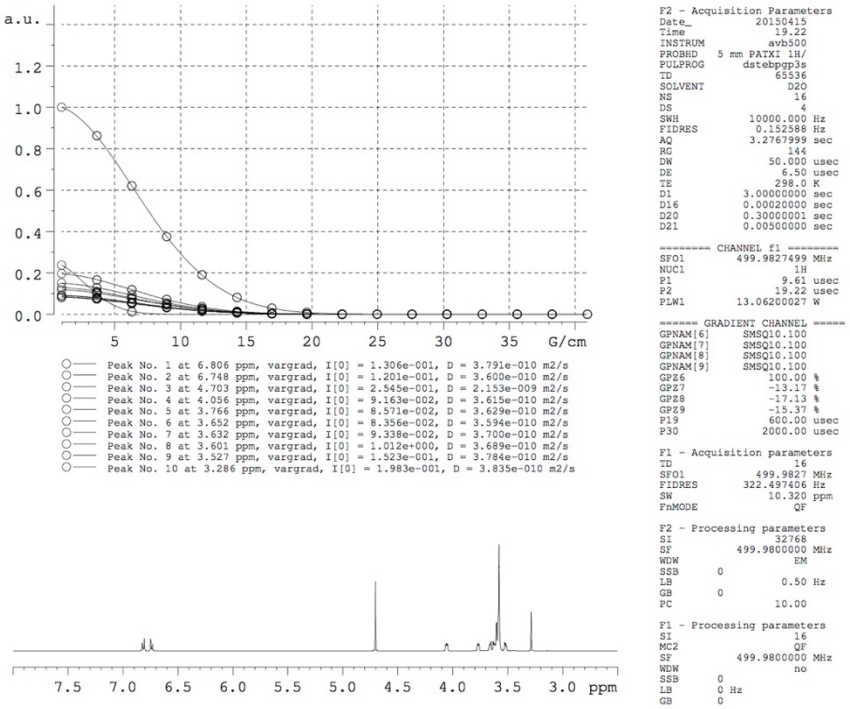



**Figure 2.5.5** DOSY NMR of amine **2.2b** in $D_2O$ (50 mM) (entry 3, Table 2.3.2)

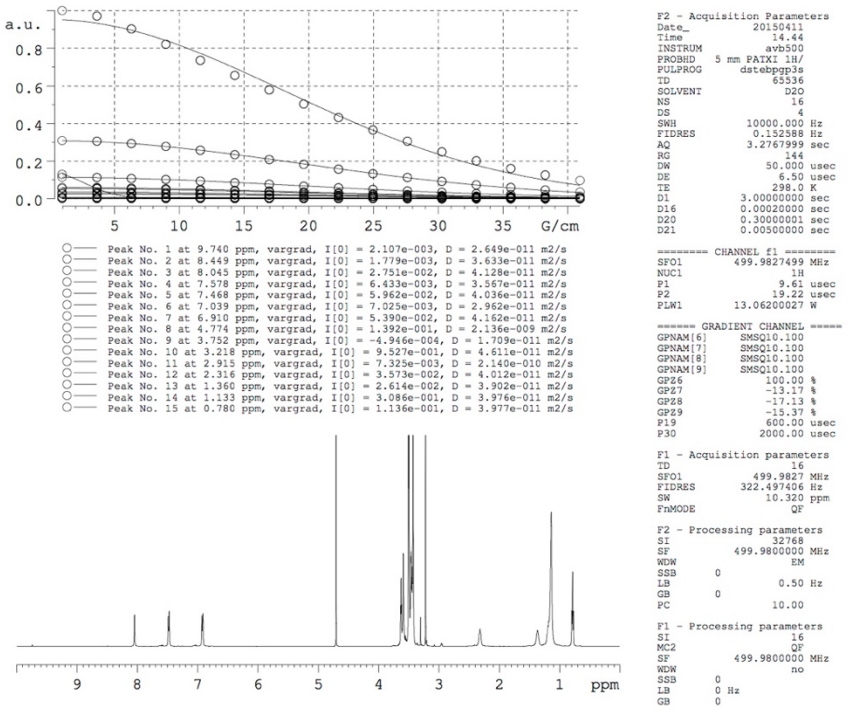



**Figure 2.5.6** DOSY NMR of imine **2.3a** in $D_2O$ (50 mM) (entry 4, Table 2.3.2)

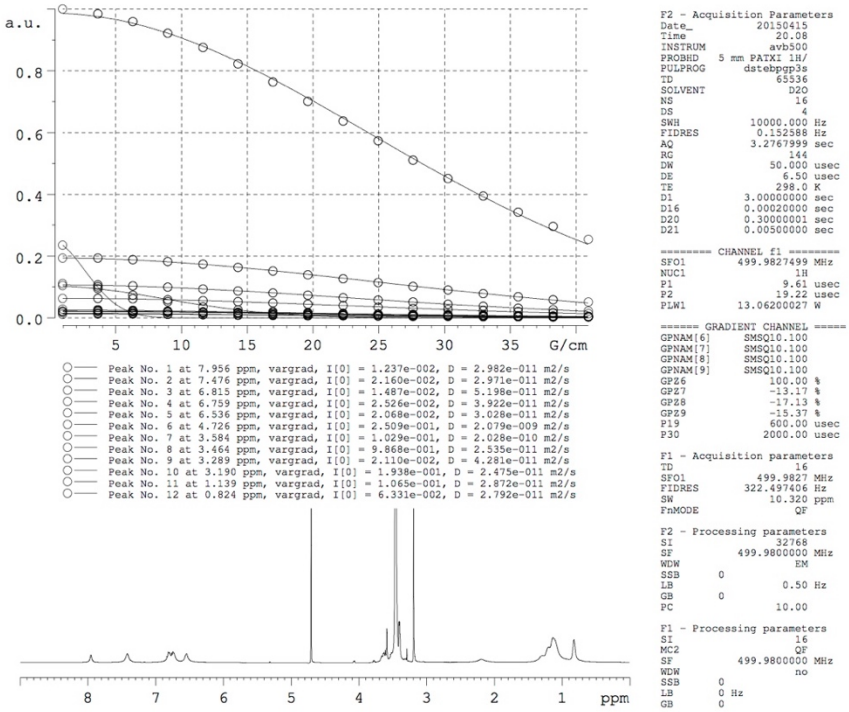



**Figure 2.5.7** DOSY NMR of imine **2.3b** in $D_2O$ (50 mM) (entry 5, Table 2.3.2)

## 2.5.2.2 In $d_3$-MeCN (Table 2.5.1)

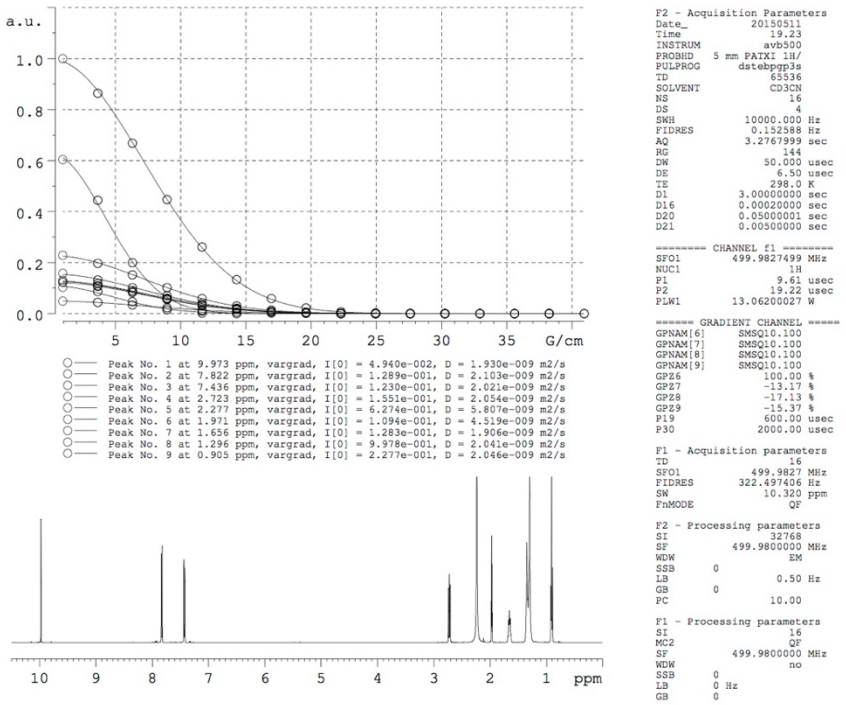



**Figure 2.5.8** DOSY NMR of aldehyde **2.1** in $d_3$-MeCN (50 mM) (Entry 1, Table 2.5.1)

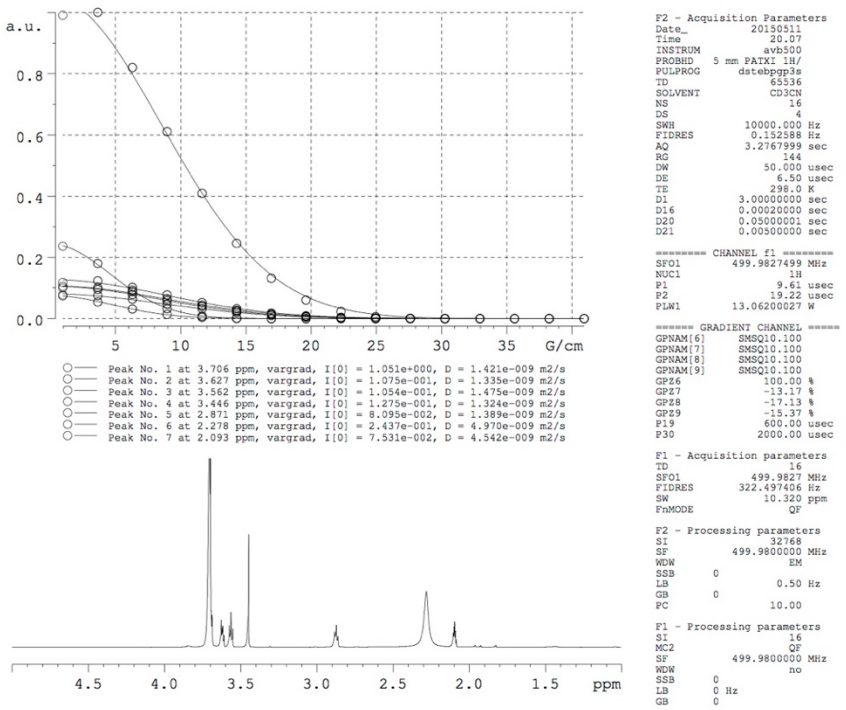



**Figure 2.5.9** DOSY NMR of amine **2.2a** in $d_3$-MeCN (50 mM) (Entry 2, Table 2.5.1)

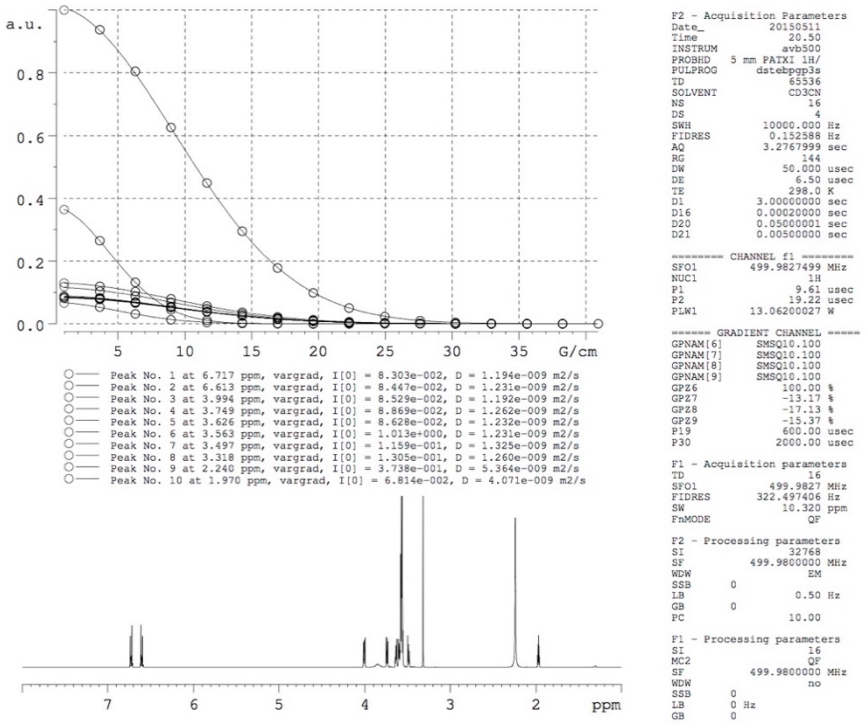



**Figure 2.5.10** DOSY NMR of amine **2.2b** in $d_3$-MeCN (50 mM) (Entry 3, Table 2.5.1)

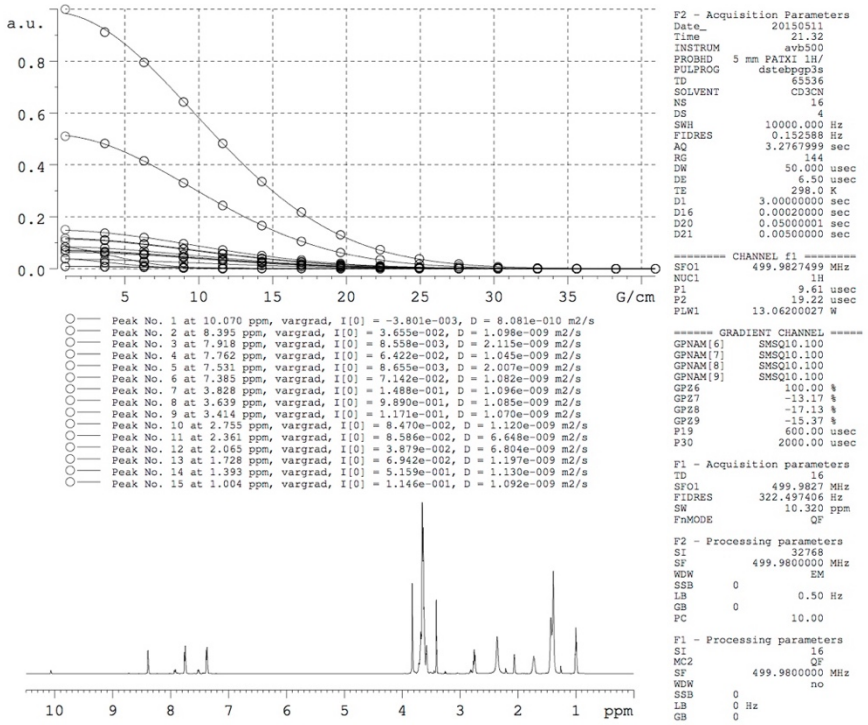



**Figure 2.5.11** DOSY NMR of equilibrated reaction amine **2.2a** + aldehyde **2.1**, both 50 mM in $d_3$-MeCN (Figure 2.3.1 and Entry 4, Table 2.5.1)

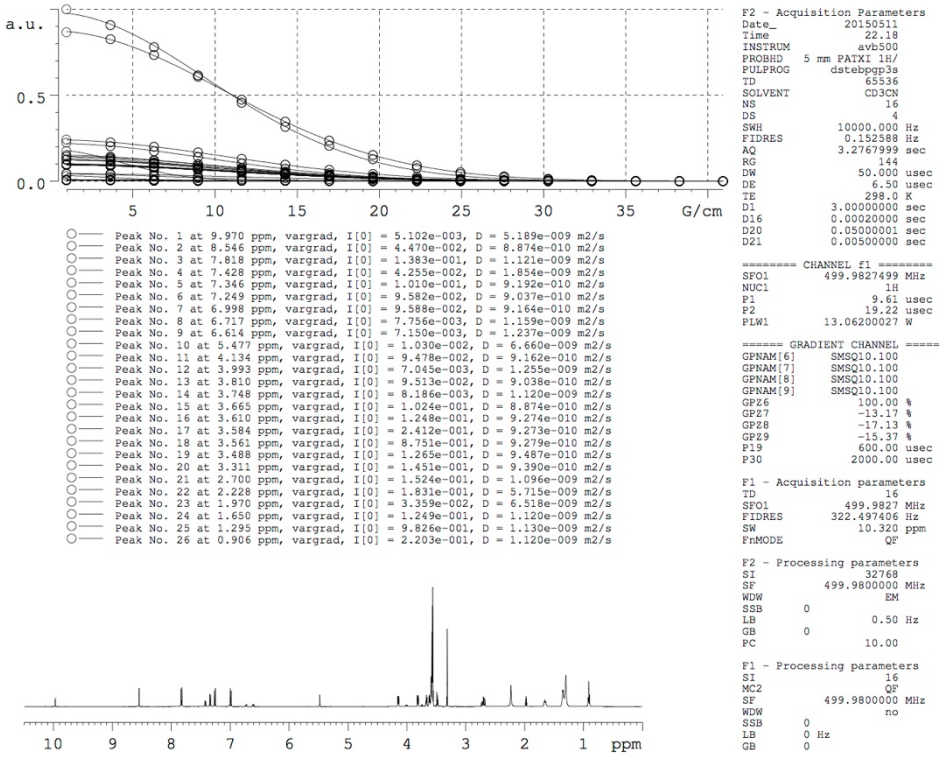



**Figure 2.5.12** DOSY NMR of equilibrated reaction amine **2.2b** + aldehyde **2.1**, both 50 mM in $d_3$-MeCN (Figure 2.3.1 and Entry 5, Table 2.5.1)

## 2.5.2.3 Diffusion coefficients in $d_3$-MeCN

| | | Diffusion coefficient D/$10^{-10}$ $m^2s^{-1}$ | | | | |
|---|---|---|---|---|---|---|
| Entry | Species present | **2.1** | **2.2a** | **2.2b** | **2.3a** | **2.3b** |
| 1 | **2.1** | 19.3 | - | - | - | - |
| 2 | **2.2a** | - | 13.9 | - | - | - |
| 3 | **2.2b** | - | - | 12.1 | - | - |
| 4 | Reaction: **2.1** + **2.2a** (Figure 2.3.1) | 20.6 | n.d.[a] | - | 11.0 | - |
| 5 | Reaction: **2.1** + **2.2b** (Figure 2.3.1) | 18.5 | - | 12.0 | - | 8.87 |

**Table 2.5.1** Diffusion coefficients taken from DOSY measurements in $d_3$-MeCN.

[a] Not determined due to overlapping peaks of species **2.2a**, **2.3a**.

## 2.5.2.4 Calculation of hydrodynamic radii

Using the diffusion coefficients (D) obtained by DOSY NMR, we used the Stokes-Einstein equation to calculate hydrodynamic radii:

$$R_h = \frac{kT}{6\pi\eta D}$$

For $H_2O$, $\eta$ = 0.894 × $10^{-3}$ $kgm^{-1}s^{-1}$ at 25 °C.

The data from the measurements in $D_2O$ are summarised in Tables 2.3.1 and 2.3.2.

## 2.5.3 NMR spectroscopy data

### 2.5.3.1 Imine **2.3a** in $D_2O$

A 50 mM solution of imine **2.3a** in $D_2O$ was prepared and its $^1H$ NMR spectrum was recorded every 15 minutes over a period of 15 hours (Figure 2.5.13). The sample showed extensive hydrolysis to **2.2a** and **2.1**. A $^1H$ NMR spectrum taken of the NMR sample 3 days after the experiment showed complete hydrolysis. No improvement in stability was observed at pD 12.45.

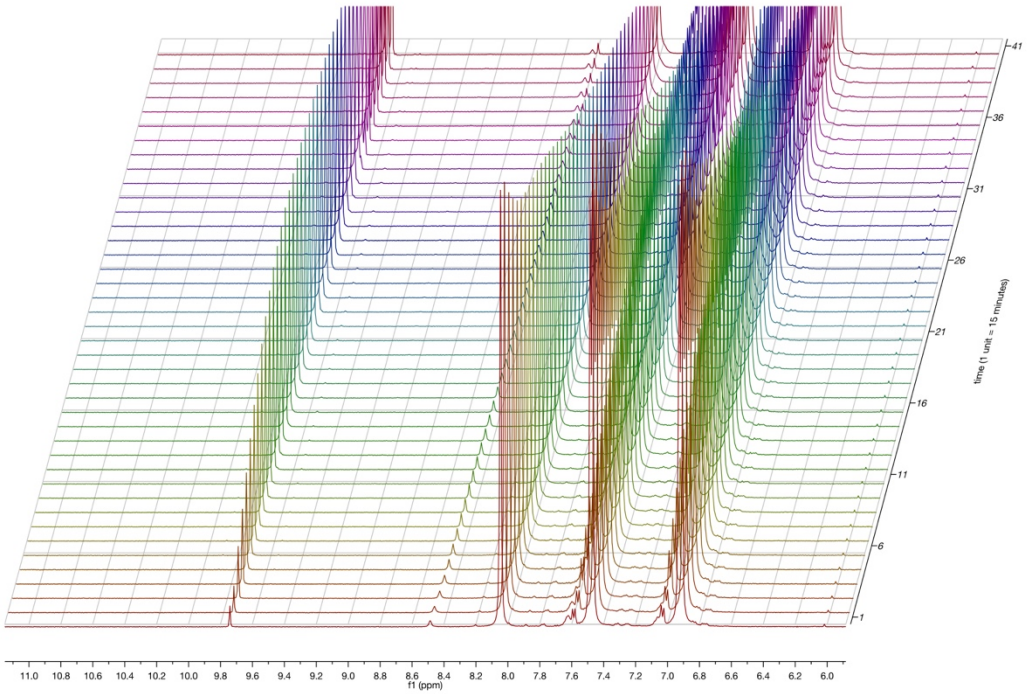



**Figure 2.5.13** $^1H$ NMR spectra in the region ~ 6.0–11.0 ppm of imine **2.3a** in $D_2O$ (50 mM) recorded every 15 minutes over 15 hours.

## 2.5.3.2 Imine **2.3b** in $D_2O$

A 50 mM solution of imine **2.3b** in $D_2O$ was prepared and its $^1H$ NMR spectrum was recorded every 15 minutes over a period of 15 hours (Figure 2.5.14). The sample showed complete hydrolysis to **2.2b** and **2.1**. The imine **2.3b** was, however, stable to hydrolysis at pD 12.45 over at least 13 hours.

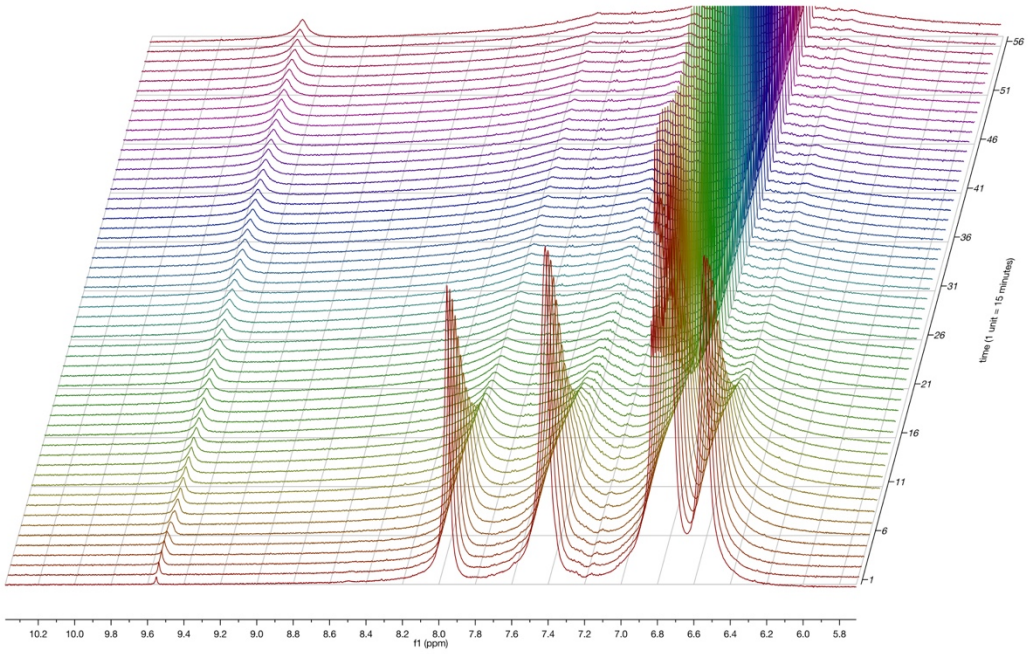
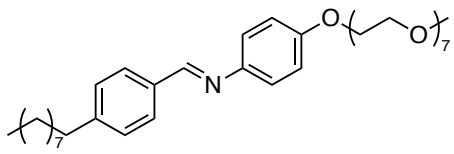



**Figure 2.5.14** $^1H$ NMR spectra in the region ~ 5.8–10.2 ppm of imine **2.3b** in $D_2O$ (50 mM) recorded every 15 minutes over 15 hours.

## 2.5.4 DLS data

### 2.5.4.1 Imine **2.3b**



Imine **2.3b** was dissolved in MilliQ $H_2O$ (50 mM). DLS measurements were recorded on a DLS Viscotek 802 instrument. The solution was filtered using syringe filters PTFE (0.2 µm, 13 mm diameter) from Camlab prior to measurement.

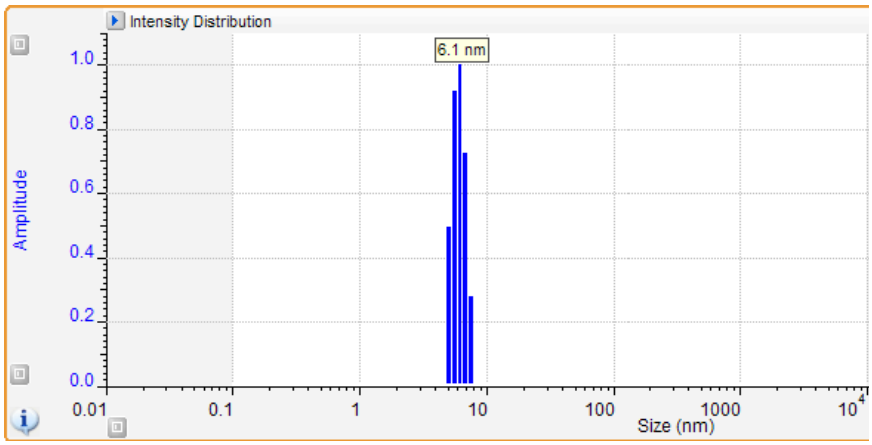



**Figure 2.5.15** DLS measurement for imine **2.3b** (50 mM in $H_2O$). Size distribution by intensity.

## 2.5.5 iSCAT: sample preparation and image processing

All measurements were made under the supervision of Dr. Andrew Bissette, Fletcher group.

Coverslips were washed with distilled $H_2O$, EtOH, and again with distilled $H_2O$ prior to sonication for 15 minutes in 0.1 M HCl and further washing with MilliQ $H_2O$. After drying under $N_2$ (g) a silicone gasket washed with MilliQ $H_2O$ and EtOH, obtained from grace biolabs, with wells of 4.5 mm diameter, 1.7 mm depth, was placed on the coverslip surface. Individual experiments were performed in these individual wells.

All components were filtered using syringe filters PTFE (0.2 μm, 13 mm diameter) from Camlab prior to measurement.

Raw data was recorded at 1.0 kHz with 333× magnification (31.8 nm/pixel) over an area of 8.1 $\mu m^2$ and was processed with background subtraction *via* temporal median filtering. Large artefacts were removed using a size 5 filter (in-house software).

All images are the average of 100 frames with 2 × 2 pixel binning (*i.e.* 63.6 nm/pixel). Images were generated using ImageJ (Fiji distribution) and in-house software. Further details of image processing can be found in a previous publication.[6] The bar below each image represents the contrast range; the individual contrast of each aggregate provides a measure of its size.

### 2.5.5.1 Aldehyde **2.1**

Neat aldehyde **2.1** (3 μL) was added to MilliQ $H_2O$ (10 μL) (Figure 2.5.16).




**Figure 2.5.16** iSCAT image of aldehyde **2.1**. Scale bar = 1 μm.

### 2.5.5.2 Amine **2.2b**

A solution of amine **2.2b** in MilliQ $H_2O$ (100 mM; 10 μL) was added to MilliQ $H_2O$ (10 μL) (Figure 2.5.17).

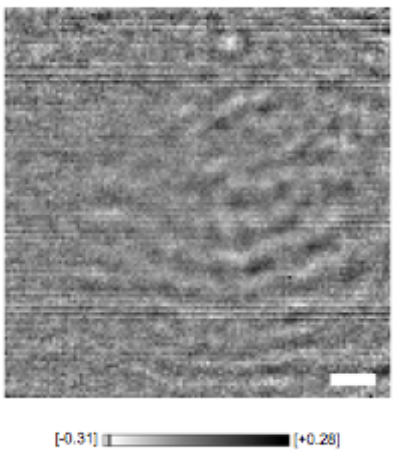



**Figure 2.5.17** iSCAT image of amine **2.2b.** Scale bar = 1 μm.

### 2.5.5.3 Imine **2.3b**

A solution of Imine **2.3b** in MilliQ $H_2O$ (5 mM; 5 µL) was added to MilliQ $H_2O$ (20 µL) to result in a sample of imine **2.3b** ~ 1 mM in MilliQ $H_2O$ (imine **2.3b** not very soluble, so approximate). The so-obtained images of aggregate binding are shown in Figure 2.3.2.

The particles highlighted in Figure 2.3.2, with their contrast recorded in Table 2.5.2, represent both frequently recorded particles (contrast ~ 0.18) and rare, larger aggregates (contrast > 0.3), which are easier to visualise by eye and so are over-represented by these images. The probability density function we obtain (Figure 2.5.18) is consistent with our previous measurement of micelles by iSCAT.[6]

| Image | Particle | Contrast (%) |
|---|---|---|
| **A** | **1** | 0.43 |
| | **2** | 0.28 |
| | **3** | 0.34 |
| | **4** | 0.18 |
| **B** | **5** | 0.23 |
| | **6** | 0.64 |
| | **7** | 0.27 |
| | **8** | 0.85 |
| | **9** | 0.25 |

**Table 2.5.2** Contrast of particles in Figure 2.3.2.

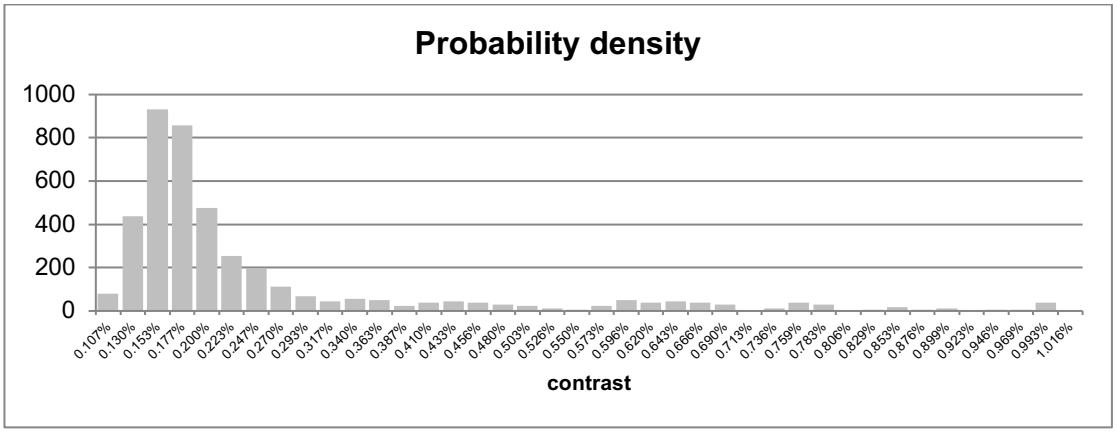
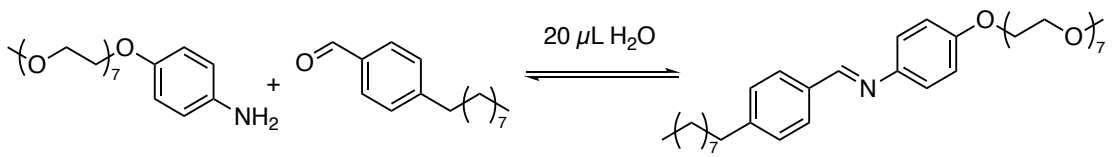



**Figure 2.5.18** Probability density function of the contrast recorded in images A and B (Figure 2.3.2).

## 2.5.5.4 Reaction on a microscope coverslip

MilliQ $H_2O$ (10 µL) was added to the well under observation, followed by neat aldehyde **2.1** (13 µL). A solution of amine **2.2b** in MilliQ $H_2O$ (100 mM; 10 µL) was then added to the well. No micelle formation was observed between amine **2.2b** and aldehyde **2.1** (Figure 2.5.19).




**2.2b**
$c_i$ = 50 mM
1.0 eq.

**2.1**
13 µL
~ 13.0 eq.

**2.3b**

**Figure 2.5.19** Reaction on a microscope coverslip between amine **2.2b** and aldehyde **2.1**.

## 2.6 References


1. Morrow, S. M., Bissette, A. J. & Fletcher, S. P. Potential for minimal self-replicating systems in a dynamic combinatorial library of equilibrating imines. *Tetrahedron* **73,** 5005–5010 (2017).
2. Li, J., Nowak, P. & Otto, S. Dynamic Combinatorial Libraries: From Exploring Molecular Recognition to Systems Chemistry. *J. Am. Chem. Soc.* **135,** 9222–9239 (2013).
3. Otto, S. Dynamic Molecular Networks: From Synthetic Receptors to Self-Replicators. *Acc. Chem. Res.* **45,** 2200–2210 (2012).
4. Nguyen, R., Allouche, L., Buhler, E. & Giuseppone, N. Dynamic Combinatorial Evolution within Self-Replicating Supramolecular Assemblies. *Angew. Chem. Int. Ed.* **48,** 1093–1096 (2009).
5. Bissette, A. J., Odell, B. & Fletcher, S. P. Physical autocatalysis driven by a bond-forming thiol–ene reaction. *Nat. Commun.* **5,** 4607 (2014).
6. Ortega-arroyo, J., Bissette, A. J., Kukura, P. & Fletcher, S. P. Visualization of the spontaneous emergence of a complex, dynamic, and autocatalytic system. *Proc. Natl. Acad. Sci.* **113,** 11122–11126 (2016).
7. Post, E., Bissette, A. & Fletcher, S. P. Self-reproducing micelles coupled to a secondary catalyst. *Chem. Commun.* **54,** 8777–8780 (2018).
8. Ortega-Arroyo, J. & Kukura, P. Interferometric scattering microscopy (iSCAT): new frontiers in ultrafast and ultrasensitive optical microscopy. *Phys. Chem. Chem. Phys.* **14,** 15625–36 (2012).
9. Xu, S. & Giuseppone, N. Self-duplicating amplification in a dynamic combinatorial library. *J. Am. Chem. Soc.* **130,** 1826–1827 (2008).
10. Jouault, N., Nguyen, R., Rawiso, M., Giuseppone, N. & Buhler, E. SANS, SAXS, and light scattering investigations of pH-responsive dynamic combinatorial mesophases. *Soft Matter* **7,** 4787 (2011).
11. Nguyen, R., Buhler, E. & Giuseppone, N. Dynablocks: Structural Modulation of Responsive Combinatorial Self-Assemblies at Mesoscale. *Macromolecules* **42,** 5913–5915 (2009).
12. Nguyen, R. *et al.* Core-shell inversion by pH modulation in dynamic covalent micelles. *Soft Matter* **10,** 3926–3937 (2014).
13. Nguyen, R. *et al.* Autopoietic Behavior of Dynamic Covalent Amphiphiles. *Chem. Eur. J.* **24,** 17125–17137 (2018).
14. Koide, Y. *et al.* Development of Novel EDG3 Antagonists Using a 3D Database Search and Their Structure-Activity Relationships. *J. Med. Chem.* **45,** 4629–4638 (2002).
15. Krężel, A. & Bal, W. A formula for correlating pKa values determined in $D_2O$ and $H_2O$. *J. Inorg. Biochem.* **98,** 161–166 (2004).

# 3

## A Chemically Fuelled Out-of-Equilibrium Replicator

The results of this chapter have been published in *Nature Communications*.[1]

## 3.1 Introduction

The behaviour of small molecule and supramolecular replicators in dynamic combinatorial libraries, as explored in Chapters 1 and 2, has some analogy with the dynamic behaviour of complex biological networks, but the closed system still heads towards the equilibrium or kinetically trapped position.

In order to approach the complexity of living systems, replication must be established in out-of-equilibrium formats.[2–6] Out-of-equilibrium dynamics characterise life: high energy, dissipative states are maintained by the consumption of chemical fuel. Their persistence and function are no longer determined by their thermodynamic stability and they are controllable in time. Since a process of evolution demands movement towards species of ever increasing 'complexity' and order, it is clear that the study of replication under out-of-equilibrium conditions is key.[7–13] However, the study of replicating molecules and supramolecular species under this regime is underexplored,[14–17] and the realisation of any out-of-equilibrium system is non-trivial.

## 3.2 The discovery of a metastable physical replicator

The design for an out-of-equilibrium replicator was detailed in Chapter 1 (Figure 1.4.3, page 38).

First, we require the autocatalytic formation of a replicator followed by its destruction to a thermodynamic, non-replicating state in a closed system (Figure 1.4.3a,b). The non-trivial translation to an out-of-equilibrium system is the maintenance of this transiently-formed and metastable product by the resupply of starting materials under open system conditions (Figure 1.4.3c,d). Though simple in appearance, neither process is well precedented, and there are few convincing demonstrations of out-of-equilibrium replication.

The system in Chapter 2, exploring a process of physical replication in a DCL, had been compromised by a lack of reactivity. It was in fact *via* exploration of another reaction commonly exploited in dynamic combinatorial libraries that we discovered a reaction which fitted the desired profile.

### 3.2.1 Surfactant formation by thiol-disulfide exchange

Our interest in reversibly-formed surfactants in dynamic combinatorial libraries had led us to consider a thiol-disulfide exchange reaction for the formation of a surfactant molecule containing a labile, reversibly-formed bond. This reaction had been studied extensively by the group of Otto in the context of molecular replication in dynamic combinatorial libraries.[18,19]

Reaction between phase-separated components octanethiol **3.1** and hydrophilic disulfide 5,5'-Dithiobis(2-nitrobenzoic acid) (DTNB) **3.2** by thiol-disulfide exchange was selected for study (Figure 3.2.1). The choice of DTNB **3.2** was inspired by the extensive literature on the reactivity of DTNB **3.2** in aqueous media, with thorough investigation into the kinetics of the exchange reaction.[20–23] Octanethiol was chosen to give a good balance between low solubility in water, to ensure phase separation, and sufficient nucleophilicity, to ensure that the reaction would not be too slow.

Under the basic conditions required for thiol-disulfide exchange the carboxylic acid group of amphiphilic **3.4** would be deprotonated and therefore act as a suitable water-soluble head group, inducing aggregation (Figure 3.2.1).

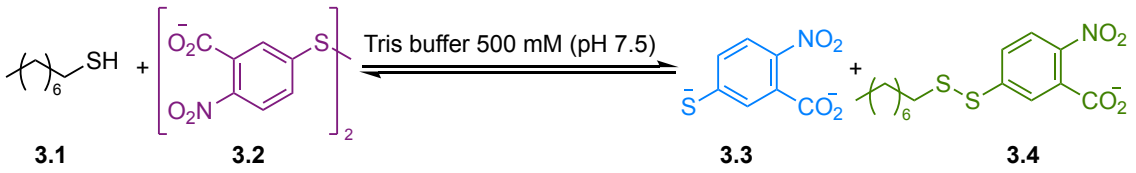



**Figure 3.2.1** Thiol-disulfide exchange between **3.1** and **3.2** would result in the production of surfactant **3.4** at equilibrium.

Aggregation of the surfactant into micelles would result in increased mixing between the phase-separated components, increasing the rate of the reaction between **3.1** and **3.2** to form **3.4**. The micelles would catalyse the reaction to form their own components and would therefore replicate.

### 3.2.2 Surfactant characterisation

The surfactant product **3.4** derived from octanethiol **3.1** (Figure 3.2.1) was synthesised under homogeneous conditions and was found to be soluble at pH 7.5 in Tris buffer (500 mM). Its aggregation properties were probed by dynamic light scattering (DLS), which revealed the formation of micelles of hydrodynamic diameter 15 – 20 nm, depending on concentration (Section 3.5.2.2). The critical micelle concentration (cmc) of the pure surfactant was determined by ring tensiometry as approximately 0.2 mM, a relatively low value that promised the ready observation of autocatalysis (Section 3.5.2.3).

### 3.2.3 A metastable replicator

The kinetics of the reaction were first examined in an experiment shown in Figure 3.2.2, following the reaction by Ultra Performance Liquid Chromatography (UPLC). In stark contrast to the system based on imine bond formation in Chapter 2, the formation of the mixed disulfide **3.4** was observed under biphasic conditions (green squares, Figure 3.2.2b).

A test for autocatalysis was conducted by seeding the reaction with the mixed disulfide surfactant **3.4** (Figure 3.2.2a and Figure 3.2.3). If the product **3.4** is an autocatalyst then seeding the reaction should result in an enhancement in reaction rate over the control reaction. Excitingly, in the reaction seeded with product **3.4**, both the rate of starting material **3.2** consumption and product **3.4** formation were markedly increased (solid *vs.* dotted lines, Figure 3.2.3;

comparison of initial rates in Section 3.5.4.1.1). It appeared that the reaction was autocatalytic. There was no obvious lag period, but this was indicative both of a relatively fast background reaction, as well as the very low cmc of **3.4**.

Further examination of the entire reaction profile (Figure 3.2.2b) revealed that the production of disulfide **3.4** did not match the production of thiolate **3.3**. This was the first indication of the thermodynamic instability of the disulfide surfactant **3.4** to the production of thiolate **3.3** and disulfide **3.5** (Figure 3.2.2a) and the first step towards the realisation of an out-of-equilibrium system.

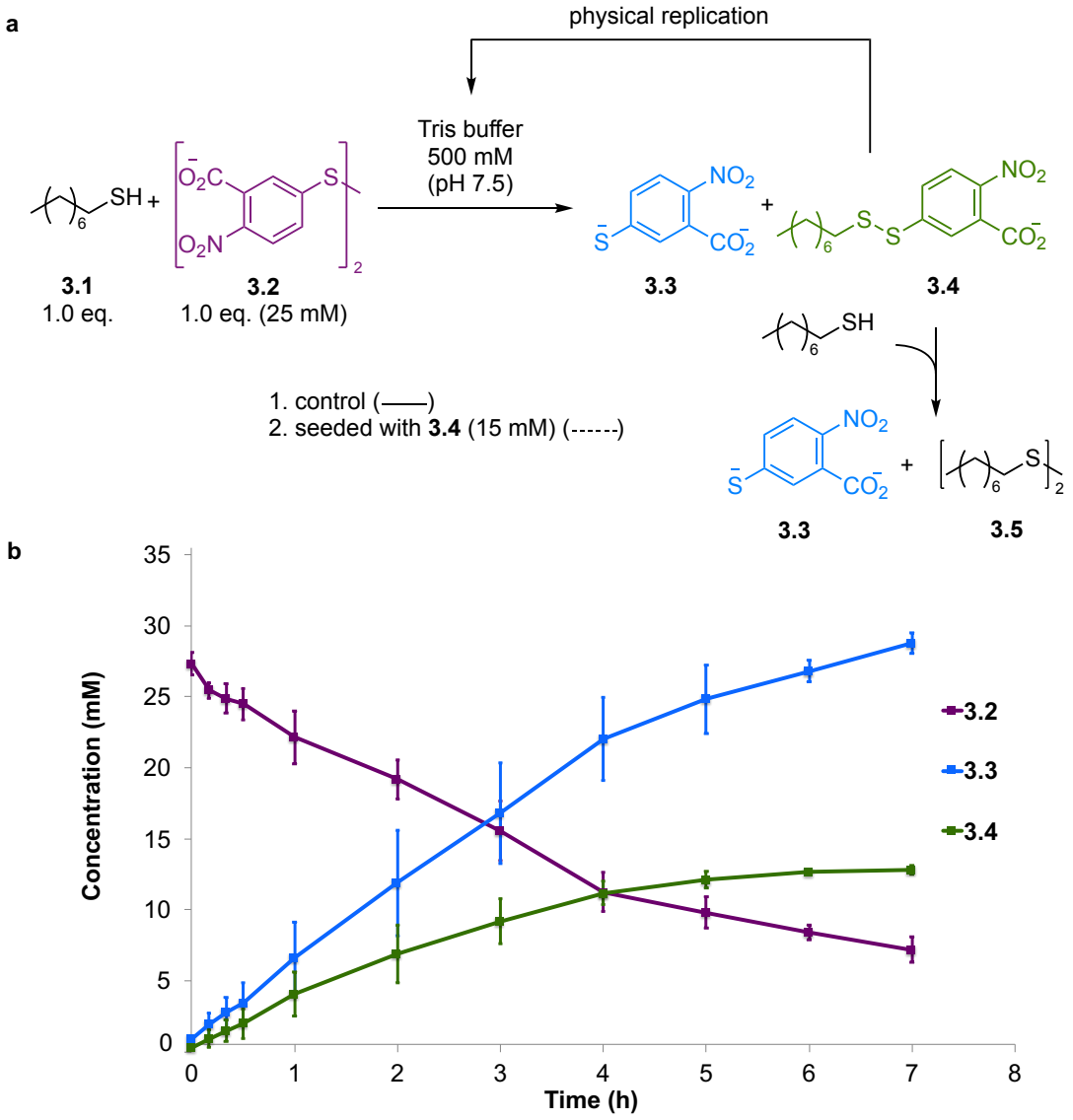



**Figure 3.2.2 a** Autocatalytic thiol-disulfide exchange between **3.1** and **3.2** produces surfactant **3.4** and thiolate **3.3**. A second thiol-disulfide exchange forms disulfide **3.5** and thiolate **3.3**. Two sets of experiments were conducted: one containing starting materials **3.1** and **3.2** only (control), and one seeded with disulfide **3.4**. Data for the seeded reaction are shown in Figure 3.2.3. **b** Concentration of all UV active components in the control reaction. The concentration of reaction components was monitored by UPLC. Each plotted point is the average of three entire experimental repeats and the error bars represent the standard deviation (n=3). Lines between points are drawn to guide the eye.

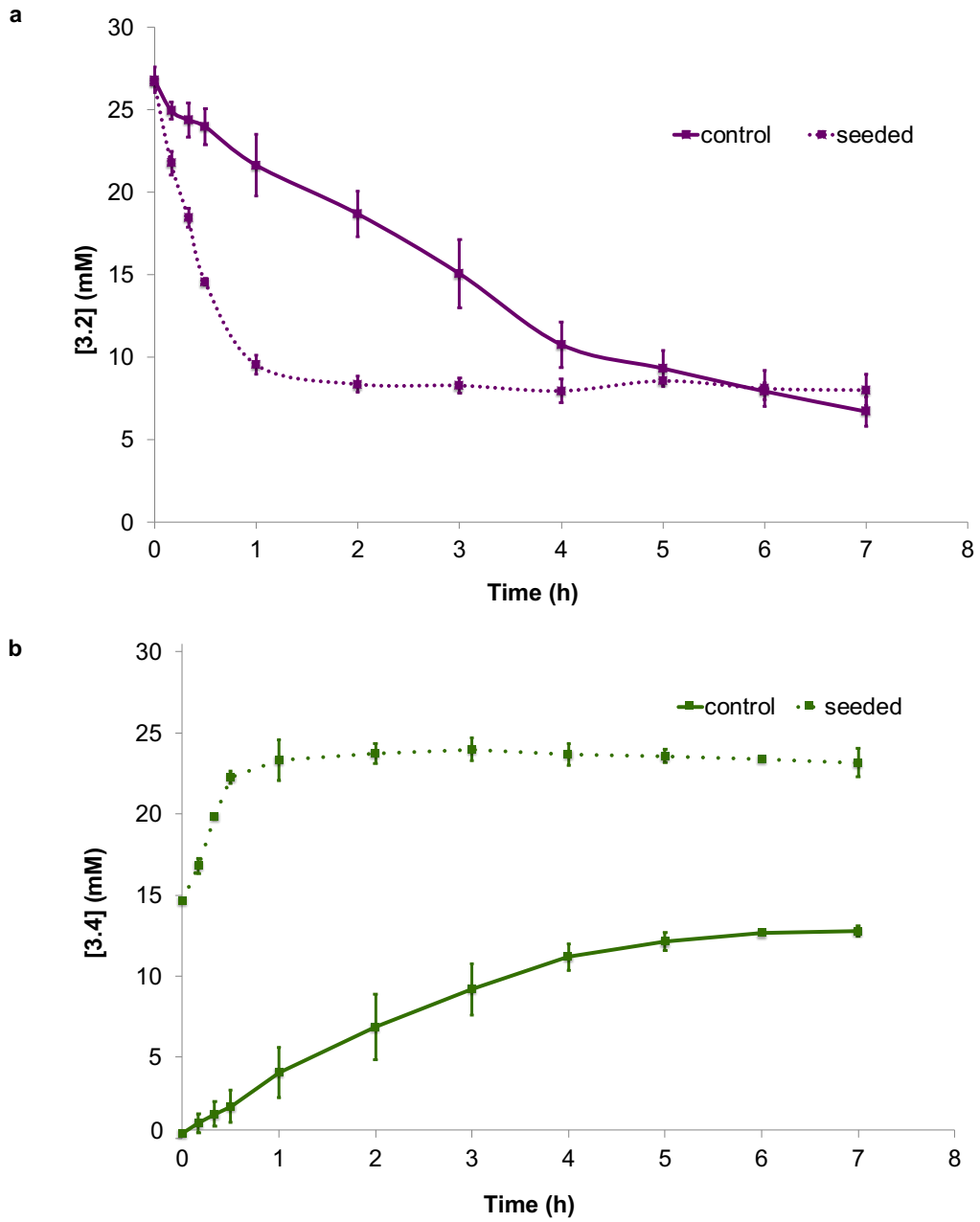



**Figure 3.2.3** Reaction profiles for control and seeded reactions conducted as in Figure 3.2.2a: **a** Concentration of **3.2**. **b** Concentration of **3.4**. The concentration of reaction components was monitored by UPLC. Each plotted point is the average of three entire experimental repeats and the error bars represent the standard deviation (n=3). Lines between points are drawn to guide the eye. Initial rates extracted from these experiments are shown in Section 3.5.4.1.1.

The kinetics and equilibrium position of the reaction under conditions of excess octanethiol **3.1** were therefore examined (Figure 3.2.4). Under these conditions, the mixed disulfide **3.4** built up in concentration before subsequent, slower destruction to form thiolate **3.3** and hydrophobic disulfide **3.5**, the thermodynamic minimum of the system. The thermodynamic drive to these products could be ascribed primarily to the electron-withdrawing groups on thiolate **3.3**, which stabilise the anion and make it a good leaving group and poor nucleophile.[23]

Other attempts to establish physical replicators under out-of-equilibrium regimes,[24,25] including our own group's study of metastable surfactant formation by alkene metathesis,[26] relied on the thermodynamic instability and destruction of the physical replicator in a closed system, or the removal of material from the system. The discovery of the thermodynamic instability of surfactant **3.4** was therefore ideal for the development of a dissipative out-of-equilibrium replicator.

To test whether the reaction remained autocatalytic under these conditions, further control and seeding experiments were performed under conditions of excess thiol (Figures 3.2.4 and 3.2.5; comparison of initial rates in Section 3.5.4.1.1). Considering the very low cmc of our surfactant (0.2 mM), reactions were also conducted at much reduced concentrations of product, testing its catalytic power and the relationship between initial reaction rate and seed concentration (Figure 3.2.6 and 3.2.7). Acceleration of the reaction was still observed (though it was less evident under conditions of excess octanethol **3.1**) and the rate was increased with increasing quantity of seed (Figures 3.2.5, 3.2.6 and 3.2.7).

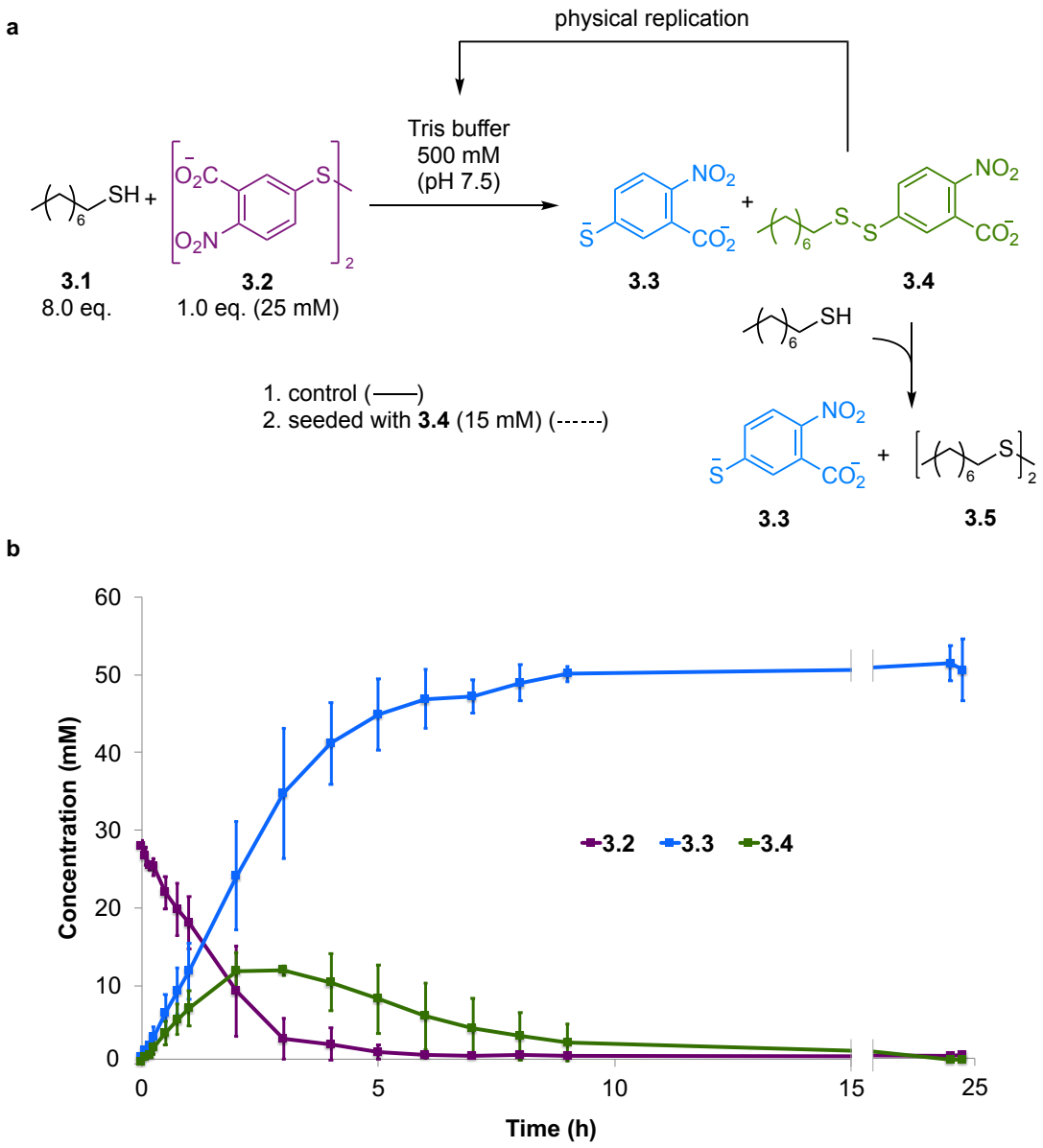



**Figure 3.2.4 a** Control and seeded reactions conducted with 8.0 equivalents of octanethiol **3.1**. **b** Concentration of all UV active species over the full course of the control reaction. Surfactant **3.4** is unstable towards attack by **3.1** to give waste products **3.3** and **3.5**; the equilibrium position of the system is for complete degradation of **3.4**. The concentration of reaction components was monitored by UPLC. Each plotted point is the average of three entire experimental repeats and the error bars represent the standard deviation (n=3). Lines between points are drawn to guide the eye.

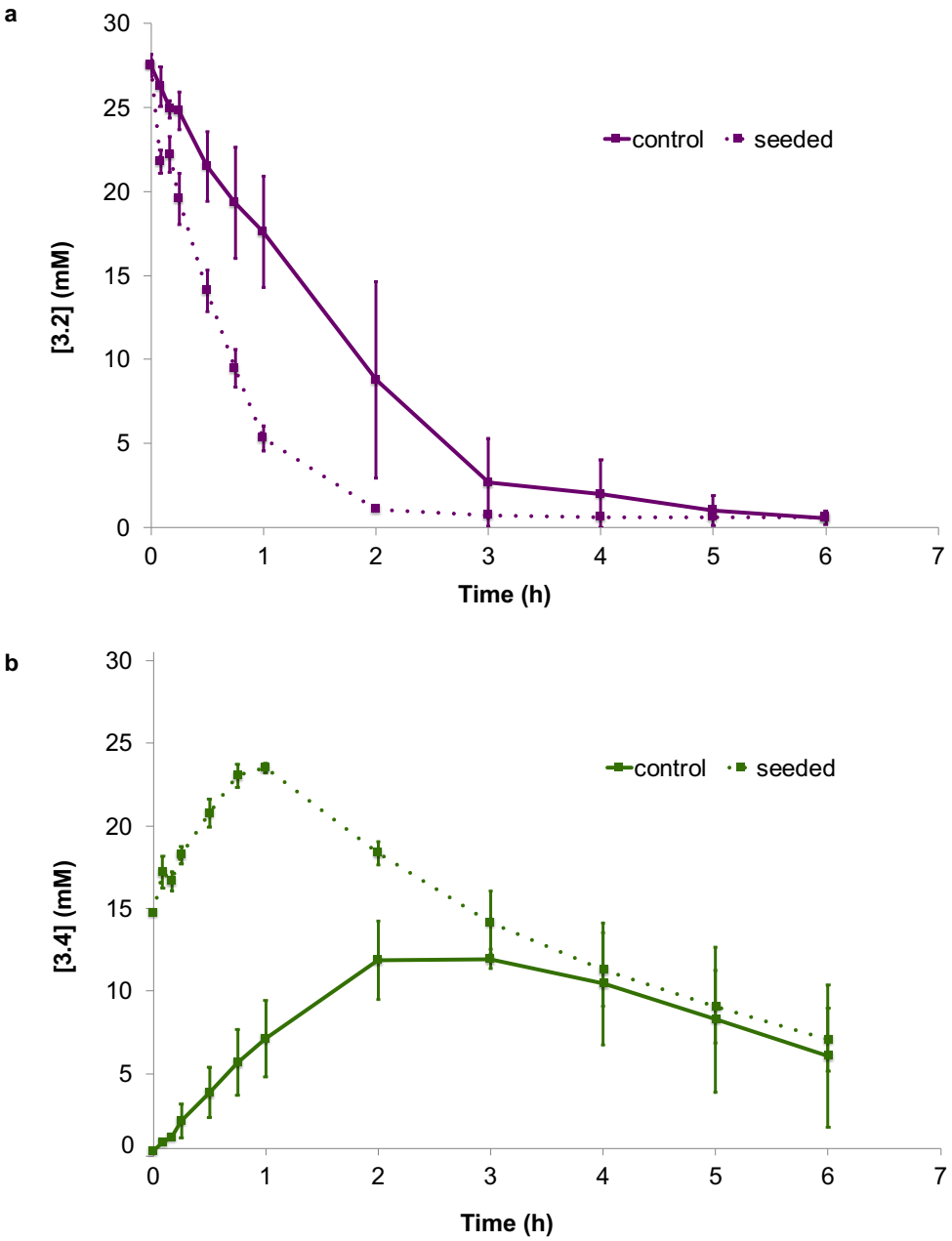
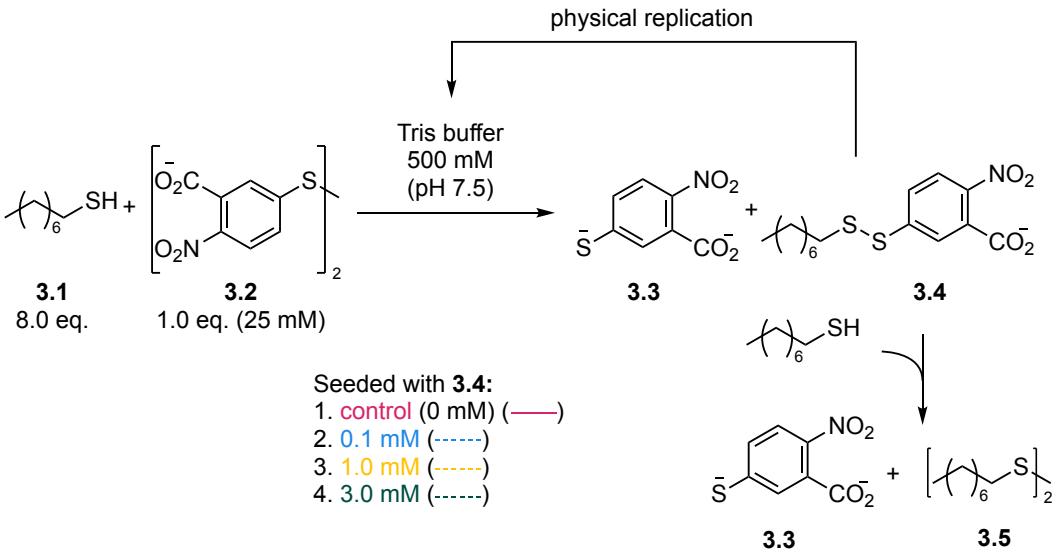



**Figure 3.2.5** Reaction profiles for control and seeded reactions conducted as Figure 3.2.4a: **a** Concentration of **3.2**. **b** Concentration of **3.4**. The concentration of reaction components was monitored by UPLC. Each plotted point is the average of three entire experimental repeats and the error bars represent the standard deviation (n=3). Lines between points are drawn to guide the eye. Initial rates extracted from these experiments are shown in Section 3.5.4.1.1.



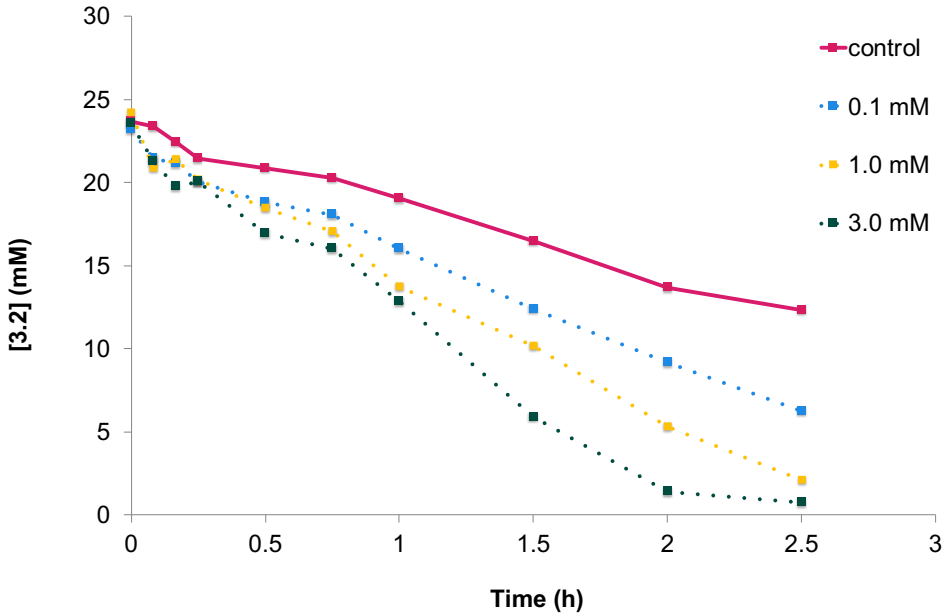




**Figure 3.2.6 a** Additional seeded reactions conducted at lower initial concentration of **3.4**. **b** Concentration of **3.2** over the course of reaction with varying quantity of seeded **3.4** (0 mM, 0.1 mM, 1.0 mM, and 3.0 mM). The concentration of reaction components was monitored by UPLC. The plots are the reaction profiles of single experiments. Lines between points are drawn to guide the eye. Initial rates extracted from these experiments are shown in Section 3.5.4.2.1.

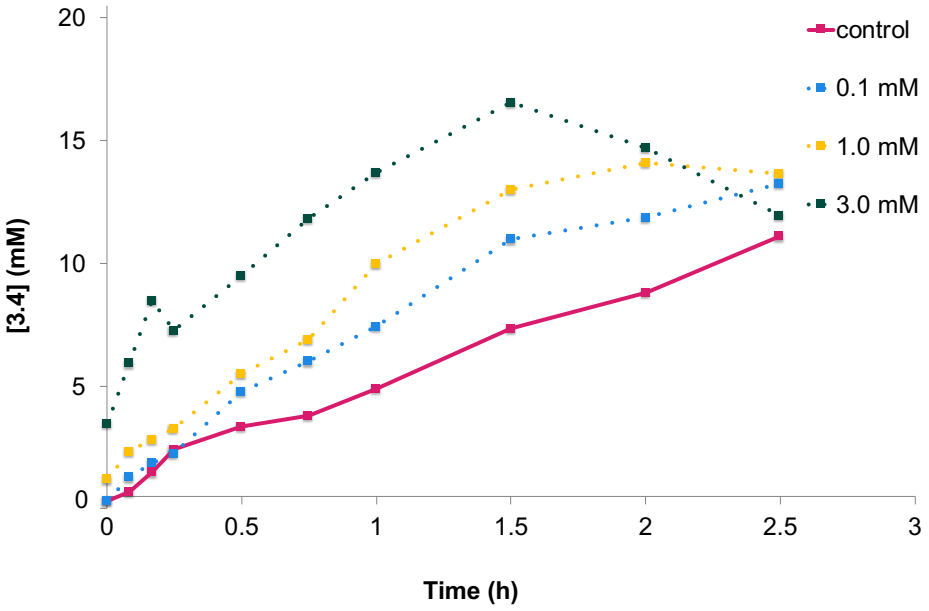



**Figure 3.2.7** Concentration of **3.4** over the course of reaction with varying quantity of seeded **3.4** (0 mM, 0.1 mM, 1.0 mM, and 3.0 mM), conducted as in Figure 3.2.6a. The concentration of reaction components was monitored by UPLC. The plots are the reaction profiles of single experiments. Lines between points are drawn to guide the eye. Initial rates extracted from these experiments are shown in Section 3.5.4.2.1.

Mechanistic investigation into the second thiol-disulfide exchange, forming thermodynamic products **3.3** and **3.5**, was also conducted (Section 3.5.4.4). In contrast to surfactant formation the destruction step did not appear to be accelerated by aggregate formation. Thus, a rapid autocatalytic step built up the replicator before the slower destruction step took over, consuming the surfactant and forming thermodynamic products **3.3** and **3.5**.

## 3.3 Out-of-equilibrium replication

According to Figure 1.4.3c,d (page 38), maintenance of the transiently formed replicator would require the continuous fuelling of the system and the resupply of otherwise limited starting materials. The external supply of starting materials in the acyclic system depicted in Figure 1.4.3c had linked previous experimental realisations of out-of-equilibrium physical replicators discussed in Chapter 1.

The nature of our reaction, however, allowed us to consider a simpler and neater system in which starting materials for the production of the replicator could be regenerated *in situ*.

### 3.3.1 System design: a cyclic system

Figure 3.3.1 depicts a progression from the system in Figure 1.4.3c,d (page 38) in which the starting materials for replicator construction are not resupplied by an external source, but are instead regenerated within the system from waste products by a smaller chemical fuel. A system like this has much greater analogy to the out-of-equilibrium systems of biology. In microtubule formation, for example, GTP-tubulin is regenerated from “waste” GDP-tubulin for the continued production of microtubule components (Figure 1.4.1, page 32). Furthermore, this recycling process avoids the build up of increasing quantities of waste products, which could otherwise disturb the out-of-equilibrium system.[6,27]

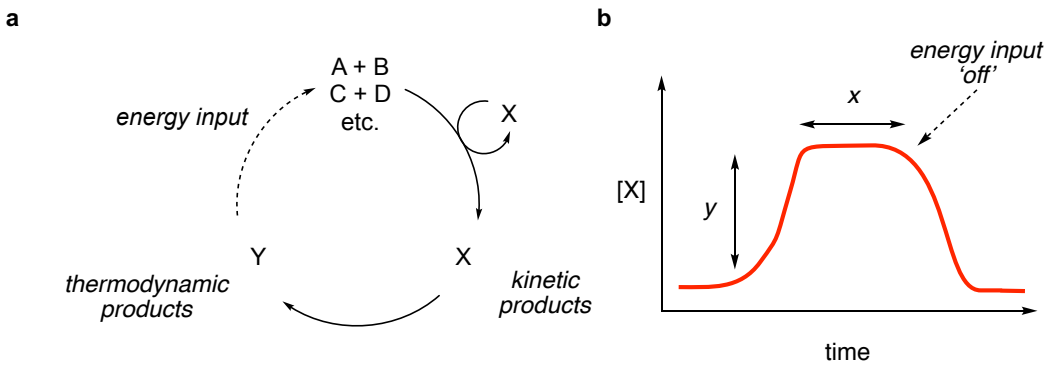



**Figure 3.3.1 a** In this open system, precursors for replicator formation are regenerated *in situ* by the external supply of energy. **b** The kinetic product X may be maintained out-of-equilibrium and its concentration (*y*) and persistence in time (*x*) controlled by fuel supply.

The detailed design and components of our system are depicted in Figure 3.3.2. High energy materials for the building of the surfactant would be generated *via* a simple oxidation reaction of waste products of the system. New batches of ready-made starting material would not be required and switching on the cycle by the continuous addition of fuel would enable the replicator to persist and retain replicator function. The design was akin to metabolic cycles as observed in biology.[28,29] Notably, in this system octanethiol **3.1** is not regenerated and two equivalents are consumed in each cycle. It is therefore present in excess from the beginning of the reaction and could be considered as a fuel source itself.

The effective irreversibility of each reaction, driven by the formation of thiolate **3.3**, would provide an important directionality for the replicator cycle and the system as a whole.[30] The clockwise and continuous flux of substrates in the cycle (Figure 3.3.2) reflects the system's desire to regain the equilibrium position,

moving in the direction of thermodynamic products which would be continuously removed from the system by recycling.[6]

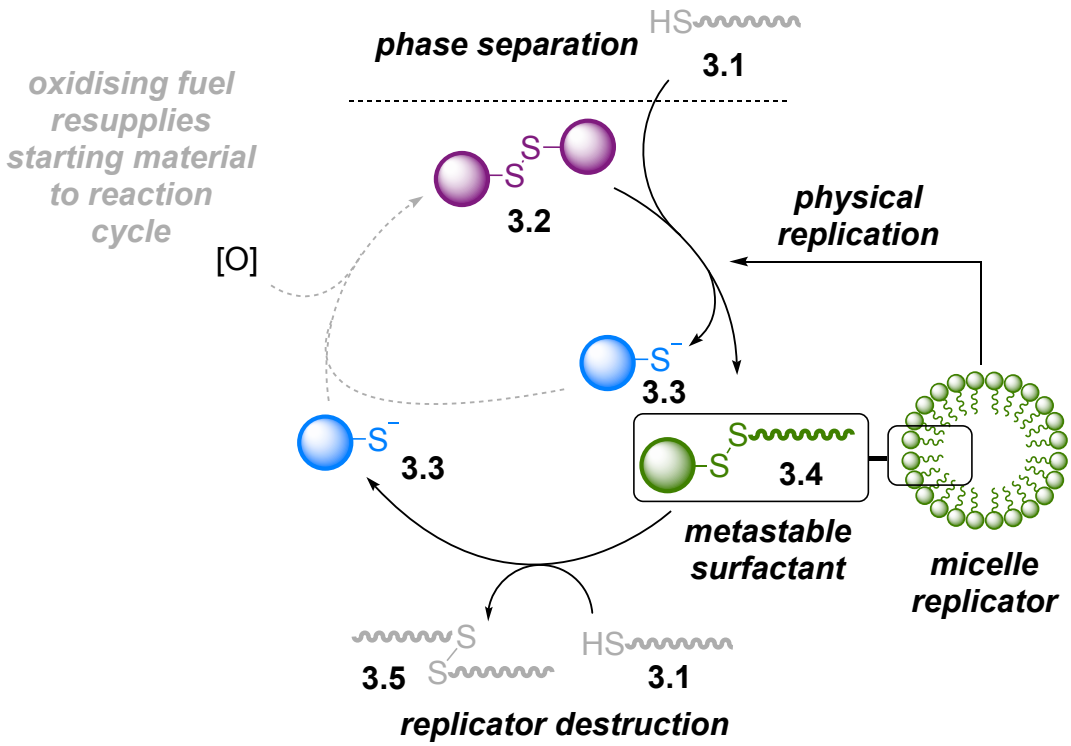



**Figure 3.3.2** The out-of-equilibrium cycle of a chemically fuelled replicator: at equilibrium, in a closed system (solid arrows), the surfactant **3.4** is destroyed. Addition of an oxidising fuel (dashed grey arrows) regenerates starting disulfide **3.2** from waste **3.3** and allows the replicator population to be maintained in an out-of-equilibrium state. At the steady state, successive cycles consume both oxidising fuel and thiol **3.1**, whilst intermediates **3.2**, **3.3** and **3.4** remain at the same concentration. Once fuel supply is halted the replicator stops being re-formed and the system degrades to equilibrium.

## 3.3.2 Experimental realisation

The search for an appropriate water-soluble oxidising agent, supplied by syringe pump, was short. Both $KMnO_4$ and $H_2O_2$ were tested, but the reaction was more tolerant to experiments conducted with $H_2O_2$ (a shutdown of reactivity was observed with high loading of $KMnO_4$) and so we decided to focus on this oxidising agent for screening of reaction conditions.

The reaction was difficult to set up: the addition of the fuel to the aqueous phase of the system introduced multiple new variables and was likely to disturb the sensitive biphasic reaction. A series of experiments with variation in reaction stoichiometry, rate of oxidant addition, stirring rate and pH was conducted to find the most reproducible system, with an out-of-equilibrium state that was observable over an appropriate time scale. A successful system would maintain a population of the replicator at a steady state, under the influence of an oxidising fuel, and be responsive to the removal of this fuel source by degradation to thermodynamic equilibrium.

It was found that the continuous supply of a 1.2 M solution of hydrogen peroxide in water, at a rate of 10 $\mu L h^{-1}$, to a reaction containing 8.0 equivalents of octanethiol **3.1** allowed us to establish a reproducible steady state in the population of replicator **3.4** (Figure 3.3.3), at which point the rates of replicator formation and destruction were neatly balanced.

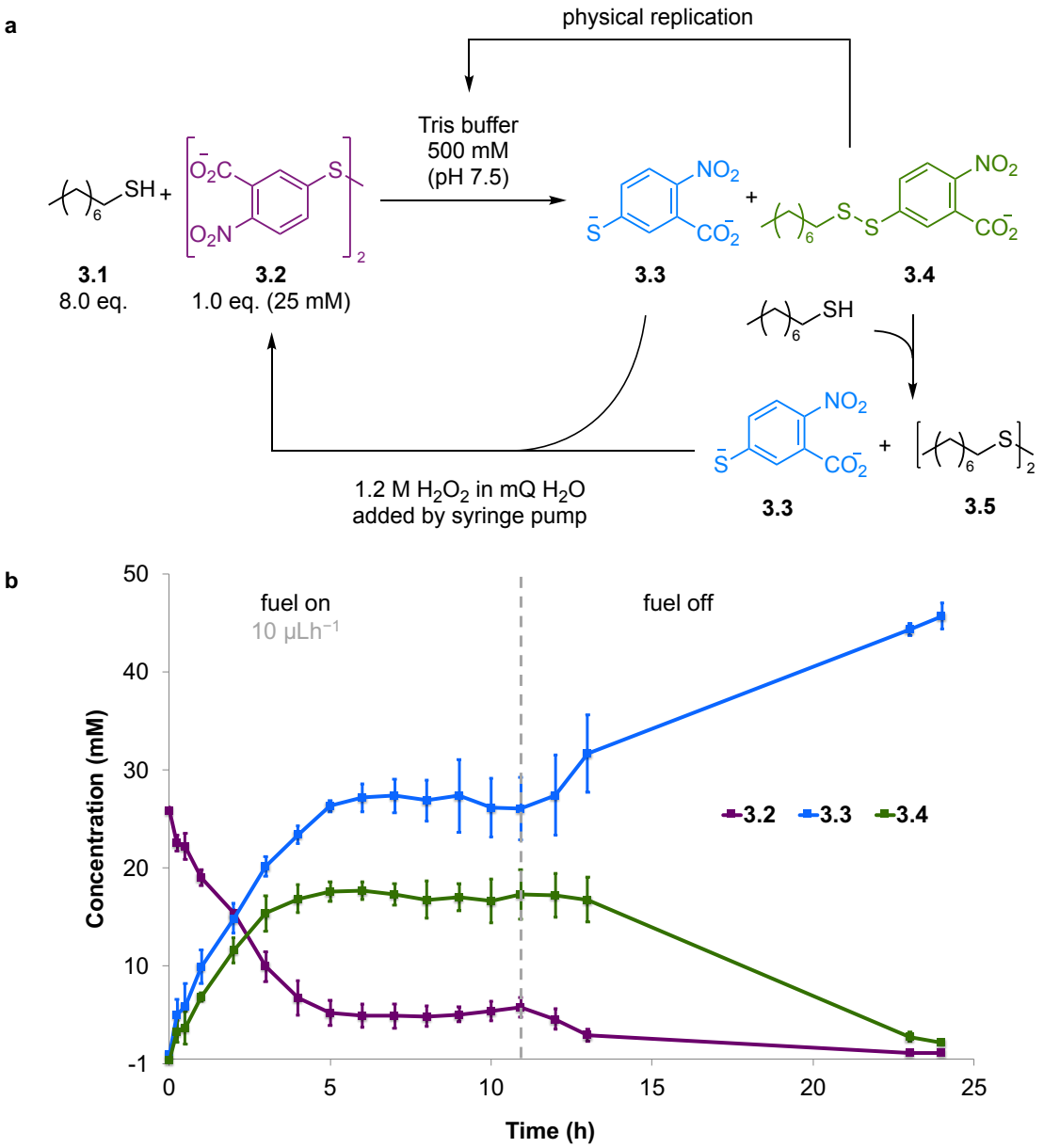



**Figure 3.3.3 a** Supply of a 1.2 M solution of $H_2O_2$ to the system allows recycling of thiolate **3.3**. **b** Continuous supply of an oxidising fuel to the aqueous phase (10 $\mu Lh^{-1}$ by syringe pump) allows **3.4** to reach a steady state. Once fuel supply is halted, the entire system degrades towards equilibrium with the destruction of **3.4** by excess **3.1**. The concentration of reaction components was monitored by UPLC. Each plotted point is the average of three entire experimental repeats and the error bars represent the standard deviation (n=3). Lines between points are drawn to guide the eye.

The observation of the steady state was really exciting; individual replicators were continuously being formed and destroyed while the population as a whole remained steady. A higher concentration of the surfactant **3.4** was observed under chemically-fuelled conditions than was observed even transiently under closed system conditions (*cf.* Figure 3.2.4 and Figure 3.3.3). Under fuelled conditions, building blocks for surfactant formation are never completely depleted as a result of the continuous recycling of thiolate **3.3**. The inherently faster replicator formation step may therefore continue to compete with replicator destruction, and so **3.4** reaches a higher concentration before the destruction step can catch up. The system eventually reaches a stable and elevated, but dynamic, population at which the rate of replicator formation is equal to that of replicator destruction.

The ability to maintain the system under a *continuous* supply of fuel was in contrast to out-of-equilibrium systems which had been limited by the batchwise addition of fuel.[30–32] Importantly, upon halting this continuous fuel supply, the entire system moved towards the thermodynamic minimum and the replicator was completely consumed by the excess octanethiol **3.1**. This allowed us to be certain that the observed steady state population of replicator was not the equilibrium position, nor a kinetically trapped position. The descent to the equilibrium position represented a release of energy; in the dissipative out-of-equilibrium state, therefore, the system was able to store energy.[30]

### 3.3.3 Adaptability

One characteristic of many out-of-equilibrium systems is their adaptability.[33] Rapid movement of the system to a different state with different properties can be achieved by simple variation in the fuel supply, without large changes in environment or the alteration of the relative thermodynamic stabilities of each component.

With variation in the rate of fuel supply in our system we were able to control the replicator concentration. An experiment was begun at a fuel supply of 10 $\mu Lh^{-1}$ and after 8 hours the rate was reduced to 5 $\mu Lh^{-1}$. At the lower rate (5 $\mu Lh^{-1}$), the system was no longer able to support such a high concentration of replicator – fewer building blocks were produced in the substrate cycle – and so the system shifted to a lower concentration of surfactant **3.4** (Figure 3.3.4a). Again, halting fuel supply caused the entire replicator population to be degraded and for the system to reach thermodynamic equilibrium.

Similarly, the system was able to recover from an initially limited supply of fuel to achieve higher concentrations of surfactant **3.4** when fuel was more abundant (Figure 3.3.4b). At an initial rate of 5 $\mu Lh^{-1}$ the replicator was little able to counteract the degradation towards equilibrium and only a low concentration of **3.4** was supported. However, increasing the fuel supply to 10 $\mu Lh^{-1}$ allowed the population of **3.4** to recover. Again, finally halting the fuel supply allowed the system to move to equilibrium.

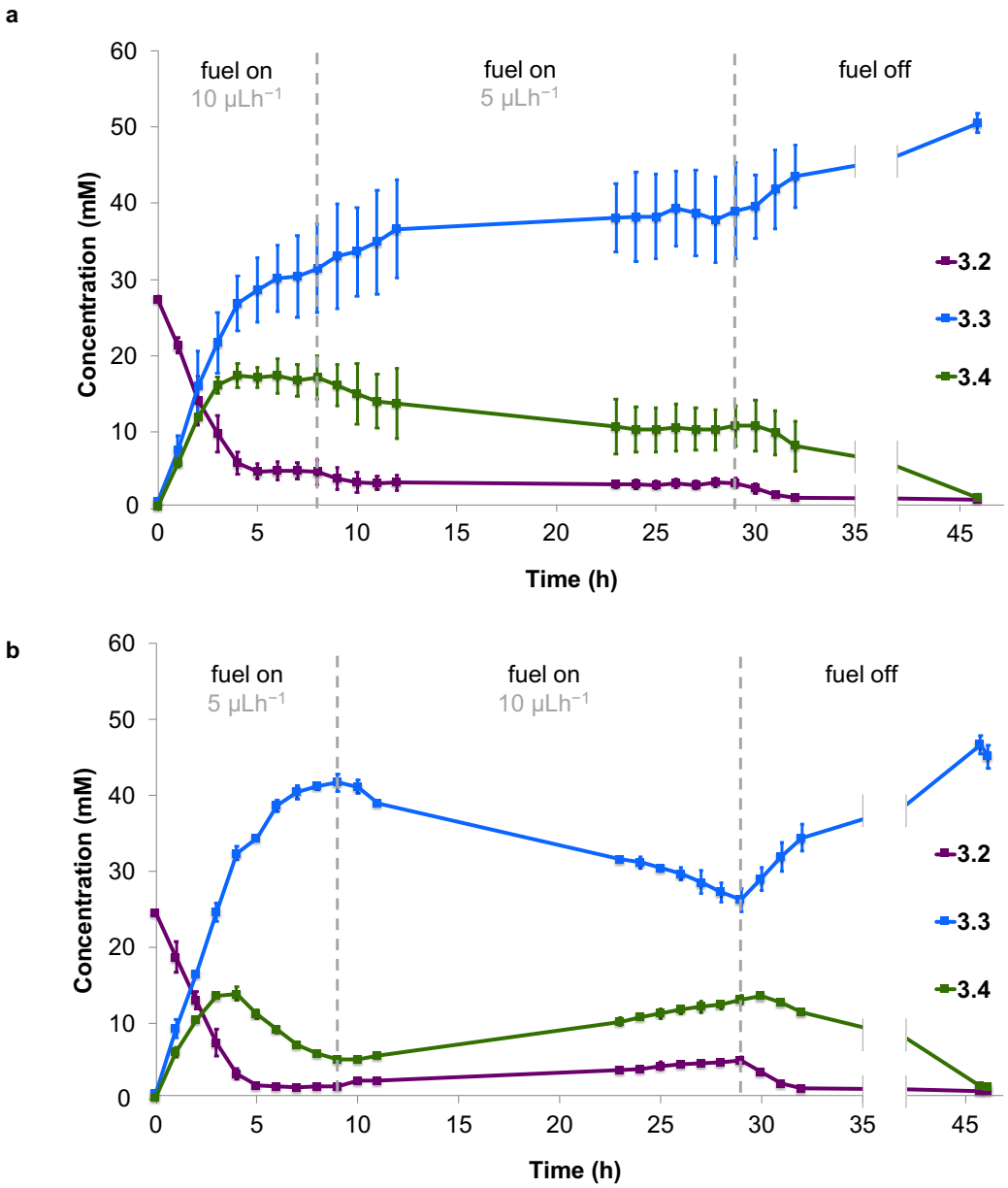



**Figure 3.3.4** The system's response to variation in the rate of fuel addition. Reactions were conducted as shown in Figure 3.3.3a. **a** Initial fuel supply 10 µLh$^{-1}$ for 8 hours, then 5 µLh$^{-1}$ for 21 hours. **b** Initial fuel supply 5 µLh$^{-1}$ for 9 hours, then 10 µLh$^{-1}$ for 20 hours. The concentration of reaction components was monitored by UPLC. Each plotted point is the average of three (**a**) or two (**b**) entire experimental repeats and the error bars represent the standard deviation (n=3) (**a**) or the range of measurements (**b**). Lines between points are drawn to guide the eye.

The adaptability of the system to the fuel supply was yet another demonstration of the emergent behaviour observable under out-of-equilibrium conditions.

## 3.4 Conclusions

The discovery of a thermodynamically unstable surfactant, both constructed and degraded by thiol-disulfide exchange, allowed us to establish a system of replicating micelles maintained in an out-of-equilibrium state by the action of a chemical fuel. The production of a functional aggregate system capable of catalysis, compartmentalisation and replication under out-of-equilibrium conditions approaches lifelike dynamics, with control over replicator concentration and function in time, and the system has obvious analogy with the maintenance of high-energy biological structures, such as microscale microtubules or even a macroscale replicating organism.

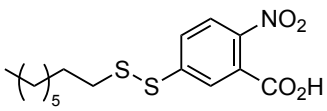
In contrast to previous attempts of the realisation of out-of-equilibrium supramolecular replicators, the system did not rely on the direct supply of new starting materials. Instead, a chemical fuel was used to establish a substrate cycle, reminiscent of simple metabolic pathways observed throughout biology.[28,29] The simple design was enabled by the biphasic nature of the reaction, which was also responsible for the observation of autocatalysis and for the formation of supramolecular structure. Further, unlike other supramolecular assemblies which persist out-out-equilibrium, the system was not limited by the batchwise supply of fuel.[30–32]

This simple system was therefore ripe for development; in Chapter 6, chiral variants of the system are investigated, and in Chapter 7 we highlight some potential future work, looking towards what might be the ultimate emergent behaviour of an out-of-equilibrium replicator: a process of open-ended evolution and the emergence of life.

## 3.5 Experimental

### 3.5.1 Synthesis and characterisation of the compounds used in this study

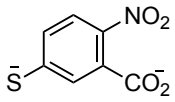
#### 3.5.1.1 Disulfide **3.4**, 2-Nitro-5-(octyldisulfaneyl)benzoic acid




A flame-dried round-bottom flask was charged with 5,5'-Dithiobis-(2-nitrobenzoic acid) (DTNB) (1.19 g, 3.00 mmol, 1.00 eq.), octanethiol (0.52 mL, 3.0 mmol, 1.0 eq.) and $CH_2Cl_2$ (25 mL) under an argon atmosphere. $Et_3N$ (1.5 mL, 11 mmol, 3.5 eq.) was added and the reaction was stirred for 2 hours. The solvent was removed *in vacuo* before quenching with 1 M HCl (20 mL) and extraction with EtOAc (3× 20 mL). The organics were dried over $MgSO_4$, filtered and concentrated *in vacuo*. The crude product was purified by column chromatography ($SiO_2$, $CH_2Cl_2$:MeOH:AcOH 97:2:1) and freeze-dried to yield disulfide **3.4** as an orange solid (440 mg, 43% yield). **$^1$H NMR** (400 MHz, $(CD_3)_2SO$): δ 8.03 (1H, d, *J* = 8.5 Hz, C(Ar)–H), 7.91 (1H, d, *J* = 2.0 Hz, C(Ar)–H), 7.87 (1H, dd, *J* = 8.5 Hz, 2.0 Hz, C(Ar)–H), 2.83 (2H, t, *J* = 7.0 Hz, SS–$CH_2$),

1.62–1.54 (2H, m, SS–$CH_2CH_2$), 1.34–1.19 (10H, m, 5× $CH_2$), 0.82 (3H, t, $J$ = 7.0 Hz, $(CH_2)_7CH_3$); **$^{13}$C NMR** (101 MHz, $(CD_3)_2SO$): δ 165.7 (C=O), 145.7 (4° C(Ar)), 144.6 (4° C(Ar)), 128.9 (4° C(Ar)), 128.2 (C(Ar)–H), 125.7 (C(Ar)–H), 124.9 (C(Ar)–H), 38.2 (SS–$CH_2$), 31.2 (1× $CH_2$), 28.5 (2× $CH_2$), 28.3, 27.6, 22.0 (3× $CH_2$), 13.9 ($(CH_2)_7CH_3$); **HRMS** (ESI+, m/z): calc. for $C_{15}H_{21}O_4NNaS_2^+$ $[M+Na]^+$ 366.0810, found 366.0803; **IR** $\tilde{\nu}_{max}$ (film)/$cm^{-1}$: 2925, 2854, 1710, 1610, 1568, 1526.

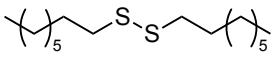
### 3.5.1.2 Thiol **3.3**, 5-mercapto-2-nitrobenzoic acid




A two-necked round-bottom flask equipped with a dropping funnel and an exit needle was charged with a suspension of 5,5'-dithiobis-(2-nitrobenzoic acid) (420 mg, 1.06 mmol, 1.00 eq) in EtOH (80% v/v in $H_2O$, 5.0 mL). $NaBH_4$ (320 mg, 8.50 mmol, 8.00 eq.) in distilled $H_2O$ (2.0 mL) was added dropwise to the suspension at 0 °C. The reaction was stirred at room temperature until gas evolution subsided and was then diluted with EtOH (5 mL) and $H_2O$ (5 mL) before acidification with 1 M HCl (10 mL). The mixture was extracted with $CH_2Cl_2$ (3× 20 mL) and the combined organic layers dried over $MgSO_4$, filtered, and concentrated *in vacuo* to yield thiol **3.3** as an orange solid (405 mg, 96% yield). NMR spectra were recorded in $(CD_3)_2SO$ and in a 500 mM Tris buffer solution in $D_2O$ to completely avoid oxidation. This solution was prepared by dissolution of Trizma® base (0.303 g, 2.50 mmol) in $D_2O$ (5.0 mL) before adjustment to pH* ~ 9 with DCl (0.5 M in $D_2O$). Dissolution of **3.3** (20 mg, 0.10 mmol) in this buffered solution resulted in a

solution of pH* ~ 8. **$^1$H NMR** (400 MHz, $(CD_3)_2SO$): δ 8.03 (1H, d, *J* = 8.5 Hz, C(Ar)–H), 7.93 (1H, br. s, C(Ar)–H), 7.86 (1H, br. d, *J* = 8.5 Hz, C(Ar)–H); **$^1$H NMR** (400 MHz, 500 mM TRIS in $D_2O$, pH* ~ 8): δ 7.81 (1H, d, *J* = 8.5 Hz, C(Ar)–H), 7.38 (1H, dd, *J* = 9.0 Hz, 2.0 Hz, C(Ar)–H), 7.26 (1H, d, *J* = 2.0 Hz, C(Ar)–H); **$^{13}$C NMR** (101 MHz, $(CD_3)_2SO$): δ 165.5 (C=O), 146.4 (4° C(Ar)), 141.9 (4° C(Ar)), 129.1 (4° C(Ar)), 129.0 (C(Ar)–H), 126.7 (C(Ar)–H), 125.3 (C(Ar)–H); **$^{13}$C NMR** (101 MHz, 500 mM TRIS in $D_2O$, pH* ~ 8): δ 176.0 (C=O), 163.4 (4° C(Ar)), 137.2 (4° C(Ar)), 135.9 (4° C(Ar)), 132.5 (C(Ar)–H), 130.2 (C(Ar)–H), 123.8 (C(Ar)–H); **HRMS** (ESI-, m/z): calc. for $C_7H_4O_4NS^-$ $[M-H]^-$ 197.98665, found 197.98660. **IR** $\tilde{\nu}_{max}$ (film)/$cm^{-1}$: 1704, 1642, 1604, 1570, 1510. The $^1$H NMR data in $(CD_3)_2SO$ are consistent with those reported in *J. Am. Chem. Soc.* **126**, 16395-16404 (2004).[34]

### 3.5.1.3 Disulfide **3.5**, 1,2-dioctyldisulfane



A round-bottom flask was charged with a solution of octanethiol (0.47 mL, 2.7 mmol, 1.0 eq.) in $Et_2O$ (9.0 mL). To the solution was added an aqueous solution of $H_2O_2$ (50 wt%, 160 µL, 1.0 eq.) and NaI (tip of spatula). After stirring for 10 minutes the reaction was quenched with sat. aq. $Na_2S_2O_3$ (5 mL) and extracted with $Et_2O$ (3× 5 mL). The combined organics were dried over $MgSO_4$, filtered, and concentrated *in vacuo* to yield disulfide **3.5** as a clear oil (314 mg, 79% yield). **$^1$H NMR** (400 MHz, $CDCl_3$): δ 2.68 (4H, t, *J* = 7.5 Hz, 2× S–$CH_2$), 1.70–1.63 (4H, m, 2× S–$CH_2C\mathit{H}_2$), 1.41–1.27 (20 H, m, 10× $CH_2$), 0.88 (6H, t, *J* = 7.0 Hz, 2× $(CH_2)_7C\mathit{H}_3$); **$^{13}$C NMR** (101 MHz, $CDCl_3$): δ 39.4 (2× S–$CH_2$), 32.0, 29.4, 29.4, 29.3, 28.7, 22.8 (12× $CH_2$), 14.2 (2× $(CH_2)_7\mathit{C}H_3$); **HRMS** (APCI, m/z): calc. for

$C_{16}H_{35}S_2^+$ $[M+H]^+$ 291.21747, found 291.21737; **IR** $\tilde{\nu}_{max}$ (film)/$cm^{-1}$: 2955, 2923, 2853. The data are consistent with those reported in *Synlett* **26**, 1185-1190 (2015).[35]

## 3.5.2 Physical characterisation of surfactant **3.4**

### 3.5.2.1 Preparation of 500 mM TRIS buffer

Per 50 mL TRIS buffer: Trizma® base obtained from Sigma Aldrich (3.029 g, 25.00 mmol) was dissolved in MilliQ $H_2O$ (approx. 45 mL). The solution was adjusted to pH ~ 7.8 – 8.0 with 12 M HCl (unless otherwise indicated in procedure) and the volume made up to 50 mL with MilliQ $H_2O$. The buffer solution was stored at 4 °C before use. In general, a 25 mM solution of DTNB **3.2** prepared in this buffer would be pH ~ 7.5. Any subsequent adjustment of pH is indicated in procedures.

### 3.5.2.2 Dynamic Light Scattering

Analyses were performed using a Malvern Zetasizer Nano ZEN5600 model system recording particle and molecule size. Instrument control and data processing were performed using Zetasizer software. A 50 mM solution of disulfide **3.4** was prepared by dissolution of disulfide **3.4** (86 mg, 0.25 mmol) in Tris buffer (500 mM, pH 7.8 – 8.0, 5.0 mL). The solution was adjusted to pH 7.5 with a few drops of 1 M HCl. Subsequent 2-fold serial dilutions were made with a Tris buffer solution (500 mM, pH 7.5). Disposable plastic cuvettes were used with

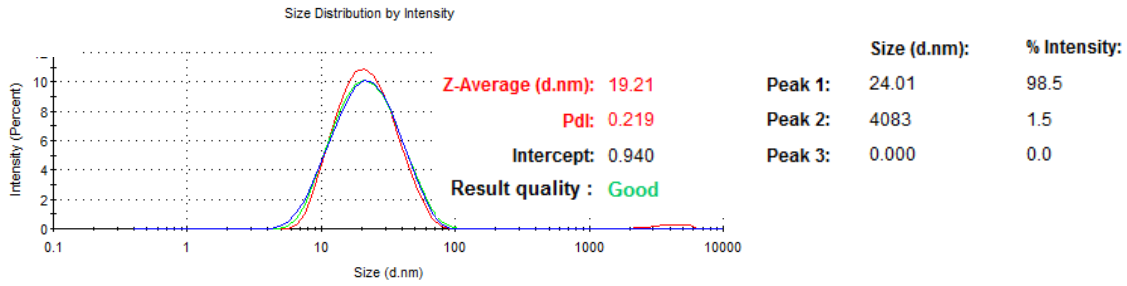
1.0 mL of sample solution, which was filtered through a 200 nm filter immediately before measurement. Three repetitions of ten measurements were taken for every concentration. Measurements were performed using an equilibrated heating probe at 25 °C, setting the following parameters for Tris buffer 500 mM (calculated internally using the software's complex solvent builder):

Refractive index = 1.339

Viscosity = 1.0780 mPa · s

Over the series of concentrations 50 mM to 3.125 mM, aggregates were detected with a diameter of 15 to 20 nm, with relatively tight polydispersity (Figures 3.5.1, 3.5.2).

**a**




**b**

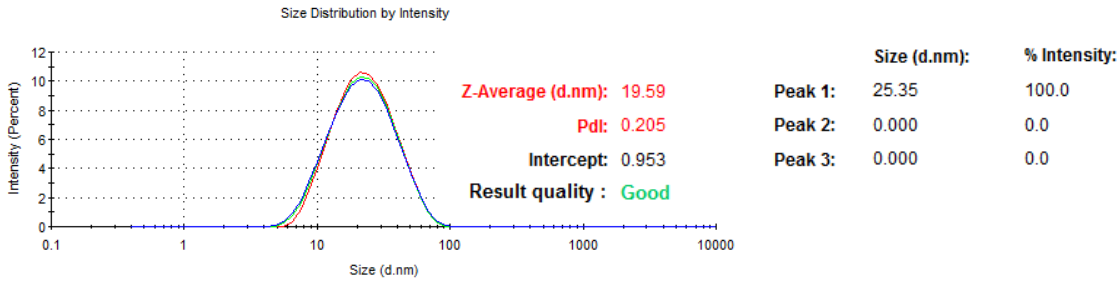



**Figure 3.5.1** Size distribution by intensity of **3.4** in 500 mM TRIS buffer pH 7.5. **a** 50 mM **b** 25 mM. Over the concentration range 50 – 3.125 mM aggregates of tight polydispersity were observed, from 15 – 20 nm in hydrodynamic diameter.

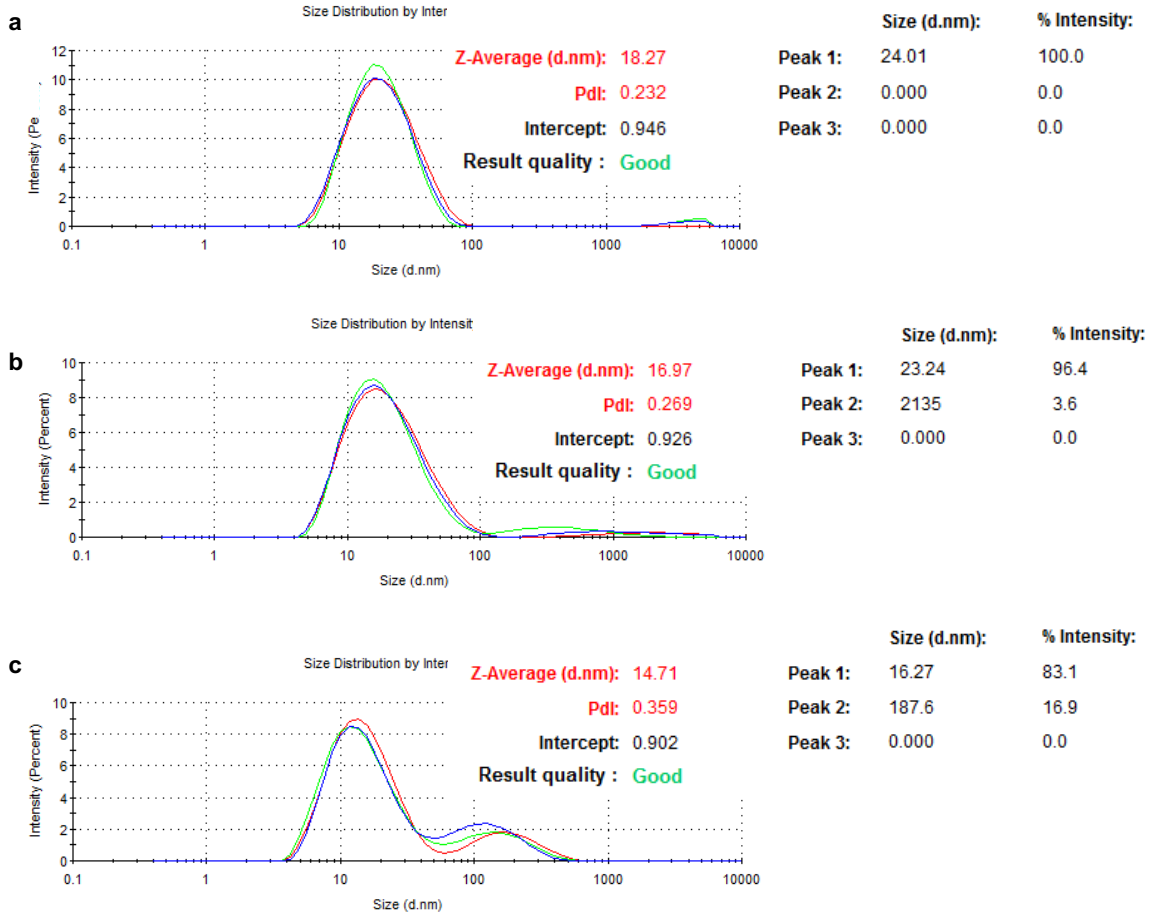



**Figure 3.5.2** Size distribution by intensity of **3.4** in 500 mM TRIS buffer pH 7.5 **a** 12.5 mM **b** 6.25 mM **c** 3.125 mM. Over the concentration range 50 – 3.125 mM aggregates of tight polydispersity were observed, from 15 – 20 nm in hydrodynamic diameter.

At lower concentrations, a higher degree of polydispersity was found (Figure 3.5.3), and at 0.39 mM it was determined that the count rate was decreasing (Figure 3.5.3c). When the sample concentration is too low, the scattering from the particles is weak and there is greater influence of noise from unwanted sources e.g. dust particles which may overwhelm the sample. This may explain the apparent increase in polydispersity. A lower count rate indicates reduced aggregation at low concentration.

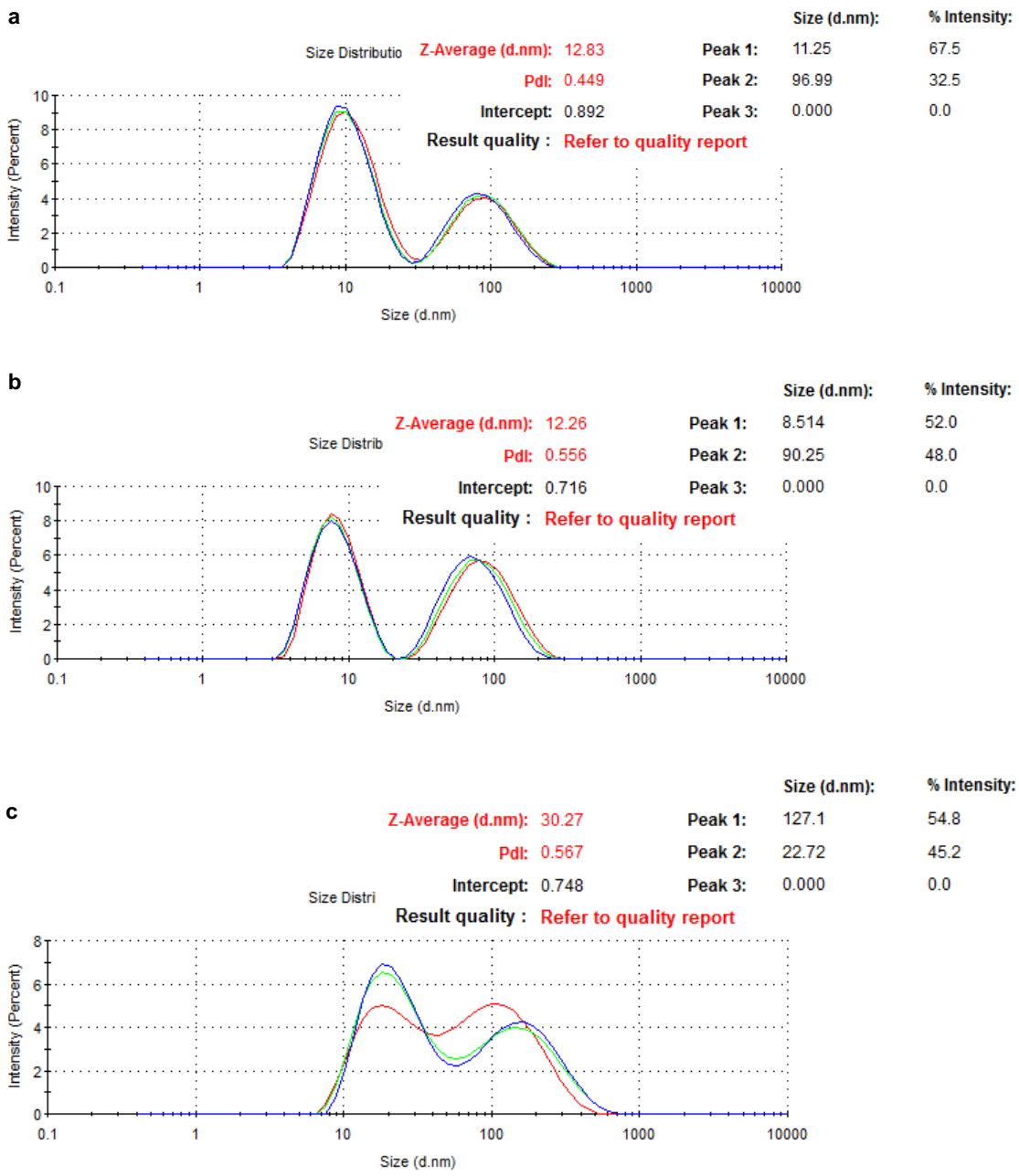



**Figure 3.5.3** Size distribution by intensity of **3.4** in 500 mM TRIS buffer pH 7.5 **a** 1.56 mM **b** 0.78 mM **c** 0.39 mM. In **a** and **b** a higher degree of polydispersity was observed compared to higher concentrations (Figure 3.5.1, 3.5.2). In **c**, count rate was significantly decreased, indicating reduced aggregation.

### 3.5.2.3 Ring tensiometry for calculation of critical micelle concentration

The critical micelle concentration of surfactant **3.4** was determined using a Krus K10ST tensiometer, measuring the surface tension of solutions at different concentration of **3.4** in Tris buffer.

Prior to buffer preparation, Trizma® base was recrystallised twice from 20% EtOH/$H_2O$, and dried over $P_2O_5$ overnight.

50 mL of 500 mM Tris buffer was prepared at pH ~ 7.9 with recrystallised Trizma® base. This solution was used for the initial dissolution of **3.4**. For the initial 40 mM stock solution, **3.4** (275 mg, 0.8 mmol) was dissolved in buffer (20 mL) and adjusted to pH ~ 7.5 with a very small quantity of 12 M HCl.

A further 130 mL of 500 mM Tris buffer was prepared at pH ~ 7.5 for dilutions. From the stock 40 mM solution, 2-fold serial dilutions were made down to a solution of concentration $4.9 \times 10^{-3}$ mM. 10 mL of each concentration was prepared.

Prior to measurement on the tensiometer, the instrument was calibrated with the surface tension of pure water. Measurements were performed at 25 °C. All measurements were taken on the same day.

The plot of surface tension vs. ln[**3.4**] reveals a critical micelle concentration of approximately 0.2 mM (Figure 3.5.4). The critical micelle concentration is the point at which the surface tension no longer decreases with increasing concentration. Error bars for the standard deviation of the three measurements at each concentration are plotted but are too small to be visible.

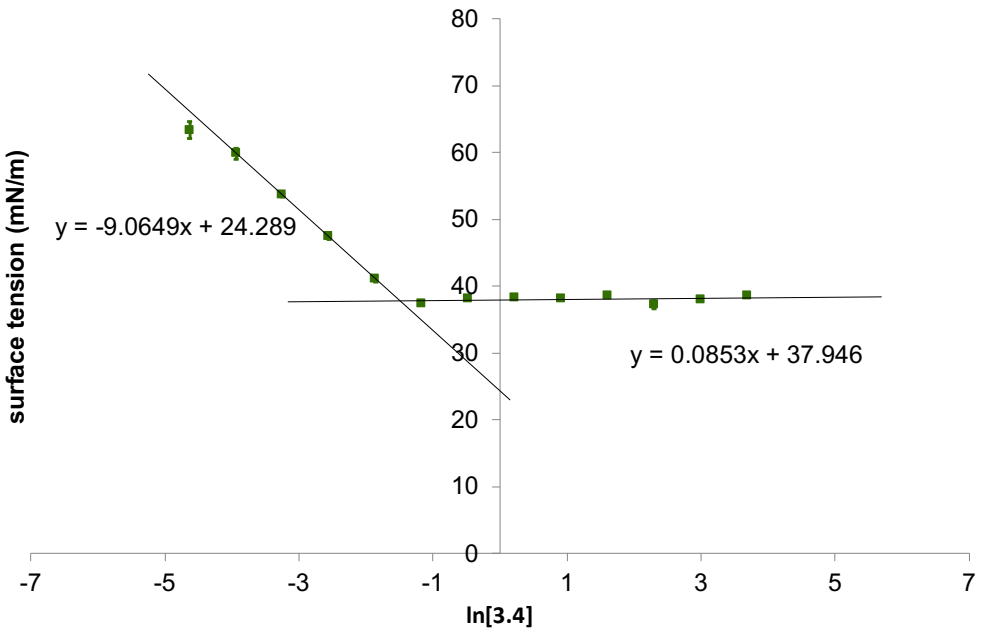



**Figure 3.5.4** Determination of critical micelle concentration by ring tensiometry. A plot of surface tension, measured by ring tensiometry, against ln[**3.4**] with trendlines plotted both above and below the cmc (above the cmc there is no longer a decrease in surface tension with concentration of surfactant). The intercept of the two lines allows us to calculate the cmc.

At the intercept:

$$x = -1.4925$$

$$[\mathbf{3.4}] = 0.22\ \mathrm{mM}$$

## 3.5.3 Methods of analysis for biphasic experiments

### 3.5.3.1 UPLC details

Calibrations and subsequent analysis of reactions were made using a Waters Acquity ultra performance liquid chromatography (UPLC) H-Class system with photodiode array (PDA) detector. Instrument control and data processing were performed using Empower software. An ACQUITY UPLC BEH C18 column (130 Å, 1.7 µm, 2.1 mm × 50 mm) was used. The gradient used to acquire every chromatogram is shown in Table 3.5.1.

| Time (minutes) | Flow ($mLmin^{-1}$) | Composition of eluent solution (%) | | | Curve |
|---|---|---|---|---|---|
| | | MilliQ $H_2O$ | MeCN | 5 % TFA in MilliQ $H_2O$ | |
| initial | 0.600 | 93 | 2 | 5 | initial |
| 0.25 | 0.600 | 93 | 2 | 5 | 6 |
| 4.00 | 0.600 | 0 | 95 | 5 | 6 |
| 4.40 | 0.600 | 0 | 95 | 5 | 6 |
| 4.50 | 0.600 | 93 | 2 | 5 | 10 |
| 5.00 | 0.600 | 93 | 2 | 5 | 10 |

**Table 3.5.1** Gradient for chromatogram acquisition on UPLC.

### 3.5.3.2 Aliquot procedure and determination of concentration of reaction components

All measurements were performed with an external standard. The standard solution was first prepared by the dissolution of 3-methyl-2-nitrobenzoic acid (100 mg, 0.55 mmol) in DMSO (10 mL). 2.5 mL of this solution was diluted with MilliQ $H_2O$ to a total volume of 500 mL in a volumetric flask, giving an overall concentration of 0.05 $mgmL^{-1}$ (0.276 mM). To this standard solution was added maleimide (120 mg per 20 mL), which acted as a quench.

To monitor the reactions (unless otherwise specified within the procedure) a small volume of the reaction mixture (aqueous phase) was withdrawn at specified time points by plastic syringe. 25 µL of this withdrawn solution was then measured by microsyringe and placed into an MS vial, before quenching with 1.0 mL of external standard solution containing maleimide. A chromatogram of each sample was recorded by UPLC by 1.0 µL injection following the conditions in Section 3.5.3.1. Peak areas were integrated at a wavelength of 215 nm. The area of the peak of interest over the area of the external standard peak was recorded to ascertain the concentration of all reaction components, using the calibrations in Section 3.5.3.3. For every experiment the total concentration of known UV active components was also monitored to ensure it remained constant, indicating no unexpected side reactivity.

### 3.5.3.3 UPLC calibration

Stock solutions **3.2**:

**3.2** (19.8 mg, 50.0 μmol), obtained from Sigma Aldrich, was dissolved in 2.0 mL Tris buffer (500 mM, pH 7.8 – 8.0) ([**3.2**] = 25 mM). 2-fold serial dilutions of this solution were made down to a solution of concentration 1.5625 mM (5 different concentrations in total).

Stock solutions **3.3**:

**3.3** (19.9 mg) was dissolved in 2.0 mL Tris buffer (500 mM, pH 7.8 – 8.0) ([**3.3**] ≈ 50 mM). The solution was not exactly 50 mM in **3.3** on account of a small quantity, approx. 4%, of **3.2** observed by UPLC. 2-fold serial dilutions of this solution were made down to a solution of concentration ≈ 1.5625 mM (5 different concentrations in total). Another solution was prepared following observation of **3.2** in the UPLC trace, dissolving **3.3** prepared according to section 3.5.1.2 (21.5 mg) in 2.0 mL Tris buffer (500 mM, pH 7.8 – 8.0) for a solution of observed concentration [**3.3**] = 50.3 mM (giving 6 solutions in total).

Stock solutions **3.4**:

**3.4** (85.9 mg, 250 μmol) was dissolved in 5.0 mL Tris buffer (500 mM, pH 7.8 – 8.0) ([**3.4**] = 50 mM). 2-fold serial dilutions of this solution were made down to a solution of concentration = 3.125 mM (5 different concentrations in total).

25 µL of each stock solution prepared above was measured by microsyringe into an MS vial and 1.0 mL of external standard solution, containing maleimide, was added to each.

Three successive 1.0 µL injections of each resultant solution were taken and the chromatogram was recorded by UPLC as in Section 3.5.3.1. Peak areas were integrated at a wavelength of 215 nm. The area of the peak of interest over the area of the external standard peak was recorded and the average of the three measurements was plotted against the concentration of the original solutions (Figures 3.5.5, 3.5.6, 3.5.7). Error bars of standard deviation for the three measurements are plotted but are too small for observation.

This resulted in a linear fit for components **3.2** and **3.3** (Figure 3.5.5, 3.5.6). For component **3.4**, there was a linear fit in the region 0 – 25 mM (Figure 3.5.7), but this became non-linear once the 50 mM solution was included. Only the region 0 – 25 mM is considered in our experiments for this component.

The calibration above leads to the following equations for the determination of component concentration (provided the procedures above and as detailed in Sections 3.5.3.1 and 3.5.3.2 were followed):

$$[\mathbf{3.2}] = \frac{\frac{\text{Area } \mathbf{3.2}}{\text{Area standard}} + 0.0868}{0.2692}$$

$$[\mathbf{3.3}] = \frac{\frac{\text{Area } \mathbf{3.3}}{\text{Area standard}} + 0.0517}{0.1268}$$

$$[\mathbf{3.4}] = \frac{\frac{\text{Area } \mathbf{3.4}}{\text{Area standard}} - 0.0302}{0.1574}$$

Where concentrations are measured in mM.

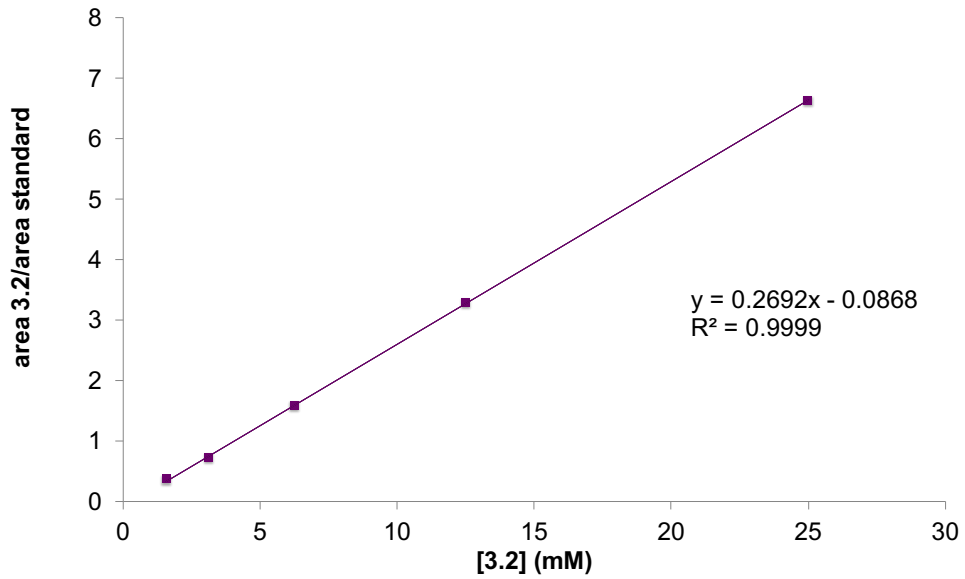



**Figure 3.5.5** UPLC calibration of **3.2**

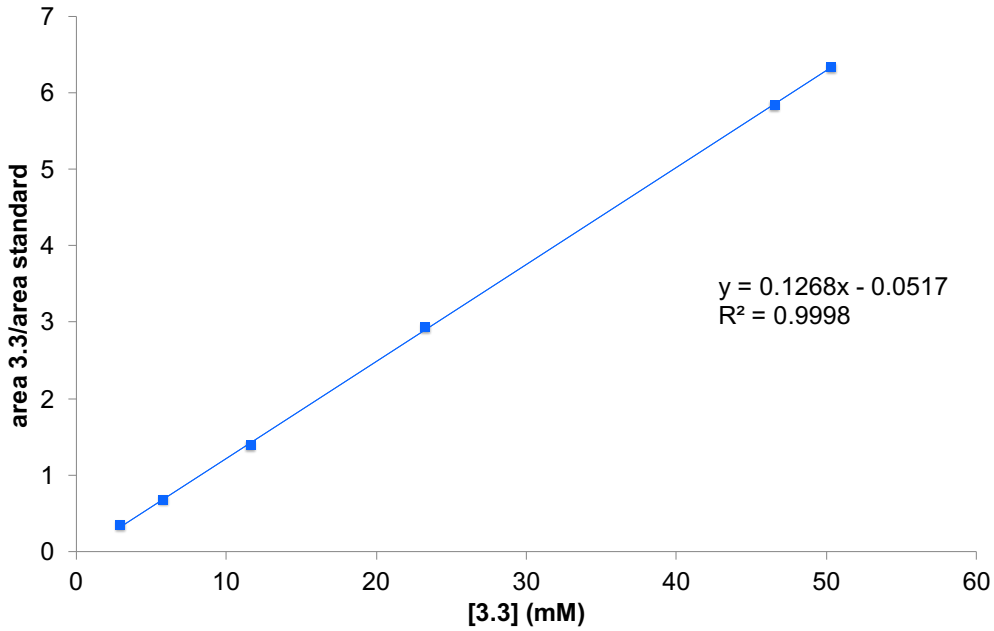



**Figure 3.5.6** UPLC calibration of **3.3**

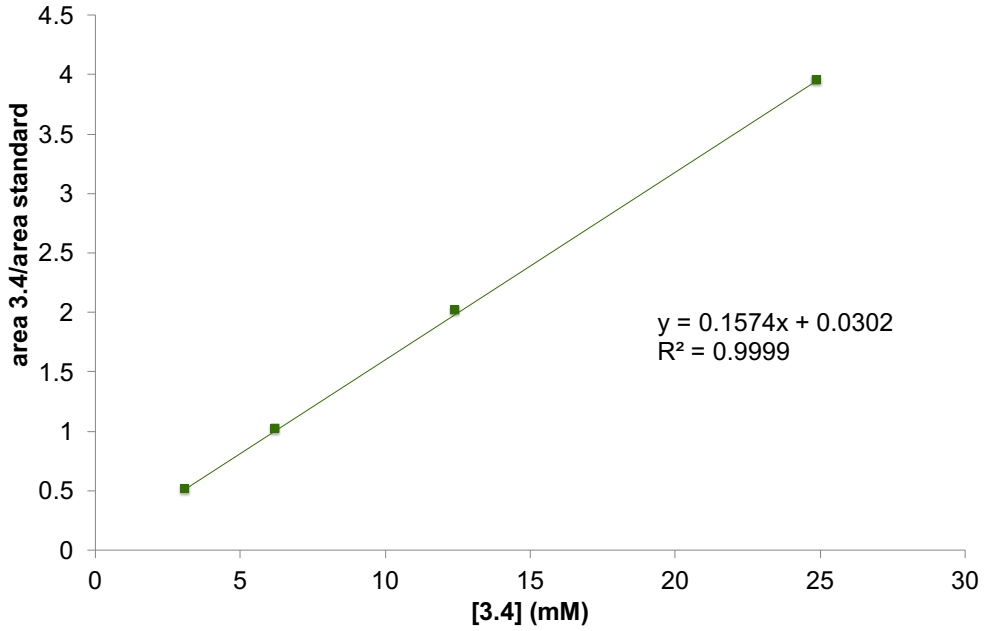



**Figure 3.5.7** UPLC calibration of **3.4**.

## 3.5.4 Procedures for biphasic experiments

### 3.5.4.1 Control and seeded experiments

(Data in Figures 3.2.2, 3.2.3, 3.2.4, 3.2.5)

**Control:** 5,5'-Dithiobis-(2-nitrobenzoic acid) (DTNB) (**3.2**) (119 mg, 300 μmol) was dissolved by sonication in 12 mL Tris buffer (500 mM, pH 7.8 – 8.0) to reach pH ~ 7.5. Any necessary adjustment was made with a few drops of 12 M HCl.

**Seeded (15 mM)**: 5,5'-Dithiobis-(2-nitrobenzoic acid) (DTNB) (**3.2**) (60 mg, 0.15 mmol) was dissolved by sonication in 6 mL Tris buffer (500 mM, pH 7.8 – 8.0). To this solution was added disulfide **3.4** (31 mg, 90 μmol) with sonication for

dissolution, to reach a pH of ~ 7.5 (matching the pH of the control). Any necessary adjustment was made with a few drops of 12 M HCl.

5 mL of each solution was placed in a 10 mL round bottomed flask and stirring was started at 100 rpm. Octanethiol (22 µL, 0.13 mmol, 1.0 eq. OR 174 µL, 1.00 mmol, 8.00 eq.) was placed dropwise onto the surface of the solution, and the beginning of this addition was considered time zero.

For 1.0 equivalent **3.1**: an aliquot was taken every 10 minutes for the first 30 minutes, followed by an aliquot at a total reaction time of 1 hour after which point aliquots were taken every hour for a total reaction time of 7 hours.

For 8.0 equivalents **3.1**: an aliquot was taken every 5 minutes for the first 15 minutes, followed by aliquots every 15 minutes until a total reaction time of 1 hour. After this point, aliquots were taken every hour for a total reaction time of 9 hours. The reaction was left to stir overnight and two final aliquots were taken at 23 hours and 24 hours.

It is noted that, in general, the production of a high concentration of **3.3** cannot be buffered (the pH of the reaction decreases over 24 hours by 1 - 2 pH units). However, thiol-disulfide exchange is still in operation, as evidenced by the destruction of **3.4** even at high concentration of **3.3** towards the end of reaction.

#### 3.5.4.1.1 Measurement of initial rates for control and seeded reactions

Figures 3.5.8 and 3.5.9 are plots of the concentration of **3.2** and **3.4** with time in both control and seeded (15 mM) reactions at the beginning of the reaction, varying in the equivalents of octanethiol **3.1** (*i.e.* initial time points of Figures 3.2.3 and 3.2.5). Linear trendlines are plotted and their associated equations are a measure of the initial rate of each reaction. Seeding the reaction with **3.4** (15 mM) under conditions of 1.0 (Figure 3.5.8) and 8.0 equivalents (Figure 3.5.9) of octanethiol **3.1** results in an acceleration in the consumption of **3.2** and the production of **3.4**.

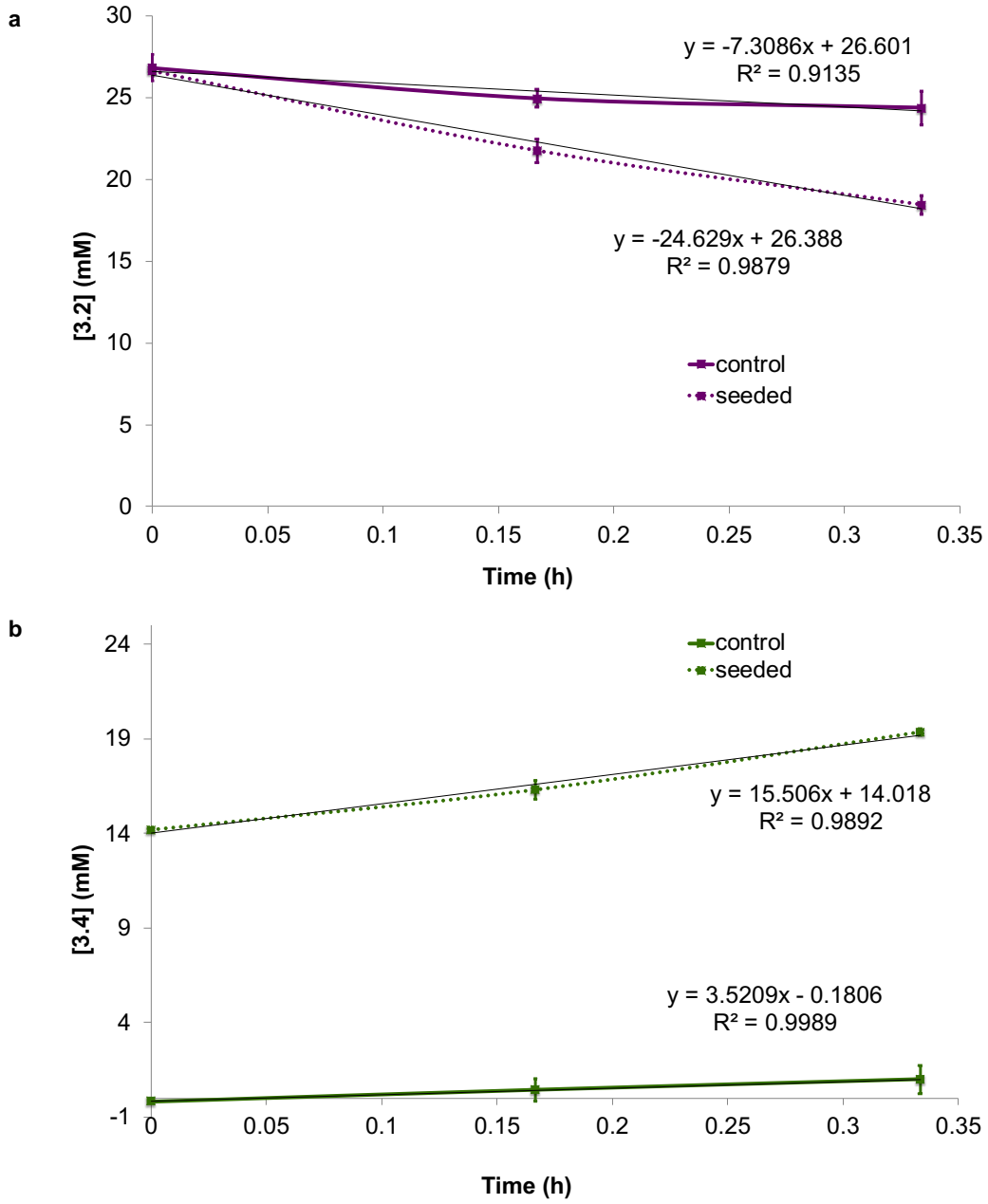



**Figure 3.5.8** Concentration of (**a**) **3.2** and (**b**) **3.4** for control and seeded reactions conducted as Figure 3.2.2a (1.0 eq. **3.1**). The concentration of reaction components was monitored by UPLC. Each plotted point is the average of three entire experimental repeats and the error bars represent the standard deviation (n=3). Lines between points are drawn to guide the eye. Linear trendlines and their associated equations are displayed as a measure of initial rate.

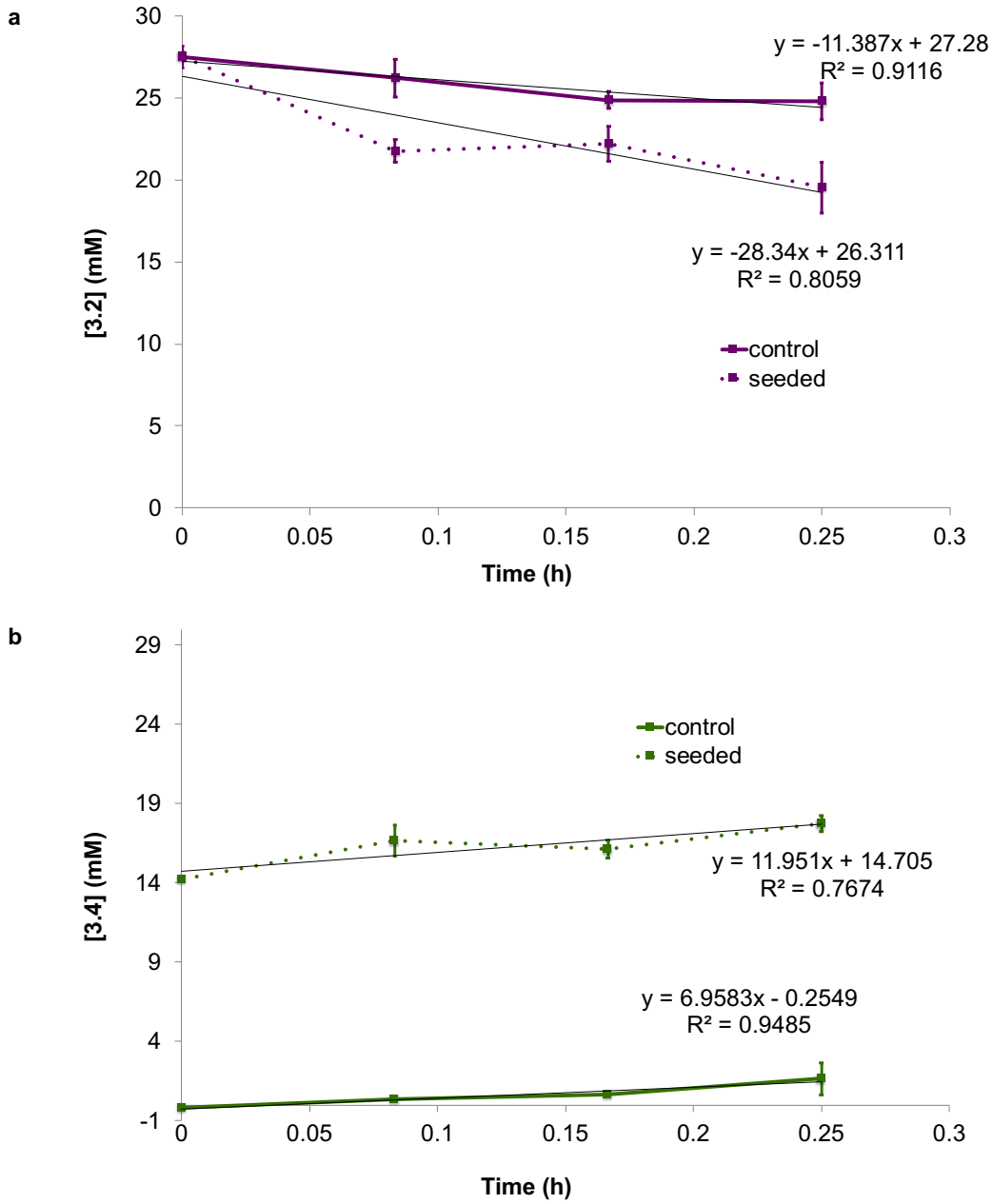



**Figure 3.5.9** Concentration of (**a**) **3.2** and (**b**) **3.4** for control and seeded reactions conducted as Figure 3.2.4a (8.0 eq. **3.1**) The concentration of reaction components was monitored by UPLC. Each plotted point is the average of three entire experimental repeats and the error bars represent the standard deviation (n=3). Lines between points are drawn to guide the eye. Linear trendlines and their associated equations are displayed as a measure of initial rate.

### 3.5.4.2 Additional seeding experiments

For these experiments, no additional pH adjustment was made on dissolution of disulfides **3.2** or **3.4** in buffer to avoid significant difference in reaction volume between experiments. Thus, pH is likely to have varied slightly between experiments conducted with different quantity of the seeded product **3.4**. The data are shown in Figures 3.2.6 and 3.2.7.

**Control**: DTNB **3.2** (60 mg, 0.15 mmol) was dissolved in 6 mL Tris buffer (500 mM, pH 7.8 – 8.0) with sonication. 5 mL of this solution was placed in a 10 mL round bottomed flask and stirring was started at 100 rpm. Octanethiol (174 µL, 1.00 mmol, 8.00 eq.) was placed dropwise onto the surface of the solution, and the beginning of this addition was considered time zero. The reaction was monitored every 5 minutes for the first 15 minutes, followed by aliquots every 15 minutes until a total reaction time of 1 hour. After this point, the reaction was monitored every 30 minutes for a total reaction time of 2.5 hours.

**3.0 mM seeding**: Disulfide **3.4** (6.2 mg, 18 µmol) and DTNB **3.2** (60 mg, 0.15 mmol) were dissolved in 6 mL Tris buffer (500 mM, pH 7.8 – 8.0). 5 mL of this solution was taken for the reaction conducted exactly as the control.

**0.1 mM and 1.0 mM seeding**: Seeding reactions conducted with 0.1 mM and 1 mM disulfide **3.4** were conducted by first preparing a stock solution (2.5 mM) of disulfide **3.4**:

**Preparation of a stock solution (2.5 mM) of disulfide 3.4**: Disulfide **3.4** (17.2 mg, 50.0 μmol) was dissolved by sonication in 20 mL Tris buffer (500 mM, pH 7.8 – 8.0).

**0.1 mM seeded reaction**: 0.24 mL of the 2.5 mM stock solution was diluted to 6.0 mL with Tris buffer (500 mM, pH 7.8 – 8.0). To this solution was added 5,5'-dithiobis-(2-nitrobenzoic acid) (DTNB) (60 mg, 0.15 mmol) with sonication for dissolution. 5 mL of this solution was taken for the reaction conducted exactly as the control.

**1.0 mM seeded reaction**: 2.4 mL of the 2.5 mM stock solution was diluted to 6.0 mL with Tris buffer (500 mM, pH 7.8 – 8.0). To this solution was added 5,5'-dithiobis-(2-nitrobenzoic acid) (DTNB) (60 mg, 0.15 mmol) with sonication for dissolution. 5 mL of this solution was taken for the reaction conducted exactly as the control.

### 3.5.4.2.1 Initial rates for additional seeding experiments

Figure 3.5.10 depicts the change in initial rate with quantity of seed for additional seeding experiments.

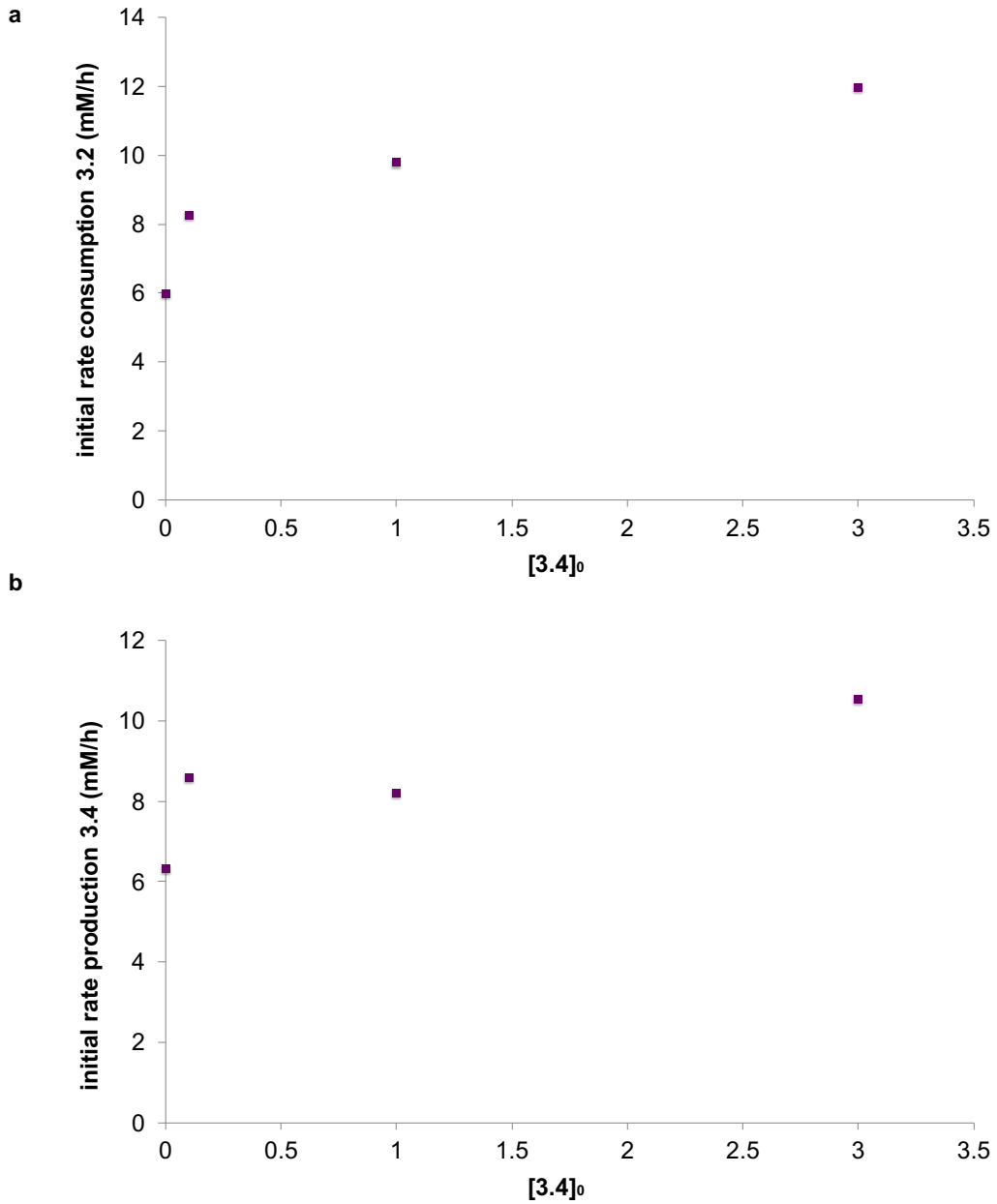



**Figure 3.5.10 a** The measured initial rate of disulfide **3.2** consumption vs. the initial concentration of surfactant **3.4** (extracted from Figure 3.2.6). **b** The measured initial rate of surfactant **3.4** production vs. the initial concentration of surfactant **3.4** (extracted from Figure 3.2.7).

### 3.5.4.3 Fuelled experiments

5,5'-Dithiobis-(2-nitrobenzoic acid) (DTNB) (**3.2**) (119 mg, 300 μmol) was dissolved by sonication in 12 mL Tris buffer (500 mM, pH 7.8 – 8.0) to reach pH ~ 7.5. Any necessary adjustment was made with a few drops of 12 M HCl. 5 mL of this solution was placed in a 10 mL round bottomed flask and stirring was started at 100 rpm.

Preparation of oxidant solution: 36 μL of an aqueous solution of $H_2O_2$ (50% wt.) was added to 64 μL of MilliQ $H_2O$. To this was added an additional 0.45 mL of MilliQ $H_2O$. The solution was placed into a 1.0 mL plastic syringe and the solution pushed to the needle tip before placing in the syringe pump assembly and tightening the assembly. Excess solution from the needle tip was wiped away before lowering into the aqueous solution. The syringe pump was then turned on and run at 10 $\mu L h^{-1}$. Octanethiol **3.1** was added dropwise by microsyringe onto the top of the solution momentarily after starting the pump. The beginning of this addition was considered time zero.

Constant rate of fuel addition (data in Figure 3.3.3): the reaction was monitored every 15 minutes for the first 30 minutes, an aliquot taken at a reaction time of 1 hour, and then aliquots taken every hour for a total reaction time of 11 hours. After a reaction time of 11 hours, the syringe pump was stopped. Two further aliquots were taken at a total reaction time of 12 and 13 hours before leaving to stir overnight. Two final aliquots were taken at 23 hours and 24 hours.

Variation in rate of fuel addition (10 $\mu Lh^{-1}$ to 5 $\mu Lh^{-1}$) (data in Figure 3.3.4a): the reaction was begun according to the general method. The reaction was monitored every hour for the first 8 hours. After a reaction time of 8 hours and 12 minutes, the rate of fuel addition was reduced to 5 $\mu Lh^{-1}$. An aliquot was taken at a total reaction time of 9 hours before again removing aliquots every hour for a total reaction time of 12 hours. The reaction was left to stir overnight and fuel addition was continued at 5 $\mu Lh^{-1}$. Measurements were restarted at a total reaction time of 23 hours and continued every hour for a total reaction time of 29 hours. The injection of fuel was stopped at 29 hours and 8 minutes, and final aliquots taken at a total reaction time of 30 hours and every hour until a total reaction time of 32 hours. The reaction was again left to stir overnight and a final aliquot taken at a total reaction time of 47 hours.

Variation in rate of fuel addition (5 $\mu Lh^{-1}$ to 10 $\mu Lh^{-1}$) (data in Figure 3.3.4b): the reaction was begun according to the general method, but at an initial rate of fuel addition of 5 $\mu Lh^{-1}$. The reaction was monitored every hour for the first 9 hours. After a reaction time of 9 hours and 10 minutes, the rate of fuel addition was increased to 10 $\mu Lh^{-1}$. Aliquots were then taken at a total reaction time of 10 and 11 hours. The reaction was left to stir overnight and fuel addition was continued at 10 $\mu Lh^{-1}$. Measurements were restarted at a total reaction time of 23 hours and continued every hour for a total reaction time of 29 hours. The injection of fuel was stopped at 29 hours and 10 minutes, and final aliquots taken at a total reaction time of 30 hours and every hour until a total reaction time of 32 hours. The reaction was again left to stir overnight and final aliquots taken at a total reaction time of 47 and 48 hours.

## 3.5.4.4 Investigation into the destruction step

The second thiol-disulfide exchange, forming thermodynamic products **3.3** and **3.5**, occurs between hydrophobic thiol **3.1** and water-soluble surfactant **3.4**. Mechanistic investigation into this step was therefore important since it was possible that this step was also catalysed by the formation of aggregates.

To investigate the destruction step, the initial rates of the reactions in Figure 3.5.11 with variation in $[\mathbf{3.4}]_0$ both below and above the cmc were measured.

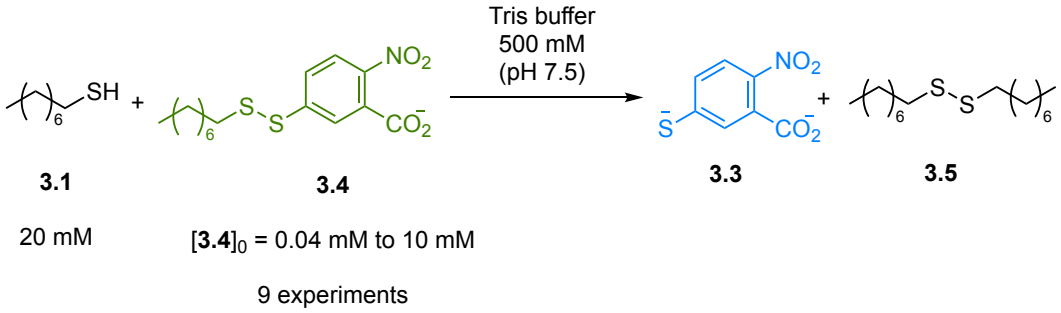



**Figure 3.5.11** Octanethiol **3.1** reacts with **3.4** to produce thiolate **3.3** and disulfide **3.5**. The initial rate of this reaction over a series of $[\mathbf{3.4}]_0$ was measured to test if the reaction was catalysed by aggregates of **3.4**.

Solutions prepared in Section 3.5.2.3 with varying concentration of **3.4**, both below and above the measured cmc, were used for this study (Table 3.5.2).

5 mL of each solution was placed in a 10 mL round bottomed flask and stirring was started at 100 rpm. Octanethiol (20 µL, 0.10 mmol) was added dropwise by microsyringe onto the top of the solution and the start of this addition was

considered time zero. Aliquots were taken as detailed in Table 3.5.2 at 2, 5, 10, 15, 30 and 60 minutes, and then every hour for a total reaction time of 3 hours. The aliquot and UPLC injection procedures were altered from the standard procedure on account of the very low initial concentration of **3.4** (Table 3.5.2). At each individual concentration, however, the aliquot and UPLC injection procedure remained the same throughout the experiment.

| $[\mathbf{3.4}]_0$ (mM) | Aliquot volume (μL) | External standard (+ maleimide) volume (mL) | Injection volume UPLC (μL) |
|---|---|---|---|
| 10 | 100 | 1.0 | 1 |
| 5 | 100 | 1.0 | 2.5 |
| 2.5 | 100 | 1.0 | 5 |
| 1.25 | 100 | 1.0 | 10 |
| 0.625 | 100 | 1.0 | 10 |
| 0.3125 | 100 | 1.0 | 10 |
| 0.15625 | 100 | 0.5 | 10 |
| 0.078125 | 100 | 0.5 | 10 |
| 0.0390625 | 200 | 0.4 | 10 |

**Table 3.5.2** Aliquot procedures for experiments conducted in Figure 3.5.11.

The initial rates of the degradation of **3.4** and the production of **3.3** were extracted and plotted against $[\mathbf{3.4}]_0$ (Figures 3.5.12 and 3.5.13).

Within experimental error, the rate of production of **3.3** and the rate of degradation of **3.4** appeared to correlate linearly with the initial concentration of surfactant **3.4**; it did not appear that the formation of aggregates accelerated the reaction rate.

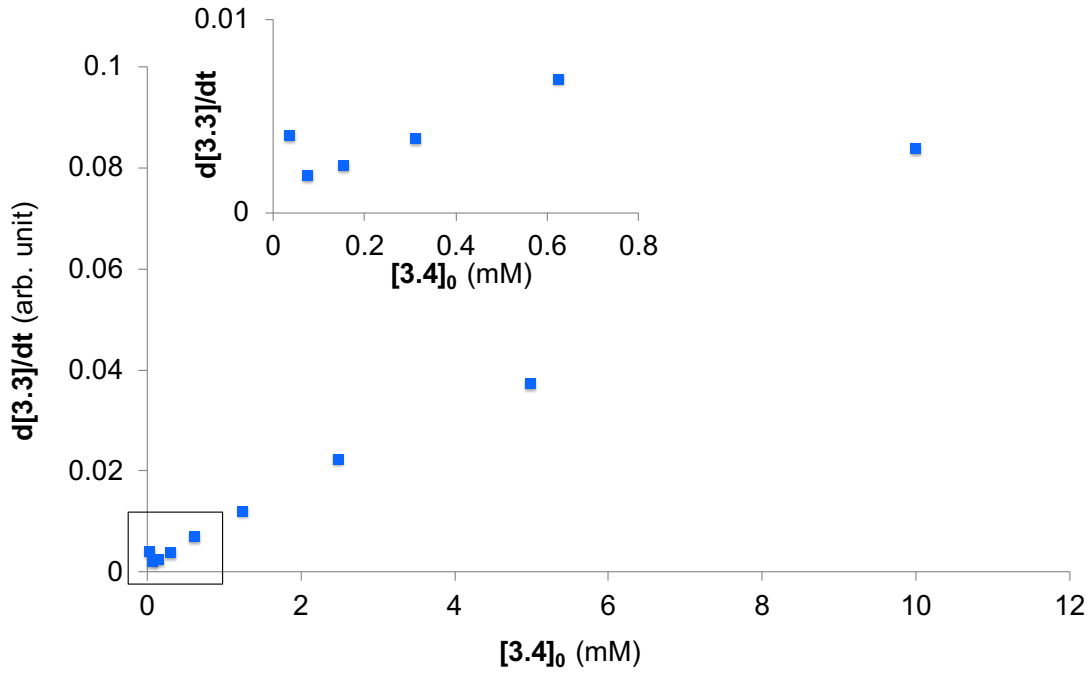



**Figure 3.5.12** Initial rate of production of **3.3** with variation in [**3.4**]$_0$ for reaction in Figure 3.5.11. The inset graph is the expanded data (from box in main graph) where [**3.4**]$_0$ approaches the measured cmc.

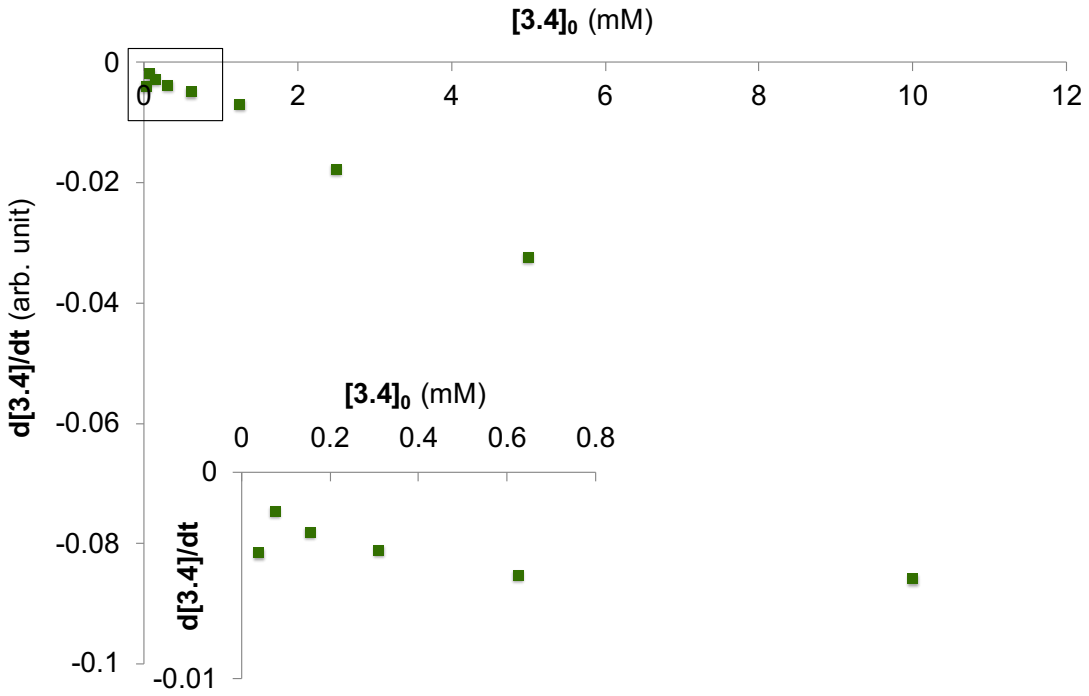



**Figure 3.5.13** Initial rate of degradation of **3.4** with variation in [**3.4**]$_0$ for reaction in Figure 3.5.11. The inset graph is the expanded data (from box in main graph) where [**3.4**]$_0$ approaches the measured cmc.

We recognised that this experiment was limited and the likelihood of experimental error was very high. We therefore also conducted a reaction as detailed in Figure 3.5.14, measuring the rate of decomposition of **3.4** below its cmc in the absence and presence of a spectator anionic surfactant, sodium dodecyl sulfate (sds).

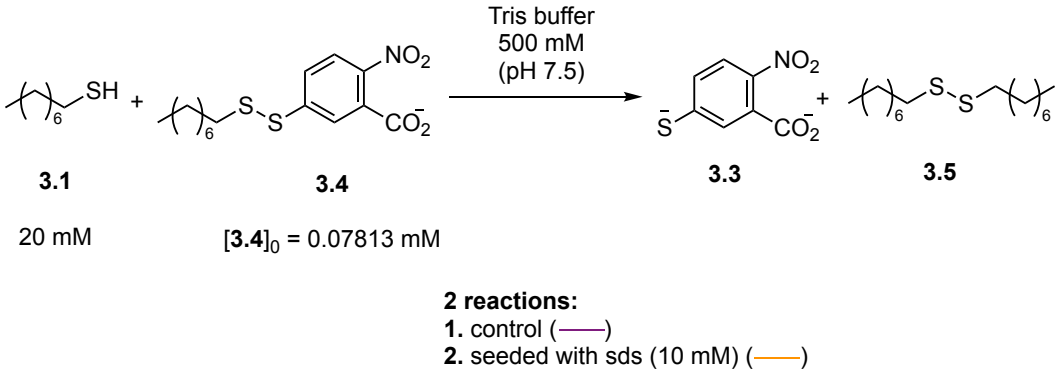



**Figure 3.5.14** Octanethiol **3.1** reacts with **3.4** to produce thiolate **3.3** and disulfide **3.5**. The intial rate of this reaction in the absence and presence of a spectator anionic surfactant was measured.

To two 10 mL round bottom flasks, one containing sodium dodecyl sulfate (7.0 mg, 25 μmol), was added 2.5 mL each of a solution of [**3.4**]$_0$ = 0.7813 mM (prepared in Section 3.5.2.3) and stirring was started at 100 rpm. Octanethiol (20 μL, 0.10 mmol) was added dropwise by microsyringe onto the top of each solution and the start of this addition was considered time zero. 100 μL aliquots were taken at 2, 5, 10, 15, 30, 60 and 120 minutes. To each aliquot was added 0.5 mL of external standard containing maleimide. 10 μL injections were made on the UPLC. Since this procedure was not equivalent to the procedure detailed in Section 3.5.3, only the relative change in concentration of reaction components could be extracted. The plots of [**3.3**] and [**3.4**] in arbitrary units against time are shown in Figures 3.5.15 and 3.5.16 and the linear trendlines are an estimate of initial rates in arbitrary units. The addition of the spectator surfactant, far from accelerating reaction, appeared to slow the rate of reaction.

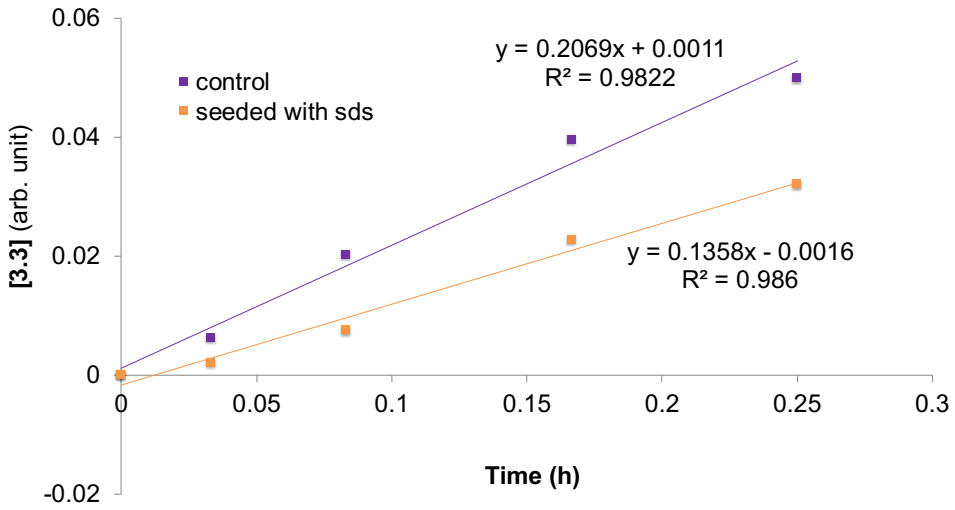



**Figure 3.5.15** Plot of [**3.3**] in arbitrary units *vs.* time for 2 reactions as detailed in Figure 3.5.14. Linear trendlines and associated equations are displayed as a measure of rate.

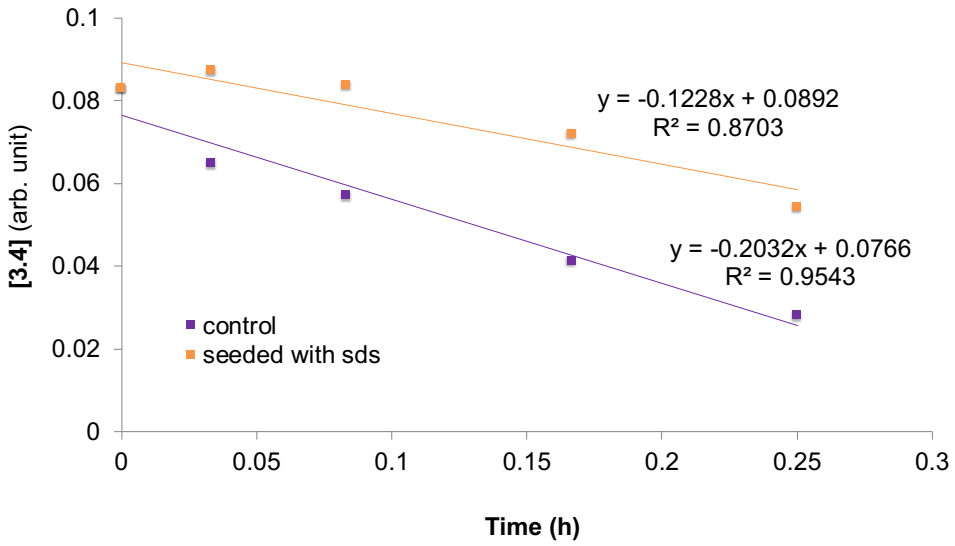



**Figure 3.5.16** Plot of [**3.4**] in arbitrary units *vs.* time for 2 reactions as detailed in Figure 3.5.14. Linear trendlines and associated equations are displayed as a measure of rate.

## 3.6 References


1. Morrow, S. M., Colomer, I. & Fletcher, S. P. A chemically fuelled self-replicator. *Nat. Commun.* **10**, 1011 (2019).
2. Kosikova, T. & Philp, D. Exploring the emergence of complexity using synthetic replicators. *Chem. Soc. Rev.* **46,** 7274–7305 (2017).
3. Grzybowski, B. A., Fitzner, K., Paczesny, J. & Granick, S. From dynamic self-assembly to networked chemical systems. *Chem. Soc. Rev.* **46,** 5647–5678 (2017).
4. Grzybowski, B. A. & Huck, W. T. S. The nanotechnology of life-inspired systems. *Nat. Nanotechnol.* **11,** 585–592 (2016).
5. Mattia, E. & Otto, S. Supramolecular systems chemistry. *Nat. Nanotechnol.* **10,** 111–119 (2015).
6. Ashkenasy, G., Hermans, T. M., Otto, S. & Taylor, A. F. Systems chemistry. *Chem. Soc. Rev.* **46,** 2543–2554 (2017).
7. Schwille, P. How Simple Could Life Be ? *Angew. Chem. Int. Ed.* **56,** 10998–11002 (2017).
8. Duim, H. & Otto, S. Towards open-ended evolution in self-replicating molecular systems. *Beilstein J. Org. Chem.* **13,** 1189–1203 (2017).
9. Higgs, P. G. Chemical Evolution and the Evolutionary Definition of Life. *J. Mol. Evol.* **84,** 225–235 (2017).
10. Pross, A. *What is Life? How chemistry becomes biology*. (Oxford University Press, 2016).
11. England, J. L. Dissipative adaptation in driven self-assembly. *Nat. Nanotechnol.* **10,** 919–923 (2015).
12. England, J. L. Statistical physics of self-replication. *J. Chem. Phys.* **139,** 121923 (2013).
13. Pascal, R., Pross, A. & Sutherland, J. D. Towards an evolutionary theory of the origin of life based on kinetics and thermodynamics. *Open Biol.* **3,** 130156 (2013).
14. Bottero, I., Huck, J., Kosikova, T. & Philp, D. A Synthetic Replicator Drives a Propagating Reaction-Diffusion Front. *J. Am. Chem. Soc.* **138,** 6723–6726 (2016).
15. Semenov, S. N. *et al.* Rational design of functional and tunable oscillating enzymatic networks. *Nat. Chem.* **7,** 160–165 (2015).
16. Semenov, S. N. *et al.* Autocatalytic, bistable, oscillatory networks of biologically relevant organic reactions. *Nature* **537,** 656–660 (2016).
17. Mukherjee, R., Cohen-Luria, R., Wagner, N. & Ashkenasy, G. A Bistable Switch in Dynamic Thiodepsipeptide Folding and Template-Directed Ligation. *Angew. Chem. Int. Ed.* **54,** 12452–12456 (2015).
18. Carnall, J. M. A. *et al.* Mechanosensitive self-replication driven by self-organization. *Science* **327,** 1502–1506 (2010).
19. Sadownik, J. W., Mattia, E., Nowak, P. & Otto, S. Diversification of self-replicating molecules. *Nat. Chem.* **8,** 264–269 (2016).
20. Whitesides, G. M., Lilburn, J. E. & Szajewski, R. P. Rates of thiol-disulfide interchange reactions between mono- and dithiols and Ellman's Reagent. *J. Org. Chem.* **42,** 332–338 (1977).
21. Moss, R. A. & Swarup, S. Transvesicular Reactions of Thiols with Ellman's Reagent. *J. Org. Chem.* **53,** 5860–5866 (1988).

22. Fendler, J. H. & Hinze, W. L. Reactivity Control in Micelles and Surfactant Vesicles. Kinetics and Mechanism of Base-Catalyzed Hydrolysis of 5,5'-Dithiobis(2-nitrobenzoic acid) in Water, Hexadecyltrimethylammonium Bromide Micelles, and Dioctadecyldimethylammonium Chloride Surfactant V. *J. Am. Chem. Soc.* **103,** 5439–5447 (1981).
23. Singh, R. & Whitesides, G. M. Thiol-disulfide interchange. in *The Chemistry of Functional Groups, Supplement S: The Chemistry of Sulphur-Containing Functional Groups* (eds. Patai, S. & Rappoport, Z.) 633–658 (John Wiley & Sons, 1993).
24. Buhse, T., Pimienta, V., Lavabre, D. & Micheau, J. C. Experimental Evidence of Kinetic Bistability in a Biphasic Surfactant System. *J. Phys. Chem. A* **101,** 5215–5217 (1997).
25. Zepik, H. H., Blöchliger, E. & Luisi, P. L. A Chemical Model of Homeostasis. *Angew. Chem. Int. Ed.* **40,** 199–202 (2001).
26. Colomer, I., Morrow, S. M. & Fletcher, S. P. A transient self-assembling self-replicator. *Nat. Commun.* **9,** 2239 (2018).
27. Sorrenti, A., Leira-Iglesias, J., Sato, A. & Hermans, T. M. Non-equilibrium steady states in supramolecular polymerization. *Nat. Commun.* **8,** 15899 (2017).
28. Newsholme, E. A. *Regulation in Metabolism*. (John Wiley & Sons, 1973).
29. Curi, R. *et al.* Regulatory principles in metabolism - then and now. *Biochem. J.* **473,** 1845–1857 (2016).
30. Ragazzon, G. & Prins, L. J. Energy consumption in chemical fuel-driven self-assembly. *Nat. Nanotechnol.* **13,** 882–889 (2018).
31. Boekhoven, J., Hendriksen, W. E., Koper, G. J. M., Eelkema, R. & van Esch, J. H. Transient assembly of active materials fueled by a chemical reaction. *Science* **349,** 1075–1079 (2015).
32. Tena-Solsona, M., Wanzke, C., Riess, B., Bausch, A. R. & Boekhoven, J. Self-selection of dissipative assemblies driven by primitive chemical reaction networks. *Nat. Commun.* **9,** 2044 (2018).
33. van Rossum, S. A. P., Tena-Solsona, M., van Esch, J. H., Eelkema, R. & Boekhoven, J. Dissipative out-of-equilibrium assembly of man-made supramolecular materials. *Chem. Soc. Rev.* **46,** 5519–5535 (2017).
34. Dong, Z. *et al.* Aryl Thiol Substrate 3-Carboxy-4-Nitrobenzenethiol Strongly Stimulating Thiol Peroxidase Activity of Glutathione Peroxidase Mimic 2,2'-Ditellurobis(2-Deoxy-β-Cyclodextrin). *J. Am. Chem. Soc.* **126,** 16395–16404 (2004).
35. Abbasi, M., Mohammadizadeh, M. R., Moosavi, H. & Saeedi, N. One-Pot Synthesis of Organic Disulfides (Disulfanes) from Alkyl Halides Using Sodium Sulfide Trihydrate and Hexachloroethane or Carbon Tetrachloride in the Poly(ethylene glycol) (PEG-200). *Synlett* **26,** 1185–1190 (2015).

# 4

## Molecular Replication and the Amplification of Chirality

## 4.1 A hallmark of life

In the first three chapters of this thesis we have discussed the dynamics that define living systems and our attempts to mimic those characteristics in the laboratory, culminating in the construction of a replicating molecule out-of-equilibrium.

Another characteristic which is considered to be a 'biosignature', or a hallmark of life, is biomolecular homochirality, *i.e.* the exclusive presence of single enantiomers of biologically relevant molecules such as L-amino acids and D-sugars. This property is essential for molecular recognition and processes of biological catalysis and replication, and is therefore intimately tied up with the origins of life itself.[1] However, the mechanism by which this process of complete symmetry breaking was achieved is unknown.

Theories agree on two fundamental processes that may have led to homochirality: first, an initial source of symmetry breaking (or a stochastic event) causing a chiral imbalance; second, amplification of the initial imbalance to homochirality.[1,2]

The initial imbalance in the enantiomeric ratio could be ascribed to a number of sources, from the action of circularly polarised light, to extraterrestrial origins, to name but a couple.[2] Of greater interest to us is the subsequent amplification of this initial imbalance; autocatalysis is a process of amplification and would have the power to amplify small chiral imbalances to enantiopurity.

## 4.2 Autocatalysis and the amplification of chirality

The Frank model provided a theoretical basis for the amplification of chirality by an autocatalytic reaction.[1,3] A general scheme for the Frank model is depicted in Figure 4.2.1. Each of the arbitrary enantiomers L and D is an asymmetric and enantioselective autocatalyst, thus capable of promoting the formation of the product of its own configuration.

Enantioselective autocatalysis alone, however, is not enough. If a catalyst is not 100% selective, it will eventually generate its product antimers which are, by definition, autocatalysts themselves. Thus, the overall enantioselectivity of the reaction would inevitably degrade over time.[4]

The system must include an additional ‘mutual antagonism’, which arises when substrates L and D react or combine together to form an inactive complex that is unable to replicate. Over time, the enantiomeric excess of the system is increased.

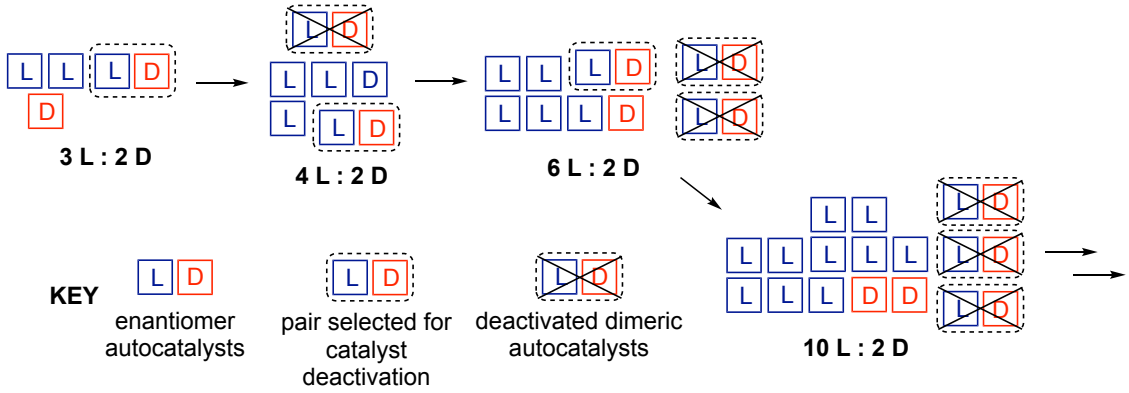



**Figure 4.2.1** The Frank model for the attainment of a homochiral state *via* enantioselective autocatalysis and deactivation of the minor enantiomer *via* mutual antagonism. Adapted with permission from reference[1].

The key, therefore, is to have both an enantioselective reaction and inhibition of the minor enantiomer. The challenge is a formidable one.

## 4.2.1 Experimental demonstration of asymmetric autocatalysis and the amplification of chirality

The *only* robust demonstration of the amplification of chirality *via* an enantioselective autocatalytic reaction is the Soai reaction, depicted in Figure 4.2.2,[5] which may be seen as an experimental realisation of the Frank model.[6] Here, the chiral product alcohol **4.1H** can act as an enantioselective autocatalyst by forming catalytically active chiral aggregates with diisopropyl zinc **4.2** which promote the enantioselective addition of diisopropyl zinc to prochiral aldehyde **4.3**. Catalytically inactive heterochiral and catalytically active homochiral aggregates of **Zn(4.1)($^{i}$Pr)** form with essentially no preference for heterochiral

over homochiral, giving a statistical distribution. Thus, the minor enantiomer is sequestered into the inactive heterochiral aggregates whilst the homochiral aggregates continue to catalyse the reaction enantioselectively. As a result, the absolute amount of chiral material and the ee increase over the course of reaction, with the amount of substrate as the only limitation. Continued rounds of the reaction, *i.e.* the addition of the product from one reaction batch to new starting material, allows the ee to increase in an effectively unlimited fashion until effective homochirality is reached.

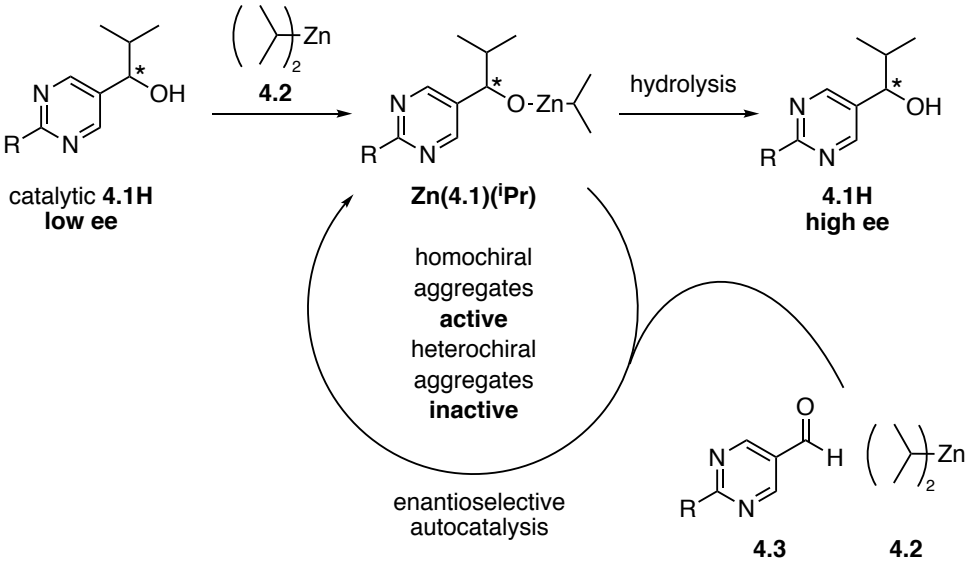



**Figure 4.2.2** The Soai reaction:[5–7] aggregates are formed from a catalytic quantity of alkanol **4.1H** of low ee and diisopropylzinc **4.2**. The minor enantiomer of the alkanol **4.1H** is sequestered into catalytically inactive heterochiral aggregates, whilst homochiral aggregates of the product **4.1H** and diisopropyl zinc **4.2** catalyse the addition of diisopropylzinc **4.2** to aldehyde **4.3** enantioselectively, increasing the ee of the forming alkanol **4.1H**. Adapted with permission from reference[5].

The system is idiosyncratic and tolerant only to small variation. Attempts to realise other autocatalytic reactions with the amplification of chirality, such as the small molecule template replicators that we touched upon in the first chapter of this thesis, have, unsurprisingly, been unsuccessful.[8,9]

The closest attempt is the design and realisation of an enantioselective peptide replicator, in which each homochiral template (**4.4$_{LL}$** or **4.4$_{DD}$**) was observed to be a "selfish" autocatalyst, promoting the formation of templates of its own handedness alone (Figure 4.2.3).[10] The heterochiral **4.4$_{LD}$**/**4.4$_{DL}$** templates were inactive. The origin of this enantioselectivity was the thermodynamic stability of the coiled coils made up of homochiral templates of the same handedness (*i.e.* dimer **4.4$_{LL}$.4.4$_{LL}$** was more stable than **4.4$_{LL}$.4.4$_{DD}$**). Notably, this work did not consider the amplification of chirality experimentally; the starting materials **4.5** and **4.6** were racemic and both enantiomers **4.4$_{LL}$** and **4.4$_{DD}$** were produced in equal quantity. Two later theoretical treatments considered the conditions that would be required to experimentally observe the amplification of chirality in this system,[11,12] including the formation of a **4.4$_{LL}$.4.4$_{DD}$** dimer. No explicit statement of mutual antagonism, or the catalytic inactivity of this dimer, was made, but the optical inactivity of the *meso* dimer would 'silence' the minor enantiomer. This process has not yet been born out experimentally.

It is important to note that in this case, unlike the Soai reaction, the absolute amount of chiral material would not increase over the course of the reaction; it is instead redistributed from starting materials to products. Nevertheless, it would

still represent an “amplification” from the ee in the starting materials to the ee in the products.

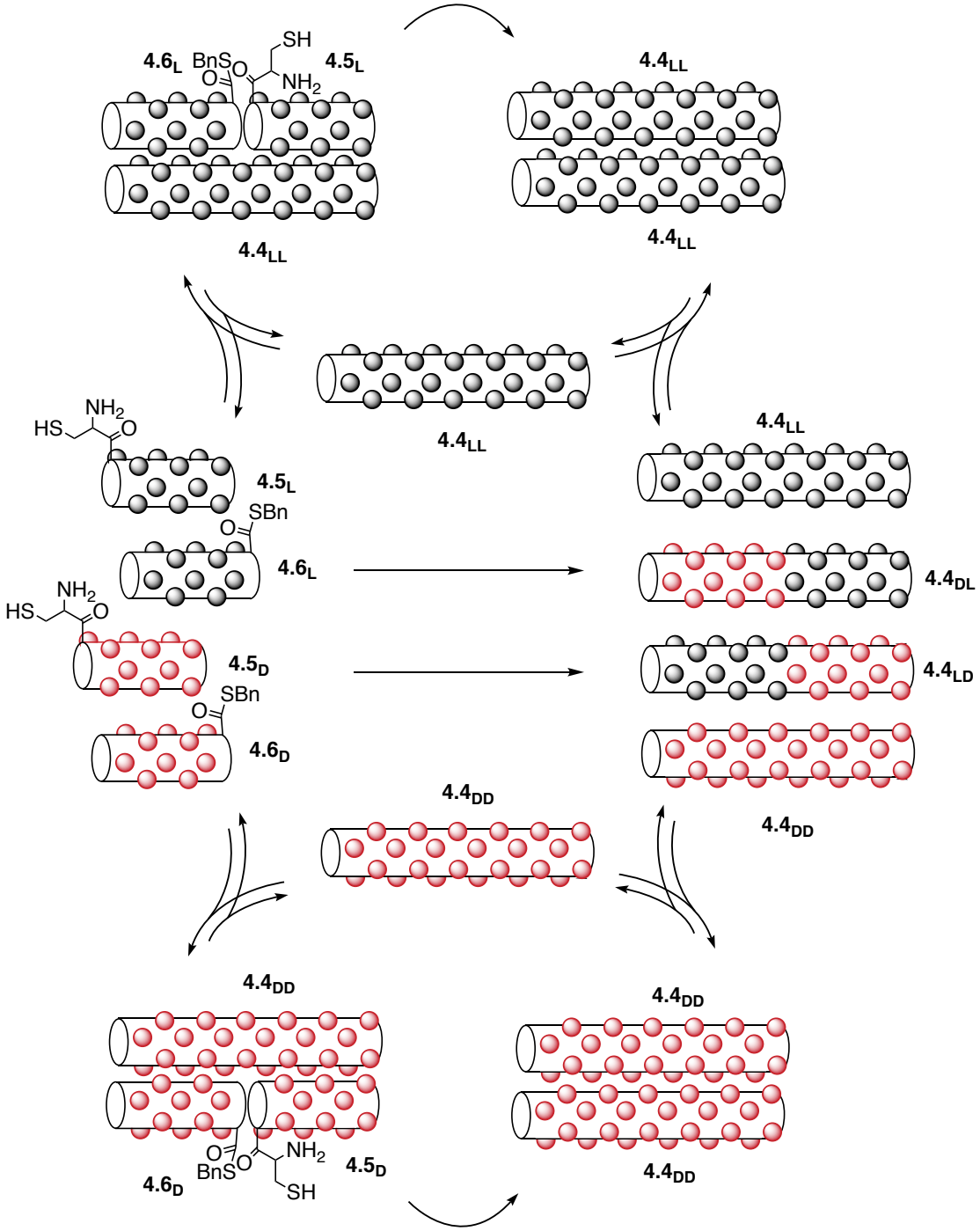



**Figure 4.2.3** An enantioselective peptide replicator. Templates **4.4$_{LL}$** and **4.4$_{DD}$** are enantioselective autocatalysts. Templates **4.4$_{DL}$** and **4.4$_{LD}$** are catalytically inactive. Adapted with permission from reference[10].

The enantioselective catalysis achieved in the system in Figure 4.2.3, and the aggregate formation in the Soai reaction, suggests to us that more general success in the amplification of chirality for systems undergoing a process of replication could be found for large, supramolecular molecules or structures with a great number and degree of chiral intermolecular interactions. The increased number of hierarchical interactions relative to the interactions between small molecules might render their chiral recognition ability more strong, and their sense of 'handedness' more readily transmitted.[8,13] Naturally, therefore, we look to supramolecular autocatalysts and replicators as candidates for the amplification of chirality. The following section considers how physical autocatalysis might lead to the amplification of chirality.

## 4.3 Replication of micelles and the amplification of chirality

The basic requirements for an autocatalytic and enantioselective reaction which displays an amplification of chirality would also apply to a system of replicating micelles, but this research area is underexplored.[14,15] Firstly, a chiral surfactant would have to be capable of enantioselective autocatalysis, promoting the formation of itself as a single enantiomer over the formation of the product of opposite chirality. Secondly, the catalytic activity of the minor enantiomer must be inhibited.

By analogy with the Frank model, we have designed a general scheme for the amplification which is presented in Figure 4.3.1, beginning with chiral starting materials. We repeat here the important point that, unlike the Soai reaction, the

absolute amount of chiral material will not increase over the course of the reaction since we begin with chiral starting materials rather than a prochiral substrate. Instead it is redistributed from starting materials to products. The “amplification of chirality” refers to the increase in the ee from starting materials to products, enabled by a process of enantioselective autocatalysis coupled with the inhibition of the catalytic activity of the minor enantiomer.

In a system consisting of 50% ee in the starting materials, the ee of surfactant molecules formed at the interface in the uncatalyzed reaction is 50% (Figure 4.3.1). However, in the ideal case, once the critical micelle concentration is reached the surfactant enantiomers undergo partitioning into enantiopure micelles, derived from the major enantiomer of starting material, and a racemic species which acts to sequester the minor enantiomer. The enantiopure micelles would be catalytically active and enantioselective, promoting the formation of new surfactants of their own chirality only. Further, the racemic surfactant would be rendered catalytically inactive by differing in its physical properties from the enantiopure (greater propensity for crystallisation, for example). Continued surfactant formation would therefore result in the amplification of chirality, or the increase in enantiomeric excess from starting materials to products, in a process akin to a kinetic resolution.

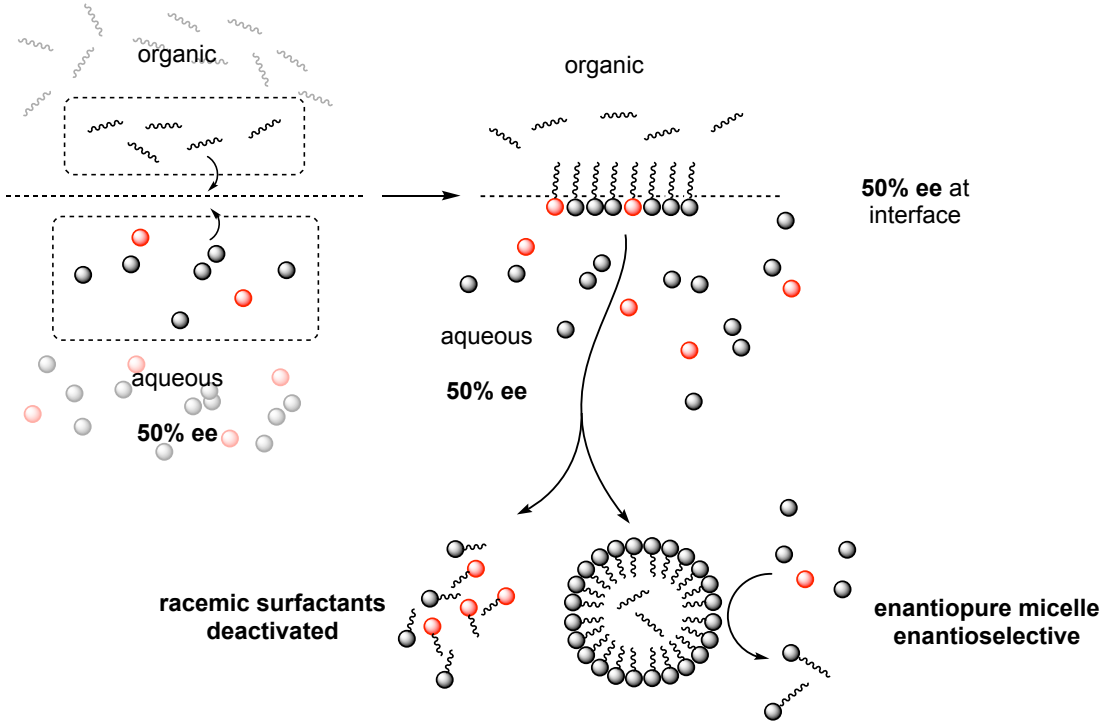



**Figure 4.3.1** Our proposed model for the amplification of chirality by physical autocatalysis based on the Frank model. We require that the minor enantiomer is sequestered into a catalytically inactive species, whilst the major enantiomer forms an enantiopure micelle which undergoes enantioselective autocatalysis.

The precedent for both mutual antagonism in surfactant assembly and enantioselective micelle catalysis are limited; these properties are explored in the following sections.

## 4.3.1 Mutual antagonism

The first requirement for the amplification of chirality is the inhibition of the minor enantiomer by reduced activity of the heterochiral species. In the case of a

physical replicator, or surfactant, significantly different physical properties may be observed between racemic and enantiopure states.

Investigation into an enantioselective variant of Luisi's classical vesicle replicators arrived in 1997 with work by Morigaki *et al.*.[14] Carboxylic acids **(*R*)-4.7** and **(*S*)-4.7** were prepared as chiral variants of a previous vesicle forming autocatalytic system (Figure 4.3.2).[16–18]

Observable differences between the enantiopure and racemic species arose on thermal analysis of the vesicles. The phase transition temperature of the vesicles was highly dependent on the enantiomeric composition; a racemic bilayer was shown to have a higher phase transition temperature than the enantiopure bilayer, and the minimum phase transition temperatures were obtained at a composition that reflected the eutectic ee (Figure 4.3.2). The shape of the binary phase diagram indicated that **4.7** crystallised as a racemate, and this was in agreement with the observation that a racemic sample of vesicles appeared to crystallise more easily than the enantiopure. Further, it was demonstrated that exchange between vesicles was rapid; mixing pre-prepared enantiopure vesicle suspensions of **(*R*)-4.7** and **(*S*)-4.7** quickly resulted in the formation of racemic vesicles. These properties resulted in the much reduced catalytic activity of the racemic system compared to the enantiopure at a temperature of 10 °C. This was below the phase transition temperature of the racemic vesicles, but above that of the enantiopure vesicles (*i.e.* a temperature at which the racemate would precipitate out whilst the enantiopure would remain solvated).

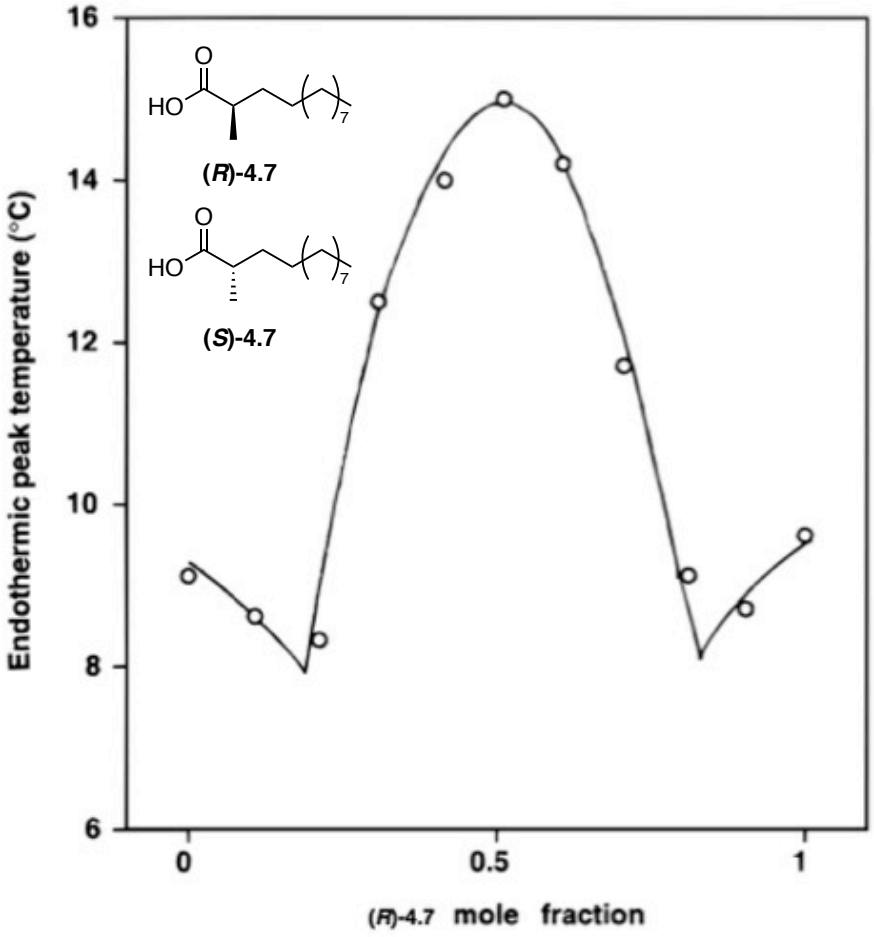



**Figure 4.3.2** The phase transition temperature dependence of vesicles of **4.7** on their enantiomeric composition ([**4.7**] = 100 mM, solution pH = $pK_a$ **4.7**). Enantiopure vesicles are observed to have a lower phase transition temperature than racemic vesicles. Reproduced with permission from reference[14].

## 4.3.2 Enantioselective micelle catalysis

Examples of enantioselective micelle catalysis, where a chiral surfactant assembles into chiral micelles and provides a chiral reaction environment, are relatively rare. Despite the highly dynamic nature of the micelles and the ill-defined reaction environment, small ee's have been realised in some cases.[19–22]

The chiral morphology and chiral recognition afforded by some chiral surfactants has also been studied.[22]

For the system described in Section 4.3.1,[14] however, the non-trivial test of enantioselective autocatalysis was negative; there was no significant difference in the rates of hydrolysis between the hydrolysis of anhydride **(*R,R*)-4.8** in the presence of vesicles of its own chirality, compared to hydrolysis in the presence of vesicles of the opposite chirality (Figure 4.3.3).

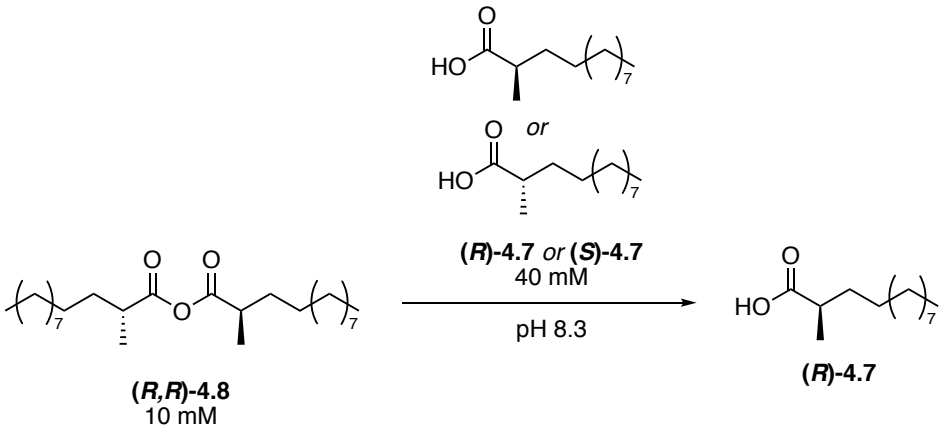



**Figure 4.3.3** The rate of hydrolysis of **(*R,R*)-4.8** to **(*R*)-4.7** was, within experimental error, the same between reactions catalysed by **(*R*)-4.7** or by **(*S*)-4.7**. Vesicles of **4.7** do not perform enantioselective hydrolysis.[14]

Nevertheless, an element of diastereoselectivity could be observed in the system (Figure 4.3.4):[14] in comparing the rates of hydrolysis of **(*R,R*)-4.8** and **4.8(mix)** (Figure 4.3.4), catalysed by **(*R*)-4.7**, an enhanced rate was observed for the hydrolysis of **(*R,R*)-4.8** (Figures 4.3.4 and 4.3.5).

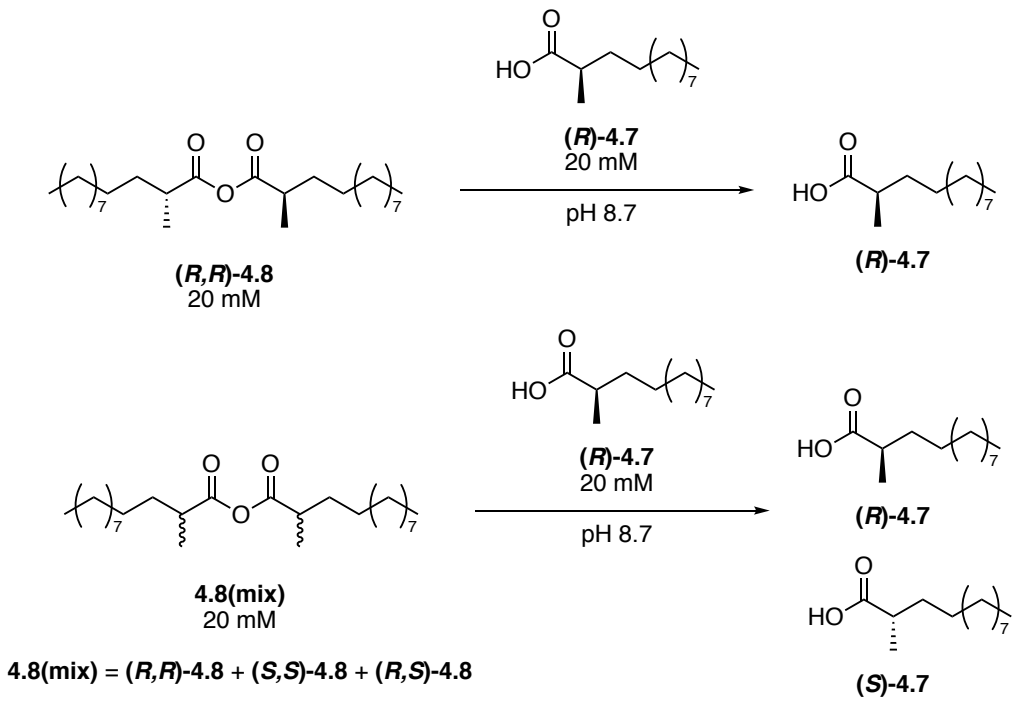



**Figure 4.3.4** Diastereoselectivity in anhydride hydrolysis was tested by comparing the rates of the hydrolysis of **(*R,R*)-4.8** and **4.8(mix)** catalysed by **(*R*)-4.7**.[14]

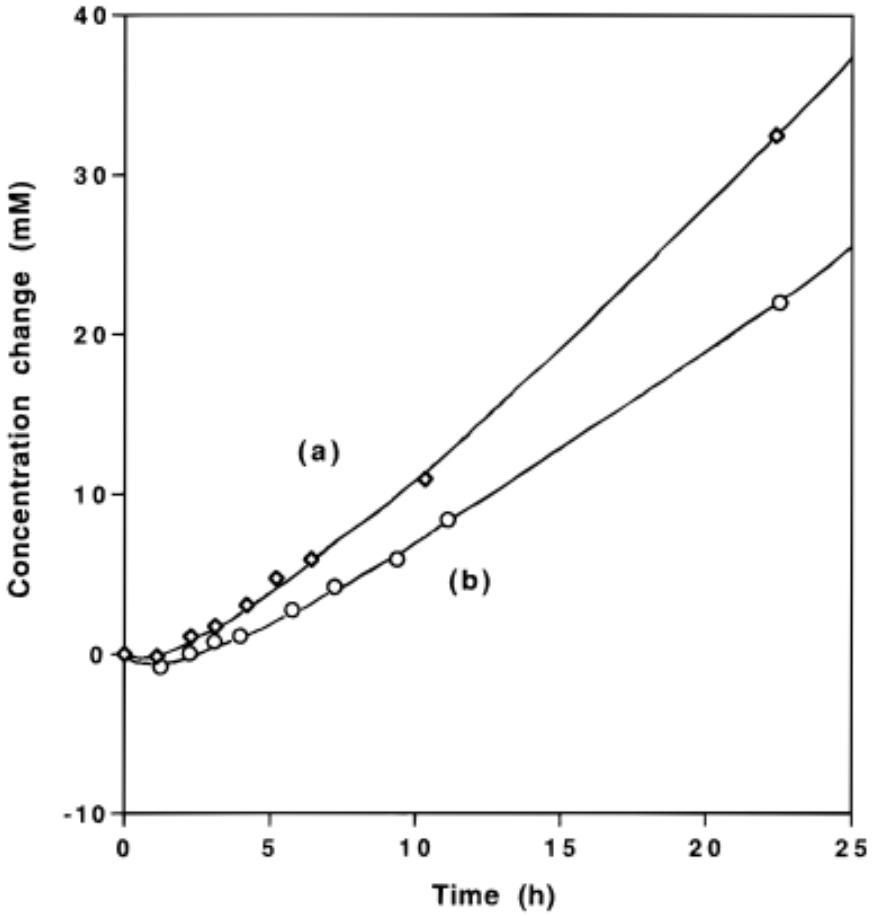



**Figure 4.3.5** Plot of [**4.7**] vs. time for the hydrolysis of **(*R,R*)-4.8** (**a**) or **4.8(mix)** (**b**), catalysed by **(*R*)-4.7**. Reaction conditions are shown in Figure 4.3.4. Reproduced with permission from reference[14].

In total, despite the opportunities offered by physical differentiation between racemic and enantiopure states within supramolecular assemblies of surfactants, no asymmetric autocatalytic reaction had been realised for this system.

## 4.4 Project Aim

The title of the Soai reaction as the *only* robust demonstration of the amplification of chirality *via* an autocatalytic reaction makes a search for other, more general reactions with the power to amplify chirality of fundamental interest.

The well explored chiral recognition and amplification that can be achieved in supramolecular assemblies suggested to us that the study of the replication of large, supramolecular structures might lead us to the amplification of chirality.[13] Indeed, other supramolecular replicators have been examined for these properties, albeit with limited success.[10,14,15] Though a very challenging task, our success in the realisation of replicating micelles encouraged us to consider the construction of chiral replicating micelles capable of chiral amplification.

The ability of a chiral micelle to provide a chiral reaction environment and induce enantioselectivity was, albeit to a limited extent, known.[19–22] Similarly, there was precedent for the ability to differentiate the racemic and enantiopure states of surfactants by their physical properties.[14]

Chapters 5 and 6 detail two designs for a system as pictured in Figure 4.3.1. One is based on a novel system whose amphiphilic components are formed by an irreversible reaction, and one is a chiral variant of the surfactant constructed by thiol-disulfide exchange as realised in Chapter 3. The examination of the amplification of chirality for a system of replicating supramolecular aggregates was underexplored and the results would be unpredictable.

## 4.5 References


1. Blackmond, D. G. The origin of biological homochirality. *Cold Spring Harb. Perspect. Biol.* **2,** a002147 (2010).
2. Feringa, B. L. & van Delden, R. A. Absolute Asymmetric Synthesis: The Origin, Control, and Amplification of Chirality. *Angew. Chem. Int. Ed.* **38,** 3418–3438 (1999).
3. Frank, F. C. On spontaneous asymmetric synthesis. *Biochim. Biophys. Acta* **11,** 459–463 (1953).
4. Blackmond, D. G. Asymmetric autocatalysis and its implications for the origin of homochirality. *Proc. Natl. Acad. Sci.* **101,** 5732–5736 (2004).
5. Soai, K., Shibata, T., Morioka, H. & Choji, K. Asymmetric autocatalysis and amplification of enantiomeric excess of a chiral molecule. *Nature* **378,** 767–768 (1995).
6. Blackmond, D. G., McMillan, C. R., Ramdeehul, S., Schorm, A. & Brown, J. M. Origins of Asymmetric Amplification in Autocatalytic Alkylzinc Additions. *J. Am. Chem. Soc.* **123,** 10103–10104 (2001).
7. Soai, K., Kawasaki, T. & Matsumoto, A. Asymmetric Autocatalysis of Pyrimidyl Alkanol and Its Application to the Study on the Origin of Homochirality. *Acc. Chem. Res.* **47,** 3643–3654 (2014).
8. Kindermann, M., Stahl, I., Reimold, M., Pankau, W. M. & Von Kiedrowski, G. Systems chemistry: Kinetic and Computational Analysis of a Nearly Exponential Organic Replicator. *Angew. Chem. Int. Ed.* **117,** 6908–6913 (2005).
9. Wang, B. & Sutherland, I. O. Self-replication in a Diels–Alder reaction. *Chem. Commun.* 1495–1496 (1997).
10. Saghatellan, A., Yokobayashi, Y., Soltani, K. & Ghadiri, M. R. A chiroselective peptide replicator. *Nature* **409,** 797–801 (2001).
11. Rivera Islas, J., Pimienta, V., Micheau, J. C. & Buhse, T. Kinetic analysis of artificial peptide self-replication. Part II: The heterochiral case. *Biophys. Chem.* **103,** 201–211 (2003).
12. Islas, J. R., Micheau, J. & Buhse, T. KINETIC ANALYSIS OF SELF-REPLICATING PEPTIDES: POSSIBILITY OF CHIRAL AMPLIFICATION IN OPEN SYSTEMS. *Orig. life Evol. Biosph.* **34,** 497–512 (2003).
13. Morrow, S. M., Bissette, A. J. & Fletcher, S. P. Transmission of chirality through space and across length scales. *Nat. Nanotechnol.* **12,** 410–419 (2017).
14. Morigaki, K., Dallavalle, S., Walde, P., Colonna, S. & Luisi, P. L. Autopoietic Self-Reproduction of Chiral Fatty Acid Vesicles. *J. Am. Chem. Soc.* **119,** 292–301 (1997).
15. Bukhryakov, K. V., Almahdali, S. & Rodionov, V. O. Amplification of Chirality through Self-Replication of Micellar Aggregates in Water. *Langmuir* **31,** 2931–2935 (2015).
16. Bachmann, P. A., Luisi, P. L. & Lang, J. Autocatalytic self-replicating micelles as models for prebiotic structures. *Nature* **357,** 57–59 (1992).
17. Morigaki, K., Dallavalle, S., Walde, P., Colonna, S. & Luisi, P. L. Autopoietic Self-Reproduction of Fatty Acid Vesicles. *J. Am. Chem. Soc.* **116,** 11649–11654 (1994).
18. Wick, R., Walde, P. & Luisi, P. L. Light Microscopic Investigations of the

Autocatalytic Self-Reproduction of Giant Vesicles. *J. Am. Chem. Soc.* **117,** 1435–1436 (1995).
19. Dwars, T., Paetzold, E. & Oehme, G. Reactions in micellar systems. *Angew. Chem. Int. Ed.* **44,** 7174–99 (2005).
20. La Sorella, G., Strukul, G. & Scarso, A. Recent advances in catalysis in micellar media. *Green Chem.* **17,** 644–683 (2015).
21. Jiang, J., Ouyang, G., Zhang, L. & Liu, M. Self-Assembled Chiral Nanostructures as Scaffolds for Asymmetric Reactions. *Chem. Eur. J.* **23,** 9439–9450 (2017).
22. Sorrenti, A., Illa, O. & Ortuno, R. M. Amphiphiles in aqueous solution: well beyond a soap bubble. *Chem. Soc. Rev.* **42,** 8200–8219 (2013).

# 5

## Chiral Surfactant Formation by Native Chemical Ligation

## 5.1 Introduction

In the first attempt to achieve a process of enantioselective physical autocatalysis with the increase in ee from starting materials to surfactant products, we were interested in the construction of a chiral replicator formed *via* an irreversible reaction.

## 5.2 System design

In a search for a simple bond-forming reaction for chiral amphiphile formation, we were inspired by a publication from Brea *et al.*, with work on the construction of synthetic phospholipids by native chemical ligation (Figure 5.2.1).[1,2] In this work, a native chemical ligation reaction between a water-soluble cysteine-functionalised lysolipid **5.1** and a water-soluble long chain acyl thioester **5.2** resulted in the generation of phospholipids **5.3**, which were able to self-assemble *in situ* to form membrane-bound vesicles.

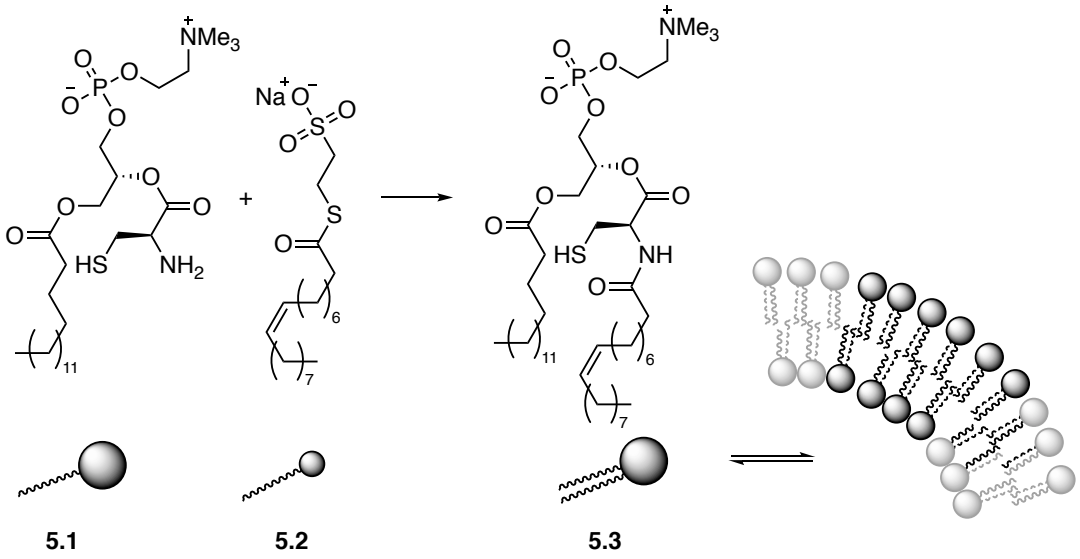



**Figure 5.2.1** Native chemical ligation between lysolipid **5.1** and thioester **5.2** (both water-soluble) results in the formation of phospholipid **5.3**, which is able to self-assemble into vesicular structures.[1]

The simple, neat, and biologically-relevant reaction for the construction of chiral phospholipids in aqueous conditions inspired us to consider a native chemical ligation reaction for the synthesis of a chiral, single-tailed surfactant, with an amino acid as the polar head group. Other surfactants rendered chiral by single amino acid groups had been shown to form chiral phases and perform chiral recognition, properties which would be essential for a process of enantioselective autocatalysis.[3]

Native chemical ligation between an achiral, hydrophobic thioester **5.4** and the amino acid cysteine would result in the formation of a simple, chiral surfactant **5.5** (Figure 5.2.2), which would ideally partition into a catalytically active enantiopure phase, and an inactive racemic phase. If subsequent surfactant formation, catalysed by the enantiopure micelle, were enantioselective then this would

constitute a mechanism for the amplification of chirality from a small initial imbalance in starting materials, to a large enantiomeric excess in products, as discussed in Chapter 4.

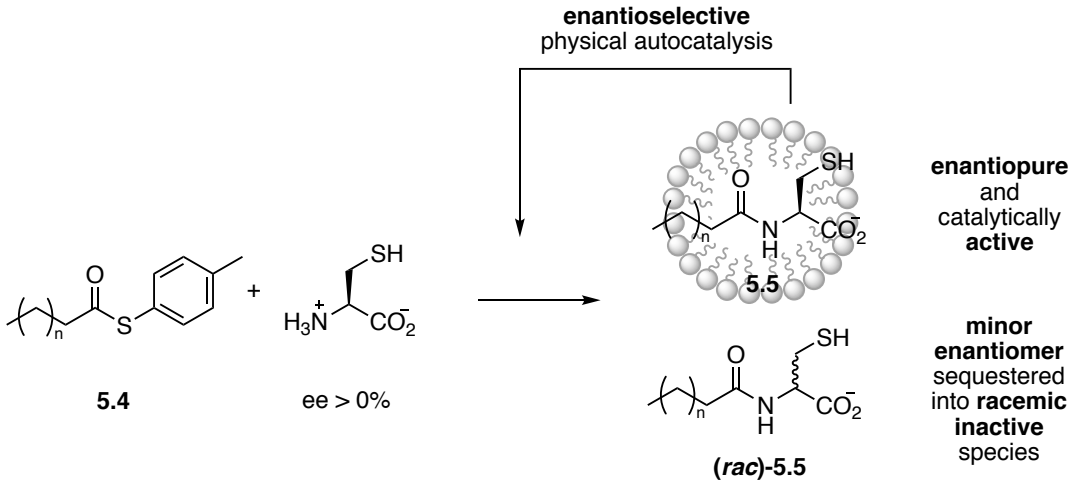



**Figure 5.2.2** Design for the amplification of chirality *via* an autocatalytic native chemical ligation between achiral thioester **5.4** and cysteine. Partitioning of surfactant **5.5** into a catalytically active, enantiopure and enantioselective phase alongside an inactive racemic phase would result in the increase in ee in product **5.5** relative to the starting materials.

## 5.3 Surfactant characterisation

We focused on two simple long chain hydrophobic thioester molecules **5.6a** and **5.6b**. The target surfactants **5.7a** and **5.7b** were first synthesised as the enantiopure products under homogeneous conditions (Figure 5.3.1). On reacting L-cysteine with thioesters **5.6a** and **5.6b** (under reducing conditions with $NaBH_4$), both reactions showed conversion to the desired products **(*R*)-5.7a** and **(*R*)-5.7b** without side product formation (Figure 5.3.1).

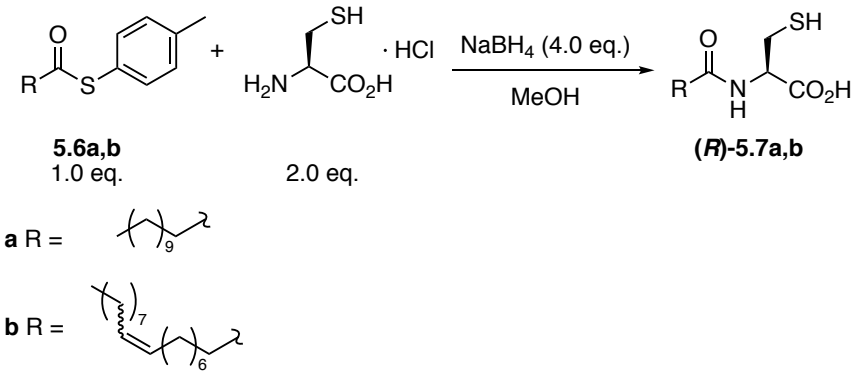



**Figure 5.3.1** Synthesis of surfactants **(*R*)-5.7a** and **(*R*)-5.7b** under homogeneous conditions.

The aggregation properties of enantiopure surfactants **5.7a** and **5.7b** were tested by dynamic light scattering (DLS) (Section 5.8.2.1). At a concentration of 10 mM in Tris buffer (pH 8.6), and in the presence of a reducing agent (TCEP) to prevent oxidation, the enantiopure surfactants **5.7a** and **5.7b** formed micelles ($R_h$ = 5.5 nm and 7.5 nm respectively). We were also able to directly observe aggregates of **5.7b** via interferometric scattering microscopy (Section 5.8.2.2).

## 5.4 Optimisation of the biphasic reaction

Early optimisation of the reaction under biphasic conditions began with thioester **5.6a**. It was quickly established that the use of anaerobic conditions and a water soluble reducing agent, tris(2-carboxyethyl)phosphine (TCEP), was essential for the observation of starting material conversion. On account of the slow biphasic reaction (~ 48 hours) and the propensity of L-cysteine to undergo oxidation, a high concentration of reducing agent (TCEP) was required to maintain aqueous cysteine in the reduced state and for reaction to reach adequate conversion. Use

of excess reducing agent would also prevent the oxidation of the surfactant **(*R*)-5.7a** to disulfide **(*R,R*)-5.8a** (Table 5.4.1).

A more thorough optimisation began with the reaction scheme detailed in Table 5.4.1, with product distributions determined by $^1$H NMR spectroscopy in $(CD_3)_2SO$, in which all components were fully soluble, with reference to an external standard (maleic acid). Conditions of excess L-cysteine were employed since this would enable us eventually to monitor any enantiomeric enrichment that would come about under non-racemic reaction conditions.

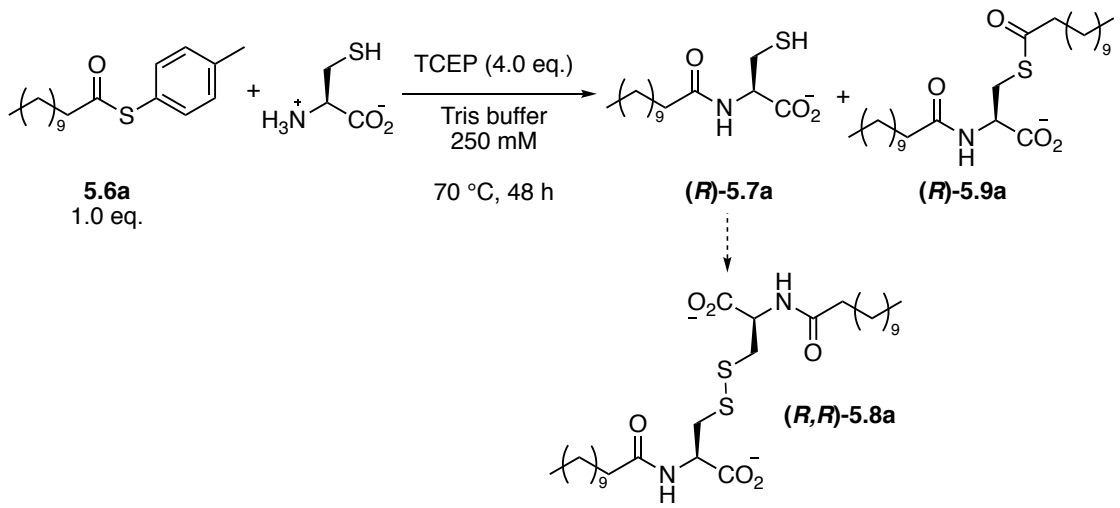
Under these conditions, ≥ 96% conversion of thioester **5.6a** could be achieved, as well as avoiding the formation of **(*R,R*)-5.8a**. However, in stark contrast to the homogeneous reaction, conversion to a dual addition product **(*R*)-5.9a** was observed despite the use of excess L-cysteine. Conversion to this product was variable between reactions performed under the same conditions (*cf.* entries 1 and 2, Table 5.4.1).

No control over the formation of **(*R*)-5.9a** could be achieved with pH *(cf.* entries 2,3 and 4, Table 5.4.1). indeed, the reaction shut down below pH 8.0; the deprotonation of the L-cysteine side chain residue ($pK_a$ 8.16) was presumably essential for reactivity (entry 3, Table 5.4.1).

Tentatively, we ascribe the formation of product **(*R*)-5.9a** to the biphasic reaction conditions. Solvation of thioester **5.6a** in the aqueous phase by surfactant **(*R*)-5.7a** increases its local concentration and makes it more likely that reaction

between surfactant **(*R*)-5.7a** and thioester **5.6a** will take place. Thioester **(*R*)-5.9a**, a two-tailed amphiphilic molecule, may be of interest in its own right as a potential autocatalyst and vesicle-forming compound. In total, however, the lack of consistency between experiments makes it difficult to formulate any theory for its formation and stability under biphasic conditions.

Full conversion to the target single tail surfactant **(*R*)-5.7a** was achieved consistently on the use of an increased number of equivalents of L-cysteine, from 2.0 to 4.0, under the conditions as detailed in Table 5.4.1.

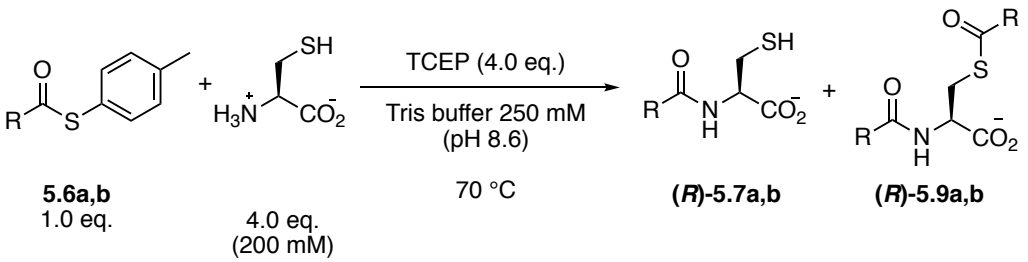


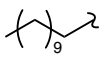

| Entry | pH | Equivalents cysteine | Conversion (%)[a] | |
|---|---|---|---|---|
| | | | **(*R*)-5.7a** | **(*R*)-5.9a** |
| 1 | 8.6 | 2.0 (100 mM) | 64 | 34 |
| 2 | 8.6 | 2.0 | 84 | 16 |
| 3 | 7.8 | 2.0 | 0 | 0 |
| 4 | 8.0 | 2.0 | 42 | 54 |
| 5 | 8.6 | 4.0 (200 mM) | 97 | 0 |

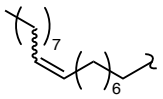
**Table 5.4.1** Optimisation of the biphasic reaction between thioester **5.6a** and L-cysteine. Each entry details the results from a single reaction. [a] Conversions were determined by $^1$H NMR spectroscopy in $(CD_3)_2SO$ with maleic acid as an external standard.

Having observed the shift in reactivity for thioester **5.6a** from homogeneous to biphasic reaction conditions, we were interested in the reactivity of thioester **5.6b** with a longer hydrophobic tail. The reactivity of thioester **5.6b** was tested alongside that of thioester **5.6a** under the conditions optimised for thioester **5.6a** (Table 5.4.2). It was clear that the dual addition product **(*R*)-5.9b** formed far more readily than **(*R*)-5.9a**, with significant conversion after only 5 hours accompanied by the appearance of precipitate in the reaction. Over the same time period for

the reaction with thioester **5.6a**, low conversion to the single addition product **(*R*)-5.7a** alone was observed (*cf.* entries 1 and 2, Table 5.4.2). Interestingly, the reaction conditions also appeared to induce isomerisation of the oleyl chain, but this was not quantified.[4]




**a** R = 

**b** R = 

| Entry | Thioester | Time (h) | Conversion (%)[a] | |
|---|---|---|---|---|
| | | | Single addition **(*R*)-5.7a,b** | Dual addition **(*R*)-5.9a,b** |
| 1 | **5.6a** | 5 | 18 | 0 |
| 2 | **5.6b** | 5 | Trace[b] | 47[b] |
| 3 | **5.6b** | 16 | 100 | 0 |

**Table 5.4.2** Comparison of reactivity of thioesters **5.6a** and **5.6b** under conditions optimised for the biphasic reaction of **5.6a**. Each entry details the results from a single reaction. [a] Conversions were determined by $^1$H NMR spectroscopy in $(CD_3)_2SO$ with maleic acid as an external standard. [b] Conversions were determined by $^1$H NMR spectroscopy in $(CD_3)_2CO$ with maleic acid as an external standard.

Despite the observation of dual addition product **(*R*)-5.9b** at low conversion, its formation appeared reversible; exclusive formation of the single addition product **(*R*)-5.7b** was achieved at full conversion (entry 3, Table 5.4.2). Full conversion of **5.6b** required a reaction time of only 16 hours, with comparison to a reaction time of 48 hours for full conversion of thioester **5.6a** (entry 5, Table 5.4.1).

Both the significant difference in reaction time and product distribution between reactions of thioesters **5.6a** and **5.6b** highlight the importance of the physical properties of molecules on their reactivity in biphasic systems. Differences in solubility and in the nature of aggregates formed can significantly alter reactivity.

## 5.5 Test for autocatalysis

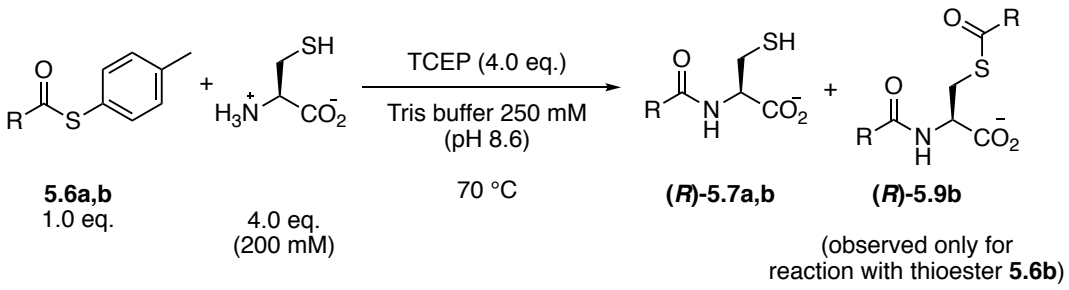
With full conversion to the target surfactants achieved under biphasic conditions, and with the observation of product aggregation (Section 5.3), the autocatalytic nature of the biphasic reactions could be tested.

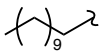
The low UV activity of the components of our system precluded the use of UPLC to monitor the reaction. Other methods for the real-time analysis of the system were explored, such as conducting the reaction in a $D_2O$ buffer, but gave poor and inconsistent data; minimal disturbance would be required for the sensitive biphasic reaction.

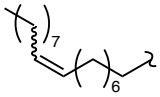
Therefore, instead of monitoring product formation over the entire course of the reaction, we decided to compare the extent of conversion of thioester **5.6a,b** in

the presence and absence of enantiopure surfactants **(*R*)-5.7a,b** after a fixed reaction time. Conversion would be calculated by $^{1}$H NMR spectroscopy with reference to an external standard. If surfactants **(*R*)-5.7a,b** act as autocatalysts, then seeding the reaction with **(*R*)-5.7a,b** at t = 0 should significantly increase the extent of thioester **5.6a,b** conversion.

Seeding the biphasic reactions with 20 mM **(*R*)-5.7a** or **(*R*)-5.7b** resulted only in tentative evidence for autocatalytic behaviour for thioester **5.6a** (Table 5.5.1). The reaction of thioester **5.6a** seeded with **(*R*)-5.7a** reached completion after 18 hours whilst the control reaction, containing **5.6a** and L-cysteine alone, remained below full conversion of thioester **5.6a** (*cf.* entries 1 and 2, Table 5.5.1). Thioester **5.6b** showed no significant difference in conversion between control and seeded reactions, with the seeded reaction apparently reaching lower conversion (*cf.* entries 3 and 4, Table 5.5.1).




**a** R = 

**b** R = 

| Entry | Thioester | Conditions | Time (h) | Conversion (%)[a] |
|---|---|---|---|---|
| 1 | **5.6a** | Control | 18 | 88 |
| 2 | **5.6a** | + **(*R*)-5.7a** (20 mM) | 18 | 100 |
| 3 | **5.6b** | Control | 4 | 68 |
| 4 | **5.6b** | + **(*R*)-5.7b** (20 mM) | 4 | 62 |

**Table 5.5.1** Conversion of thioesters **5.6a,b** to all products in control and seeded reactions. Each entry details the results from a single reaction. [a] Conversions were determined by $^1$H NMR spectroscopy in $(CD_3)_2SO$ with maleic acid as an external standard.

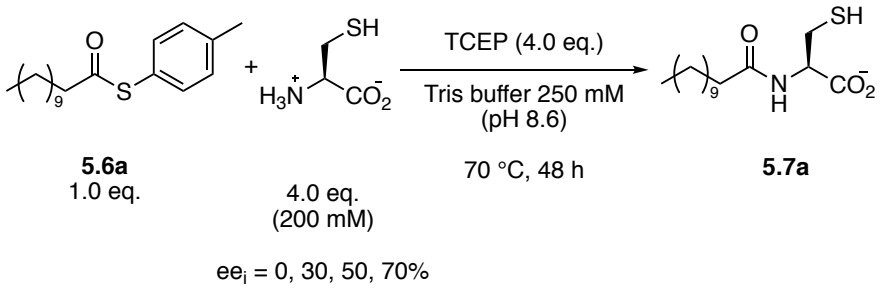
Considering the very sensitive and variable nature of the individual biphasic reactions, monitoring the reaction at a single time point was limiting. Without a reliable *in situ* method the presence of autocatalysis could not be thoroughly tested. We could not confirm a robust autocatalytic behaviour based on the experiments in Table 5.5.1.

## 5.6 Test for the amplification of chirality

In a final probe of the system, the effect of varying the initial ee of cysteine on reaction with thioester **5.6a** was tested. The observation of non-linear effects would indirectly suggest the presence of autocatalysis as well as fulfilling our ultimate aim of the amplification of chirality as detailed in Figure 5.3.1. Reactions were performed as detailed in Figure 5.6.1a, reacting thioester **5.6a** with racemic and scalemic cysteine.

However, the ee of reaction product **5.7a** correlated linearly with that of the initial ee of cysteine; no amplification of chirality had taken place (Figure 5.6.1b).

**a**




**5.6a**
1.0 eq.

4.0 eq.
(200 mM)

$ee_i$ = 0, 30, 50, 70%

**5.7a**

**b**

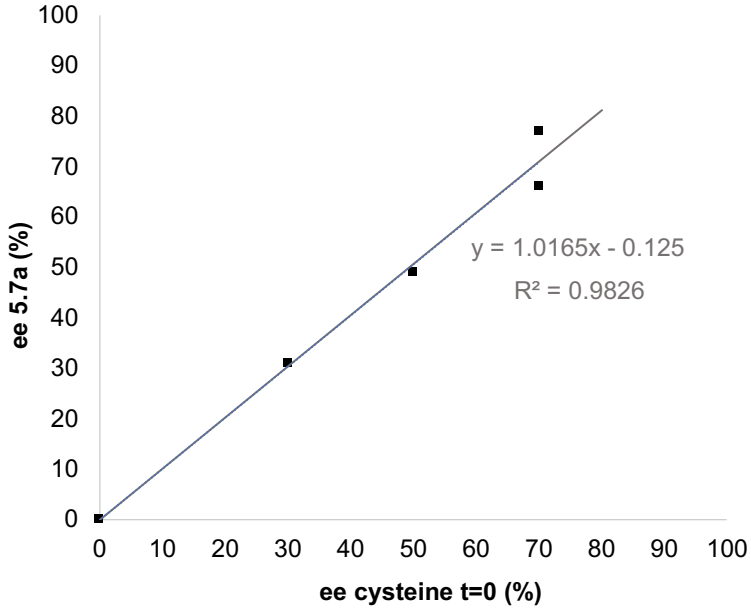



**Figure 5.6.1 a** Reactions were performed with variation in the initial ee of cysteine, from 0 to 70% ee. **b** ee of cysteine at t = 0 *vs* the ee of **5.7a** at the end of the reaction (at full conversion of thioester **5.6a**). ee's of **5.7a** were determined by chiral HPLC. Each plotted point is the outcome of a single experiment (experiment at 70% ee conducted twice).

## 5.7 Conclusions

Over the course of this project, two biphasic native chemical ligation reactions were developed. Their products showed evidence of supramolecular aggregate formation and were therefore predicted to induce physical autocatalysis, but we

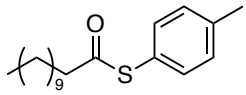
were not able to observe evidence of this kind of reactivity and were limited in particular by a lack of reliable analytical techniques for this biphasic system. In the absence of autocatalysis, the amplification of chirality from starting materials to products was also precluded.

The formation of the dual addition products **(*R*)-5.9a** and **(*R*)-5.9b** under biphasic conditions was in contrast to the behaviour under homogeneous conditions. Further, there was a significant difference in reaction rates and product distribution between thioesters **5.6a** and **5.6b**. These observations highlight the importance of physical properties on reactivity under biphasic conditions. The aggregation properties of the dual addition product, which appears to be reversibly formed (at least for thioester **5.6b**), may be interesting to explore and investigation into the interaction between amphiphilic components **5.7a,b** and their equivalent hydrophobic thioesters **5.6a,b** must be examined in future work on this system.

## 5.8 Experimental

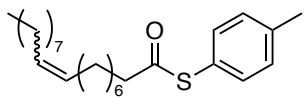
### 5.8.1 Synthesis and characterisation of the compounds used in this study

#### 5.8.1.1 Thioester **5.6a**



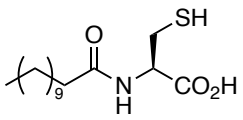
A round-bottom flask was charged with a solution of dodecanoic acid (3.00 g, 15.0 mmol, 1.10 eq.) in $CH_2Cl_2$ (15 mL). 4-dimethylaminopyridine (DMAP) (166 mg, 1.36 mmol, 10.0 mol%) and 4-methylbenzenethiol (1.69 g, 13.6 mmol, 1.00 eq.) were added. *N,N'*-dicyclohexylcarbodiimide (DCC) (3.09 g, 15.0 mmol, 1.1 eq.) was then added at 0 °C. The solution was allowed to warm to rt and stirred for 17 hours. The solution was filtered and the filtrate was concentrated *in vacuo*. The crude product was purified by column chromatography ($SiO_2$, petrol ether 100% *to* petrol ether:$Et_2O$ 9:1) to afford thioester **5.6a** as a clear oil (3.08 g, 74% yield). **$^1$H NMR** (400 MHz, $CDCl_3$): δ 7.29 (2H, d, *J* = 8.0 Hz, 2× C(Ar)–H), 7.22 (2H, d, *J* = 8.0 Hz, 2× C(Ar)–H), 2.64 (2H, t, *J* = 7.5 Hz, 1× $CH_2$), 2.38 (3H, s, C(Ar)-$CH_3$), 1.71 (2H, m, 1× $CH_2$), 1.38–1.27 (16H, m, 8× $CH_2$), 0.89 (3H, t, *J* = 7.0 Hz, $(CH_2)_{10}CH_3$); **$^{13}$C NMR** (101 MHz, $CDCl_3$): δ 198.2 (C=O), 139.6 (4° C(Ar)), 134.6 (2× C(Ar)–H)), 130.1 (2× C(Ar)–H)), 124.6 (4° C(Ar)), 43.8, 32.0 (2× $CH_2$), 29.7 (2× $CH_2$), 29.6, 29.5, 29.4, 29.1, 25.8, 22.8 (6× $CH_2$), 21.5 (C(Ar)-$CH_3$), 14.3 ($(CH_2)_{10}CH_3$); **HRMS** (ESI+, m/z): calc. for $C_{19}H_{31}OS$ $[M+H]^+$ 307.2090, found 307.2092; **IR** $\tilde{\nu}_{max}$ (film)/$cm^{-1}$: 2923, 2835, 1708, 1599. The data are consistent with those reported in *J. Am. Chem. Soc.* **122**, 11260-11261 (2000).[5]

## 5.8.1.2 Thioester **5.6b**



A round bottom flask was charged with oleic acid (2.3 mL, 7.1 mmol, 1.1 eq.) and $CH_2Cl_2$ (7 mL). 4-dimethylaminopyridine (DMAP) (79 mg, 0.64 mmol, 10 mol%) and 4-methylbenzenethiol (800 mg, 6.43 mmol, 1.00 eq.) were added. *N,N'*-dicyclohexylcarbodiimide (DCC) (1.46 g, 7.08 mmol, 1.1 eq.) was then added at 0 °C. The solution was allowed to warm to rt and stirred for 17 hours. The solution was filtered and the filtrate was concentrated *in vacuo*. The crude product was purified by column chromatography ($SiO_2$, petrol ether 100% *to* petrol ether:$Et_2O$ 9:1) to afford thioester **5.6b** as a clear oil (1.88 g, 75% yield). **$^1$H NMR** (400 MHz, $CDCl_3$): δ 7.29 (2H, d, *J* = 8.0 Hz, 2× C(Ar)–H), 7.22 (2H, d, *J* = 8.0 Hz, 2× C(Ar)–H), 5.40–5.31 (2H, m, HC=CH), 2.64 (2H, t, *J* = 7.5 Hz, 1× $CH_2$), 2.37 (3H, s, C(Ar)–$CH_3$), 2.03–2.00 (4H, m, 2× $CH_2$), 1.35–1.27 (22H, m, 11× $CH_2$), 0.88 (3H, t, *J* = 7.0 Hz, $(CH_2)_7CH_3$); **$^{13}$C NMR** (101 MHz, $CDCl_3$): δ 198.2 (C=O), 139.6 (4° C(Ar)), 134.6 (2× C(Ar)–H), 130.1 (HC=CH), 130.1 (2× C(Ar)–H), 129.8 (HC=CH), 124.6 (4° C(Ar)), 43.7, 32.0, 29.9, 29.8, 29.7 (5× $CH_2$), 29.5 (2× $CH_2$), 29.3, 29.2, 29.1, 27.4, 27.3, 25.7, 22.8 (7× Alk$CH_2$), 21.5 (C(Ar)–$CH_3$), 14.3 ($(CH_2)_7CH_3$); **HRMS** (EI, m/z): calc. for $C_{25}H_{40}OS$ $[M]^+$ 388.2800, found 388.2807; **IR** $\tilde{\nu}_{max}$ (film)/$cm^{-1}$: 3004, 2923, 2853, 1709, 1599.

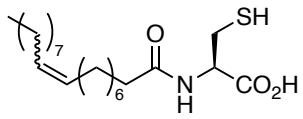
## 5.8.1.3 Surfactant **(*R*)-5.7a**



A round bottom flask was charged with a solution of L-cysteine hydrochloride (206 mg, 1.31 mmol, 2.00 eq.) in MeOH (15 mL). $NaBH_4$ (99 mg, 2.6 mmol, 4.0 eq.) was added portionwise to the solution and the mixture was stirred for 1 h before the addition of a solution of thioester **5.6a** (200 mg, 0.650 mmol, 1.00 eq.) in MeOH (5 mL). The reaction was stirred for 1.5 h before the solvent was removed *in vacuo*. 1 M HCl (20 mL) was added and the aqueous solution was extracted with EtOAc (2× 20 mL). The combined organics were dried over $MgSO_4$, filtered and concentrated *in vacuo* before purification by column chromatography on ($SiO_2$, $Et_2O$:AcOH 99:1). Following purification the product was taken into EtOAc (10 mL) and washed once with 1 M HCl (10 mL) before being dried over $MgSO_4$, filtered and concentrated *in vacuo* to yield surfactant ***(R)*-5.7a** as a white solid (100 mg, 51% yield). **$^1$H NMR** (500 MHz, $CDCl_3$): δ 6.45 (1H, d, *J* = 7.0 Hz, NH), 4.89–4.86 (1H, m, CH), 3.15–3.09 (1H, m, C*H*$_a$H$_b$), 3.02–2.96 (1H, m, CH$_a$*H*$_b$), 2.30 (2H, t, *J* = 8.0 Hz, 1× $CH_2$), 1.68–1.63 (2H, m, 1× $CH_2$), 1.48 (1H, t, *J* = 9.0 Hz, SH), 1.34–1.26 (16H, m, 8× $CH_2$), 0.88 (3H, t, *J* = 7.0 Hz, $(CH_2)_{10}CH_3$); **$^{13}$C NMR** (125 MHz, $CDCl_3$): δ 174.4 (C=O), 173.0 (C=O), 53.6 (CH), 36.6, 32.1 (2× $CH_2$), 29.8 (2× $CH_2$), 29.6, 29.5, 29.5, 29.4 (4× $CH_2$), 26.7 ($CH_aH_b$), 25.8, 22.8 (2× $CH_2$), 14.3 ($(CH_2)_{10}CH_3$); **HRMS** (ESI+, m/z): calc. for $C_{15}H_{30}O_3NS$ $[M+H]^+$ 304.1941, found 304.1942; **IR** $\tilde{\nu}_{max}$ (film)/cm$^{-1}$: 3232, 2924, 2854, 1730, 1626, 1533; $\alpha_D$ (c = 1.0, $CHCl_3$): +44.0.

Following the procedure described for surfactant **(*R*)-5.7a**, surfactant ***(S)*-5.7a** was synthesised from D-cysteine hydrochloride (154 mg, 980 μmol, 2.00 eq.). Thioester **(*S*)-5.7a** was isolated as a white solid (110 mg, 73% yield). $\alpha_D$ (c = 1.0, $CHCl_3$): −42.7.

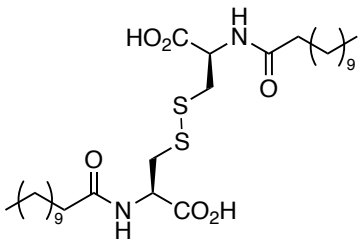
## 5.8.1.4 Surfactant (*R*)-5.7b




A round bottom flask was charged with a solution of L-cysteine hydrochloride (162 mg, 1.03 mmol, 2.00 eq.) in MeOH (15 mL). $NaBH_4$ (78 mg, 2.1 mmol, 4.0 eq.) was added portionwise to the solution and the mixture was stirred for 1 h before the addition of a solution of thioester **5.6b** (200 mg, 510 μmol, 1.00 eq.) in MeOH (5 mL). The reaction was stirred for 1.5 h before the solvent was removed *in vacuo*. 1 M HCl (20 mL) was added and the aqueous solution was extracted with EtOAc (2× 20 mL). The combined organics were dried over $MgSO_4$, filtered and concentrated *in vacuo* before purification by column chromatography on ($SiO_2$, $Et_2O$:AcOH 99:1). Following purification the products were taken into EtOAc (10 mL) and washed once with 1 M HCl (10 mL) before being dried over $MgSO_4$, filtered and concentrated *in vacuo* to yield surfactant **(*R*)-5.7b** as a yellow oil and as a mixture of olefinic isomers (1.29:1) (98 mg, 50% yield). **$^1$H NMR** (500 MHz, $CDCl_3$): δ 6.51 (1H, d, *J* = 7.0 Hz, NH), 5.42–5.37 (major isomer) and 5.35–5.31 (minor isomer) (2H, m, HC=CH), 4.90–4.87 (1H, m, CH), 3.14–3.08 (1H, m, C$H_a$H$_b$), 3.03–2.98 (1H, m, CH$_a$$H_b$), 2.31–2.27 (2H, t, *J* = 7.5 Hz, 1× $CH_2$), 2.05–1.99 (minor isomer) and 1.98–1.94 (major isomer) (4H, m, 2× $CH_2$), 1.68–1.62 (2H, m, 1× $CH_2$), 1.44 (1H, t, *J* = 9.0 Hz, SH), 1.32–1.26 (20H, m, 10× $CH_2$), 0.88

(3H, t, *J* = 7.0 Hz, $(CH_2)_7CH_3$); **$^{13}$C NMR** (125 MHz, $CDCl_3$): δ 174.4 (C=O), 173.0 (C=O), 130.6 (major isomer), 130.3 (major isomer), 130.2 (minor isomer), 129.8 (minor isomer) (HC=CH), 53.6 (CH), 36.6, 32.8, 32.7, 32.1, 30.5, 29.9, 29.9, 29.8, 29.7, 29.7, 29.6, 29.5, 29.4, 29.3, 29.3, 29.3, 29.1, 27.4, [27.3 ($CH_aH_b$)], 26.7, 25.7, 22.8 (14× $CH_2$), 14.3 ($(CH_2)_7CH_3$); **HRMS** (ESI+, m/z): calc. for $C_{21}H_{40}O_3NS$ $[M+H]^+$ 386.2723, found 386.2719; **IR** $\tilde{\nu}_{max}$ (film)/$cm^{-1}$: 2981, 2924, 2854, 2731 1648, 1540**;** $\alpha_D$ (c = 1.025, $CHCl_3$): +34.8.

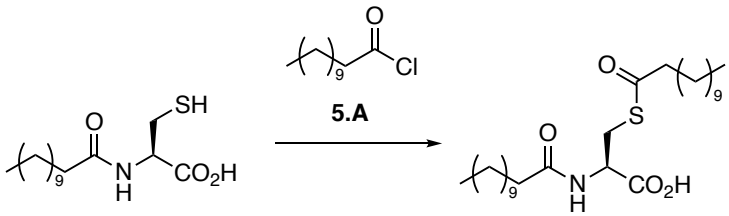
## 5.8.1.5 Disulfide **(*R,R*)-5.8a**




Surfactant **(*R*)-5.7a** was dissolved in $H_2O$ (0.5 mL) and the solution was adjusted to pH ~ 9 with 1 M $NH_4OH$. A crystal of $Fe(II)Cl_2$ was added and the reaction was stirred open to the air for 18 h. The solution was acidified to pH ~ 1 with 1 M HCl and extracted with EtOAc (3× 15 mL). The combined organics were dried over $MgSO_4$, filtered and concentrated *in vacuo* to afford disulfide **(*R,R*)-5.8a** as an off-white solid (22 mg, quant. yield). **$^1$H NMR** (400 MHz, $(CD_3)_2CO$): δ 7.53 (2H, d, *J* = 8.0 Hz, 2× NH), 4.82–4.77 (2H, m, 2× CH), 3.28 (2H, dd, *J* = 14.0 Hz, 5.0 Hz, 2× $CH_aH_b$), 3.14 (2H, dd, *J* = 14.0 Hz, 8.0 Hz, 2× $CH_aH_b$), 2.27 (4H, t, *J* = 7.5 Hz, 2× $CH_2$), 1.62 (4H, m, 2× $CH_2$), 1.35–1.29 (32H, m, 16× $CH_2$), 0.88 (6H, m, 2× $(CH_2)_{10}CH_3$); **$^{13}$C NMR** (101 MHz, $(CD_3)_2CO$): δ 173.7 (2× C=O), 172.0 (2× C=O), 52.5 (2× CH), 41.4 (2× $CH_aH_b$), 36.4, 32.6, 30.4, 30.4, 30.3, 30.2, 30.1,

30.0, 26.3, 23.3 (20× $CH_2$), 14.4 (2× $(CH_2)_{10}CH_3$); **HRMS** (ESI+, m/z): calc. for $C_{30}H_{55}O_6N_2S_2$ $[M\text{-}H]^-$ 603.3507, found 603.3516; **IR** $\tilde{\nu}_{max}$ (film)/$cm^{-1}$: 3295, 2956, 2923, 2853, 1726, 1651, 1540; $\alpha_D$ (c = 0.67, $(CH_3)_2CO$): −26.4.

## 5.8.1.6 Thioester **(*R*)-5.9a**




**(*R*)-5.7a** **(*R*)-5.9a**

**5.A**

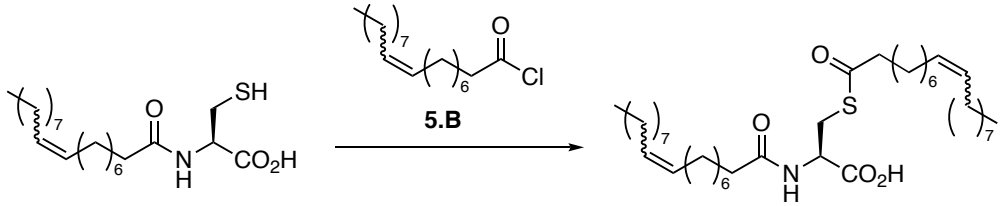
A round bottom flask was charged with a solution of dodecanoic acid (1.50 g, 7.59 mmol, 1.00 eq.) in THF (20 mL). Oxalyl chloride (1.2 mL, 13 mmol, 1.9 eq.) and DMF (4 drops, cat.) were added. The solution was stirred for 2 h and the solvent was removed *in vacuo* to afford acid chloride **5.A**. The crude product was used in the next step without further purification.

Thioester **(*R*)-5.9a**

A round bottom flask was charged with a solution of surfactant **(*R*)-5.7a** (50 mg, 0.16 mmol, 1.0 eq.) in THF (2.0 mL). TMSCl (42 µL, 0.33 mmol, 2.0 eq.) was added and the reaction was stirred for 2 h at 45 °C. Triethylamine (56 µL, 0.33 mmol, 2.0 eq.) and a solution of acid chloride **5.A** (72 mg, 0.33 mmol, 2.0 eq.) in THF (0.5 mL) were added at 0 °C. The solution was allowed to warm to rt and stirred for 2 h. The solvent was removed *in vacuo*. 1 M HCl (15 mL) was added and the solution was extracted with EtOAc (2× 15 mL). The organics were dried

over $MgSO_4$, filtered, and concentrated in vacuo. The crude product was purified by column chromatography ($SiO_2$, $Et_2O$:AcOH 99:1) to yield thioester **(*R*)-5.9a** as a white solid (56 mg, 72% yield). **$^1$H NMR** (500 MHz, $CDCl_3$): δ 6.72 (1H, d, *J* = 5.0 Hz, NH), 4.61–4.60 (1H, m, CH), 3.37–3.36 (2H, m, $CH_aH_b$), 2.59 (2H, t, *J* = 7.5 Hz, 1× $CH_2$), 2.23 (2H, t, *J* = 7.5 Hz, 1× $CH_2$), 1.68–1.64 (2H, m, 1× $CH_2$), 1.62–1.59 (2H, m, 1× $CH_2$), 1.28–1.26 (32H, m, 16× $CH_2$), 0.88 (6H, m, 2× $(CH_2)_{10}CH_3$); **$^{13}$C NMR** (125 MHz, $CDCl_3$): δ 201.9 (C=O), 175.8 (C=O), 171.9 (C=O), 54.3 (CH), 44.1, 36.5, 32.1, 32.1, 29.9, 29.8, 29.8, 29.8, 29.8, 29.7, 29.6, 29.5, 29.5, 29.4, 29.3, 29.1, 25.8, 25.6, 22.8 (21× $CH_2$), 14.3 (2× $(CH_2)_{10}CH_3$); **HRMS** (ESI-, m/z): calc. for $C_{27}H_{50}O_4NS$ $[M-H]^-$ 484.34660, found 484.34705; **IR** $\tilde{\nu}_{max}$ (film)/$cm^{-1}$: 3305, 2955, 2921, 2852, 1726, 1697, 1537; **$\alpha_D$** (c = 1.14, $CHCl_3$): +0.42.

## 5.8.1.7 Thioester **(*R*)-5.9b**




**(*R*)-5.7b** **(*R*)-5.9b**

**5.B**

A round bottom flask was charged with a solution of oleic acid (1.00 g, 3.54 mmol, 1.00 eq.) in THF (10 mL). Oxalyl chloride (0.6 mL, 7.1 mmol, 2.0 eq.) and DMF (4 drops, cat.) were added. The solution was stirred for 2 h and the solvent was removed *in vacuo* to afford acid chloride **5.B**. The crude product was used in the next step without further purification.

Thioester **(*R*)-5.9b**

A round bottom flask was charged with a solution of surfactant **(*R*)-5.7b** (50 mg, 0.13 mmol, 1.0 eq.) in THF (2 mL). TMSCl (33 µL, 0.26 mmol, 2.0 eq.) was added and the solution was stirred for 2 h at 45 °C. Triethylamine (36 µL, 0.26 mmol, 2.0 eq.) and a solution of acid chloride **5.B** (78 mg, 0.26 mmol, 2.0 eq.) in THF (0.5 mL) were added at 0 °C. The solution was stirred for 2 h warming to rt before removal of the solvent *in vacuo*. 1 M HCl (15 mL) was added and the aqueous solution extracted with EtOAc (2× 15 mL). The organics were dried over $MgSO_4$, filtered, and concentrated *in vacuo*. The crude product was purified by column chromatography ($SiO_2$, $Et_2O$:AcOH 99:1) to yield thioester **(*R*)-5.9b** as a yellow oil and as a mixture of olefinic isomers (not quantified) (43 mg, 50% yield); **$^1$H NMR** (400 MHz, $CDCl_3$): δ 6.61 (1H, d, *J* = 6.5 Hz, NH), 5.38–5.29 (4H, m, HC=CH), 4.71–4.66 (1H, m, CH), 3.42–3.32 (2H, m, $CH_aH_b$), 2.58 (2H, t, *J* = 7.5 Hz, 1× $CH_2$), 2.22 (2H, t, *J* = 7.5 Hz, 1× $CH_2$), 2.05–1.93 (8H, m, 4× $CH_2$), 1.66–1.58 (4H, m, 2× $CH_2$), 1.29–1.26 (40H, m, 20× $CH_2$), 0.87 (6H, t, *J* = 6.5 Hz, 2× $(CH_2)_7CH_3$); **$^{13}$C NMR** (101 MHz, $CDCl_3$): δ 201.0 (C=O), 175.1 (C=O), 172.7 (C=O), 130.6, 130.3, 130.2, 130.1, 129.8, 129.8 (4× HC=CH), 53.5 (CH), 44.1, 36.4, 32.8, 32.7, 32.0, 30.4, 30.0, 29.9, 29.9, 29.8, 29.8, 29.7, 29.6, 29.5, 29.4, 29.3, 29.3, 29.3, 29.2, 29.2, 29.1, 27.4, 27.3, 27.3, 25.8, 25.5, 22.8 (29× $CH_2$), 14.3 (2× $(CH_2)_7CH_3$); **HRMS** (ESI+, m/z): calc. for $C_{39}H_{72}O_4NS$ $[M+H]^+$ 650.5177, found 650.5162; **IR** $\tilde{\nu}_{max}$ (film)/$cm^{-1}$: 2923, 2854, 2359, 2009, 1698, 1541; $\alpha_D$ (c = 1.07, $CHCl_3$): -0.006.

## 5.8.2 Surfactant characterisation

### 5.8.2.1 Dynamic light scattering (DLS)

Solutions of surfactant **(*S*)-5.7a** and surfactant **(*R*)-5.7a** (10 mM each) in Tris buffer (250 mM, pH 8.6) were prepared. TCEP·HCl (20 mM) was added to each solution and the pH adjusted to pH 8.6 with 10 M NaOH. Solutions were measured by dynamic light scattering. DLS measurements were recorded on a DLS Viscotek 802 instrument. The solutions were filtered using syringe filters PTFE (0.2 μm, 13 mm diameter) from Camlab prior to measurement.

The resultant number and intensity distributions are shown in Figures 5.8.1 and 5.8.2 for **(*S*)-5.7a**, and Figure 5.8.3 and 5.8.4 for **(*R*)-5.7a**.

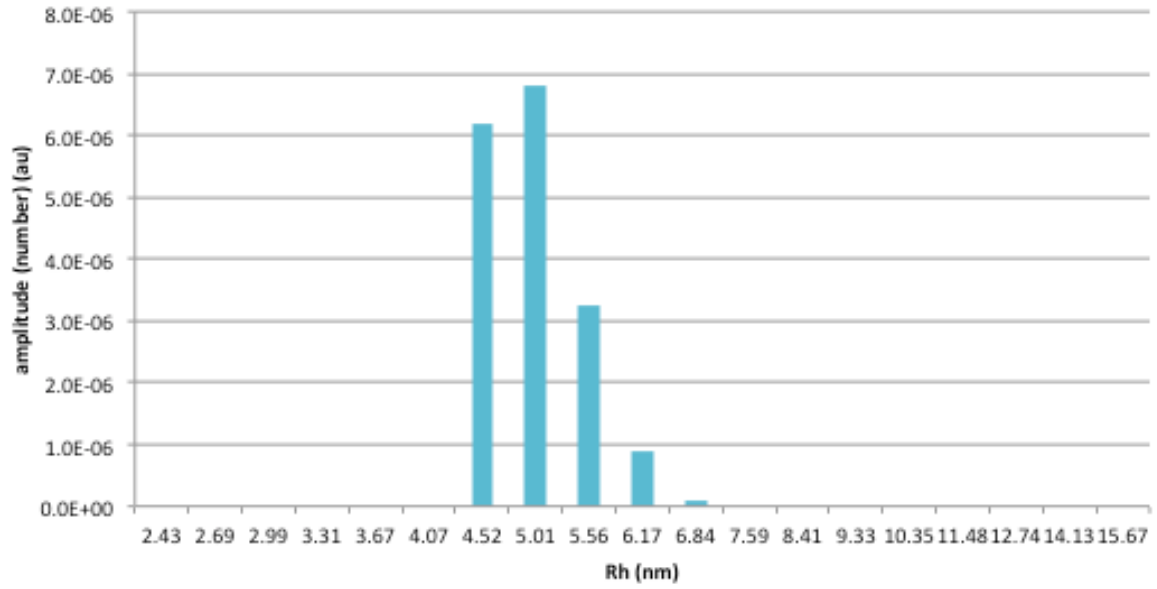



**Figure 5.8.1** Number distribution of a 10 mM solution of **(*S*)-5.7a** in Tris buffer (250 mM, pH 8.6).

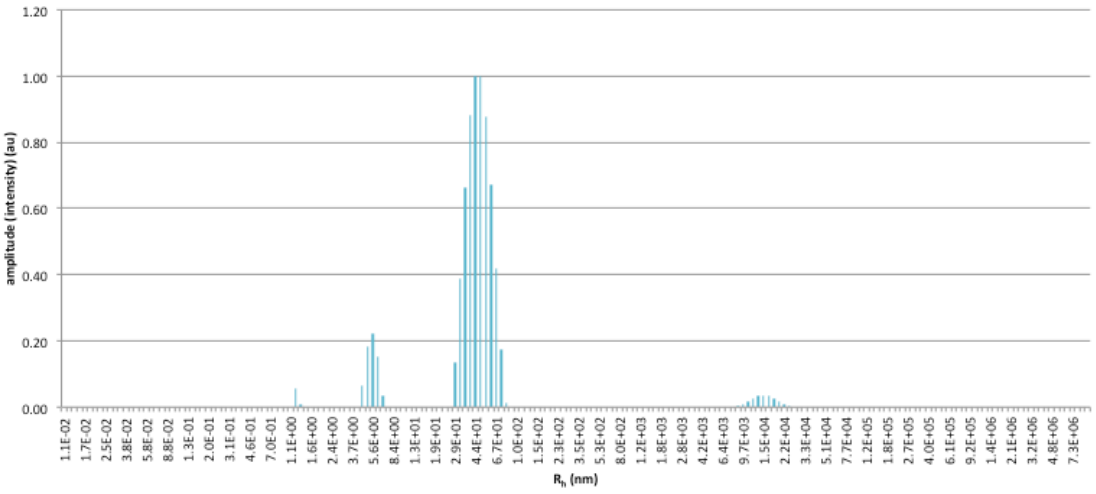



**Figure 5.8.2** Intensity distribution of a 10 mM solution of **(*S*)-5.7a** in Tris buffer (250 mM, pH 8.6).

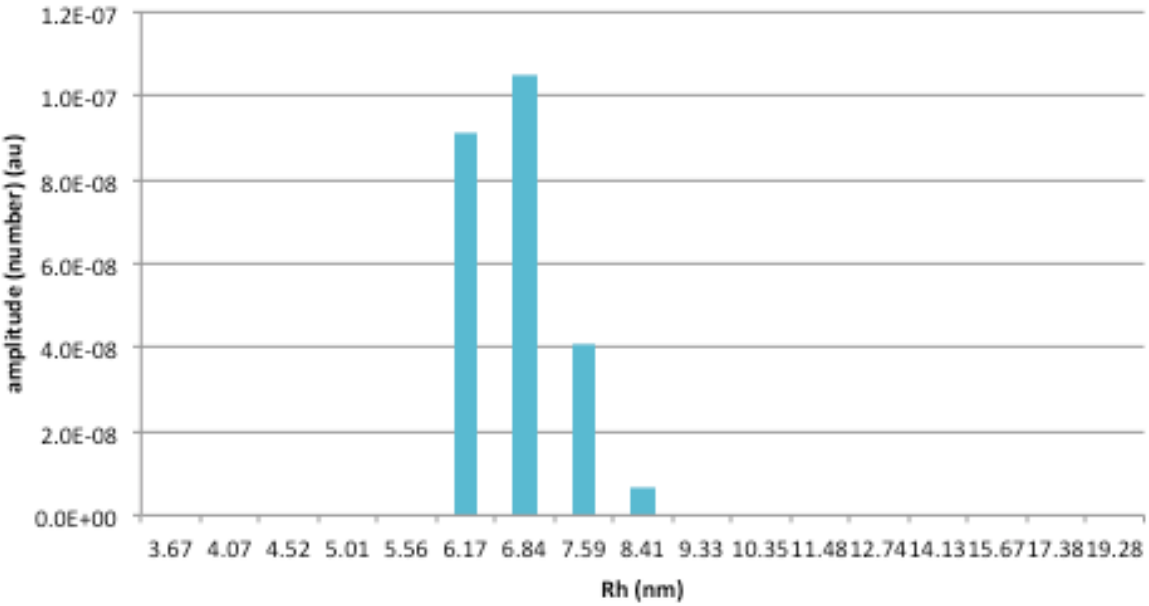



**Figure 5.8.3** Number distribution of a 10 mM solution of **(*R*)-5.7b** in Tris buffer (250 mM, pH 8.6).

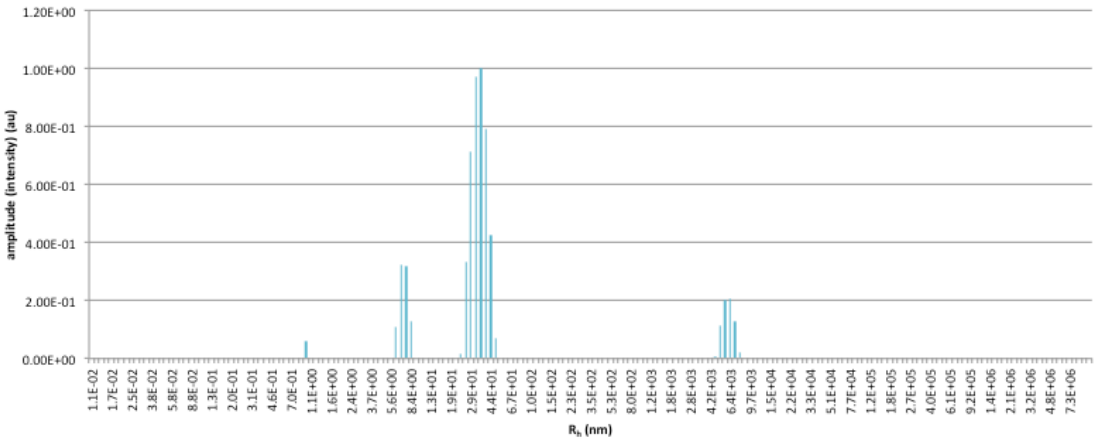



**Figure 5.8.4** Intensity distribution of a 10 mM solution of **(*R*)-5.7b** in Tris buffer (250 mM, pH 8.6).

### 5.8.2.2 Interferometric scattering microscopy

#### 5.8.2.2.1 Sample preparation and measurement

All measurements were made under the supervision of Dr. Andrew Bissette, Fletcher group.

A solution of surfactant **(*R*)-5.7b** (0.05 mM) and TCEP·HCl (40 mM) in Tris buffer (250 mM, pH 8.6) was prepared and adjusted to pH 8.6 with 10 M NaOH.

Coverslips were prepared and the above sample filtered according to the procedure in Section 2.5.5.

Raw data was recorded and processed following the procedure in Section 2.5.5, removing large artefacts with a size 10 filter (in-house software).

The resultant image is pictured in Figure 5.8.5.

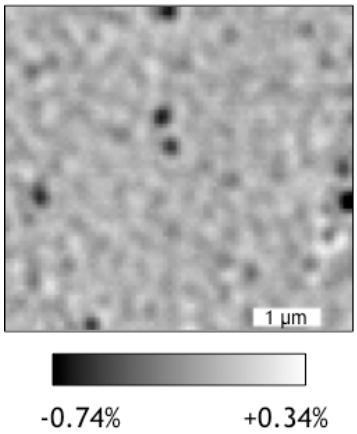



**Figure 5.8.5** Image of the binding of aggregates of **(*R*)-5.7b** captured by interferometric scattering microscopy. Scale bar = 1 µm. The bar below the image represents the contrast range; the individual contrast of each aggregate provides a measure of its size.

## 5.8.3 Biphasic reaction optimisation

A vial was charged with L-cysteine (24 mg, 0.20 mmol, 2.0 eq. OR 49 mg, 0.40 mmol, 4.0 eq.) and TCEP·HCl (115 mg, 400 µmol, 4.00 eq.). Tris buffer (~1.5 mL, 250 mM, pH 8.6) was added and the pH adjusted to the desired pH using a few drops of 10 M NaOH and Tris buffer (250 mM, pH 8.6) to reach a final volume of 2.0 mL. The solution was added to a 5 mL round bottom flask charged with thioester **5.6a** (31 mg, 0.10 mmol, 1.0 eq.) OR thioester **5.6b** (39 mg, 0.10 mmol, 1.0 eq.) under argon. The reaction was stirred rapidly (750 rpm) at the desired temperature for the reaction times specified in Tables 5.4.1 and 5.4.2. The reaction was acidified to pH < 2 using 1 M HCl and extracted with EtOAc (2× 10 mL). The combined organics were dried over $MgSO_4$, filtered and concentrated *in vacuo* to afford the crude reaction mixture for analysis by $^1$H NMR spectroscopy

in $(CD_3)_2SO$ or $(CD_3)_2CO$ with maleic acid as an external standard. The data from these experiments are recorded in Tables 5.4.1 and 5.4.2.

## 5.8.4 Procedure for control and seeding reactions

For thioester **5.6a**: A vial was charged with L-cysteine (97 mg, 0.80 mmol, 4.0 eq per reaction) and TCEP·HCl (229 mg, 800 µmol, 4.00 eq. per reaction). Tris buffer (~ 3 mL, 250 mM, pH 8.6) was added and the pH adjusted back to pH 8.6 using a few drops of 10 M NaOH and Tris buffer (250 mM, pH 8.6) to reach a final volume of 4.0 mL.

2.0 mL portions of the solution was added to two 5 mL flasks, one charged with thioester **5.6a** (31 mg, 0.10 mmol, 1.0 eq.), and one charged with a mixture of thioester **5.6a** (31 mg, 0.10 mmol, 1.0 eq.) and surfactant **(*R*)-5.7a** (12 mg, 40 µmol, 0.40 eq.) under argon. The reactions were stirred rapidly (700 rpm) at 70 °C for 18 h. The reactions were acidified to pH < 2 using 1 M HCl and extracted with EtOAc (2× 10 mL). The combined organics were dried over $MgSO_4$, filtered and concentrated *in vacuo* to afford the crude reaction mixtures for analysis by $^1H$ NMR spectroscopy in $(CD_3)_2SO$ with maleic acid as an external standard. The data from these experiments are recorded in Table 5.5.1.

For thioester **5.6b**: reactions were performed analogously to those for thioester **5.6a** but using thioester **5.6b** (39 mg, 0.10 mmol, 1.0 eq.), or a mixture of thioester **5.6b** (39 mg, 0.10 mmol, 1.0 eq.) and surfactant **(*R*)-5.7b** (15 mg, 40 µmol, 0.40 eq.) and a reaction time of 4 h. The crude reaction mixtures were analysed by $^1H$

NMR spectroscopy in $(CD_3)_2SO$ with maleic acid as a standard. The data from these experiments are recorded in Table 5.5.1.

### 5.8.5 Procedure for reactions performed with racemic and scalemic cysteine

Racemic reaction: a vial was charged with a solution of L-cysteine (24.2 mg, 200 µmol, 2.00 eq.), D-cysteine (24.2 mg, 200 µmol, 2.00 eq.), and TCEP·HCl (115 mg, 400 µmol, 4.00 eq.) in Tris buffer (~ 1.5 mL, 250 mM, pH 8.6). The pH adjusted back to pH 8.6 using a few drops of 10 M NaOH and Tris buffer (250 mM, pH 8.6) to reach a final volume of 2.0 mL. The solution was added to a 5 mL round bottom flask charged with thioester **5.6a** (31 mg, 0.10 mmol, 1.0 eq.) under argon. The reaction was stirred rapidly (700 rpm) at 70 °C for 48 h. The reactions was acidified to pH < 2 using 1 M HCl and extracted with EtOAc (2× 10 mL). The organics were dried over $MgSO_4$, filtered and concentrated *in vacuo* to afford the crude reaction mixture for analysis by $^1H$ NMR spectroscopy with 1,4-dioxane as a standard. The crude product was purified by column chromatography ($SiO_2$, $Et_2O$:AcOH 99:1) to afford surfactant **5.7a**.

The enantiomeric excess was determined by HPLC [Chiralpak® IC, hexane:iPrOH 96:4; 1.0 $mLmin^{-1}$, λ= 210 nm, $t_R$ (**(*R*)-5.7a**) = 27.553, $t_R$ (**(*S*)-5.7a**) = 35.113].

Procedures using cysteine at ee's of 30%, 50% and 70% were performed analogously to the racemic procedure but with variation in the preparation of the

L/D-cysteine solution. For reactions at 50% and 70% ee, 4.0 or 8.0 mL solutions were prepared and a 2.0 mL portion taken for reaction (to reduce measurement error). For reaction at 70% ee, two reactions were performed.

30% ee: L-cysteine (31.5 mg, 260 µmol, 2.60 eq.) and D-cysteine (17.0 mg, 140 µmol, 1.40 eq.) in Tris buffer (2.0 mL total).

50% ee: L-cysteine (72.7 mg, 600 µmol, 6.00 eq.) and D-cysteine (24.2 mg, 200 µmol, 2.00 eq.) in Tris buffer (4.0 mL total).

70% ee: L-cysteine (165 mg, 1.36 mmol, 13.6 eq.) and D-cysteine (29.1 mg, 240 µmol, 2.40 eq.) in Tris buffer (8.0 mL total).

The data from these experiments is recorded in Figure 5.6.1.

## 5.9 References


1. Brea, R. J., Cole, C. M. & Devaraj, N. K. In Situ Vesicle Formation by Native Chemical Ligation. *Angew. Chem. Int. Ed.* **53,** 14102–14105 (2014).
2. Dawson, P. E., Muir, T. W., Clark-Lewis, I. & Kent, S. B. Synthesis of proteins by native chemical ligation. *Science* **266,** 776–779 (1994).
3. Sorrenti, A., Illa, O. & Ortuno, R. M. Amphiphiles in aqueous solution: well beyond a soap bubble. *Chem. Soc. Rev.* **42,** 8200–8219 (2013).
4. Niehaus, Walter G. Thiol-Catalyzed cis-trans Isomerization of Oleic Acid. *Bioorganic Chemistry* **3**, 302-310 (1974).
5. Liebeskind, L. S. & Srogl, J. Thiol ester-boronic acid coupling. A mechanistically unprecedented and general ketone synthesis. *J. Am. Chem. Soc.* **122,** 11260–11261 (2000).

# 6

## Chiral Surfactant Formation by Thiol-Disulfide Exchange

## 6.1 Introduction

The system explored in Chapter 5 did not demonstrate a process of autocatalysis and, thus, it was far from demonstrating the amplification of chirality. The simultaneous realisation of both a novel autocatalytic reaction and the amplification of chirality was a difficult task.

Following our study in Chapter 3 on a micelle replicator constructed by thiol-disulfide exchange we were encouraged to investigate chiral variants of the system, with the hope of observing non-linear behaviour.

## 6.2 Enantioselective physical autocatalysis: system design

Two chiral variants of the thiol-disulfide exchange reaction explored in Chapter 3 were considered. In one, the chiral component was the hydrophilic disulfide, and in the other the chiral component was the hydrophobic thiol (Figure 6.2.1).

In the ideal case, following the Frank model as discussed in Chapter 4, chiral surfactants **6.2** and **6.4** would partition into enantiopure and racemic assemblies, and the racemic assembly would sequester the minor enantiomer. Whilst the enantiopure assembly would be catalytically active, the racemic assembly would be catalytically inactive. If the enantiopure, active species were enantioselective, then this would allow for the amplification of chirality *via* physical autocatalysis from a low ee in starting materials to a high ee in products.

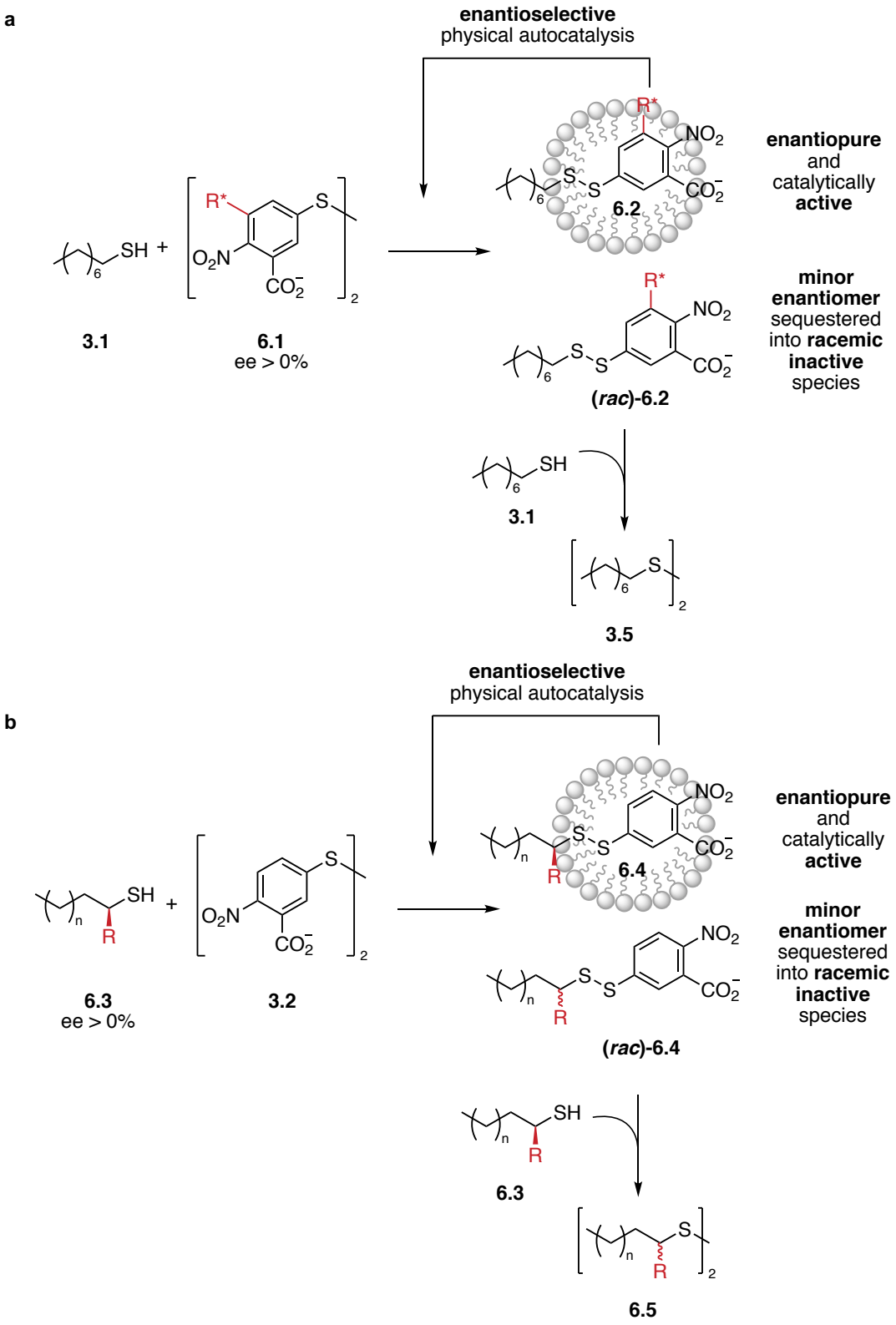



**Figure 6.2.1** Two proposed systems for the amplification of chirality *via* autocatalytic thiol-disulfide exchange: **a** based on a chiral hydrophilic disulfide; **b** based on a chiral hydrophobic thiol.

In addition, both systems had the potential to undergo a second thiol-disulfide exchange for the destruction of the chiral surfactant. The influence of the second exchange on a mixture of aggregates of **6.2** and **6.4** on the enantiomeric excess of the system could not be predicted.

For an initial examination of each system we turned our attention to the surfactant formation step and the presence of autocatalysis in the first thiol-disulfide exchange.

## 6.3 Scenario 1: a chiral hydrophilic disulfide

### 6.3.1 System design

A simple chiral variant of DTNB appended with phenylalanine, disulfide **6.6**, was designed (Figure 6.3.1). Reaction with octanethiol **3.1** would produce chiral disulfide surfactant **6.7** that, by analogy with the system in Chapter 3, would aggregate into micelles and could replicate. The simple design was partly inspired by other surfactants that, despite being rendered chiral only by a single amino acid group, produced macroscopic chiral phases.[1]

As already emphasised, but of utmost importance, the partitioning of surfactant **6.7** into enantiopure, catalytically active and enantioselective micelles and an inactive racemic phase would result in the amplification of chirality (Figure 6.3.1).

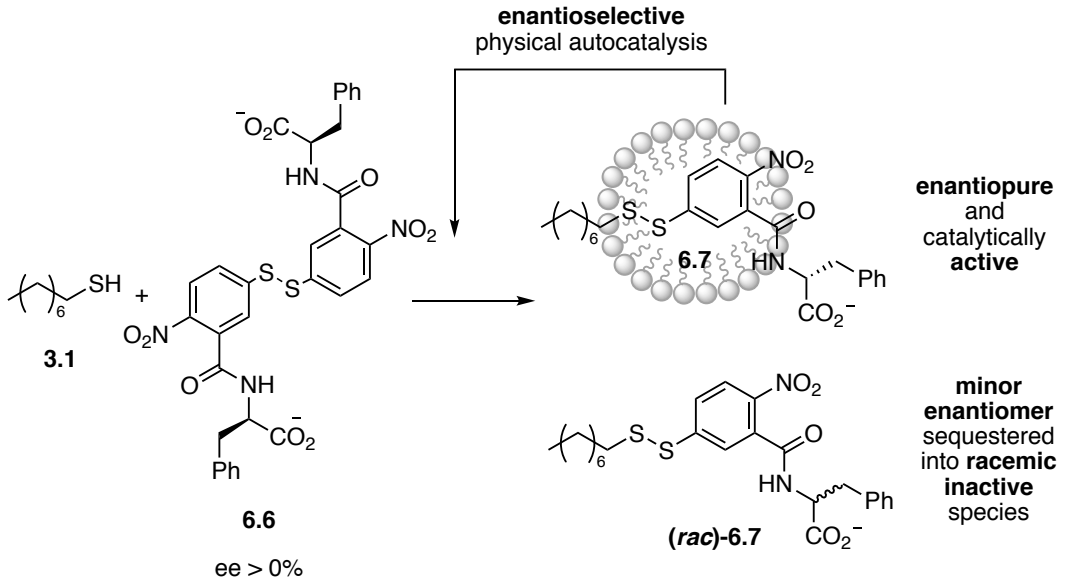


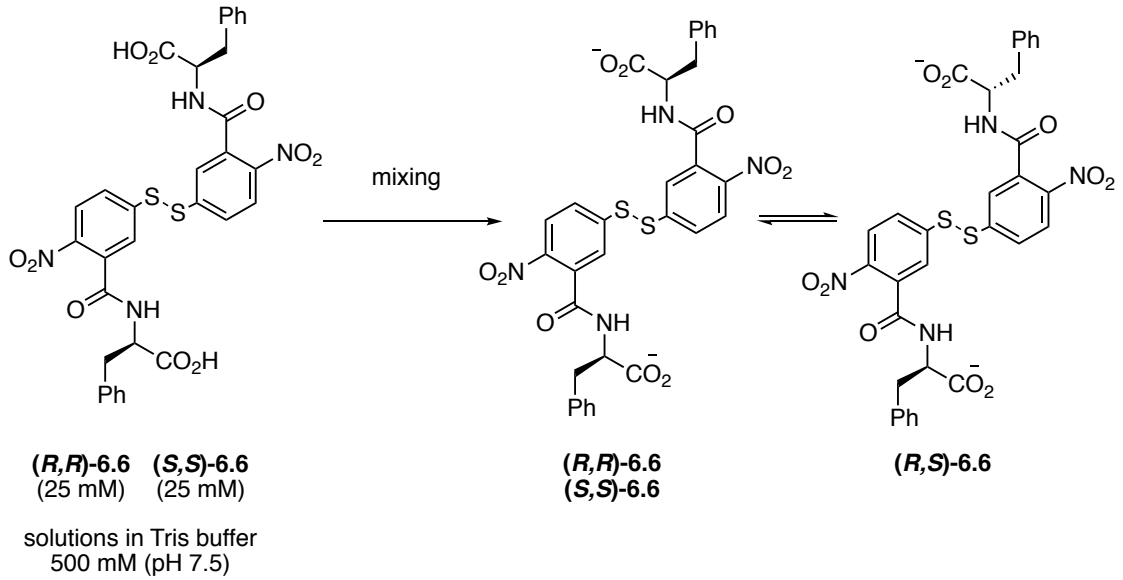

**Figure 6.3.1** System design: proposed mechanism for the amplification of chirality *via* autocatalytic thiol-disulfide exchange based on chiral hydrophilic disulfide **6.6**.

## 6.3.2 Characterisation of disulfide **6.6**

First, enantiopure disulfides **(*R,R*)-6.6** and **(*S,S*)-6.6** were synthesised (see Section 6.6.1.1) and their properties examined under reaction conditions as optimised in Chapter 3.

Whilst enantiopure disulfides **(*R,R*)-6.6** and **(*S,S*)-6.6** in Tris buffer were observed as single peaks by chiral UPLC, preparation of racemic and scalemic samples of the starting material by mixing enantiopure disulfides **(*R,R*)-6.6** and **(*S,S*)-6.6** at different ratios in Tris buffer (total concentration 25.0 mM) resulted in the appearance of three peaks. This indicated that the basic buffer promoted disulfide exchange, allowing for the formation of the *meso* disulfide **(*R,S*)-6.6** and thus

affording a diastereomeric mixture of **(*R,R*)-6.6**, **(*S,S*)-6.6**, and **(*R,S*)-6.6** (Table 6.3.1). Importantly, this equilibration effectively increased the ee of disulfide **6.6** (Table 6.3.1), a property of potential utility for the amplification of chirality in the system.




| Ratio **(*R,R*)-6.6**:**(*S,S*)-6.6** before mixing (theoretical ee) | Ratio **(*R,R*)-6.6**+**(*S,S*)-6.6**:**(*R,S*)-6.6** in solution[a] | ee **6.6** in solution (%)[a] |
|---|---|---|
| 1.2:1.0 (10% ee) | 1.06:1 | 21 |
| 3.0:1.0 (50% ee) | 1.59:1 | 76 |
| 19:1.0 (90% ee) | 5.53:1 | 97 |

**Table 6.3.1** Solutions of **(*R,R*)-6.6** and **(*S,S*)-6.6** (25.0 mM in Tris buffer) were mixed in different ratios to produce mixtures of **(*R,R*)-6.6**, **(*S,S*)-6.6** and **(*R,S*)-6.6** at equilibrium, with a resultant shift in the initial ee. [a] Measured by chiral UPLC.

## 6.3.3 Test for the amplification of chirality

To examine the behaviour of the entire system and the evolution of enantiomeric excess over time, three experiments were conducted using the solutions as prepared in Table 6.3.1 (Figure 6.3.2). In order to observe asymmetric amplification, or a kinetic resolution of starting materials, an excess of the enantiopure disulfides **(*R,R*)-** and **(*S,S*)-6.6** was employed (Figure 6.3.2). Using this component in excess would also reduce the influence of the second thiol-disulfide exchange and allow initial focus on the autocatalytic step.

The reaction profile was followed by chiral UPLC, and was plotted as a sum over all stereoisomers of each component (*i.e.* **(*R,R*)-6.6**, **(*S,S*)-6.6** and **(*R,S*)-6,6** summed together, **(*R*)-6.7** and **(*S*)-6.7** summed together). Figure 6.3.2b displays the reaction profile for the reaction conducted at 10% ee (plotted on left axis). Reactions conducted at different initial ee's, from Table 6.3.1, showed the same general reaction profile for the consumption of **6.6** and formation of **6.7**.

Reaction between **3.1** and **6.6** in Tris buffer resulted in the formation of disulfide **6.7** (Figure 6.3.2b). However, no change in enantiomeric excess was observed over the course of the reaction. The ee of product **6.7** was equal, within experimental error, to the ee of its precursor **6.6**.

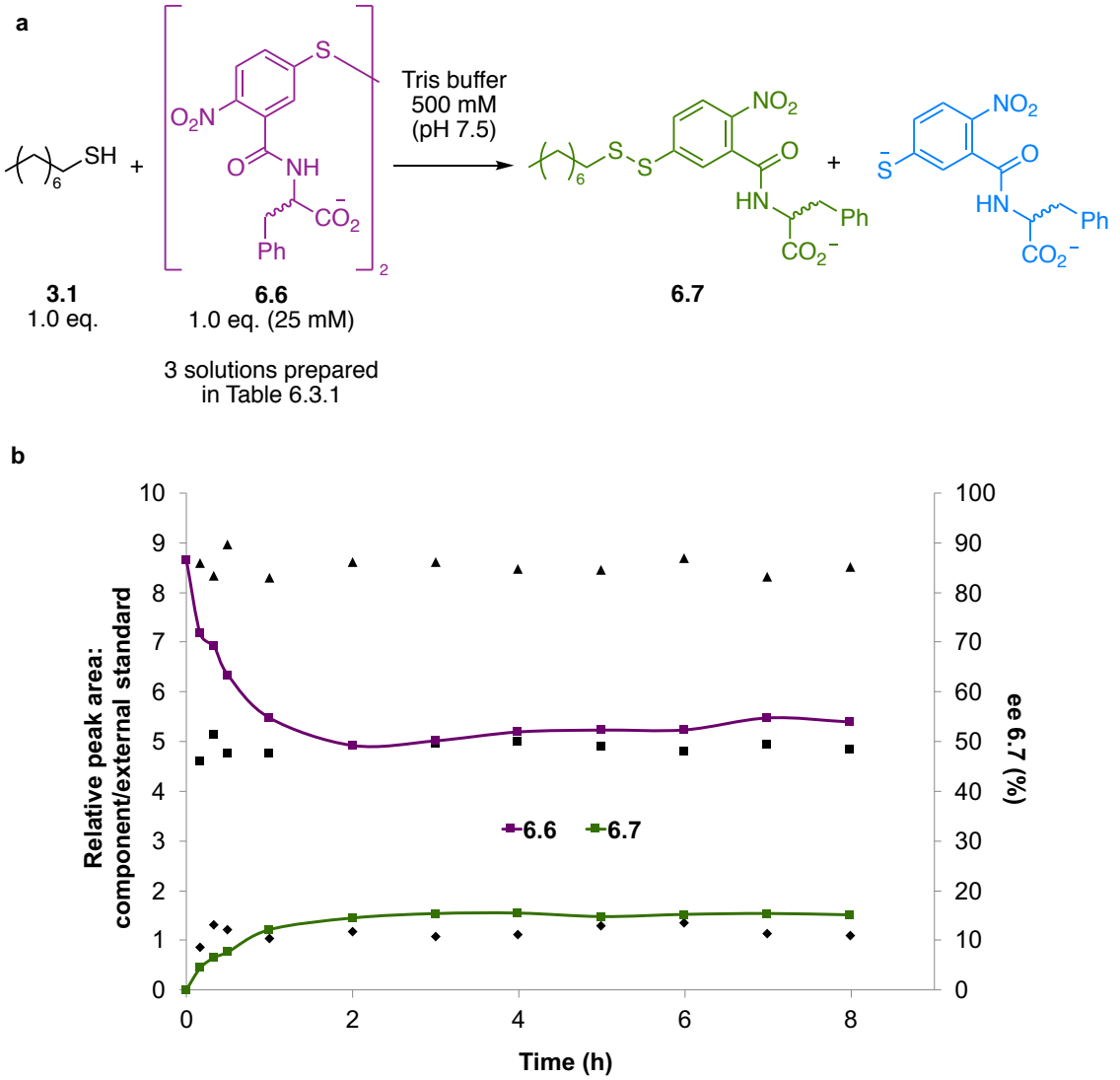



**Figure 6.3.2 a** Three reactions with different initial ee of **6.6** (prior to mixing) (Table 6.3.1) were monitored. **b** Kinetic profile for the reaction conducted at 10% ee, which is representative of all three reactions (plotted on left axis), and the evolution of ee of **6.7** over time for each reaction with different initial ee of **6.6** prior to mixing (◆) = 10% ee (■)= 50% ee (▲) = 90% ee (plotted on right axis). The reactions were monitored by chiral UPLC. Each reaction was performed once only. Lines between points are drawn to guide the eye.

Without any observation of non-linear effects, and with some difficulty in the synthesis of **6.6**, investigation into this system was stopped. A second study based on a chiral hydrophobic thiol (Section 6.4), being undertaken at the same time, appeared more promising and was more synthetically accessible. Further work therefore focused on this latter system.

## 6.4 Scenario 2: a chiral hydrophobic thiol

### 6.4.1 System design

An alternative design used the hydrophobic thiol of the reaction as the chiral component. For chiral thiol **6.8,** a significant difference in the size of the functional groups on the stereogenic centre was introduced to maximise potential enantioselectivity (Figure 6.4.1).

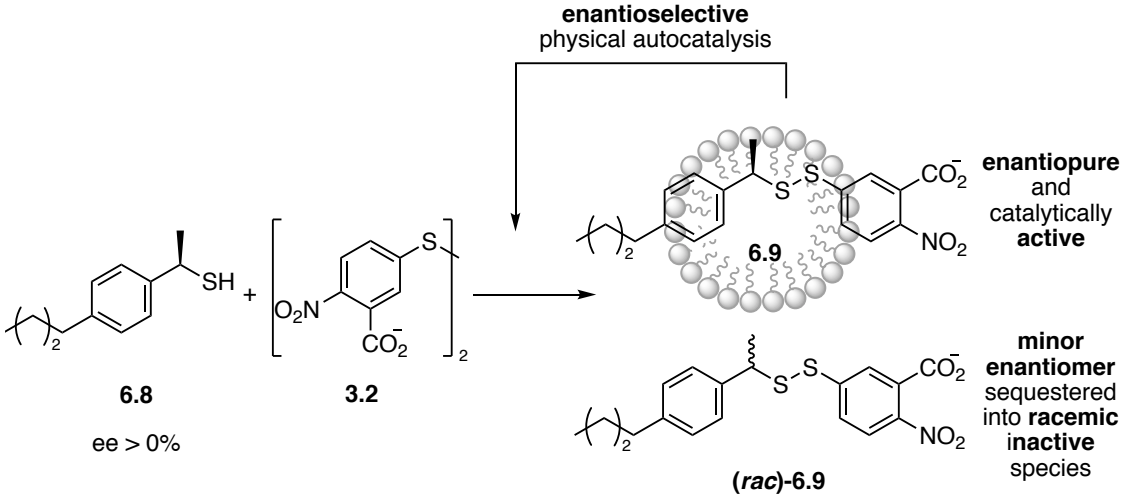



**Figure 6.4.1** System design: proposed mechanism for the amplification of chirality *via* autocatalytic thiol-disulfide exchange based on chiral hydrophobic thiol **6.8**.

The same requirements would apply; for the amplification of chirality, surfactant **6.9** would partition into an enantiopure, catalytically active and enantioselective assembly, alongside an inactive racemic assembly.

## 6.4.2 The racemic system: precipitation of the surfactant

To examine the general behaviour of the system, initial reactions were conducted between one equivalent of racemic thiol **(*rac*)-6.8** and DTNB **3.2** (Figure 6.4.2). Whilst chiral amplification would usually require the chiral component to be in excess, so that a kinetic resolution of thiol **6.8** *via* autocatalytic thiol-disulfide exchange might occur, this excess stoichiometry would likely result in a second thiol-disulfide exchange and degradation of the chiral surfactant. To begin our study, we opted to use of one equivalent of **6.8** in order to isolate the autocatalytic reaction and reduce the influence of the degradation reaction.

Two reactions were set up under identical conditions (Figure 6.4.2), and the concentration of the reaction components was followed by UPLC (Figure 6.4.2). For both reactions, the formation of disulfide **6.9** was observed. However, in one out of two reactions, precipitation of **6.9** occurred at approximately 3 hours. Comparison of the two reaction profiles showed an apparent reduction in reaction rate on precipitation; we reasoned that this might be due to a reduced quantity of solvated surfactant catalyst **6.9**. The fact that precipitation occurred only in one reaction, despite efforts to treat both reactions identically, is illustrative of the high sensitivity of the biphasic system.

The precipitation of **6.9** was an intriguing observation. First, it suggested that autocatalysis could still be in operation, since the effective removal of product from the reaction by precipitation affected the rate of the reaction. Secondly, it warranted the investigation of precipitation under non-racemic conditions; the partitioning of enantioenriched and racemic **6.9** by precipitation could lead to the realisation of an asymmetric autocatalytic reaction with amplification of chirality. Thus, if the precipitate were racemic, whilst the solubilised surfactant were enantiopure and enantioselective, then we would achieve amplification of chirality *via* the scheme in Figure 6.4.1.

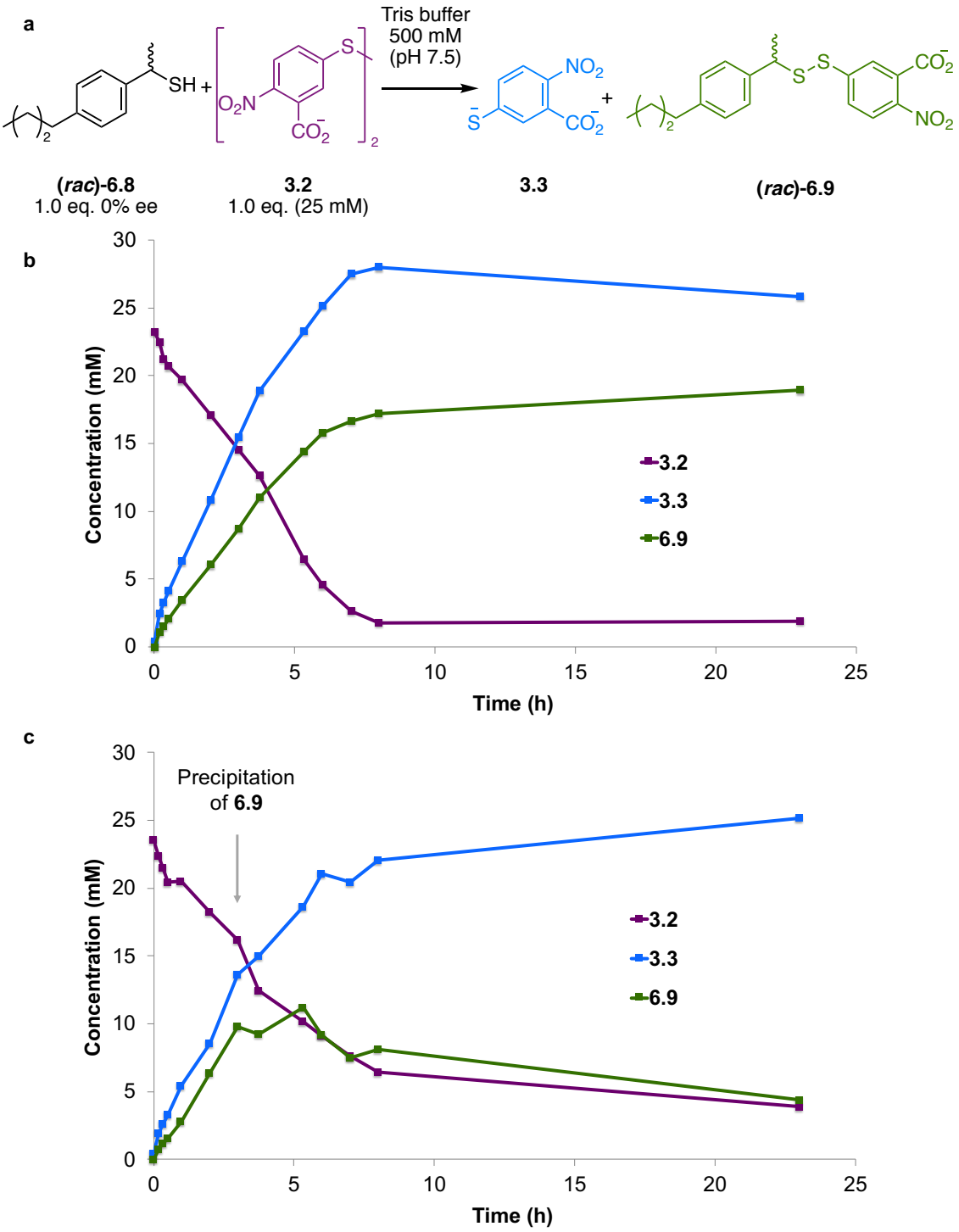



**Figure 6.4.2** **a** Two reactions under identical conditions (individual reaction profiles **b** and **c**) were conducted with **(*rac*)-6.8**. **b** Profile for reaction in which no precipitation occurred. **c** Profile for reaction in which **6.9** precipitated at ~ 3 hours. The concentration of the reaction components in solution was monitored by UPLC. Lines between points are drawn to guide the eye.

### 6.4.3 The non-racemic system

In order to examine whether the precipitation and resultant inactivity of the product could influence the enantiomeric excess of the system, the same reaction was conducted with an initial 67% ee of the hydrophobic thiol **6.8** (Figure 6.4.3).

Again, precipitation of product **6.9** occurred, and monitoring its ee in the two different phases throughout the reaction revealed that the enantiomers did indeed partition between active, solubilised **6.9** and inactive, precipitated **6.9**.

However, it was the inactive precipitate which showed a higher ee than the starting material, whilst the active catalytic species in solution tended towards a lower ee than the starting material (Figure 6.4.3c).

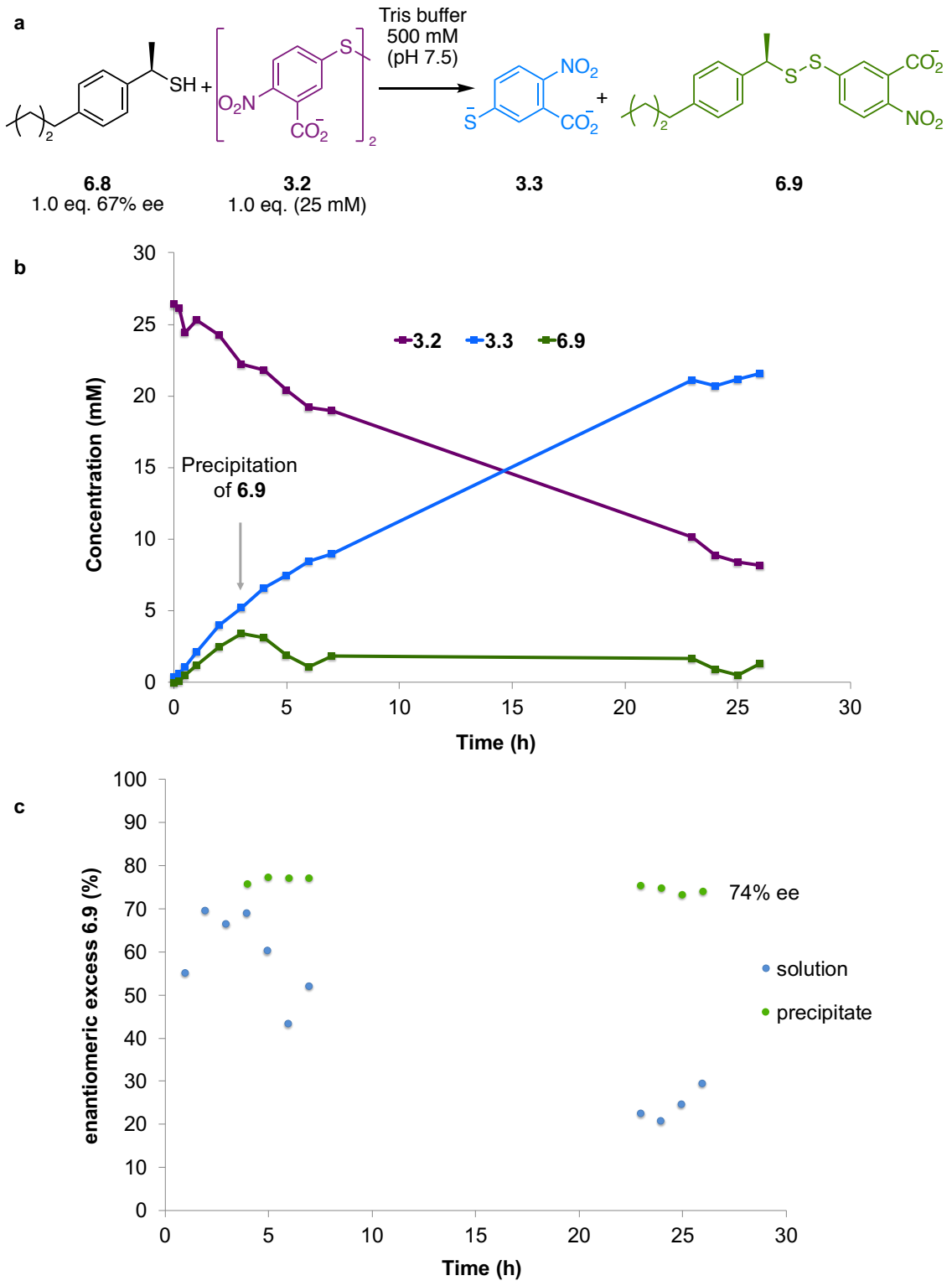



**Figure 6.4.3 a** Reaction conducted with **(*R*)-6.8** (67% ee). **b** Concentration of the reaction components in solution monitored by UPLC. Lines between points are drawn to guide the eye. **c** ee of **6.9** in solution and as precipitate monitored by chiral SFC. The data are those of a single experiment.

## 6.4.4 Characterisation of disulfide **6.9**

In order to further investigate the behaviour of disulfide **6.9**, different ee's of thiol **6.8** (30%, 49% and 82%) were used to synthesise the product **6.9** under homogeneous conditions (Section 6.6.1.4). The resultant ee of the isolated product **6.9** was equal to that of the starting materials, as expected from a reaction under homogeneous conditions in which all components remain solvated. Subsequent dissolution of **6.9** of known ee in Tris buffer, aiming to mimic the biphasic reaction conditions, resulted in the precipitation of **6.9** with enhanced ee, whilst **6.9** left in solution was of reduced ee (Table 6.4.1).

| ee **6.9** before dissolution (%) | ee **6.9** after dissolution and precipitation (%)[a] | |
|---|---|---|
| | solution phase | precipitate phase |
| 0 | 0 | 0 |
| 30 | 1 | 33 |
| 49 | 2 | 54 |
| 81 | 20 | 88 |

**Table 6.4.1** Variation in the ee of isolated surfactant **6.9** upon dissolution in Tris buffer at a concentration of 25.0 mM. [a] ee's were measured by chiral SFC.

The precipitation of an enantioenriched product, as well as the decrease in the ee of the catalytically active product left in solution, did not fit the Frank model for chiral amplification. Nevertheless, the intrinsic partitioning of the chiral surfactant **6.9** into two different phases with different ee's led us to consider a different approach for the amplification of chirality.

### 6.4.5 An alternative mechanism for the amplification of chirality

A different scenario for the amplification of chirality was designed to take advantage of the phase partitioning of disulfide **6.9** and its ability to undergo a second thiol-disulfide exchange (Figure 6.4.4).

Here, once precipitation occurred, the racemate in solution would be degraded by a second thiol-disulfide exchange with excess thiol to a mixture of chiral and *meso* disulfides **6.10** (Figure 6.4.4). We envisioned that the continued dissolution of the racemate and its destruction would result in an amplification of the enantiomeric excess in the precipitate.

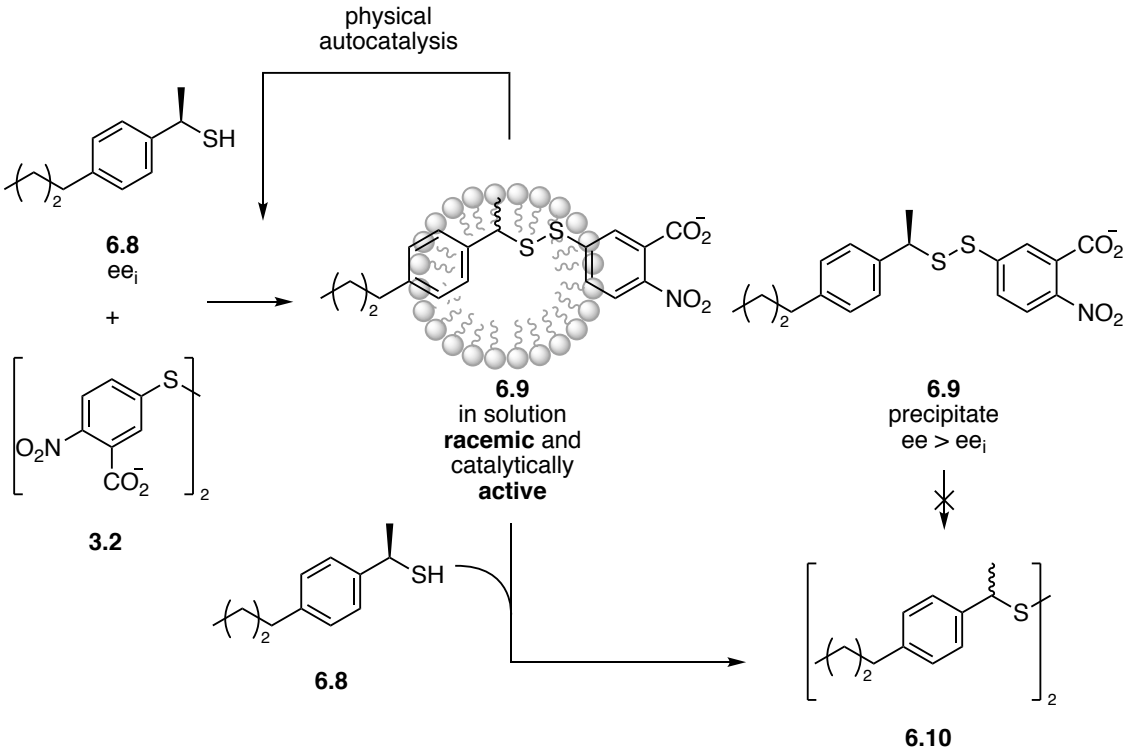
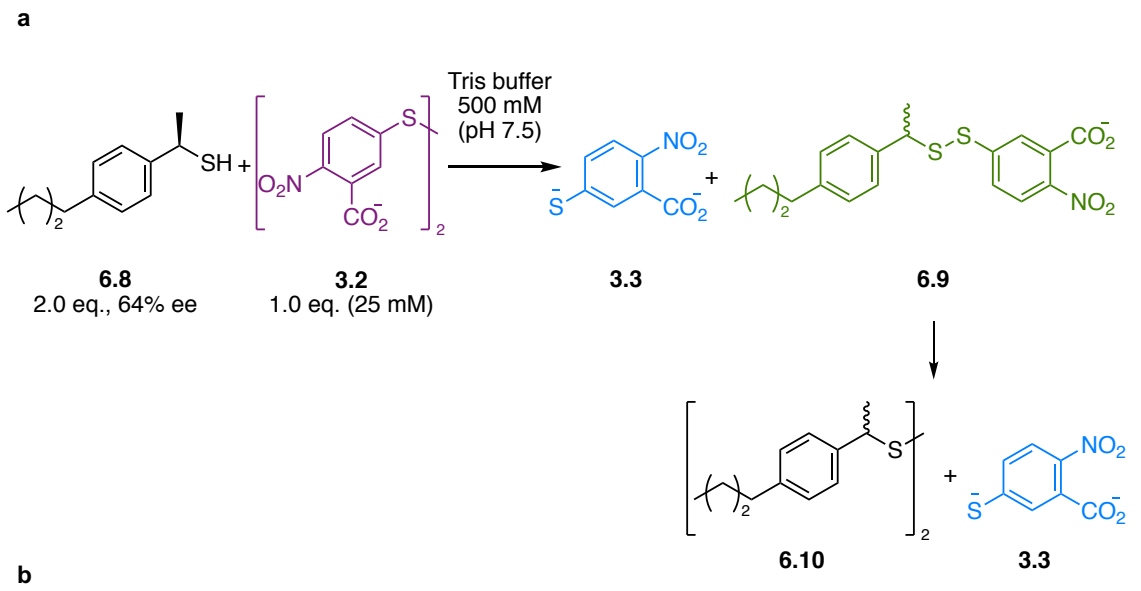



**Figure 6.4.4** An alternative proposed mechanism for the amplification of chirality: **6.9**, which tends towards the racemic state in solution, is degraded by a second thiol-disulfide exchange. Precipitated **6.9**, with enhanced ee, does not undergo degradation.

## 6.4.5.1 Experimental results

A preliminary test was conducted using 2.0 equivalents of enantioenriched thiol **6.8** (Figure 6.4.5). Precipitation of the disulfide **6.9** occurred, and the precipitate was enhanced in ee relative to the starting materials (Figure 6.4.6). However, the ee of the precipitate remained steady, within experimental error, over the course of the reaction and it did not appear to increase after the first appearance of the precipitate.



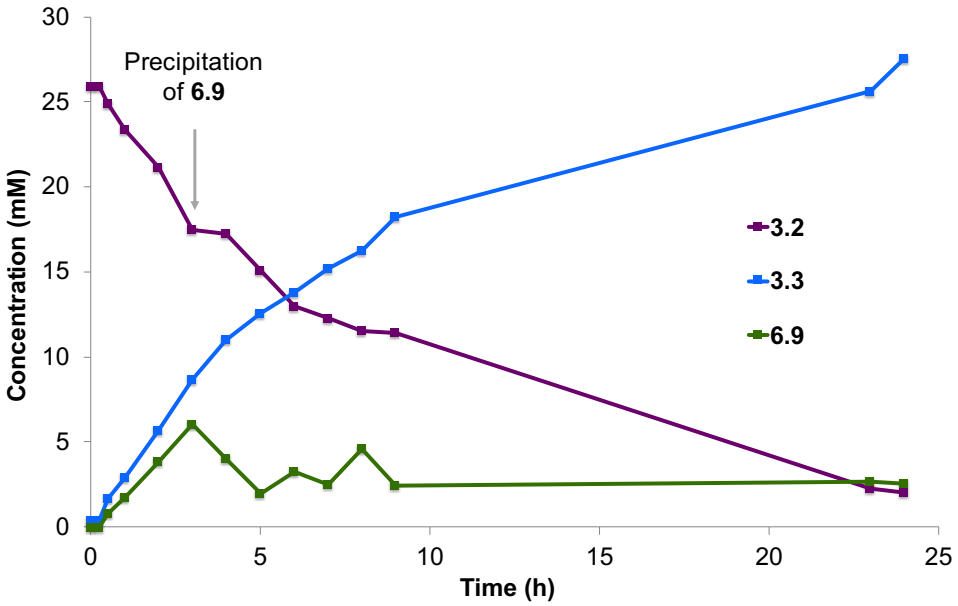




**Figure 6.4.5 a** Reaction conducted with 2.0 equivalents of enantioenriched thiol **6.8** (64% ee). **b** Concentration of the reaction components in solution monitored by UPLC (precipitation of **6.9** was observed at ~ 3 hours). Lines between points are drawn to guide the eye. The reaction profile is that of a single experiment.

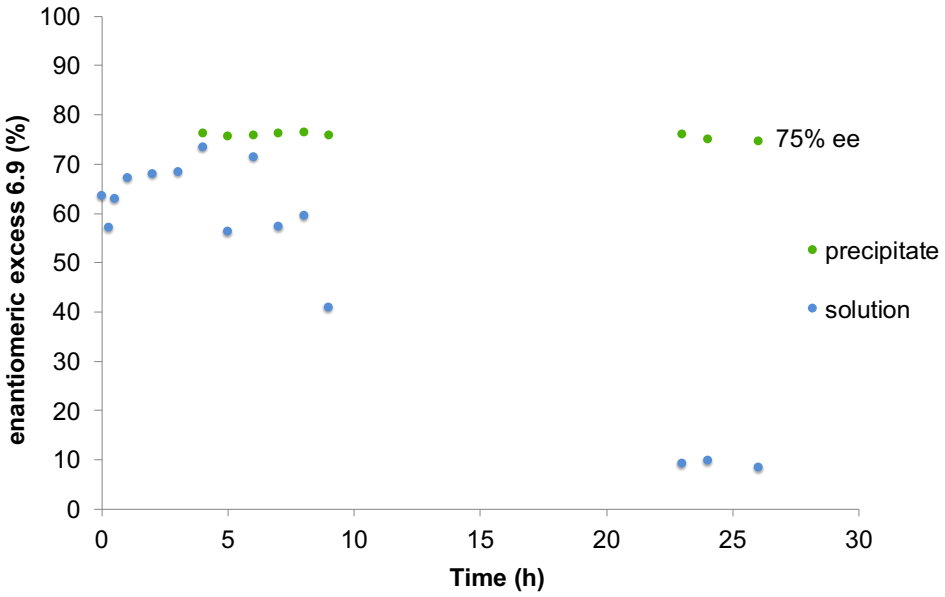



**Figure 6.4.6** ee of **6.9** in solution and in the precipitate monitored over time for the experiment depicted in Figure 6.4.5b. ee's were measured by chiral SFC.

Repeating these experiments produced variable results. Where precipitation of **6.9** occurred, this was always accompanied by an enhancement in ee; nevertheless, in some cases no precipitation occurred, and throughout the reaction the ee of **6.9** in solution remained equal to that of starting materials. Further, the reliable monitoring of each phase with minimal disturbance of the system proved difficult.

In order to increase the influence of the second thiol-disulfide exchange, with the aim of degrading the racemic solution phase and obtaining an obvious enhancement in the precipitate ee over time, a final reaction was conducted using 8.0 equivalents of thiol **6.8** (Figure 6.4.7).

However, whilst the product **6.9** was observed to reach a significant concentration, no precipitation was observed under these conditions. The second exchange was relatively rapid and disulfide **6.9** was degraded before it could precipitate. The ee of **6.9** in solution remained constant and the same as that of the starting materials throughout the reaction (Figure 6.4.8).

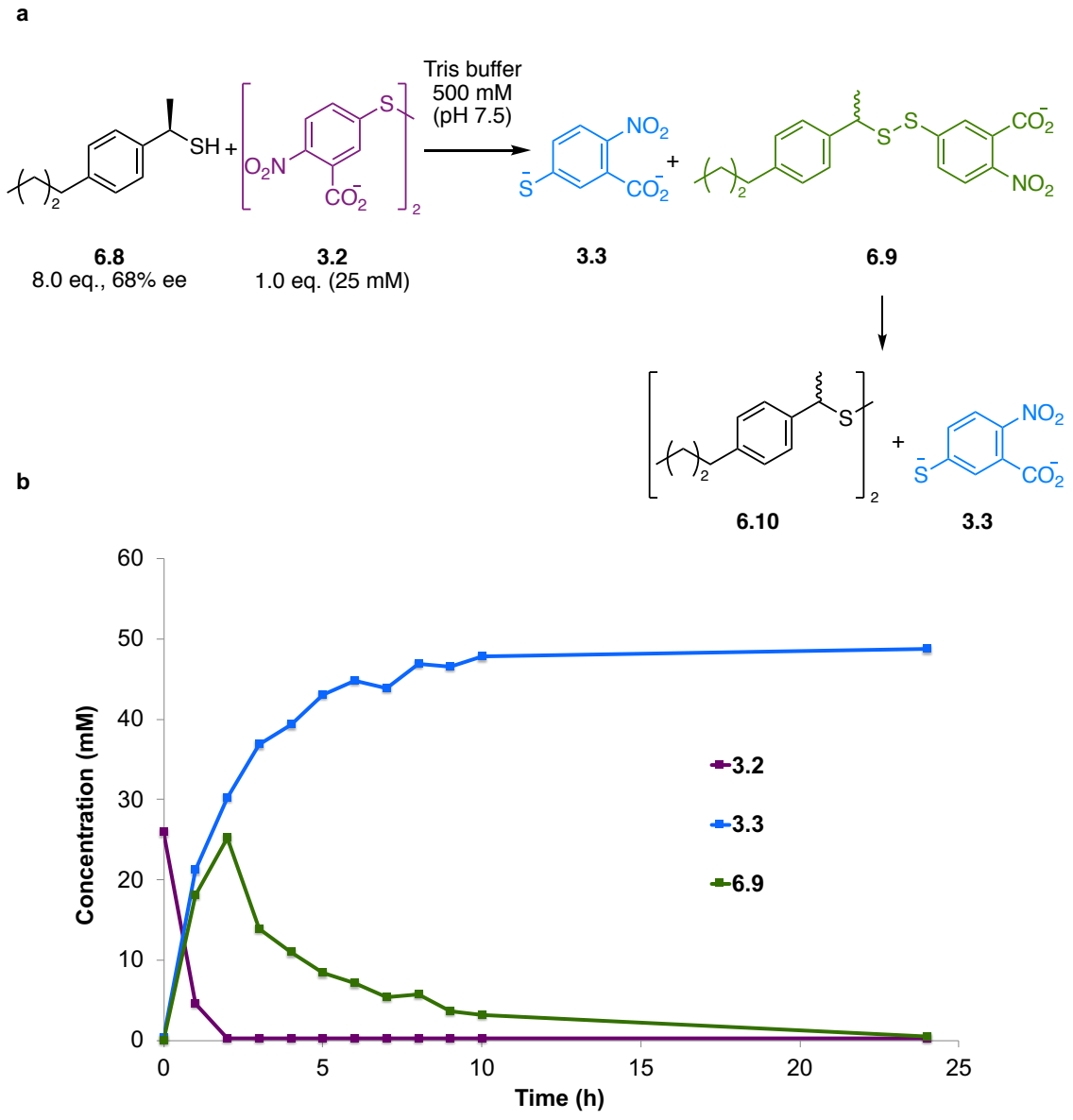



**Figure 6.4.7 a** Reaction conducted with 8.0 equivalents of thiol **6.10** (68% ee). **b** Concentration of the reaction components in solution monitored by UPLC. Lines between points are drawn to guide the eye. The reaction profile is that of a single experiment.

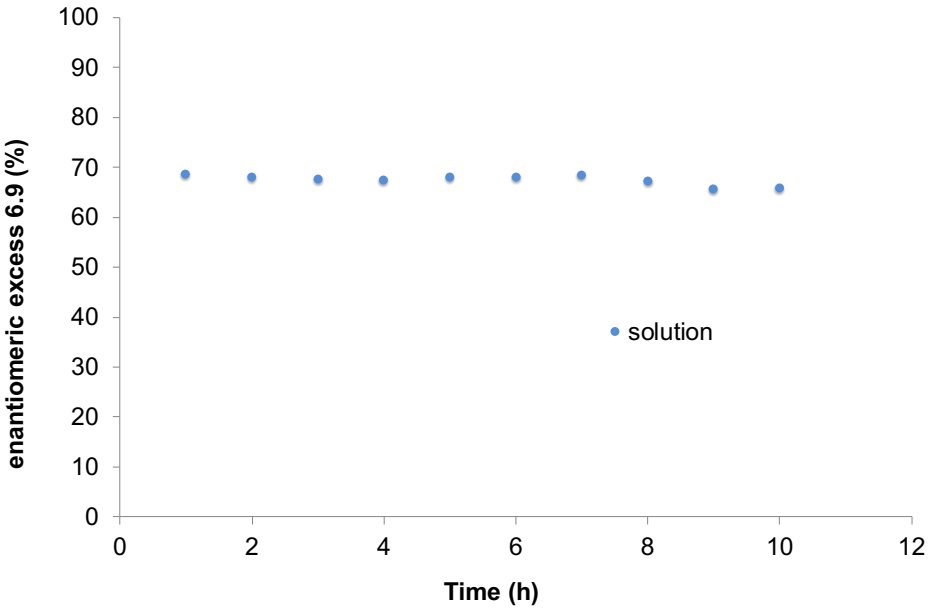



**Figure 6.4.8** ee of **6.9** over the course of the experiment depicted in Figure 6.4.7b. ee's were measured by chiral SFC.

## 6.5 Conclusions

In an effort to find new and general autocatalytic reactions for the amplification of chirality, chiral variants of the autocatalytic thiol-disulfide exchange system in Chapter 3 were carefully examined in search of non-linear behaviour.

For the system based on chiral disulfide **6.6**, mixing disulfides **(*R,R*)-** and **(*S,S*)-6.6** resulted in the formation of *meso* disulfide **(*R,S*)-6.6,** which sequestered racemic material and led to an enhanced ee in the major enantiopure disulfide **6.6**. Unfortunately this did not translate into an enhancement in the ee of the surfactant product **6.7** on reaction of **6.6** with thiol **3.1**.

Instead, a system based on chiral hydrophobic thiol **6.8** appeared much more promising, with the precipitation of enantioenriched **6.9** from the reaction mixture. Despite not being in line with the Frank model for the amplification of chirality, the nature of our system would allow a second thiol-disulfide exchange to occur and, in principle, to selectively degrade racemic product left in solution. However, given the difficulties encountered in reliably producing a precipitated phase, as well as in monitoring the reaction without introducing disturbances, further optimisation of the system would be required.

## 6.6 Experimental

### 6.6.1 Synthesis and characterisation of the compounds used in this study

#### 6.6.1.1 Disulfides **6.6**

The general procedure for the synthesis of disulfides **(*S,S*)-6.6** and **(*R,R*)-6.6** is illustrated in Figure 6.6.1 with the synthesis of **(*S,S*)-6.6** from L-phenylalanine.

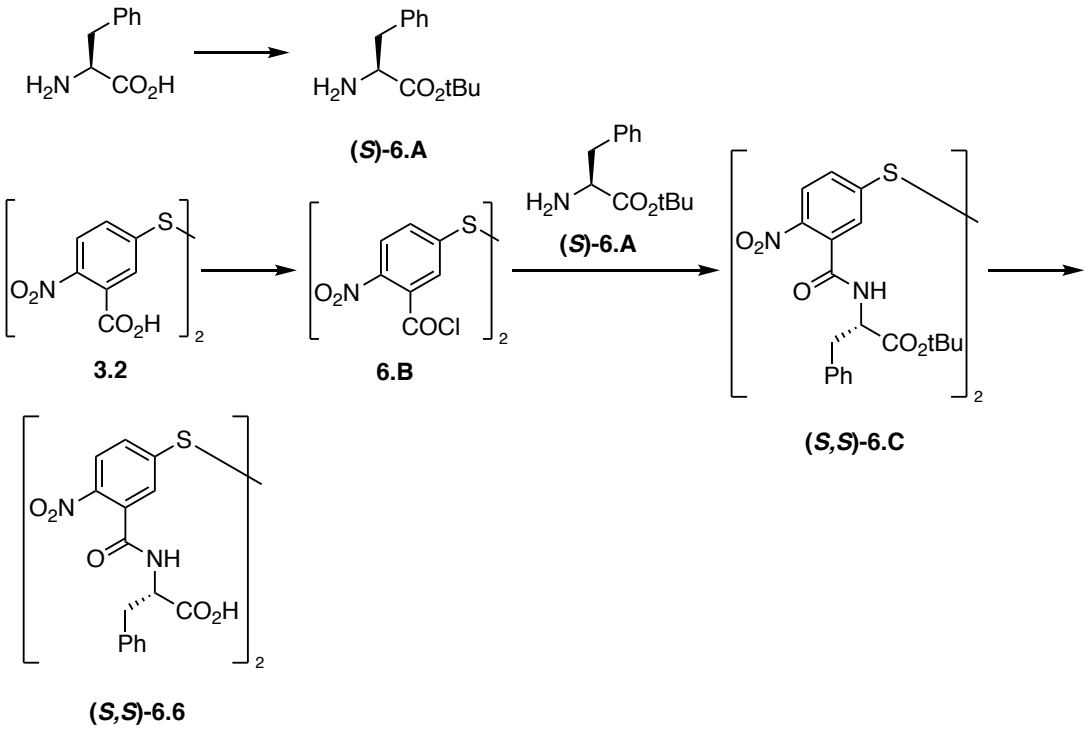



**Figure 6.6.1** General scheme for the synthesis of disulfides **(*S,S*)-6.6** and **(*R,R*)-6.6**, illustrated with the synthesis of disulfide **(*S,S*)-6.6** from L-phenylalanine.

**(*S*)-6.A**

A round-bottom flask was charged with L-phenylalanine (990 mg, 6.00 mmol, 1.00 eq.) and tert-butyl acetate (13.5 mL, 101 mmol, 16.8 eq.). $HClO_4$ (70 wt% in $H_2O$; 0.75 mL, 8.7 mmol, 1.4 eq.) was added dropwise at 0 °C and the reaction was left to warm to rt and stirred overnight. 1 M HCl (15 mL) was added and the solution was adjusted to pH 9 with an aqueous solution of $K_2CO_3$ (10 wt%, 100 mL). The mixture was extracted with $CH_2Cl_2$ (3× 20 mL) and the organic layers dried over $MgSO_4$, filtered, and concentrated *in vacuo*. The crude product was used in the next step without further purification.

**6.B**

A flame-dried round-bottom flask was charged with 5,5'-Dithiobis-(2-nitrobenzoic acid) (DTNB) **3.2** (1.88 g, 4.73 mmol, 1.00 eq.), THF (45 mL) and DMF (5 drops). Oxalyl chloride $(COCl)_2$ (1.0 mL, 11 mmol, 2.4 eq.) was added dropwise to the solution at 0 °C and stirred for 5 minutes. The reaction was concentrated *in vacuo* and the crude product was used in the next step without further purification.

**(*S,S*)-6.C**

A round-bottom flask was charged with **(*S*)-6.A** (1.07 g, 4.85 mmol, 2.05 eq.), THF (10 mL) and propylene oxide (5.0 mL). A solution of **6.B** (1.02 g, 2.37 mmol, 1.00 eq.) in THF (5.0 mL) and propylene oxide (1.5 mL) was added at 0 °C. The reaction was stirred for 1.5 hours, then diluted with $H_2O$ (10 mL) and extracted with EtOAc (3× 10 mL). The organic layers were dried over $MgSO_4$, filtered, and concentrated *in vacuo*. The crude product was purified by column chromatography ($SiO_2$, $CH_2Cl_2$:MeOH 99.5:0.5) to yield disulfide **(*S,S*)-6.C** as a

yellow solid (868 mg, 46% yield). **$^1$H NMR** (400 MHz, $CDCl_3$): δ 8.07 (2H, d, *J* = 8.5 Hz, 2× C(Ar)–H), 7.53 (2H, dd, *J* = 8.5 Hz, 2.0 Hz, 2× C(Ar)–H), 7.34–7.19 (12H, m, 12× C(Ar)–H), 5.00–4.95 (2H, m, 2× CH), 3.06–2.97 (4H, m, 2× $CH_2$), 1.25 (18H, s, 2× $C(CH_3)_3$); **$^{13}$C NMR** (101 MHz, $CDCl_3$): δ 171.8 (2× C=O), 165.7 (2× C=O), 144.1 (2× 4° C(Ar)), 143.1 (2× 4° C(Ar)), 136.1 (2× 4° C(Ar)), 134.5 (2× 4° C(Ar)), 129.6 (4× C(Ar)–H), 128.6 (4× C(Ar)–H), 127.2 (2× C(Ar)–H), 126.8 (2× C(Ar)–H), 125.4 (2× C(Ar)–H), 125.3 (2× C(Ar)–H), 83.4 (2× *C*$(CH_3)_3$), 53.9 (2× CH), 38.3 (2× $CH_2$), 27.9 (2× C(*C*$H_3)_3$); **HRMS** (ESI+, m/z): calc. for $C_{40}H_{43}O_{10}N_4S_2^+$ $[M+H]^+$ 803.2415, found 803.2412; **IR** $\tilde{\nu}_{max}$ (film)/ $cm^{-1}$: 2980, 2361, 2342, 1731, 1656, 1529; $\alpha_D$ (c = 0.2, MeOH): −16.3.

Following the procedure described for **(*S,S*)-6.C**, **(*R,R*)-6.C** was synthesised from D-phenylalanine (990 mg, 6.00 mmol, 1.00 eq.). **(*R,R*)-6.C** was isolated as a yellow solid (1.12 g, 59% yield). $\alpha_D$ (c = 0.2, MeOH): +18.5.

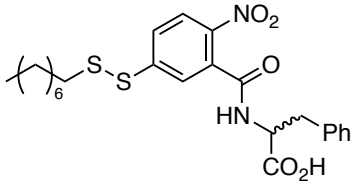
**(*S,S*)-6.6**

A round-bottom flask was charged with a solution of ester **(*S,S*)-6.C** (0.93 g, 1.2 mmol, 1.0 eq.) in $CH_2Cl_2$ (5 mL). Trifluoroacetic acid (2.7 mL, 35 mmol, 30 eq.) was added at 0 °C. The reaction was left to warm to rt and stirred overnight. The reaction mixture was concentrated *in vacuo*, dissolved in $CH_2Cl_2$ (20 mL) and washed with $H_2O$. The organic layer was dried over $MgSO_4$, filtered, and concentrated *in vacuo*. The crude product was purified by column chromatography ($SiO_2$, $CH_2Cl_2$:MeOH:AcOH 94:5:1) to yield disulfide **(*S,S*)-6.6** as a pale yellow solid (537 mg, 68% yield). **$^1$H NMR** (400 MHz, $(CD_3)_2SO$): δ 9.16 (2H, d, *J* = 8.0 Hz, 2× NH), 8.06 (2H, d, *J* = 8.5 Hz, 2× C(Ar)–H), 7.78 (2H, dd, *J*

= 8.5 Hz, 2.0 Hz, 2× C(Ar)–H), 7.45 (2H, d, *J* = 2.0 Hz, 2× C(Ar)–H), 7.30–7.19 (10H, m, 10× C(Ar)–H), 4.64–4.58 (2H, m, 2× CH), 3.18–3.13 (2H, dd, *J* = 14.0 Hz, 5.0 Hz, 2× C$H_aH_b$), 2.96 (2H, dd, *J* = 14.0 Hz, 9.5 Hz, 2× $CH_aH_b$); **$^{13}$C NMR** (101 MHz, $(CD_3)_2SO$): δ 172.4 (2× C=O), 164.5 (2× C=O), 145.6 (2× 4° C(Ar)), 141.6 (2× 4° C(Ar)), 137.4 (2× 4° C(Ar)), 133.0 (2× 4° C(Ar)), 129.1 (4× C(Ar)–H), 128.3 (4× C(Ar)–H), 127.8 (2× C(Ar)–H), 126.6 (2× C(Ar)–H), 126.3 (2× C(Ar)–H), 125.5 (2× C(Ar)–H), 53.8 (2× CH), 36.7 (2× $CH_2$); **HRMS** (ESI+, m/z): calc. for $C_{32}H_{27}O_{10}N_4S_2^+$ $[M+H]^+$ 691.1163, found 691.1159; **IR** $\tilde{\nu}_{max}$ (film)/ $cm^{-1}$: 3065, 1730, 1652, 1564, 1526; **$\alpha_D$** (c = 1.13, MeOH): −16.0.

Following the procedure described for **(*S,S*)-6.6**, **(*R,R*)-6.6** was synthesised from **(*R,R*)-6.C** (1.09 g, 1.35 mmol, 1.00 eq.). **(*R,R*)-6.6** was isolated as a pale yellow solid (719 mg, 77% yield). **$\alpha_D$** (c = 1.67, MeOH): +15.8.

## 6.6.1.2 Disulfide **(*rac*)-6.7**




A round-bottom flask was charged with a solution of disulfide **(*R,R*)-6.6** (43.2 mg, 62.5 µmol, 0.500 eq.) and **(*S,S*)-6.6** (43.2 mg, 62.5 µmol, 0.500 eq.) in Tris buffer (5.0 mL; 500 mM, pH 7.8 – 7.9). The solution was stirred at 100 rpm and octanethiol (22 µL, 0.13 mmol, 1.0 eq.) was added by microsyringe. The reaction was stirred for 23 hours, then quenched with 1 M HCl (5 mL) and extracted with EtOAc (3× 10 mL). The combined organic layers were dried over $MgSO_4$, filtered, and concentrated in vacuo. The crude product was purified by column

chromatography ($SiO_2$, $CH_2Cl_2$:MeOH:AcOH 95:4:1) to yield disulfide **(*rac*)-6.7** as a yellow oil (32 mg, 53% yield). **$^1$H NMR** (400 MHz, $(CD_3)_2CO$): δ 8.04 (1H, d, *J* = 8.5 Hz, 1× C(Ar)–H), 7.81 (1H, dd, *J* = 8.5 Hz, 2.0 Hz, 1× C(Ar)–H), 7.57 (1H, d, *J* = 2.0 Hz, 1× C(Ar)–H), 7.39–7.30 (4H, m, 4× C(Ar)–H), 7.26–7.22 (1H, m, 1× C(Ar)–H), 4.97 (1H, m, CH), 3.34 (1H, dd, *J* = 14.0 Hz, 5.5 Hz, C$H_a$H$_b$), 3.18 (1H, dd, *J* = 14.0 Hz, 8.0 Hz, CH$_a$$H_b$), 2.86 (2H, t, *J* = 7.5 Hz, 1× $CH_2$), 1.72–1.65 (2H, m, 1× $CH_2$), 1.43–1.36 (2H, m, 1× $CH_2$), 1.31–1.21 (8H, m, 4× $CH_2$), 0.87 (3H, t, *J* = 7.0 Hz, $(CH_2)_7CH_3$); **$^{13}$C NMR** (101 MHz, $(CD_3)_2CO$): δ 172.0 (C=O), 165.9 (C=O), 146.1 (4° C(Ar)), 145.9 (4° C(Ar)), 138.1 (4° C(Ar)), 134.4 (4° C(Ar)), 130.3 (2× C(Ar)–H), 129.2 (2× C(Ar)–H), 127.5 (1× C(Ar)–H), 127.5 (1× C(Ar)–H), 126.3 (1× C(Ar)–H), 125.9 (1× C(Ar)–H), 54.6 (CH), 39.4 (1× $CH_2$), 38.1 (CH$_a$H$_b$), 32.5, 29.8, 29.6, 29.0, 23.3, 20.5 (6× $CH_2$), 14.3 ($(CH_2)_7CH_3$).

## 6.6.1.3 Thiols **6.8**

The general procedure for the synthesis of thiols **(*rac*)-6.8** and **(*R*)-6.8** is illustrated in Figure 6.6.2.

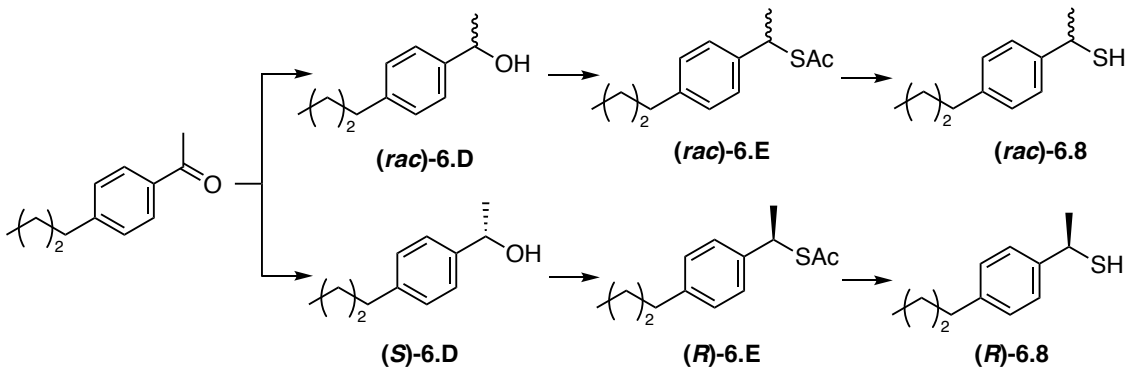



**Figure 6.6.2** General scheme for the synthesis of thiols **(*rac*)-6.8** and **(*R*)-6.8**.

**(*rac*)-6.D**

A round-bottom flask was charged with a solution of 4'-butylacetophenone (3.00 g, 17.0 mmol, 1.00 eq.) in EtOH (20 mL). $NaBH_4$ (100 mg, 25.5 mmol, 1.50 eq.) was added portionwise to the solution at 0 °C. The reaction was allowed to warm to rt and stirred for 3 hours before it was cooled back to 0 °C and quenched with 1 M HCl (10 mL). The mixture was extracted with $CH_2Cl_2$ (3× 15 mL) and the organic layers were washed with an aq. sat. solution of $NaHCO_3$ (15 mL) and brine (15 mL), dried over $MgSO_4$, filtered and concentrated *in vacuo*. The crude product was used in the next step without further purification.

**(*S*)-6.D**

A round-bottom flask was charged with $Et_3N$ (5.9 mL, 43 mmol, 2.5 eq.) and formic acid (3.9 mL, 100 mmol, 6.0 eq.) was added dropwise at 0 °C. 4'-butylacetophenone (3.1 mL, 17 mmol, 1.0 eq.) was added, followed by RuCl(*p*-cymene)[(*S*,*S*)-Ts-DPEN] (540 mg, 0.85 mmol, 5.0 mol%). The reaction was allowed to warm to rt and stirred overnight. The reaction was quenched with $H_2O$ (20 mL) and extracted with $Et_2O$ (3× 20 mL). The combined organic layers were dried over $MgSO_4$, filtered, and concentrated in vacuo. The crude product was purified by column chromatography ($SiO_2$, petrol ether:$Et_2O$ 90:10–60:40) to yield alcohol **(*S*)-6.D** as a colourless oil (2.97 g, 98% yield) (87% ee). **$^1$H NMR** (400 MHz, $CDCl_3$): δ 7.30–7.28 (2H, m, 2× C(Ar)–H), 7.18–7.16 (2H, m, 2× C(Ar)–H), 4.90–4.85 (1H, m, C*H*OH), 2.61 (2H, t, *J* = 8.0 Hz, C(Ar)–$CH_2$), 1.83 (1H, br. s, OH), 1.65–1.56 (2H, m, 1× $CH_2$), 1.49 (3H, d, *J* = 7.5 Hz, CH(OH)C$H_3$), 1.41–1.31 (2H, m, 1× $CH_2$), 0.93 (3H, t, *J* = 7.5 Hz, $(CH_2)_3CH_3$); **$^{13}$C NMR** (101 MHz, $CDCl_3$): δ 143.2 (4° C(Ar)), 142.4 (4° C(Ar)), 128.7 (2× C(Ar)–H), 125.5 (2× C(Ar)–H), 70.4 (CHOH), 35.4 (C(Ar)–*C*$H_2$), 33.8 (1× $CH_2$), 25.1 (CH(OH)*C*$H_3$), 22.5 (1× $CH_2$), 14.1 ($(CH_2)_3CH_3$); **HRMS** (EI, m/z): calc. for $C_{12}H_{18}O^+$ $[M]^+$ 178.1352, found 178.1351; **IR** $\tilde{\nu}_{max}$ (film)/ $cm^{-1}$: 3338, 2959, 2929, 2859, 2361; **$\alpha_D$** (c = 1.1, MeOH): −27.8. The data are consistent with those reported in *Chem. Eur. J.* **16**, 3090-3096 (2010).[2]

The enantiomeric excess was determined by HPLC [Chiralpak® ID, hexane:iPrOH 98:2; 1.0 $mLmin^{-1}$, λ= 210 nm, $t_R$ (**(*R*)-6.D**) = 10.66, $t_R$ (**(*S*)-6.D**) = 11.09].

**(*rac*)-6.E**

A round-bottom flask was charged with a solution of $PPh_3$ (8.93 g, 34.0 mmol, 2.00 eq.) in THF (60 mL) under argon. Diethyl azodicarboxylate (DEAD) (5.4 mL, 34 mmol, 2.0 eq.) was added dropwise to the solution at 0 °C and the reaction was stirred for 1 hour. A solution of alcohol **(*rac*)-6.D** (3.03 g, 17.0 mmol, 1.00 eq.) in THF (20 mL) and thioacetic acid (2.4 mL, 2.0 eq.) were added dropwise. The reaction was left to stir overnight before the solvent was removed *in vacuo*. The residue was suspended in hexane (50 mL), stirred for 2 hours, and filtered. The filtrate was concentrated *in vacuo* and the crude product was purified by column chromatography ($SiO_2$, petrol ether: $Et_2O$ 97:3) to yield racemic thioester **(rac)-6.E** as a yellow oil (2.78 g, 69% yield). **$^1$H NMR** (400 MHz, $CDCl_3$): δ 7.25–7.23 (2H, m, 2× C(Ar)–H), 7.14–7.12 (2H, m, 2× C(Ar)–H), 4.74 (1H, q, *J* = 7.0 Hz, C*H*($CH_3$)SAc), 2.59 (2H, t, *J* = 8.0 Hz, C(Ar)–$CH_2$), 2.30 (3H, s, $CH_3$ (Ac)), 1.66 (3H, d, *J* = 7.0 Hz, CH(C*H*$_3$)SAc), 1.62–1.55 (2H, m, 1× $CH_2$), 1.40–1.31 (2H, m, 1× $CH_2$), 0.93 (3H, t, *J* = 7.5 Hz, $(CH_2)_3CH_3$); **$^{13}$C NMR** (101 MHz, $CDCl_3$): δ 195.3 (C=O), 142.2 (4° C(Ar)), 139.8 (4° C(Ar)), 128.7 (2× C(Ar)–H), 127.1 (2× C(Ar)–H)), 42.9 (*C*H($CH_3$)SAc), 35.4 (C(Ar)–*C*$H_2$), 33.7 (1× $CH_2$), 30.6 ($CH_3$ (Ac)), 22.5 (1× $CH_2$), 22.4 (CH(*C*$H_3$)SAc), 14.1 ($(CH_2)_3CH_3$); **HRMS** (EI, m/z): calc. for $C_{14}H_{20}OS^+$ $[M]^+$ 236.1229, found 236.1235; **IR** $\tilde{\nu}_{max}$ (film)/ $cm^{-1}$: 2958, 2929, 2859, 2361, 1690, 1512.

Following the procedure described for **(*rac*)-6.E**, using diisopropyl azodicarboxylate (DIAD) (6.3 mL, 32 mmol, 2.0 eq.) in place of DEAD, **(*R*)-6.E** was synthesised from alcohol **(S)-6.D** (2.86 g, 16.1 mmol, 1.00 eq.). **(*R*)-6.E** was isolated as a yellow oil (2.47 g, 65% yield) (83% ee). **$\alpha_D$** (c = 0.92, MeOH): +219.6

The enantiomeric excess was determined by SFC [Chiralpak® IF, MeOH/$CO_2$: 1.0 to 30 %; 1.5 mLmin$^{-1}$, λ= 215 nm, $t_R$ (**(*R*)-6.E**) = 1.64, $t_R$ (**(*S*)-6.E**) = 1.84].

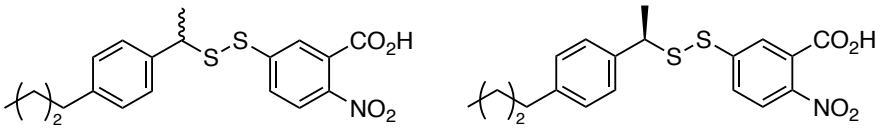
**(*rac*)-6.8**

A flame-dried round-bottom flask was charged with $Et_2O$ (35 mL) and a solution of $LiAlH_4$ in $Et_2O$ (1.0 M; 11.5 mL, 1.00 eq.). A solution of racemic thioester **(*rac*)-6.E** (2.71 g, 11.5 mmol, 1.00 eq.) in $Et_2O$ (25 mL) was added dropwise to the solution at 0 °C and the reaction was stirred for 10 minutes before quenching with 1 M HCl (15 mL). The mixture was extracted with $Et_2O$ (3× 20 mL) and the combined organics dried over $MgSO_4$, filtered, and concentrated *in vacuo*. The crude product was purified by column chromatography ($SiO_2$, petrol ether:$Et_2O$ 99.5:0.5) to afford thiol **(*rac*)-6.8** as a clear and colourless oil (1.94 g, 87% yield). **$^1$H NMR** (400 MHz, $CDCl_3$): δ 7.29–7.27 (2H, m, 2× C(Ar)–H), 7.15–7.13 (2H, m, 2× C(Ar)–H), 4.23 (1H, m, C*H*($CH_3$)SH), 2.59 (2H, t, *J* = 8.0 Hz, C(Ar)–$CH_2$), 1.99 (1H, d, *J* = 5.0 Hz, S*H*), 1.67 (3H, d, *J* = 7.0 Hz, CH(C*H*$_3$)SH), 1.63–1.55 (2H, m, 1× $CH_2$), 1.41–1.32 (2H, m, 1× $CH_2$), 0.93 (3H, t, *J* = 7.5 Hz, $(CH_2)_3$C*H*$_3$); **$^{13}$C NMR** (101 MHz, $CDCl_3$): δ 143.1 (4° C(Ar)), 142.0 (4° C(Ar)), 128.7 (2× C(Ar)–H), 126.3 (2× C(Ar)–H), 38.6 (*C*H($CH_3$)SH), 35.4 (C(Ar)–*C*$H_2$), 33.7 (1× $CH_2$), 26.3 (CH(C*H*$_3$)SH), 22.5 (1× $CH_2$), 14.1 ($(CH_2)_3$*C*$H_3$); **HRMS** (EI, m/z): calc. for $C_{12}H_{18}S^+$ $[M]^+$ 194.1124, found 194.1126; **IR** $\tilde{\nu}_{max}$ (film)/ cm$^{-1}$: 3021, 2958, 2927, 2858, 2360, 2341, 1512.

Following the procedure described for **(*rac*)-6.8**, **(*R*)-6.8** was synthesised from thioester **(*R*)-6.E** (2.47 g, 10.5 mmol, 1.00 eq.). **(*R*)-6.8** was isolated as a clear and colourless oil (1.86 g, 91% yield) (82 % ee) $\alpha_D$ (c = 1.38, MeOH): +44.1.

The enantiomeric excess was determined by SFC [Chiralpak® IF, MeOH/$CO_2$: 1.0 to 30 %; 1.5 mLmin$^{-1}$, λ= 215 nm, $t_R$ (**(*R*)-6.8**) = 1.37, $t_R$ (**(*S*)-6.8**) = 1.41].

## 6.6.1.4 Disulfides **6.9**



**(*rac*)-6.9**

A round-bottom flask was charged with 5,5'-Dithiobis-(2-nitrobenzoic acid) (DTNB) **3.2** (123 mg, 310 µmol, 1.00 eq.), racemic thiol **(*rac*)-6.8** (60.0 mg, 310 µmol, 1.00 eq.), and $CH_2Cl_2$ (5 mL) under argon. $Et_3N$ (0.15 mL, 1.1 mmol, 3.5 eq.) was added at 0 °C and the reaction was allowed to warm to rt and stirred for 1.25 hours. The reaction was quenched with 1 M HCl (15 mL) and extracted with EtOAc (3× 20 mL). The combined organics were dried over $MgSO_4$, filtered, and concentrated *in vacuo*. The crude product was purified by column chromatography ($SiO_2$, $CH_2Cl_2$:MeOH:AcOH 96:3:1) to afford racemic disulfide **(*rac*)-6.9** as a yellow oil (80 mg, 66% yield). **$^1$H NMR** (400 MHz, $(CD_3)_2SO$): δ 7.86 (1H, d, *J* = 8.5 Hz, 1× C(Ar)–H), 7.67 (1H, d, *J* = 2.0 Hz, 1× C(Ar)–H), 7.64 (1H, dd, *J* = 8.5 Hz, 2.0 Hz, 1× C(Ar)–H), 7.25–7.23 (2H, m, 2× C(Ar)–H), 7.04–7.02 (2H, m, 2× C(Ar)–H), 4.37 (1H, q, *J* = 7.0 Hz, C(Ar)–C*H*($CH_3$)), 2.46 (2H, t, *J* = 7.5 Hz, C(Ar)–$CH_2$), 1.63 (3H, d, *J* = 7.0 Hz, C(Ar)–CH(C*H*$_3$)), 1.47–1.39 (2H, m, 1× $CH_2$), 1.28–1.19 (2H, m, 1× $CH_2$), 0.86 (3H, t, *J* = 7.5 Hz, $(CH_2)_3CH_3$); **$^{13}$C NMR** (101 MHz, $(CD_3)_2SO$): δ 165.6 (C=O), 145.5 (4° C(Ar)), 144.1 (4° C(Ar)),

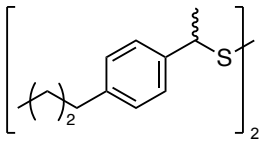
142.1 (4° C(Ar)), 137.6 (4° C(Ar)), 128.6 (4° C(Ar)), 128.3 (2× C(Ar)–H), 127.9 (1× C(Ar)–H), 127.5 (2× C(Ar)–H), 125.7 (1× C(Ar)–H), 124.4 (1× C(Ar)–H), 49.5 (C(Ar)–*C*H($CH_3$)), 34.4 (C(Ar)–*C*$H_2$). 33.0 (1× $CH_2$), 21.8 (1× $CH_2$), 19.8 (C(Ar)–CH(*C*$H_3$)), 13.7 ($CH_2$)$_3$*C*$H_3$); **HRMS** (ESI−, m/z): calc. for $C_{19}H_{20}O_4NS_2$ $[M-H]^-$ 390.0828, found 390.0845.

Following the procedure described for **(*rac*)-6.9**, **(*R*)-6.9** was prepared from thiol **(*R*)-6.8** (82% ee) (60.0 mg, 310 mmol, 1.00 eq.). This procedure afforded disulfide **(*R*)-6.9** as a yellow oil (85 mg, 70% yield) (81% ee). $\alpha_D$ (c = 0.23, MeOH:$CHCl_3$ 1:1): +61.1.

The enantiomeric excess was determined by SFC: [Chiralpak® IG, MeOH/$CO_2$: 1.0 to 30 %; 1.5 mLmin$^{-1}$, λ= 215 nm, $t_R$ (**(*R*)-6.9**) = 4.77, $t_R$ (**(*S*)-6.9**) = 4.98].

Following the procedure described for **(*rac*)-6.9**, **(*R*)-6.9** was also prepared at 49% ee and at 30% ee from mixtures of racemic thiol **(*rac*)-6.8** and **(*R*)-6.8** (82% ee). **(*R*)-6.9** (49% ee) was synthesised from a mixture of racemic thiol **(*rac*)-6.8** (23.0 mg, 118 μmol, 0.38 eq.) and thiol **(*R*)-6.8** (82% ee) (36.0 mg, 185 μmol, 0.60 eq.). **(*R*)-6.9** (30% ee) was synthesised from a mixture of racemic thiol **(*rac*)-6.8** (38.0 mg, 196 μmol, 0.63 eq.) and thiol **(*R*)-6.8** (82% ee) (22.0 mg, 113 μmol, 0.37 eq.).

### 6.6.1.5 Disulfides **6.10**



A round-bottom flask was charged with a solution of **(*rac*)-6.8** (20.0 mg, 100 µmol, 1.00 eq.) in EtOAc (1.0 mL). To the solution was added an aqueous solution of $H_2O_2$ (50 wt%, 6 µL, ~ 1.0 eq.) and NaI (tip of spatula). After stirring for 10 minutes the reaction was quenched with sat. aq. $Na_2S_2O_3$ (2 mL) and extracted with $Et_2O$ (3× 5 mL). The combined organics were dried over $MgSO_4$, filtered, and concentrated *in vacuo* to yield a mixture of disulfides **(*R,R*)-6.10**, **(*S,S*)-6.10**, and **(*R,S*)-6.10**.

The mixture of product isomers was analysed by chiral SFC [Chiralpak® IC, MeOH/$CO_2$: 1.0 to 30 %; 1.5 mLmin$^{-1}$; $t_R$ = 2.00, $t_R$ = 2.22, $t_R$ = 2.28].

## 6.6.2 Procedures for biphasic experiments

### 6.6.2.1 Preparation and general methods of analysis

Tris buffer (500 mM) was prepared as described in Section 3.5.2.1. No additional pH adjustment was made on dissolution of the disulfides **6.6** or **3.2** in the pre-prepared buffer (pH 7.8–7.9 prior to dissolution of the disulfides).

External standard solution containing maleimide was prepared as described in Section 3.5.3.2. Aliquots were taken from the reaction as described in Section 3.5.3.2.

## 6.6.2.2 Experiments conducted using chiral disulfide **6.6**

Experiments were analysed by chiral UPLC on a Chiralpak® IC-U column (1.7 μm, 3.0 mm × 10 mm), using the gradient shown in Table 6.6.1.

| Time (minutes) | Flow ($mLmin^{-1}$) | Composition of eluent solution (%) | | | Curve |
|---|---|---|---|---|---|
| | | MilliQ $H_2O$ | MeCN | 5 % TFA in MilliQ $H_2O$ | |
| initial | 0.600 | 80 | 15 | 5 | initial |
| 0.25 | 0.600 | 80 | 15 | 5 | 6 |
| 4.00 | 0.600 | 0 | 95 | 5 | 6 |
| 4.40 | 0.600 | 0 | 95 | 5 | 6 |
| 4.50 | 0.600 | 80 | 15 | 5 | 10 |
| 5.00 | 0.600 | 80 | 15 | 5 | 10 |

**Table 6.6.1** Gradient for chromatogram acquisition on chiral UPLC.

No calibration was performed for the components **6.6** or **6.7**. The points plotted for **6.6** and **6.7** in Figure 6.3.2 equal the peak area of each component over the area of the external standard.

### 6.6.2.2.1 Preparation of solutions of disulfide **6.6**

Stock solutions of disulfides **(*S,S*)-6.6** and **(*R,R*)-6.6** (25 mM) in Tris buffer (500 mM, pH 7.8 – 7.9) were prepared. They were mixed in different ratios to result in three solutions of different theoretical ee prior to mixing: *i.e.* (**(*R,R*)-6.6**: **(*S,S*)-6.6**)

1.1 mL:0.9 mL for 10% ee; 1.5 mL:0.5 mL for 50% ee; 1.9 mL: 0.1 mL for 90% ee.

The experimental ee's were determined by chiral UPLC [Chiralpak® IC-U, as Section 6.6.2.2, λ= 215 nm, $t_R$ (**(*S,S*)-6.6**) = 3.59, $t_R$ (**(*R,S*)-6.6**) = 3.69, $t_R$ (**(*R,R*)-6.6**) = 3.77] and are recorded in Table 6.3.1.

### 6.6.2.2.2 Procedure for biphasic reaction

Each 2.0 mL solution prepared in Section 6.6.2.2.1 was placed in a round-bottom flask and stirring was begun at 100 rpm. Octanethiol **3.1** (5.0 μL, 25 μmol, 0.50 eq. relative to **6.6**) was added onto the top of each solution by microsyringe and the start of the addition was considered time zero. An aliquot was taken every 10 minutes for the first 30 minutes, followed by an aliquot at a total reaction time of 1 hour after which point aliquots were taken every hour until a total reaction time of 8 hours.

Each aliquot was analysed by chiral UPLC [Chiralpak® IC-U, as Section 6.6.2.2, λ= 215 nm, $t_R$ (**(*S*)-6.7**) = 4.54, $t_R$ (**(*R*)-6.7**) = 4.67] and the ee of **6.7** throughout the reaction is recorded in Figure 6.3.2.

### 6.6.2.3 Experiments conducted using chiral thiol **6.8**

Experiments were analysed following the procedures described in Section 3.5.3, and the concentrations of reaction components **3.2** and **3.3** were determined using the calibrations made in Section 3.5.3.3.

A simple calibration of the concentration of **6.9** by UPLC was performed: first a 5.0 mM solution of **6.9** (3.9 mg, 10 µmol) in 2.0 mL Tris buffer (500 mM, pH 7.8 – 7.9) was prepared. 25 µL of this solution was placed in an MS vial and 1.0 mL of external standard solution, containing maleimide, was added. Three successive 1.0 µL injections of the solution were taken and the chromatogram was recorded by UPLC. Peak areas were integrated at a wavelength of 215 nm. The area of the peak corresponding to **6.9** over the area of the external standard peak was recorded and the average of the three measurements was taken. This measurement was taken as a calibration of a 5.0 mM solution. To calculate the concentration of **6.9** in other solutions it was (tentatively) assumed that the UPLC response was linear.

#### 6.6.2.3.1 Reactions conducted with **(*rac*)-6.8**

The general procedure is llustrated with the reaction depicted in Figure 6.4.2:

5,5'-Dithiobis-(2-nitrobenzoic acid) (DTNB) **3.2** (119 mg, 300 µmol) was dissolved by sonication in 12 mL Tris buffer (500 mM, pH 7.8 – 7.9) to reach pH ~ 7.5.

Two 5 mL portions of this solution were placed into two 10 mL round bottomed flasks and stirring was started at 100 rpm. Racemic thiol **(*rac*)-6.8** (24 mg, 0.13 mmol, 1.0 eq.) was placed dropwise onto the surface of each solution by microsyringe, and the beginning of this addition was considered time zero.

An aliquot of the solution phase was taken every 10 minutes for the first 30 minutes, followed by an aliquot at a total reaction time of 1 hour after which point aliquots were taken every hour until a total reaction time of 8 hours. The reaction was left to stir overnight before taking final aliquots at a total reaction time of 23 hours.

#### 6.6.2.3.2 Experiments conducted with non-racemic **6.8**

For each experiment, the initial enantiomeric excess of thiol **6.8** was determined by SFC [Chiralpak® IF, MeOH/$CO_2$: 1.0 to 30 %; 1.5 mLmin$^{-1}$, λ= 215 nm, $t_R$ (**(*R*)-6.8**) = 1.37, $t_R$ (**(*S*)-6.8**)= 1.41].

To determine the ee of **6.9** in different phases, a small portion of the solution phase and, when precipitation occurred, a small sample of the precipitate was removed as best as possible and placed into vials.

One drop of 1 M HCl and EtOAc (0.5 mL) was added to each vial and the vials were shaken. The organic layers were carefully removed by pipette and transferred to MS vials. The solutions were concentrated *in vacuo*. The dry samples were dissolved in hexane:isopropanol (9:1) (1.0 mL). The enantiomeric

excess of **6.9** was determined by chiral SFC [Chiralpak® IG, MeOH/$CO_2$: 1.0 to 30 %; 1.5 mLmin$^{-1}$, λ= 215 nm, $t_R$ (**(*R*)-6.9**) = 4.77, $t_R$ (**(*S*)-6.9**) = 4.98].

### 6.6.2.3.2.1 Behaviour of **6.9** under biphasic conditions

25 mM solutions of **(*rac*)-6.9**, **(*R*)-6.9** (30% ee), **(*R*)-6.9** (49% ee), and **(*R*)-6.9** (81% ee) were prepared in Tris buffer (500 mM, pH 7.8 – 7.9). No adjustment to the pH was made on dissolution. Precipitation was observed, and portions of the solution phase and the precipitate were taken and analysed. The resultant ee's are recorded in Table 6.4.1.

### 6.6.2.3.2.2 Reactions conducted with non-racemic **6.8**

**(*R*)-6.8** (82% ee) (102 mg, 525 μmol) and **(*rac*)-6.8** (18.0 mg, 93.0 μmol) were mixed by sonication in a vial to give **(*R*)-6.8** (67% ee).

The reaction was set up exactly as the reactions described in Section 6.6.2.3.1 but using **(*R*)-6.8** (67% ee) (24 mg, 0.13 mmol, 1.0 eq.).

An aliquot of the solution phase was taken every 15 minutes for the first 30 minutes, followed by aliquots at a total reaction time of 1 hour after which point measurements were taken every hour until a total reaction time of 7 hours. When it formed, samples of the precipitate were also taken for analysis at the same time points as solution phase aliquots. The reaction was left to stir overnight before

taking an aliquot at a total reaction time of 23 hours, and then every hour for a total reaction time of 26 hours. The data are recorded in Figure 6.4.3.

Reactions conducted with 2.0 and 8.0 equivalents of non-racemic thiol **6.8** were carried out following the above procedure using **(*R*)-6.8** (64% ee) (49 mg, 0.25 mmol, 2.0 eq.), and **(*R*)-6.8** (68% ee) (194 mg, 1.00 mmol, 8.0 eq.) respectively.

The thiol starting materials were prepared as follows:

**(*R*)-6.8** (82% ee) (93 mg, 479 μmol) and **(*rac*)-6.8** (17.0 mg, 87.5 μmol) were mixed by sonication in a vial to give **(*R*)-6.8** (64% ee).

**(*R*)-6.8** (82% ee) (337 mg, 1.73 mmol) and **(*rac*)-6.8** (63.0 mg, 324 μmol) were mixed by sonication in a vial to give **(*R*)-6.8** (68% ee).

For the reaction with 2.0 equivalents: an aliquot of the solution phase was taken every 15 minutes for the first 30 minutes, followed by an aliquot at a total reaction time of 1 hour after which point aliquots were taken every hour until a total reaction time of 9 hours. When it appeared, samples of the precipitate were also taken for analysis at the same time points as solution phase aliquots. The reaction was left to stir overnight before taking final aliquots at a total reaction time of 23, 24 and 26 hours. The data are recorded in Figures 6.4.5 and 6.4.6.

For the reaction with 8.0 equivalents: aliquots of the solution phase were taken every hour for a total reaction time of 10 hours. The reaction was left to stir

overnight and a final aliquot was taken at a total reaction time of 24 hours. The data are recorded in Figures 6.4.7 and 6.4.8.

## 6.7 References


1. Sorrenti, A., Illa, O. & Ortuno, R. M. Amphiphiles in aqueous solution: well beyond a soap bubble. *Chem. Soc. Rev.* **42,** 8200–8219 (2013).
2. Inagaki, T., Phong, L. T., Furuta, A. & Ito, J. Iron- and Cobalt-Catalyzed Asymmetric Hydrosilylation of Ketones and Enones with Bis(oxazolinylphenyl)amine Ligands. *Chem. Eur. J.* **16,** 3090–3096 (2010).

# 7

## Conclusions and Future Work

## 7.1 Out-of-equilibrium replication

A process of replication and reproduction, allowing persistence, mutation and evolution in the environment, is an essential characteristic of any living system. To understand the transition from “non-living” to “living” at the origins of life, the study of synthetic systems undergoing replication without the use of evolved biological machinery is important.

The work described in this thesis has focused on physical replication, or the reproduction of supramolecular aggregates, which serves as a minimal model of the replication of biological membranes. In particular, we have established a process of physical replication under out-of-equilibrium conditions, where the persistence and function of the replicator is no longer be confined by its thermodynamic stability. A process of replication out-of-equilibrium may be essential for evolution and the emergence of life.[1–7]

### 7.1.1 Replication in a dynamic combinatorial library

On the way towards an out-of-equilibrium replicator, we first explored physical replication in a dynamic combinatorial library (DCL). Replicators constructed within ‘perfect’ dynamic combinatorial libraries are formed reversibly and equilibrate between each other, therefore undergoing processes of destruction and competition likened, to some extent, to primitive lifelike processes. Their dynamic behaviour and response to their environment makes them of interest in their own right. Whilst the system still moves towards the thermodynamic or

kinetically trapped distribution, the type of reactions which are used to construct DCL replicators can be of use towards the design and construction of out-of-equilibrium replicators.

Thus, Chapter 2 was an investigation into a set of physical replicators in a dynamic combinatorial library. We were inspired by the work of Nguyen *et al.* which reported physical replicators constructed by reversible imine bond formation.[8] They could compete against each other for shared building blocks, equilibrating to the thermodynamic distribution, and their reversible formation was in contrast to our own previous studies of irreversibly formed physical replicators.[9–11] In particular, we were interested in examining this system of reversibly formed replicators at the single aggregate level using interferometric scattering microscopy (iSCAT).[11,12]

However, whilst the reported imine surfactant molecules **2.3a** and **2.3b** that we had chosen to study (Figure 2.2.1, page 56) were shown to aggregate and form micelles in aqueous solution, the surfactants were unstable to hydrolysis under neutral conditions and this precluded the observation of autocatalysis. At high pD, where one component did appear stable, autocatalysis was still not observed.

The ideal, autocatalytic behaviour for this system based on imine bond formation appeared limited to particular substrates that we had not examined; it was a sensitive system which suffered from a lack of reactivity and was not amenable for further development. Nevertheless, the study of replication within dynamic combinatorial libraries in general was important and had been argued to be the

'first step toward the far-from-equilibrium character of life'.[13] Thus, Chapter 3 began with the examination of a replicator constructed by thiol-disulfide exchange, a reaction which had been extensively used in the creation of DCLs.[14,15]

## 7.1.2 A chemically fuelled replicator

Chapter 3 examined the formation of a mixed disulfide surfactant **3.4**, constructed by thiol-disulfide exchange between octanethiol **3.1** and DTNB **3.2** (Figure 3.2.2, page 103). In sharp contrast to the system in Chapter 2, the reaction was shown to be autocatalytic.

The crucial step towards an out-of-equilibrium replicator relied on the fact that the surfactant **3.4** was also unstable towards a second thiol-disulfide exchange reaction with excess octanethiol **3.1** and was degraded to non-replicating components **3.3** and **3.5**. In a closed system, therefore, the surfactant replicator **3.4** was transiently produced before degradation towards the equilibrium state (Figure 3.2.4, page 106).

However, in an open system, an oxidising chemical fuel was used to recycle waste components of the reaction, regenerating precursors for surfactant and replicator formation. A steady state of the surfactant replicator could be established; surfactant molecules were simultaneously formed and destroyed whilst the population as a whole remained steady. Switching off the fuel supply resulted in the degradation towards thermodynamic equilibrium and the

destruction of all replicator, demonstrating that whilst under the continuous supply of fuel the system was indeed not at equilibrium nor in a kinetically trapped position (Figure 3.3.3, page 114). Therefore, fuel supply, rather than thermodynamic stability, determined both the persistence of the replicator and its concentration, which could be altered by increase or decrease in the supply of the chemical fuel (Figure 3.3.4, page 117).

Importantly, the system represented an advance over previous demonstrations of physical replicators under out-of-equilibrium conditions, and indeed over many out-of-equilibrium systems in general. Components were generated *in situ* from waste products with the *continuous* supply of chemical fuel, completing a substrate cycle. The manual input of new starting materials into the reaction or the continuous physical removal of waste products of the system was not required.

### 7.1.3 Future work

A system of self-replicating micelles in an out-of-equilibrium state could be expanded into ever-increasing network complexity and alter our understanding of lifelike processes.

First, we can imagine coupling surfactant and micelle formation to other micelle-catalysed reactions.[16–18] In theory, control over the concentration of the aggregated surfactant **3.4**, and therefore associated micelle-catalysed reactions, could be achieved; they could operate only where the consumption of fuel

allowed the micelles to persist. The nature of our aggregates as “general” catalysts, in contrast to the specificity of template replicators, makes the number of theoretical reactions broad and the resultant theoretical networks large. In turn, the products of these secondary reactions could be imagined to influence the stability, size, and numerous other aspects of the micelle compartments themselves under an out-of-equilibrium regime; the system’s behaviour would be emergent and complex.

We have already hinted at what might be the ultimate emergent behaviour of a replicator under out-of-equilibrium conditions: a process of open-ended evolution towards the emergence of life.[1–7] Whilst already explored relatively extensively in the context of RNA replication,[19,20] exactly what this looks like for a simpler synthetic system and how might can be achieved has mainly been explored theoretically and is a controversial and complicated field.[1–7] Our relatively simple replicating system, out-of-equilibrium, may allow for some experimental investigation into these theoretical requirements, such as processes of replicator mutation and selection under chemically fuelled conditions. Competition between replicators would no longer be confined to their thermodynamic stability. The potential function of our micelle replicator as a compartment, or membrane, providing all-important separation between competing molecular entities, differences in local environment, and an overall sense of inhomogeneity and asymmetry, may have important implications for theoretical scenarios of the origins of life.[21]

We believe that the interest in out-of-equilibrium supramolecular materials, coupled with the interest in processes of replication under out-of-equilibrium regimes, makes this study of replicating micelles out-of-equilibrium a valuable contribution to studies on the emergence and origins of life, as well as the synthesis of new lifelike materials and machines.

## 7.2 Replication and the amplification of chirality

In the second half of this thesis we explored another phenomenon that can be associated with a process of autocatalysis: the amplification of chirality. The only demonstration of an autocatalytic reaction with amplification of chirality is the Soai reaction;[22] the search for other, more general reactions is therefore important. We believed that investigating systems of replicating and autocatalytic supramolecular aggregates might lead us towards this research goal.

In Chapter 4 we proposed a mechanism for the amplification of chirality by a system of replicating aggregates. We required both a process of enantioselective micelle catalysis and of minor enantiomer inhibition. Demonstrations and mechanisms for both types of behaviour were known to some extent but had not been combined to demonstrate the successful amplification of chirality.[16,17,23–26] Chapters 5 and 6 detailed two designs for such a system; one was based on a surfactant constructed by native chemical ligation, and one was based on a surfactant constructed by thiol-disulfide exchange, a derivative of the system investigated in Chapter 3.

### 7.2.1 Chiral surfactant formation by native chemical ligation

Our first attempt to design a physical replicator with amplification of chirality arrived in Chapter 5, with the formation of an irreversibly formed replicator **5.7** constructed by native chemical ligation (Figures 5.2.2, page 174 and Figure 5.3.1, page 175). The change in product distribution both on moving from homogeneous to biphasic reaction conditions and on subtle changes in the physical properties of the starting materials was of interest in its own right, highlighting the sensitivity of this system and of biphasic reactions in general (Table 5.4.1, page 178 and Table 5.4.2, page 179). However, despite the ability of the designed surfactants **5.7a,b** to aggregate under biphasic conditions, the possible occurrence of autocatalysis could not be easily detected and we were limited by the lack of an appropriate *in situ* technique. A test for the amplification of chirality from starting materials to products showed no non-linear effects (Figure 5.6.1, page 184). Without the observation of autocatalysis the continued exploration of this system would not be rewarding. The simultaneous realisation of both a new autocatalytic reaction as well as one which had the power to amplify chirality was perhaps too ambitious a goal.

### 7.2.2 Chiral surfactant formation by thiol-disulfide exchange

Considering our previous success in developing an autocatalytic reaction based on thiol-disulfide exchange, we were interested in investigating chiral variants of the system and hoped to observe non-linear effects. This was the subject of Chapter 6.

Preliminary investigation focused on a chiral derivative of DTNB **3.2**, disulfide **6.6** (Figure 6.3.1, page 207). Experimentally, a process of disulfide exchange between **(*R,R*)-6.6** and **(*S,S*)-6.6** introduced into the reaction resulted in the enhancement in ee of the starting materials by formation of a *meso* disulfide **(*R,S*)-6.6** which sequestered the minor enantiomer (Table 6.3.1, page 208). However, this enhancement in ee was not translated into product formation; the ee of the resultant surfactant product **6.7** was found to be equal to that of the starting materials **6.6** introduced into the reaction (Figure 6.3.2, page 210).

A more promising derivative was the use of a chiral hydrophobic thiol **6.8** (Figure 6.4.1, page 211). Here, the surfactant product **6.9** derived from the reaction of the chiral thiol **6.8** with DTNB **3.2** was observed to precipitate from aqueous solution and a sense of asymmetry was established; the precipitate was enantiomerically enriched whilst the solution phase tended towards an ee that was lower than that of the starting materials (Figure 6.4.3, page 216). Whilst not in line with our original design for the amplification of chirality *via* physical autocatalysis, the establishment of any asymmetry in the reaction, promoted by the biphasic conditions, was interesting and led to a new design for the amplification of chirality which relied on the operation of a second thiol-disulfide exchange to destroy racemic product (Figure 6.4.4, page 219). Unfortunately, however, the experimental realisation of this design was not achieved.

### 7.2.3 Future work

For the design of replicators which fit the Frank model for amplification of chirality, general design rules for the partitioning of surfactants into enantiopure and racemic assemblies must be established. Additionally, once formed, the enantiopure micelles must catalyse subsequent reactions enantioselectively. Micelles are generally considered to be poorly-defined and highly dynamic environments, which makes processes of enantioselective micelle catalysis difficult to realise. The construction of better-defined enantiopure assemblies, which can select between enantiomers of other materials, must therefore be investigated. Study at this fundamental level is more likely to lead to success in realising a process of physical autocatalysis with amplification of chirality.

Nevertheless, the asymmetry in the system provided by the biphasic conditions for the system studied in Chapter 6 is a promising property that could be exploited for investigation of non-linear behaviours, even if it does not fit the Frank model. First, a more thorough investigation into the nature of the precipitate and solution phases will be required to ascertain the true partitioning of the system and the ee of each phase; better methods of analysis are needed which avoid unwanted disturbance of the system.

Once more robust methods have been developed it may also be interesting to explore the behaviour of the systems designed in Chapter 6, and derivatives thereof, under out-of-equilibrium conditions, with the continued production of components for replicator formation. As far as we are aware, neither theoretical

nor experimental treatments of the amplification of chirality under out-of-equilibrium conditions have been well explored.[27]

## 7.3 Concluding remarks

The design and study of out-of-equilibrium replicating systems and systems which amplify chirality are both of critical importance for our understanding of lifelike dynamics and the emergence of life from non-living components. However, both areas are underexplored and complex; there are no widely-understood and accessible design rules for the construction of synthetic systems which approach the complexity of living, biological systems. Thus, examples of these behaviours in purely synthetic systems are few and far between.

On studying a process of physical autocatalysis we have observed emergent behaviour that contributes towards both research goals. First, we have constructed an out-of-equilibrium replicator which catalyses a biphasic reaction to produce its own components and whose persistence and function is dependent on the supply of a simple chemical fuel. Secondly, investigating chiral derivatives of the same system has resulted in the emergence of enantiomerically enriched phases which cannot be achieved under homogeneous conditions. Both processes have relied on a sense of asymmetry established by the biphasic reaction conditions. The coupling of simple chemical reactivity with physical processes in these systems is fundamental to their behaviour and might be a general design rule towards the construction and understanding of synthetic systems which approach lifelike dynamics.

## 7.4 References


1. Schwille, P. How Simple Could Life Be ? *Angew. Chem. Int. Ed.* **56,** 10998–11002 (2017).
2. Duim, H. & Otto, S. Towards open-ended evolution in self-replicating molecular systems. *Beilstein J. Org. Chem.* **13,** 1189–1203 (2017).
3. Higgs, P. G. Chemical Evolution and the Evolutionary Definition of Life. *J. Mol. Evol.* **84,** 225–235 (2017).
4. Pross, A. *What is Life? How chemistry becomes biology*. (Oxford University Press, 2016).
5. England, J. L. Dissipative adaptation in driven self-assembly. *Nat. Nanotechnol.* **10,** 919–923 (2015).
6. England, J. L. Statistical physics of self-replication. *J. Chem. Phys.* **139,** 121923 (2013).
7. Pascal, R., Pross, A. & Sutherland, J. D. Towards an evolutionary theory of the origin of life based on kinetics and thermodynamics. *Open Biol.* **3,** 130156 (2013).
8. Nguyen, R., Allouche, L., Buhler, E. & Giuseppone, N. Dynamic Combinatorial Evolution within Self-Replicating Supramolecular Assemblies. *Angew. Chem. Int. Ed.* **48,** 1093–1096 (2009).
9. Bissette, A. J., Odell, B. & Fletcher, S. P. Physical autocatalysis driven by a bond-forming thiol-ene reaction. *Nat. Commun.* **5,** 4607 (2014).
10. Post, E., Bissette, A. & Fletcher, S. P. Self-reproducing micelles coupled to a secondary catalyst. *Chem. Commun.* **54,** 8777–8780 (2018).
11. Ortega-arroyo, J., Bissette, A. J., Kukura, P. & Fletcher, S. P. Visualization of the spontaneous emergence of a complex, dynamic, and autocatalytic system. *Proc. Natl. Acad. Sci.* **113,** 11122–11126 (2016).
12. Ortega-Arroyo, J. & Kukura, P. Interferometric scattering microscopy (iSCAT): new frontiers in ultrafast and ultrasensitive optical microscopy. *Phys. Chem. Chem. Phys.* **14,** 15625–36 (2012).
13. Otto, S. Dynamic Molecular Networks: From Synthetic Receptors to Self-Replicators. *Acc. Chem. Res.* **45,** 2200–2210 (2012).
14. Carnall, J. M. A. *et al.* Mechanosensitive self-replication driven by self-organization. *Science* **327,** 1502–1506 (2010).
15. Sadownik, J. W., Mattia, E., Nowak, P. & Otto, S. Diversification of self-replicating molecules. *Nat. Chem.* **8,** 264–269 (2016).
16. Dwars, T., Paetzold, E. & Oehme, G. Reactions in micellar systems. *Angew. Chem. Int. Ed.* **44,** 7174–99 (2005).
17. La Sorella, G., Strukul, G. & Scarso, A. Recent advances in catalysis in micellar media. *Green Chem.* **17,** 644–683 (2015).
18. Maiti, S., Fortunati, I., Ferrante, C., Scrimin, P. & Prins, L. J. Dissipative self-assembly of vesicular nanoreactors. *Nat. Chem.* **8,** 725–731 (2016).
19. Lincoln, T. A. & Joyce, G. F. Self-sustained replication of an RNA enzyme. *Science* **323,** 1229–1232 (2009).
20. Vaidya, N. *et al.* Spontaneous network formation among cooperative RNA replicators. *Nature* **491,** 72–77 (2012).
21. Szostak, J. W., Bartel, D. P. & Luisi, P. L. Synthesizing life. *Nature* **409,** 387–390 (2001).
22. Soai, K., Shibata, T., Morioka, H. & Choji, K. Asymmetric autocatalysis and

amplification of enantiomeric excess of a chiral molecule. *Nature* **378,** 767–768 (1995).
23. Saghatellan, A., Yokobayashi, Y., Soltani, K. & Ghadiri, M. R. A chiroselective peptide replicator. *Nature* **409,** 797–801 (2001).
24. Morigaki, K., Dallavalle, S., Walde, P., Colonna, S. & Luisi, P. L. Autopoietic Self-Reproduction of Chiral Fatty Acid Vesicles. *J. Am. Chem. Soc.* **119,** 292–301 (1997).
25. Jiang, J., Ouyang, G., Zhang, L. & Liu, M. Self-Assembled Chiral Nanostructures as Scaffolds for Asymmetric Reactions. *Chem. Eur. J.* **23,** 9439–9450 (2017).
26. Sorrenti, A., Illa, O. & Ortuno, R. M. Amphiphiles in aqueous solution: well beyond a soap bubble. *Chem. Soc. Rev.* **42,** 8200–8219 (2013).
27. Islas, J. R., Micheau, J. & Buhse, T. KINETIC ANALYSIS OF SELF-REPLICATING PEPTIDES: POSSIBILITY OF CHIRAL AMPLIFICATION IN OPEN SYSTEMS. *Orig. life Evol. Biosph.* **34,** 497–512 (2003).